CHAPTER ONE

INTRODUCTION

1.1 Plant Kingdom

Plant kingdom bestowed upon human is one of the most treasured gifts, early generations of mankind recognized their reliance on nature [1]. Plants have provided man with all his needs in terms of housing, dressing, cooking, flavoring, and perfumery as not the least, medications. Plants have built the backbone of multifaceted traditional medicine systems, which have been in presence for thousands of years and continue to provide generations with new remedies.

Natural products and their by-products represent more than 50 per cent of all the medicinces in clinical use in the world. Over the last 40 years, plenty of effective drugs have been derived from flowering plants.

Medicinal plants typically contain mixtures of many chemical components that may act separately, additively or in synergy to improve health. A single plant may contain bitter compounds that motivate digestion, anti-inflammatory compounds that decrease swellings and ache, phenolic compounds that can act as an anti-bacterial and venotonics, antioxidant and anti-fungal tannins that work as natural drugs, diuretic meterials that increase the removal of waste products and poisons and alkaloids that enhance mood and provide a sense of well-being.

People who take traditional medicines may not understand the scientific rationale behind their remedies, but they know from personal experience that some medicinal plants can be extensively active if used at healing doses. Since we have a better knowledge today of how the body acts, we are thus in a better position to understand the healing powers of plants and their potential as multi-functional chemical entities for healing complicated health conditions. Modern allopathic commonly aims to improve a patentable individual compound or a ‘magic bullet’ to heal specific

conditions. Traditional medicine often aims to make balance by using chemically multiplex plants, or by combining several different plants in order to maximize a synergistic effect or to improve the likelihood of an interaction with a relevant molecular target.

Nowadays, in most societies, allopathic and traditional systems of medicine occur shoulder to shoulder in a complimentary way. The former treats serious acute conditions, while the latter is used for chronic illnesses, to reduce symptoms and improve the quality of life in a cost-effective way.

Even though some of the therapeutic features attributed to plants have shown to be erroneous, medicinal plant remedy is based on the factual findings of hundreds and thousands of years. The first document written on brick tablets in manuscript, was from Mesopotamia and date from 2600 BC; among the essential natural products that were applied were extracts of Cedrus species (Cedar) and Cupressus sempervirens (Cypress), Papaver somniferum (Poppy juice). *Commiphora* species (Myrrh) and *Glycyrrhiza glabra* (Licorice), all of which up-to-date are in use for the remedy of illnesses ranging from colds and coughs to inflammation and parasitic infections. Egyptian medicines report on the use of bishop's weeds (Ammi majus) to treat vitiligo, a skin condition characterized by a loss of pigments. More recently, a drug, methoxypsoralen **1**, has been produced from this plant to treat psoriasis and other skin ailments, as well as T-cell lymphoma. Many drugs that are commonly used today came through the use of indigenous medicine (such as aspirin **2** from salicylic acid **3** and pethidine **4** from morphine **5)** that is through the bioscientific investigations of plants used by people throughout the world [2-4].

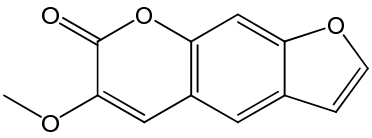

methoxypsoralen **1**

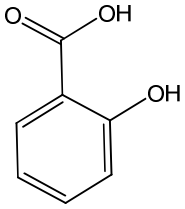

salicylic acid **2** from *Salix* sp.

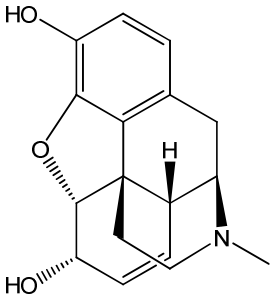

morphine **4** from *Papaver somniferum*

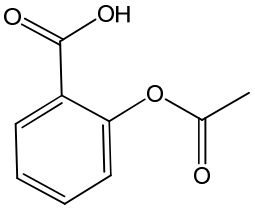

aspirin **3**

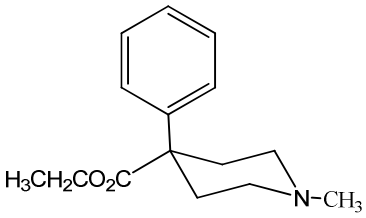

pethidine **5**

Fortunately, Malaysia is blessed with one of the oldest (approximately 130 to 150 million years old) and wealthiest flora (comprises of more than 15000 species of higher plants) in the world. Its position near the Equator confers on it a typical tropical climate, characterized by high temperature, humidity and rainfall throughout the year which are conductive to plant life and have resulted in a rich and thriving flora [5]. The tropical rain forest of Malaysia possess medicinal properties such as tongkat ali or pasak bumi *(Eurycoma longifolia),* jarum emas *(Striga asata),* kacip fatimah *(Labisia pothoina),* ketum *(Mitragyna speciosa),* ginger *(Zinziber officinale),* cekur *(Kaempferia galanga),* hempedu bumi *(Andrographis paniculata),* senduduk *(Melastoma malabathrichum),* mengkudu *(Morinda citrifolia),* ulam raja *(Cosmos caudatus),* tutup

bumi (*Elephantopus scaber), sirih (Piper betle),* dukung anak *(Phyllanthus niruri),* serusa *(Strobilanthes crispa),* petai *(Parkia speciosa),* jering *(Archidendron jiringa),* pegaga *(Centella asiatica),* bunga raya *(Hibiscus rosa-sinensis),* ati-ati *(Coleus scutellarioides)* and many others [6-7]. The earliest phytochemical report from the Malaysia Flora was on phytochemical screening of 205 plants in Sabah [8]. A few years later, the screening of 200 species have been done in Peninsular Malaysia for the presence of alkaloids [9]. These two reports marked the beginning of medicinal plant research in Malaysia. Subsequently, more plants were screened chemically for alkaloids, saponins, triterpenes and steroids [10]. Many plants have been explored and researched, and much more yet to be discovered. In this study, the author has worked on Meliaceae plants which are *Chisocheton ceramicus, Chisocheton tomentosus, and Dysoxylum macrocarpum* since plants of the Meliaceae family are known as a rich source of secondary metabolites including alkaloids [11-12].

1.2 Botanical Aspect of Meliaceae

Meliaceae, or the mahogany family, embrace over 1400 species in 51 genera of woody plants allocated in subtropical and tropical regions worldwide. Within the family, two major subfamilies [13], Melioideae and Swietenioideae, have been recognized based on seed morphology [14], wood anatomy and more recently molecular data [15]. (The name Cedreloideae has priority over Swietenioideae but is practically never used) [16]. Melioideae form a monophyletic group that includes 73% of the genera and 87% of the species of the family [15], and are characterized by naked buds, unwinged seeds, and fruits that are berries, drupes, nuts, or loculicidal capsules. Swietenioideae include 14 genera and only 51 species, most of which are used as timber worldwide. They are characterized primarily by their buds protected by scale-like leaves, septifragral capsules and winged seeds. They may be recognized at once by their usually pinnately compound leaves without stipules and by syncarpous, usually bisexual

flowers borne in panicles, cymes, spikes, or cluster. Many species are deciduous, either in dry season or in winter, but some are evergreen. Mahogany is a very bulky canopy tree, sometimes reaching over 150 feet in high, with trunks sometimes exced six feet in diameter above a large basal buttress. It is generally open-crowned tree, with gray to brownish-red fissured bark. Considering its flowers, and fruit-structure, it is undoubtedly a climax family, more advanced than Rutaceae with which it is slightly related. The flowers are mostly free petals, but more especially by the androecium with filaments variously united into a tube which sometimes resembles a corolla [17-19].

1.3.1 Classification of Genus [17-18]

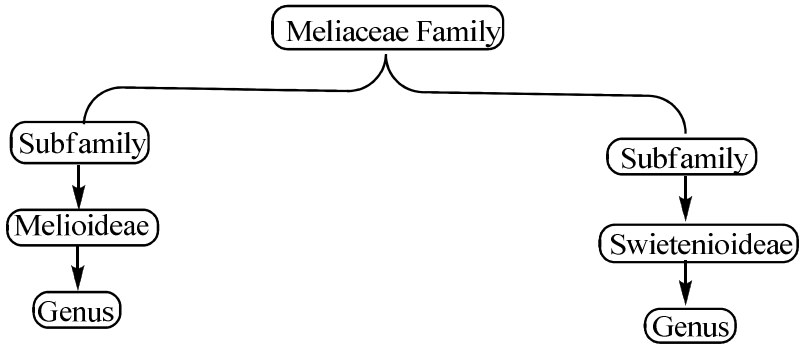

Aglaia Lour
Aphanamixis Blume
Azadirachta A. Juss
Chisocheton Blume
Cipadessa Blume
Dysoxylum Blume
Lansium Blume
Reinwardtioendron
Koordens
Sandoricum Cay.
Trichilia P. Br.
Turraea L.
Walsura Roxb.

Chukrasia A. Juss
Toona (End!.) M.J.
Roemer
Xylocarpus Koenig
Swietenia

Scheme 1.1: Classification of Malaysian Meliaceae

1.3 Genus *Chisocheton*

The genus *Chisocheton* is made up of about 50 species and distributed mainly in the tropic and subtropic region of Asia. These species are often found in the lowland rain forest with a few species in lower montane habitats. They grow under other trees.

The leaves are alternate, pinnate, leaflets opposite and the rachis terminated by bud which produces new pairs of leaflets for most of the life of leaf. It has indumentums of small, glandular hairs and unbranched or stellate eglandular hairs. Plants always dioecious, have inflorescences axillary, spicate to paniculate, sometimes epiphyllous or cauliflorous.

The flowers are articulated with pedicel or branchlets and sometimes have a pseudopedicel above point of articulation. It has three to six petals which aestivation valvate or alternative, rarely imbricate or quincuncial, connate at the base and sometimes-adnate to staminal tube. Its staminal tube is cylindrical, sometimes slightly expanded or contracted at the mouth with the margin entire to deeply lobed. The anthers are inserted within tube, 4-12, usually locellate, and antherodes somewhat more slender.

The fruit is loculicidal and sometimes rather belatedly. It is usually two to four seeded (sometimes until eight), stipitate or rostrate, rarely ridged. Its pericarp is spongy, woody or coriaceous, sometimes with white sap. The seeds have carcotesta or arillode, arillode partly free or not and have large hilum. The cotyledons are large and collateral or superposed. Some species produce oil, which is purgative, has a rancid smell and is non-drying, e.g. *Chisocheton pentandrus* and *Chisocheton cumingianus*. The extracted oil of the former is exploited commercially for making soap while the latter is used as a hair cosmetic product in Philippines. The hardwood from *Chisocheton ceramicus* is used for house building in the East Sepik and in the construction of ceremonial houses. Another species, *Chisocheton montanus*, is used as building material for houses, fences,

gardening sticks, etc. *Chisocheton morobeanus* can be used as fish poison. Its bark is beaten and then put into water in confined pool. These will effectively stunned fishes for several hours [19-21].

1.3.1 *Chisocheton ceramicus*

Chisocheton ceramicus (Figure 1.1) is a medium-sized tree (up to 30 m high), bole cylindrical (up to 40 cm diameter), its bark is grey-brown; inner bark reddish; twigs rusty tomentose. Leaves in terminal spirals on dropping branches, up to 1.5 m long, with pseudogemmula and up to 17 pairs of leaflets, from elliptic to elliptic-oblong, apex abruptly acuminate acute. Inflorescence axillaries, flowers on a branched axis, cones absent; flowers unisexual, unisexual with male and female flowers on different plants, stalked, flowers with many planes of symmetry, 13.0-18.0 mm long, diameter small (up to10 mm diam). Fruits are in frutescence arranged on branched axis, with 30.0-40.0 mm long, orange to red, not spiny, fleshy, simple, indehiscent or somewhat dehiscent, capsule. Seeds dark reddish brown, 20-24 mm long and12-15 mm diameter [19].

Figure 1. 1: *Chisocheton ceramicus* leaves and fruit KL 4973

1.3.2 *Chisocheton tomentosus*

Chisocheton tomentosus (Figure 1.2) is a medium-sized tree that can grow up to 21 m. unbranched Corner's Model or sparsely branched, often from near the base and 60 cm girth. Bole sometimes weakly fluted or with small stilt roots. Its bark is blackish brown, smooth to weakly fissured, with conspicuous shield-shape, all young parts brown tomentose with irritant hairs. Its leaves are about 2 m long, imparipinnate to pseudogetnmulate with up to at least 15 pairs of leaflets, rugose, shiny and glabrous above except for brown tomentose midrib, tomentose or tawny pubescent below where strongly reticulate with 12-30 veins on each side of midrib. Inflorescences to 1 m long, with flowers forming a terminal head in distal half. Flowers-hermaphrodite or unisexual on same tree; calyx 5-lobed; petals 5, free; filaments joined near base, terminated by a pair of thread-like appendages; anthers 10, hairy; disc small, united to base of filaments; ovary 5 (6)-locular; style head with 5 small stigmatic lobes. Fruits are small spherical with 7.5 cm diam., sub-globular, golden brown velvety with irritant detachable hairs; seeds 3-5, to 4 cm long with white sarcotesta [19].

Figure 1. 2: *Chisocheton tomentosusn* fruit and leaves KL 4251

1.4 Genus *Dysoxylum*

Dysoxylum is a genus of trees or treelets, dioecious, more rarely with hermaphrodite flowers in the family (Meliaceae), most of which occur in lowland rain forest. The leaves are opposite or spirally arranged pinnate, leaflets opposite or alternate coriaceous or sub-coriaceous, base oblique, the flowers bisexual or functionally unisexual. The fruit is a leathery capsule. There are few seeds; each has a fleshy jacket. There are about 75 species, mainly trees, were prized for their wood which is a rich red in colour and was widely used in the furniture trade [19].

1.4.1 *Dysoxylum macrocarpum*

Dysoxylum macrocarpum (Figure 1.3) is a big tree to 33 m tall and 1.5 m girth. Plank buttresses to 2 m tall and to 1 m out. Its bark smooth, grey-green, faintly hooped and finely lenticellate; inner bark cream, flecked orange, fibrous within; wood pale yellow. Leafy twigs stout with wide pith and conspicuous leaf scars and lenticels. Apical buds spike-like to 5 cm long. Leaves to 1 m long, paripinnate, subglabrous; leaflets in 3 or 4 pairs, to 30 cm long and with 13-18 veins on each side of midrib but other venation obscure. Inflorescence to 25 cm long, with spreading branches. Flowers foetid; petals 4; anthers 8 (9). Infructescence with massive axis to 8 mm diam., of 1-3 fruits, globose, 10 cm diam., bright orange-red, shallowly ridged, dehiscent; pericarp with white latex; mesocarp fleshy, orange-yellow; seeds 1-2 with dark brown (7) sarcotesta [19].

Figure 1. 3: *Dysoxylum macrocarpum* fuit and leaves KL 4302

,

1.5 Objectives of the Project

Plants in the Meliaceae (mahogany) family are common to generate a class of highly oxidized triterpenes, named the limonoids. Information acquired previously has exhibited a broad extent of biological activities for these compounds, including antifeedant, insect and growth regulating activities, along with a plenty of remedia effects in animals and humans [22]. To achieve this goal, this work was divided into three objectives:

(1) To extract, purify and isolate the chemical constituents from *Chisocheton tomentosus*, *Chisocheton ceramicus*, and *Dysoxylum macrocarpum* using column chromatographic techniques and preparative HPLC.

(2) To elucidate the structure of isolated compounds using spectroscopic methods including IR, MS (positive ion model and negative ion model), extensive 1D and 2D NMR (^{1}H, ^{13}C, DEPT, ^{1}H-^{1}H COSY, HMQC, HMBC, and NOESY), and X-ray diffraction experiments.

(3) To investigate the biological activity of some isolated compounds.

CHAPTER TWO

GENERAL CHEMICAL ASPECTS OF MELIACEAE FAMILY

1.0 Introduction

According to the recent relationship between humankind and plants; we have to recognize that the plants have provided man with all his needs in term of food, shelter, clothing, flavors and fragrance as not the least, medicines, it is important to acknowledge with gratefulness that plant extracts and products contribute substantially in our needs especially as pharmaceutical and biological agents [2].

This section highlights on some molecules and secondary metabolites that have led to the development of these pharmacological active extracts in Meliaceous plants.

2.1 Aromatic Compounds: Phenolics [23-25]

Phenolics are a huge and diverse group of aromatic compounds (containing benzene rings) usually with hydroxyl groups. Many plant phenolics have three carbon side chains and are called phenyl propanoids.

Harhorne and Simmonds [23] have classified the phenolic compounds in plants into several families as illustrated in Table 2.1, due to the diverse group of the plant phenolics.

Table 2.1 : Classification of phenolic constituents in plants

Number of carbon atoms	Families of phenols
C_6	Simple phenols
C_6-C_1	Phenolic acids and related compounds
C_6-C_2	Acetophenones and phenyllacetic acids
C_6-C_3	Cinnamic acid and related compounds
C_6-C_3	Coumarins, isocoumarins and chromones
C_{15}	Flavones
C_{15}	Isoflavones and isoflavonoid
C_{15}	Flavonols, dihydroflavanols and related compounds
C_{15}	Anthocyanidins
C_{15}	Chalcones, aurones and dihydrochalcones.
C_{30}	Biflavonyls
C_6-C_1-C_6	Benzophenones, xanthones and stilbenes.
C_6-C_2-C_6	
C_6, C_{10}, C_{14}	Quinones
C_{18}	Bentacyanins

2.1.1 The C_6-C_3 Phenolics Constituent

The C_6- C_3 skeleton is the most common and the most important. Many phenolic compounds reported possess this structure. This group includes, to begin with, the alcohols derived from the cinnamic acids, which is more commonly than their C_6-C_1 counterparts. Confineryl **6** and sinapyl **7** alcohols are constituents of woody plants: they are regarded as precursors of lignin.

Attention must also be given to two amino acids, which possesses phenolic functions, although they are not usually considered along the phenolic constituents: tyrosine **8** and 3,4-dihydroxyphenylalanine **9**. In the course of alcoholic fermentation

tyrosine is converted into *p*-hydroxyphenylethanol **10**, which is a normal constituent of fermented beverages, beer and wine. To these structures may also be added various aromatic amines, such as tyramine **11**, which are sometimes classified as alkaloids.

Phenolic substances with phenylpropane structures such as eugenol **12** and isoeugenol **13** should be placed in class of C_6-C_3 compounds. These are constituents of essential oil. Here also are to be included the lignin, C_6-C_3 dimers which are heartwood constituents associated with lignin. They are different structural types, such as the dibenzylbutyrolactones (e.g matairesinol **14**) or the diphenyltetrahydrofurofurans (pinoresinol **15)**. The last class of C_6-C_3 to be mentioned is the chromene, which are not commonly found related to the coumarins. The simplest example is that of euginin **16**.

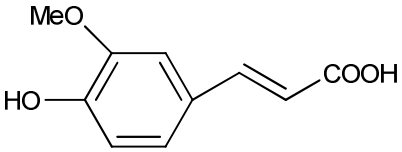

confineryl **6**

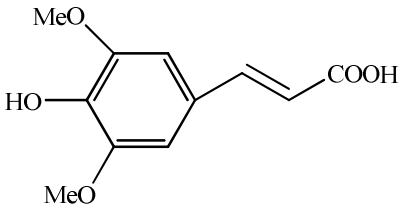

sinapyl **7**

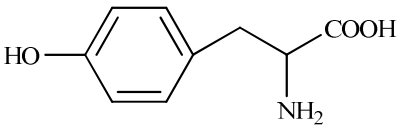

tyrosine **8**

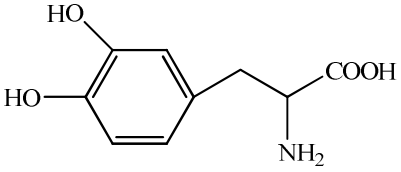

3,4-dihydroxyphenylalanine **9**

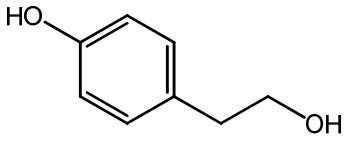

p-hydroxyphenylethanol **10**

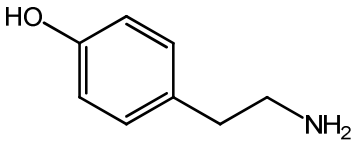

tyramine **11**

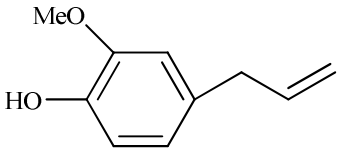

eugonol **12**

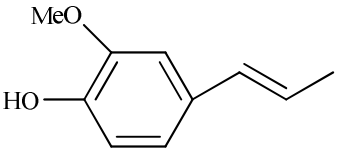

isoeugenol **13**

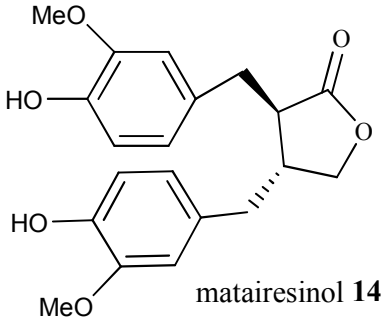

matairesinol **14**

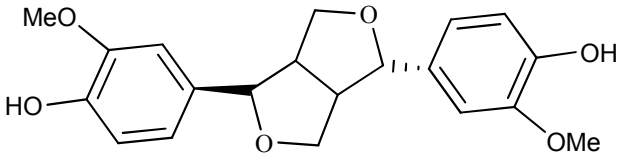

pinoresinol **15**

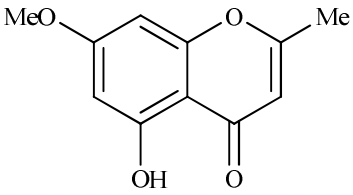

eugenin **16**

2.1.2 Biogenesis of Plant Phenolics

Plant phenolics arises from the following main pathways

i) The shikimic acid pathway

The most common pathway is in the one which, via shikimate (shikimic acid **17**) leads from monosacharides to aromatic amino acids (phenylalanine **18** and tyrosine **8**), then by deamination of the latter, to cinnamic acid and their numerous derivatives including benzoic acids, acetophenones, lignans, lignins and coumarins.

ii) The acetate or polyketide pathway

The other pathway begins with acetate and leads to poly-*β*-ketonesters, by

cyclization (Claisen or aldol condensation), products that are often polycyclic, including chromones, isocaumarins, orcinols, depsides, depsidones, xanthones and quinines.

iii) The mevalonic acid pathway

This pathway leads to the formation of aromatic terpenoids and steroids containing aromatic ring.

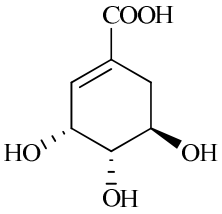

Shikimic acid **17**

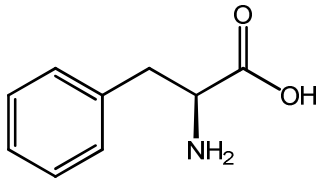

phenylalanine **18**

2.1.3 Biosynthetic Origin of Aromatic Ring (Shikimic Acid Pathway)

The shikimic acid pathway represents the principal mode of accumulation of phenolic compounds in plants. Not only the aromatic acids, but the benzoic acids and the cinnamic acid are all formed in this way. The structure of shikimic acid **17** is shown above, for which the pathway was named after.

The building blocks of shikimic acid are phosphoenolpyruvate (PEP) and D-erythrose-4-phosphate (E_4P). These combine in a reaction catalyzed by the enzyme DAHP synthase to give the 7-carbon sugar 3-deoxy-D-arabino-heptulosonic acid-7-phosphate, which is subsequently cyclised to the first carbocyclic compound, 3-dehydroquinate (DHQ). Hydrolysis of the latter gives 3-dehydroshikimate (DHS), followed by reduction of the carbonyl functional group then gives shikimate which is subsequently phosphorylated in the position-3 to form shikimate 3-phosphate (SA_3P). Attachment of a 3-carbon side chain, provided by another molecule of phosphoenolpyruvate leads to the formation of 5-enolpyruvylshikimate-3-phosphate (EPSP), followed by a 1,4-elimination of the elements of phosphoric acid then leads to

the formation of chorismate. These processes are illustrated in Scheme 2.1.

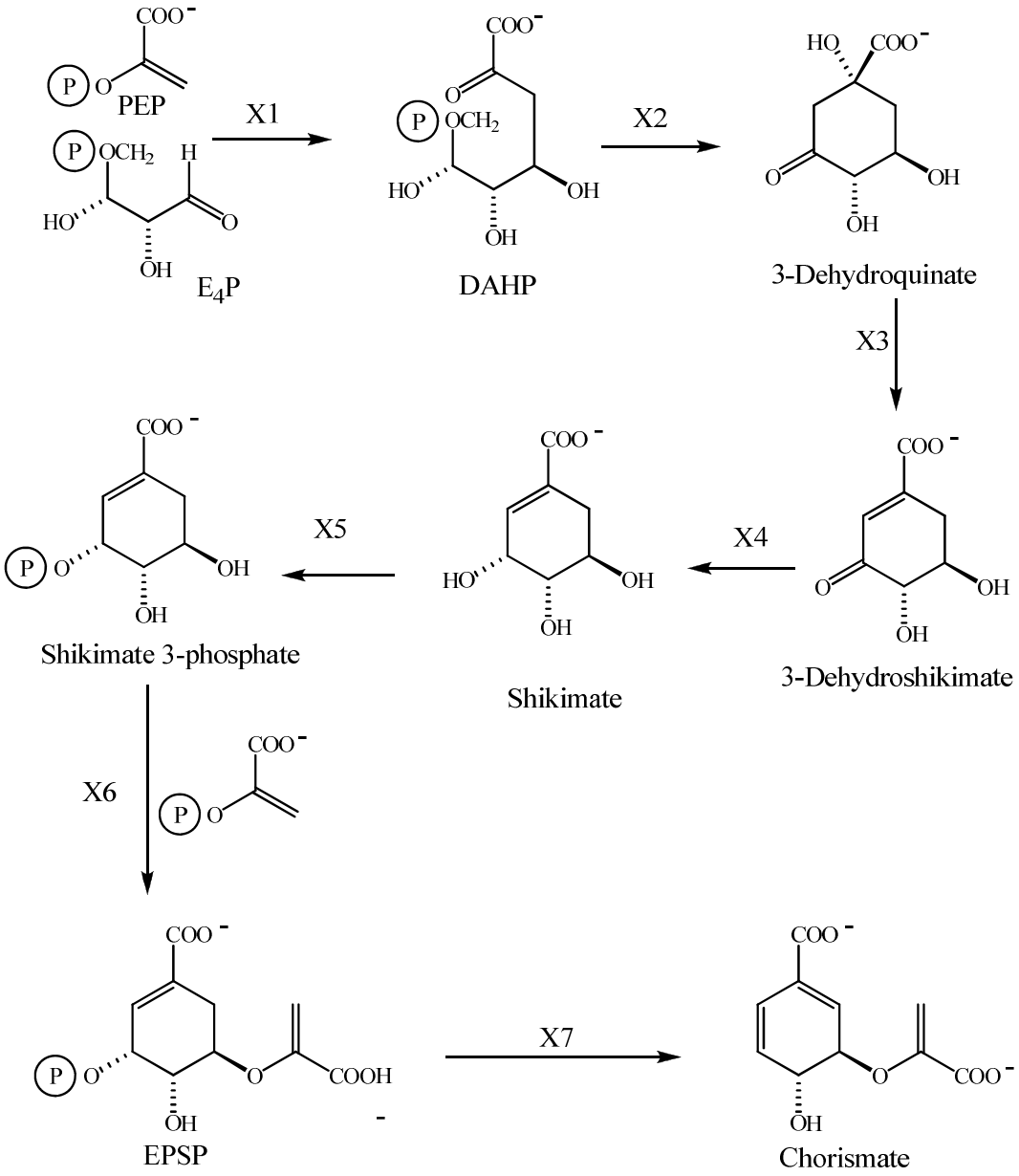

Scheme 2.1: Shikimate pathway to chorismate

X1 : 3-Deoxy-D-arabino-heptulosonate 7-phosphate synthase(DAHP syntase/synthetase
X2 : 3-Dehydroquinate synthetase
X3 : 3-Dehydroquinate hydro-lyase (DHQase)
X4 : Shikimate dehydrogenase (SHorase)
X5 : Shikimate kinase
X6 : 5-Enolpyruvylshikimate-3-phosphate synthase (EPS synthase)
X7 : Chorismate synthase

Chorismate, the product of the shikimate pathway is the key compound for the formation of coumarin via Claisen rearrangement, which leads the formation of

phenylalanine and tyrosine (Scheme 2.2). The committed step in the formation of coumarin is the *ortho*-hydroxylation of a trans-cinnamic acid, which is derived from phenylalanine by the action of phenylalanine ammonia-lyase (Scheme 2.3) [26-27].

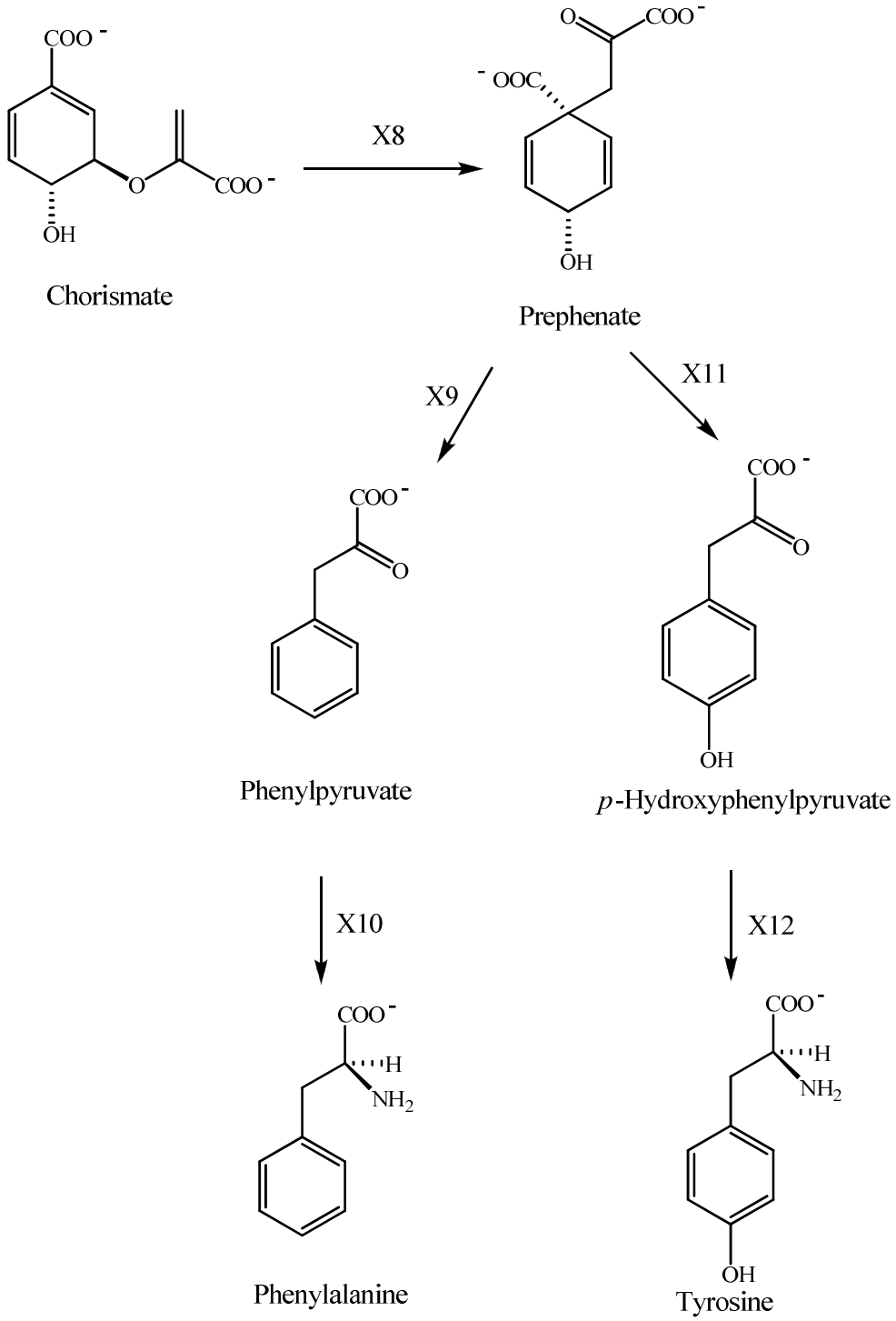

Scheme 2.2 : Pathways to phenylalanine and tyrosine

X8 : Chorismate mutase
X9 : Prephenate dehydratase
X10 : Phenylalanine aminotransferase
X11 : Prephenate dehydrogenase
X12 : Tyrosine aminotransferase

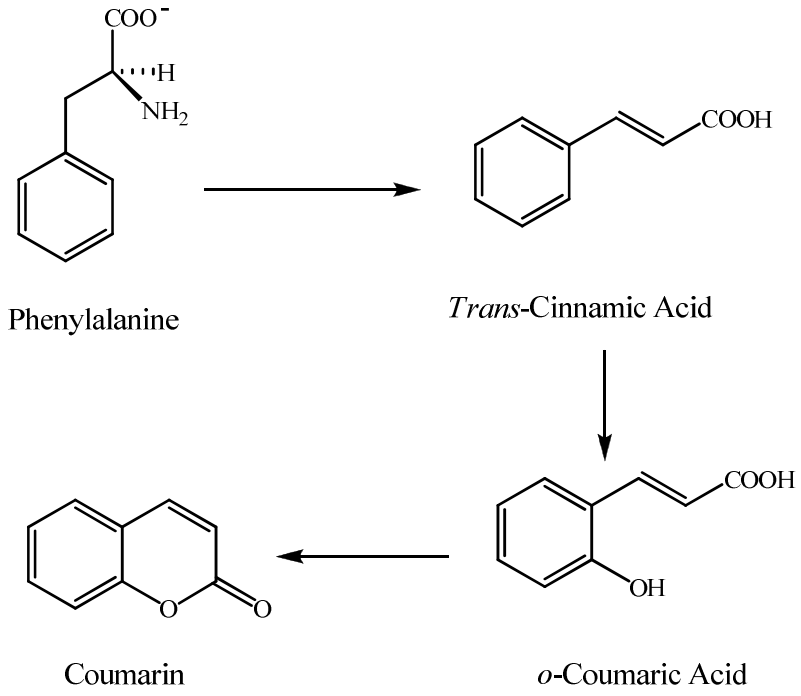

Scheme 2.3: Biosynthetic pathway from phenylalanine to coumarin

2.2 Terpenoids [28-29]

Terpenoids are naturally occurring hydrocarbons produced by plants, insects, and animals, thus, terpenoids are all based on the isoprene molecule (2-methylbutadiene) **19** and their carbon skeletons are built up from the union of two or more of these C_5 units ignoring the double bond. They are then classified according to whether they contain two (C_{10}), three (C_{15}), four (C_{20}), six (C_{30}), or eight (40) of such units. So according to the above rule, monoterpenoids are defined as compounds having carbon skeleton with two isoprene units, sesquiterpenes with three isoprene units, and so on (Table 2.2)

Table 2.2 : Common classification of terpenoid groups

Group	No. of carbons	Isoprene Units	Examples
Monoterpenoid	10	2	pinane **20**, menthol **21,** limonane **22**
Sesquiterpenoid	15	3	bisabolene **23,** arteannuic acid **24**
Diterpenoid	20	4	manool **25**, taxadiene **26**
Triterpenoid	30	6	taraxasterol **27,** squalene **28**
Tetraterpenoid	>30	8	capsanthin **29**

2-methylbutadiene **19**

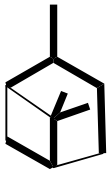

pinane **20**

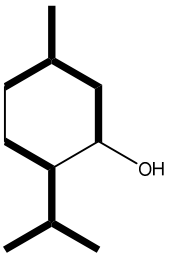

menthol **21**

limonane **22**

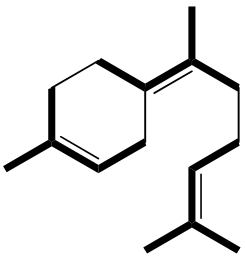

bisabolene **23**

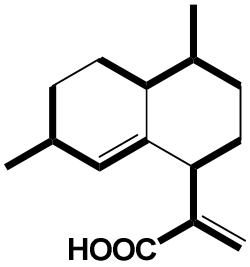

arteannuic acid **24**

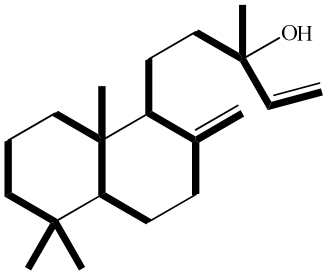

manool **25**

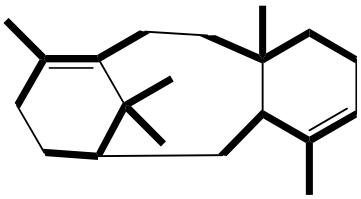

taxadiene **26**

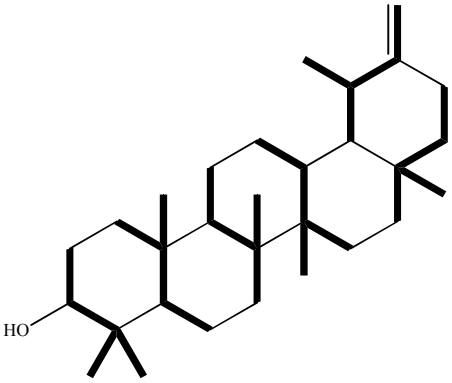

taraxasterol **27**

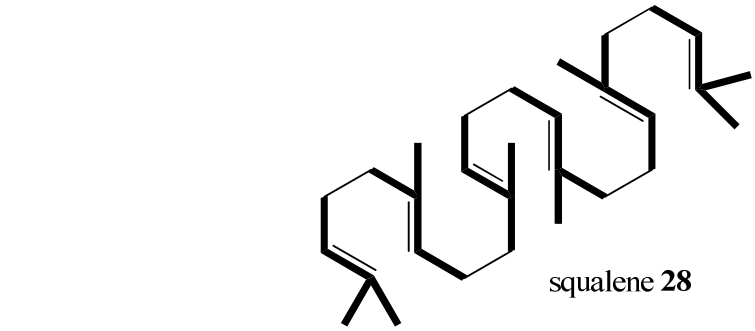

squalene **28**

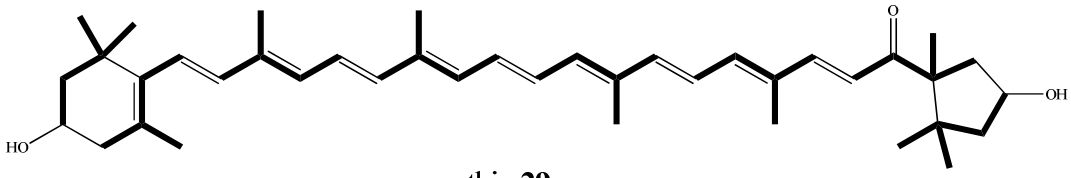

capsanthin **29**

2.2.1 Triterpenoids

Triterpenoids comprise a group of isoprenes typically containing 30 C-atoms that originate from six isoprene units. The triterpenoids form the largest group among the terpenoid classes, and are extensively allocated in the plant kingdom. Plants contain a huge variety of cyclic triterpenes that do not occur at all in animals and fungi. Structurally, triterpenoids are diversed group of natural products derived from squalene or related acyclic carbon precursor. Triterpenoids with well characterized biological activities include sterols, steroids and saponins. This large group of natural products displays well over 100 distinct skeletons. Most triterpenoids are 6-6-6-6 tetracycles, 6-6-6-6-5 pentacycles, or 6-6-6-6-6 pentacycles, but acyclic, monocyclic, bicyclic, tricyclic and hexacyclic triterpenoids have also been isolated from natural sources.

Triterpenes have high structural homogeneity and the major difference is in the type of configuration, depending on to the conformation originally adopted by the squalene epoxide. The cation resulting from the cyclization can subsequently undergo a series of 1, 2 proton methyl shifts, which can be used to rationalize the occurrence of different tetra- and pentacyclic skeleton characteristic of this group.

At first glance, it is easy to think that steroids are of triterpene type because of

the tetracyclic structure. However, steroids are different from terpenes due to the loss of at least 3 methyl groups at position 4 and 14. The losses of the methyl group are easily identifiable in the ^{1}H-NMR spectrum, thereby distinguishing steroids from triterpenes.

2.2.2 Tritepenoid Groups

Triterpenoid structures consist of various groups, squalene, lanostane, dammarane, lupane, ursane, and hopane are the most well known triterpenoid skeletons. Other types of skeleton can be found in plants and their structures were illustrated as in scheme 2.4. These skeletons exist as a result of cyclisation, rearrangement and degradation sequence of reaction. There are however several pathways known for the biosynthesis of triterpenoids, leading to different types of triterpenoid skeletons. Several skeletons have been found to undergo ring cleavage leading to seco skeletons, homologation (leading to homo and bis homo skeleton), degradations and minor rearrangement to related skeleton [30].

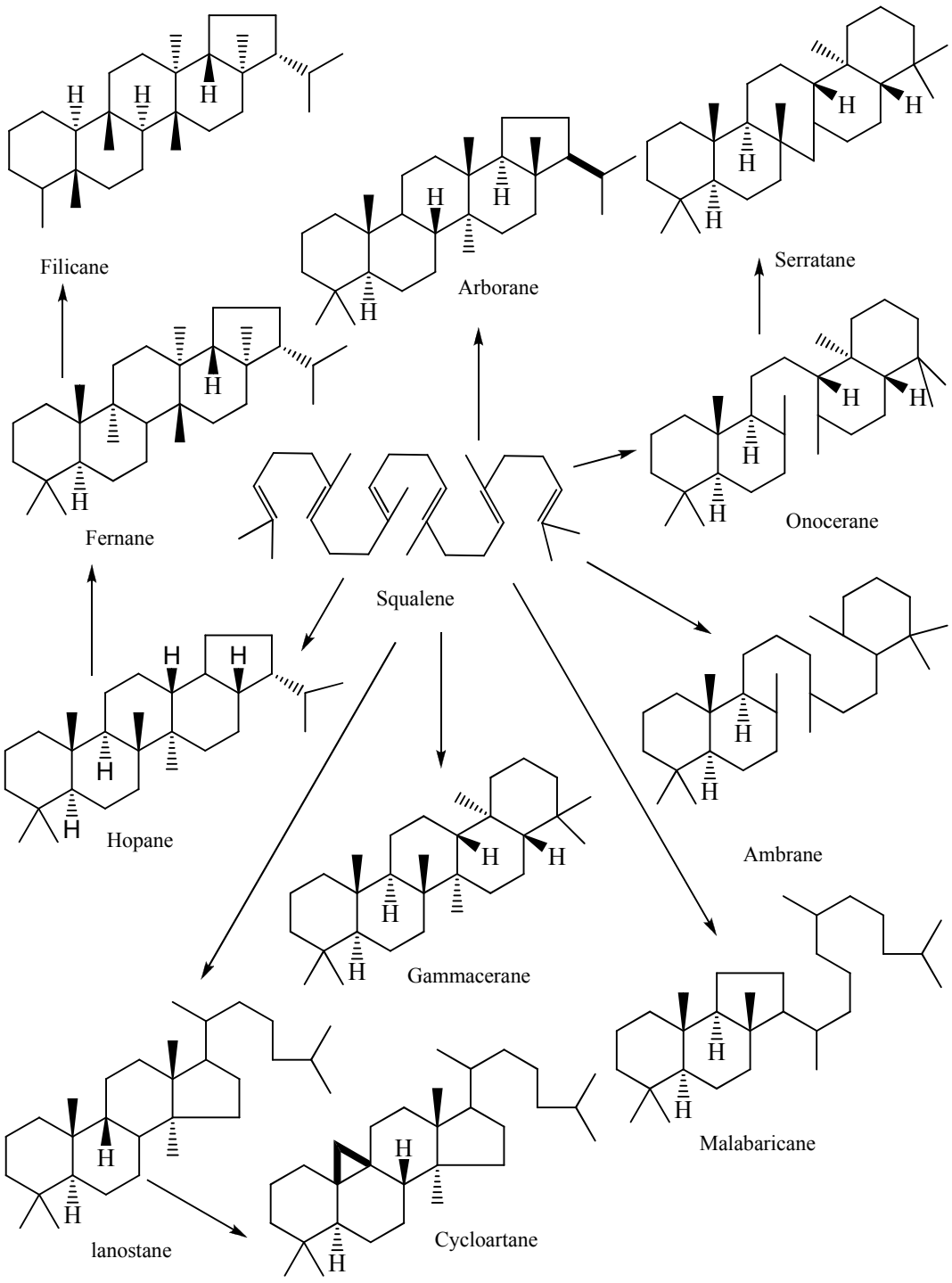
Filicane
Arborane
Serratane
Fernane
Squalene
Onocerane
Hopane
Ambrane
Gammacerane
lanostane
Cycloartane
Malabaricane

Continue

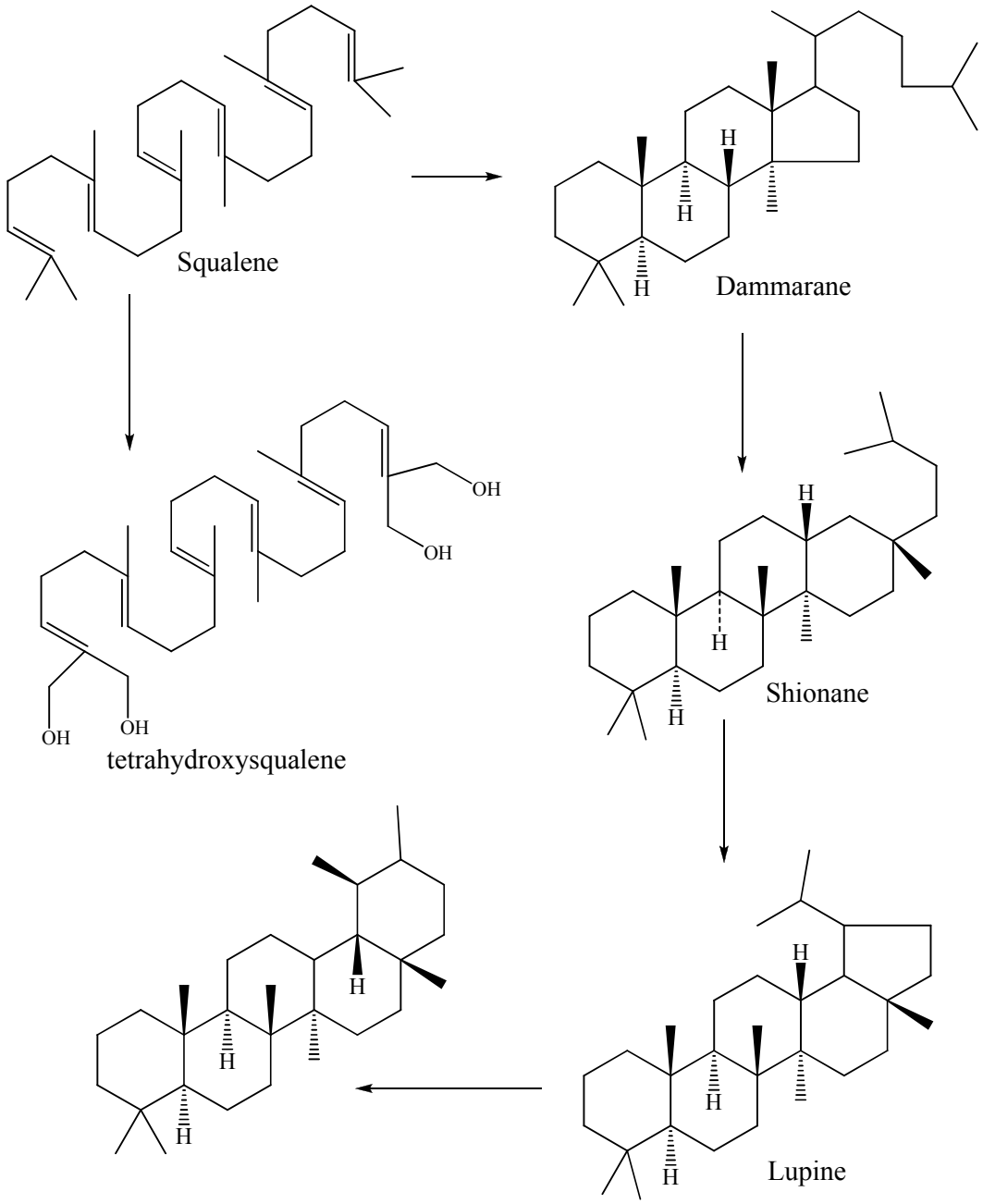

Scheme 2.4: Cyclization of squalene to various triterpene skeletons (pages 25 and 26)

2.3 Limonoids

Chemically, Meliaceous plants are characterized by the production of a class of modified triterpenoids named the tetranorterpenoids (limonoids). These are a group of plant secondary metabolites whose production is confined to the plants in the order, Rutales, in particular, the family Meliaceae, where they are diverse and abundant.

Although the chemical principles for the medicinal benefits of Meliaceous plants are still unclear, the presence of limonoids is believed to be responsible for their useful activity against insects [31].

Skeletally, the limonoids are presumed to be derived from the tetracyclic triterpenes, similar to tirucallol or euphol through series of oxidative changes interspersed with molecular rearrangements. A proposed scheme for the formation of a limonoid skeleton is shown in Scheme 2.5. The triterpene side chain is first oxidized eventually to a β-substituted furan ring, since compounds that have the 4,4,8-trimethylsteroid skeleton with an intact side but highly oxidized and often cyclised to form an ether ring are called the protolemonoids [31-34].

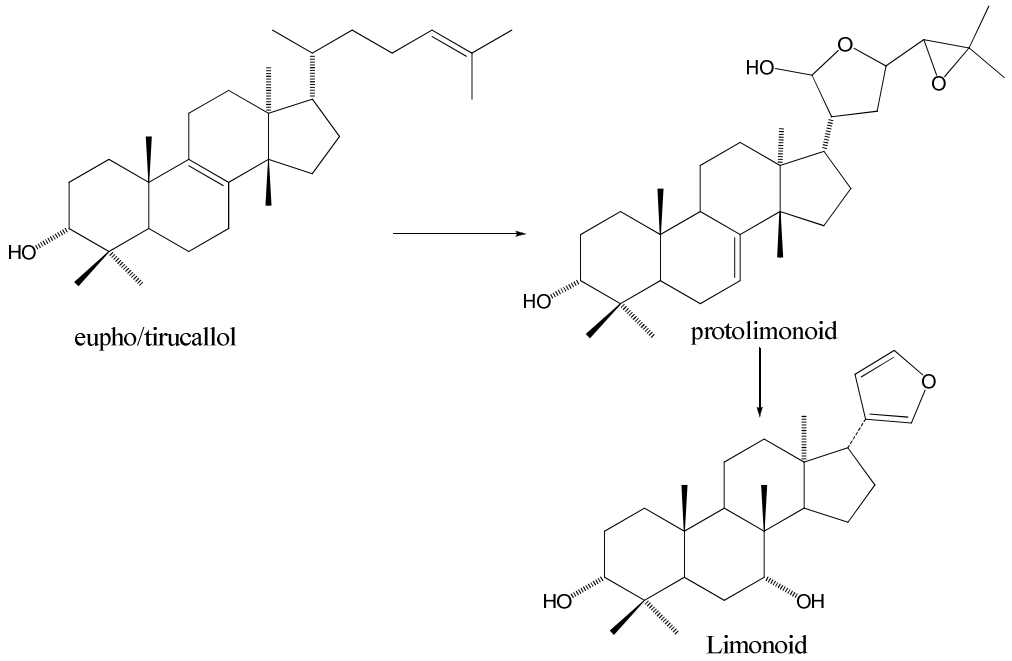

Scheme 2.5: Biogenetic pathways leading to the formation of simple limonoid with side chain oxidation

2.3.1 Classes and Biogenetic Routes of Limonoids in Meliaceae family

To date, there are twelve possible groups were found for construction of the limonoid skeleton, the classification was based on a number of oxidations and structural reconstruction that may occur on the tetra-cyclic nucleus to form a variety of structures [34-35].

2.3.1.1 Group I Protolimonoids and Related Triterpenoids

The side chain of these triterpenoids is intact, but generally extensively oxidized and cyclized to form ether ring.

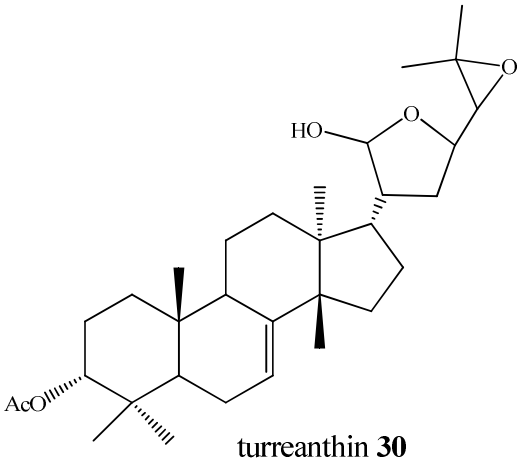

turreanthin **30**

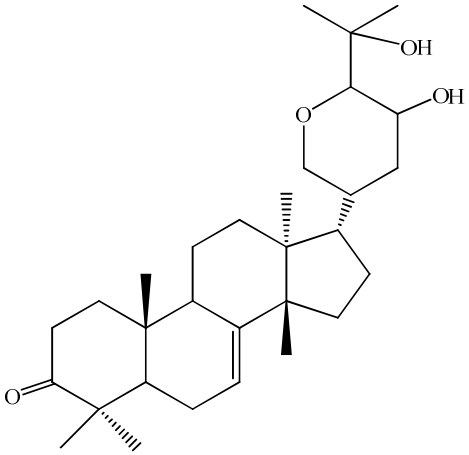

bourjotinolone A **31**

2.3.1.2 Group II Havanesin Group

This group consists of a furan side chain in the compounds and no changes in all remaining rings of skeleton.

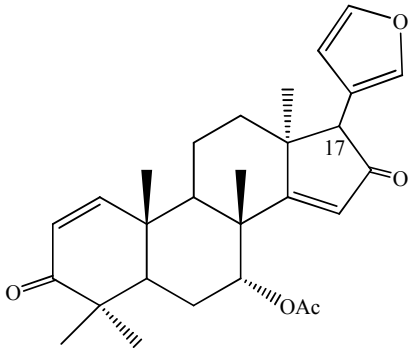

azadiradione **32**

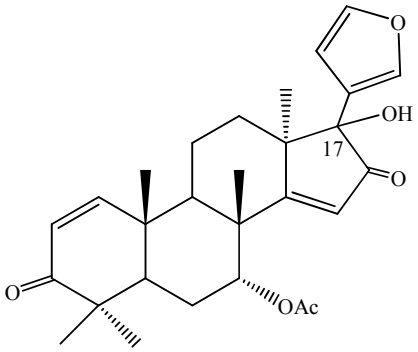

17β-hydroxyazadiradione **33**

2.3.1.3 Group III Gedunin Group (Ring D opened)

The first limonoid of this group has been discovered in Meliaceae family.

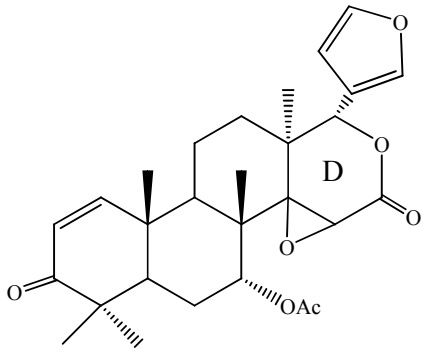

gedunin **34**

In gedunin, the biosynthesis of lactone ring D appears to be obvious, first stage is the allylic oxidation of the double bond to a 16-ketone, followed by the constitution of lactone ring as in the following scheme 2.6

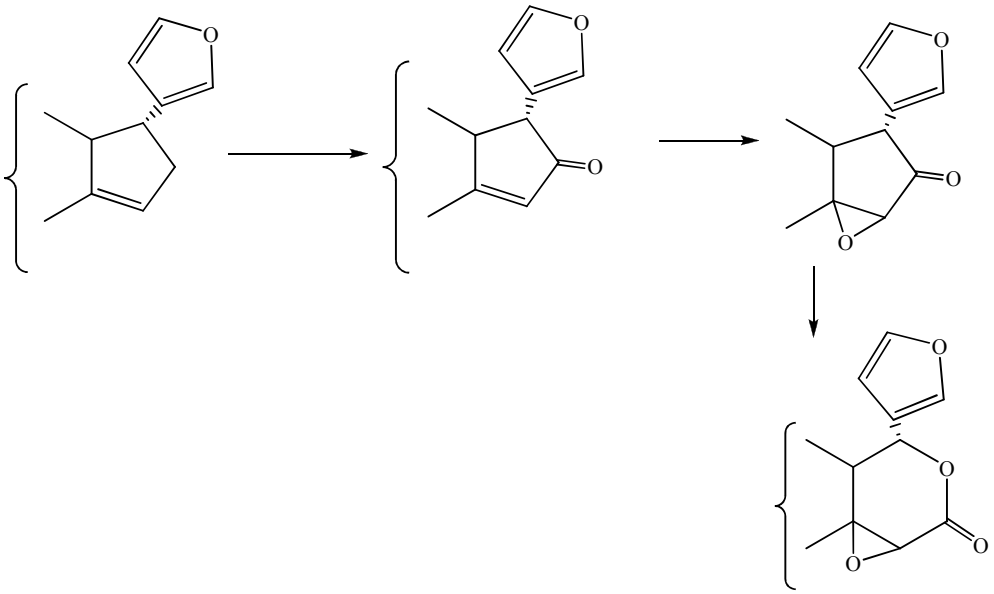

Scheme 2.6: Partial synthesis of gedunin

2.3.1.4 Group IVa Limonoids with Rings B and D opened

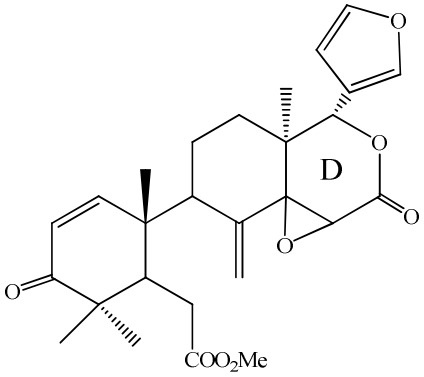

andirobin **35**

In compounds of this group, the B ring of 7-keto compounds is opened to a lactone or ester without the formation of any subsequent carbon ring see scheme 2.7

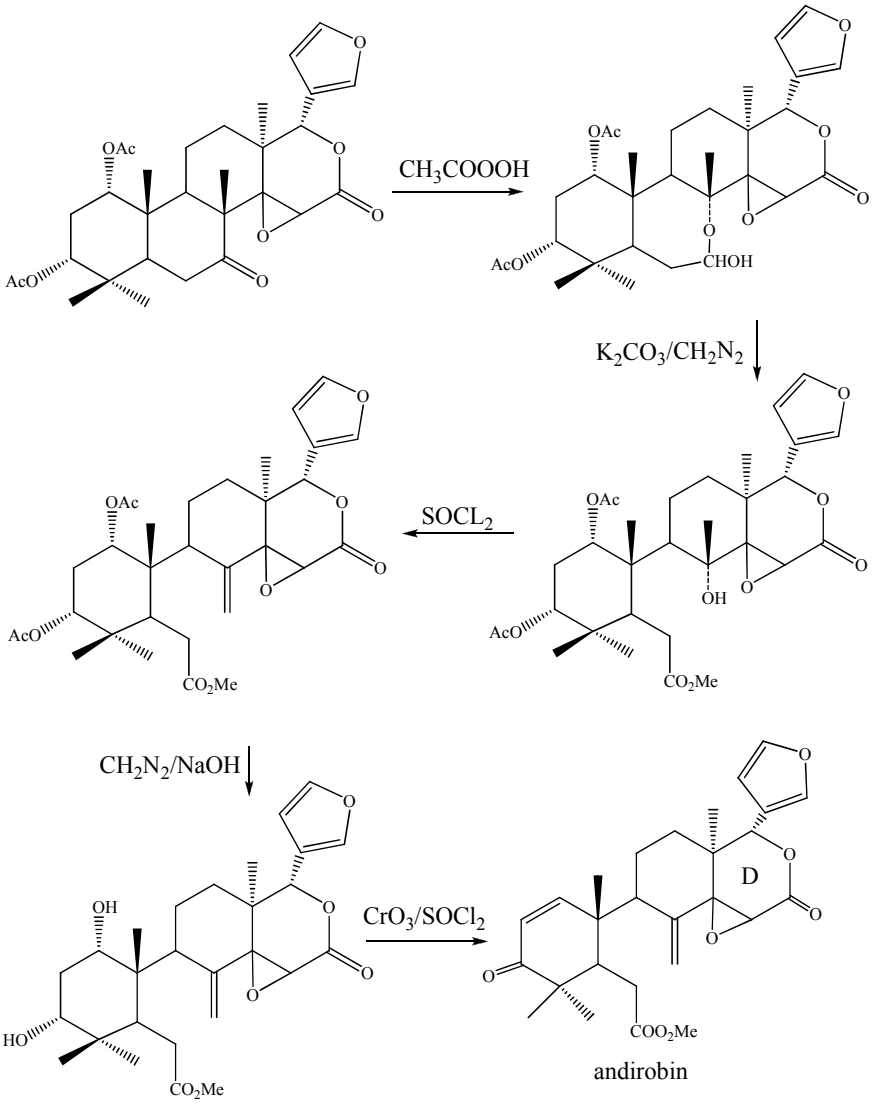

Scheme 2.7 : Partial synthesis of andirobin

2.3.1.5 Group IVb Mexiconolide Group

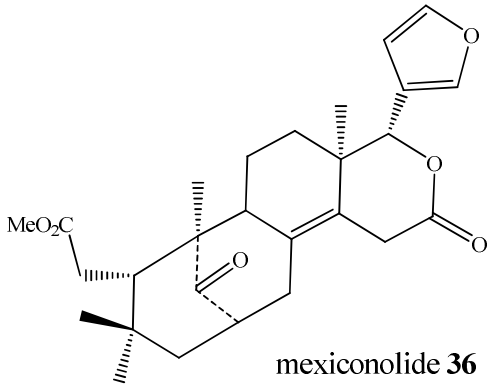

mexiconolide **36**

Mexiconolide compounds are derived from 1,3-diketodiene lactones of the andirobin group by sponataneous Michael cyclisation producing mexiconolide in the simplest case as shown in scheme 2.8

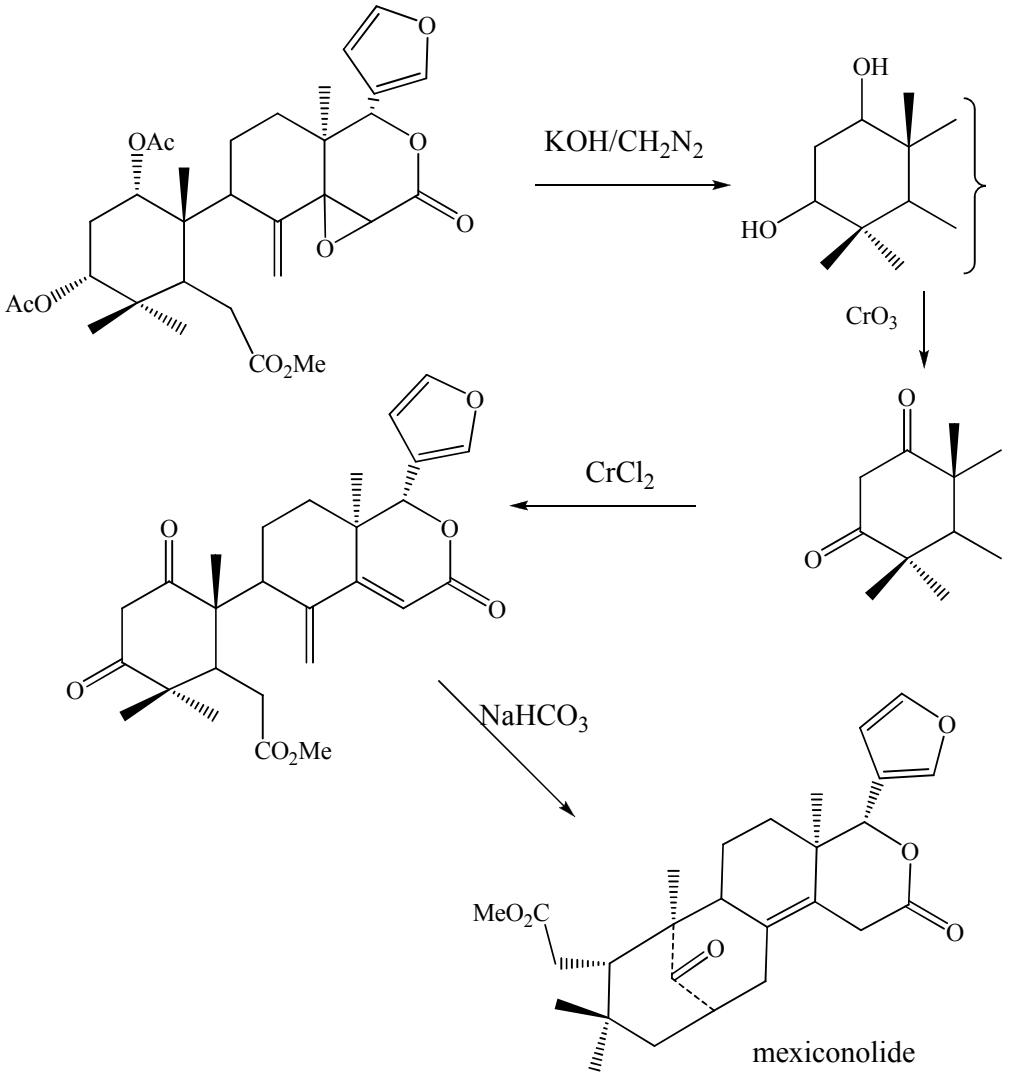

Scheme 2.8: Partial synthesis of mexiconolide

2.3.1.6 Group IVc Phragmalin Group

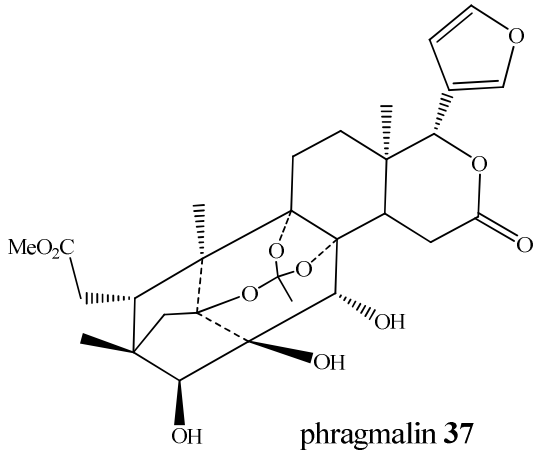

phragmalin **37**

In this group, one of the first limonoids to be isolated from Meliaceae was enthandrophragmalin **38,** it is the longest known member but the structure was obscure for long period of time until it was analyzed to be enthandrophragmalin **38** by X-ray crystallography of utilin **39**.

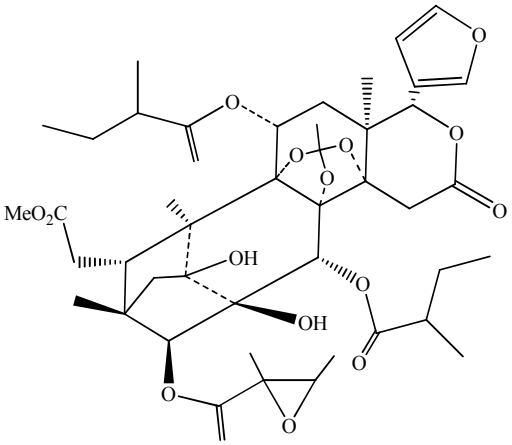

enthandrophragmalin **38**

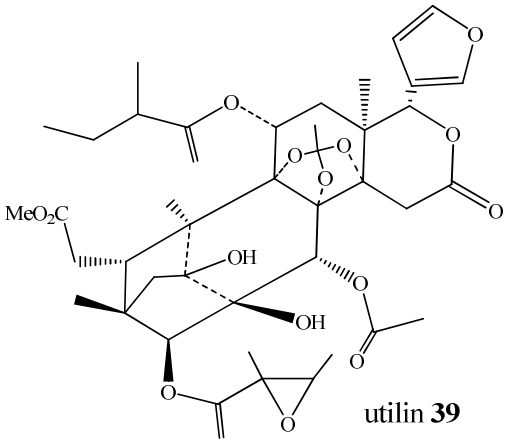

utilin **39**

It is interesting to ask how phragmalin is formed in the plant. Usually the C-29 methyl group is oxidized, but since the C-1 ketone is also reduced, the transformation from mexiconolid is actually an isomerization. It has been suggested that the precursor is a ketal of the xylocarpus type, which yields oxygen radical that finally oxidizes C-9. Since C-8 oxidation is necessary to produce the original ketal, scheme 2.9 explains why phragmalin derivatives are always oxidized at C-8 and C-9

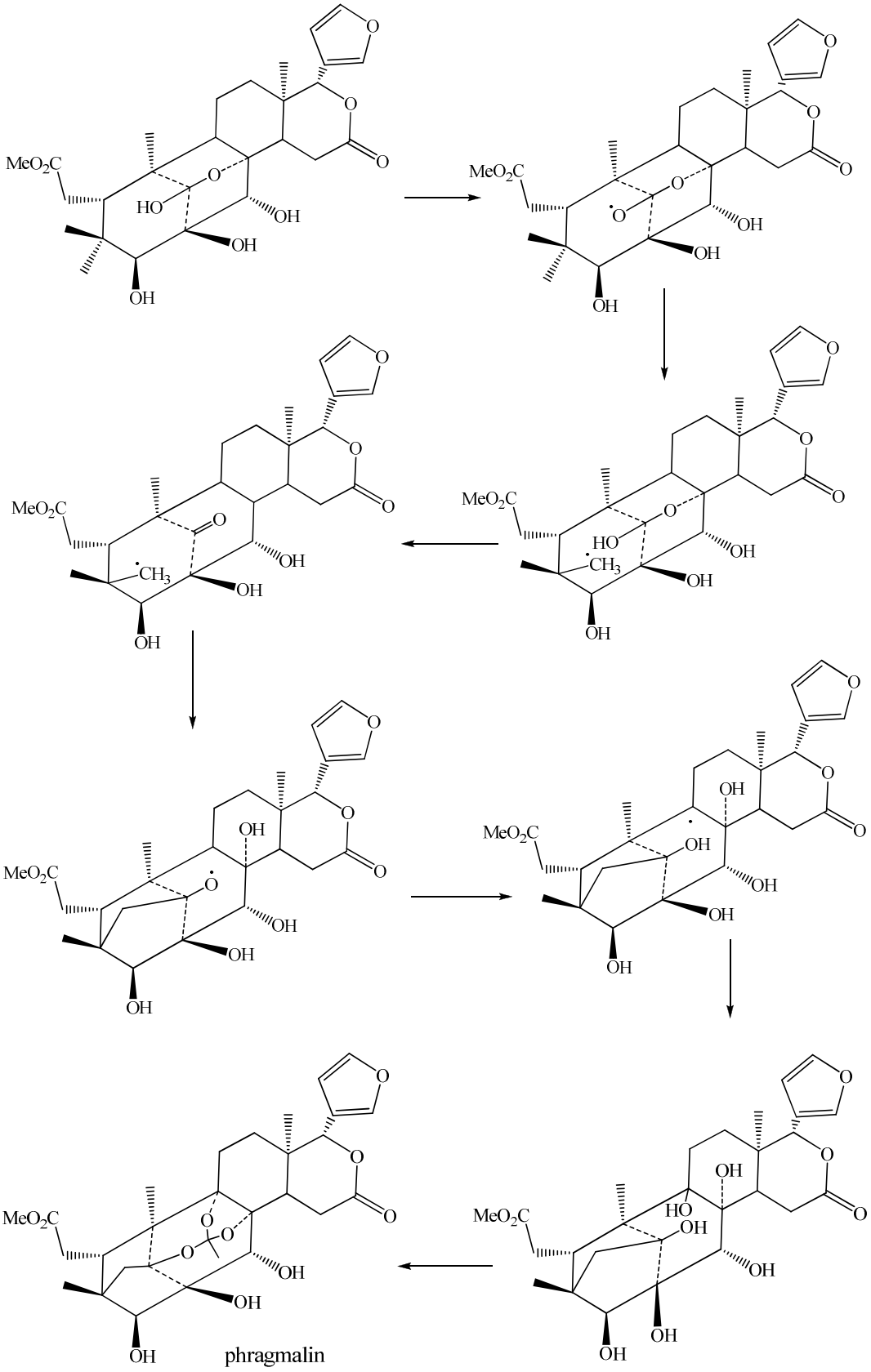

Scheme 2.9: Hypothetical biosynthesis of phragmalin

2.3.1.7 Group V Methyl Ivorensate Group (Rings A, B, D Opened)

This still is a very small group. The original member, methyl ivorensate **40** is found in small amount in *khaya ivorensis* and was synthesized by oxidation of methyl angolensate with perbenzoic acid.

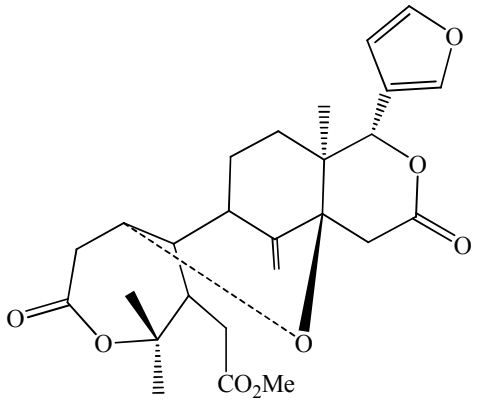

methyl ivorensate **40**

2.3.1.8 Group VI Obacunol Group (Rings A and D Opened)

This group is characteristic of the Rutaceae and rare in Meliaceae. Obacunol **41** occurs in *Lovoa trichiliodes* and in *Carapa procera*. The stereochemistry of the 6-substituent in this compound is very unusual, but seems to be correct.

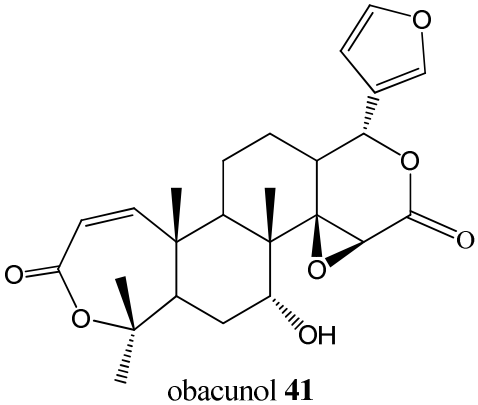

obacunol **41**

2.3.1.9 Group VII Nimbin Group (Rings C Opened)

This is large and important group containing some very complex compounds, there are no very simple members of the group, and the commonest feature in addition to the ring C opening is formation of tetrahydrofuran ring between C-28 and C-6. Given that the biosynthesis depends on the oxidative opening of ring C; similar to ring opening in other limonoids, the simplest derivative is the long known salannin **43** in which ring C is opened to a methyl ester.

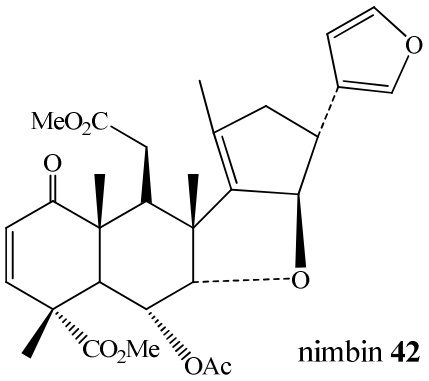

nimbin **42**

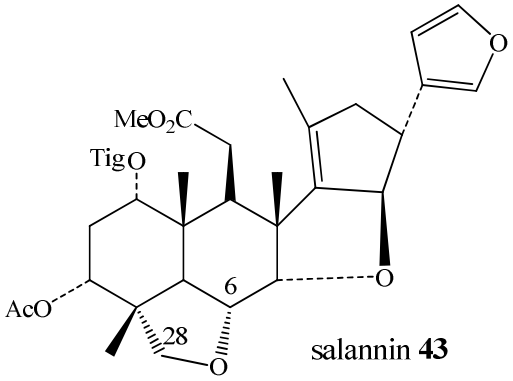

salannin **43**

The biosynthesis of nimbin **42** derivatives scheme 2.10, the intermediate will be a 12*β*-hydroxy-14, 15*β*-oxide which will be open to give a 12-aldehydo $\Delta^{13,14}$-15*β*-ol.

In heudebolin, which represents a common type in this group, the C-12-aldehyde has cyclized in a hemi-acetal with the 15-hydroxyl group. Related to this again is ohchinolide in which the hemiacetal has been replaced by a lactone.

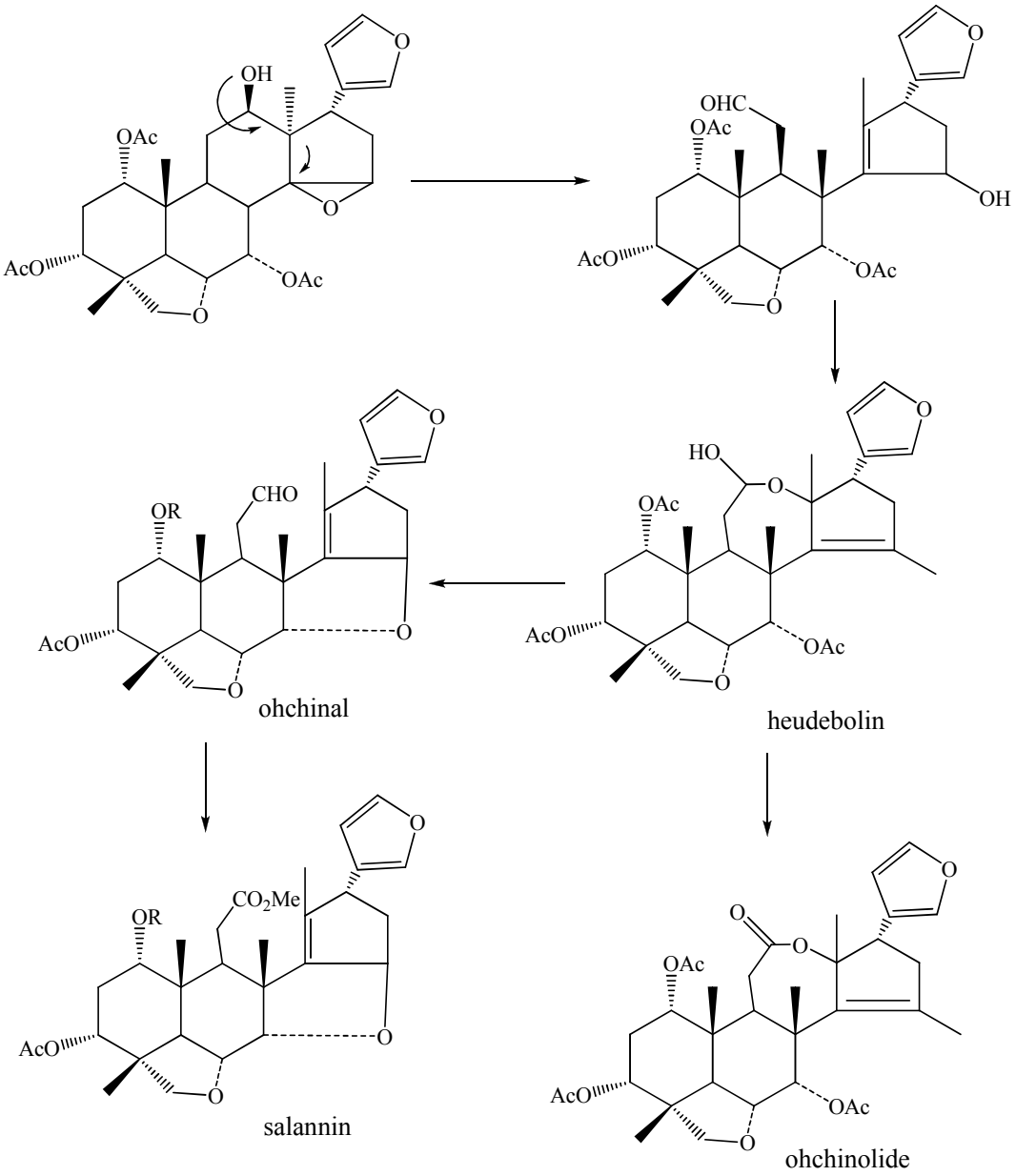

Scheme 2. 10 : Biosynthesis of nimbin derivatives

2.3.1.10 Group VIII Toonafolin Group (Rings B Opened)

Toonafolin is the ring B lactone corresponding to cedrelone with the addition of a 1,11α-ether bridge. Toonacilin has the lactone opened and has in addition an 11α, 12α,- diacetoxy system.

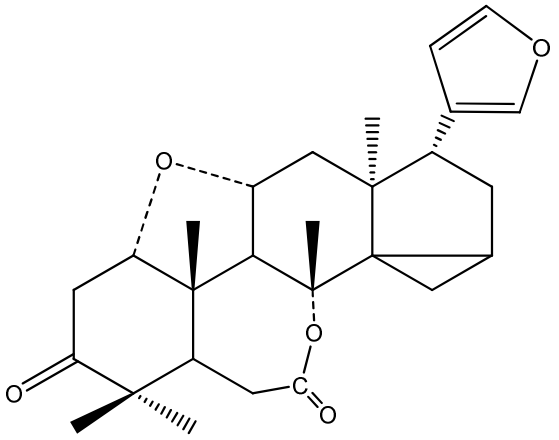

toonafolin **44**

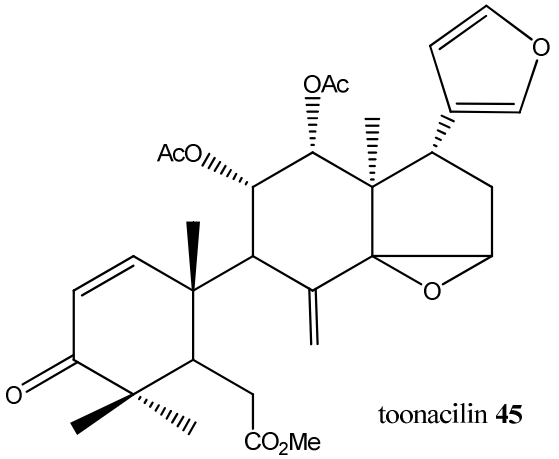

toonacilin **45**

2.3.1.11 Group IX Evodulone Group (Rings A Opened)

This group has been suspected to be precusrsors of the prieurianin group of limonoids.

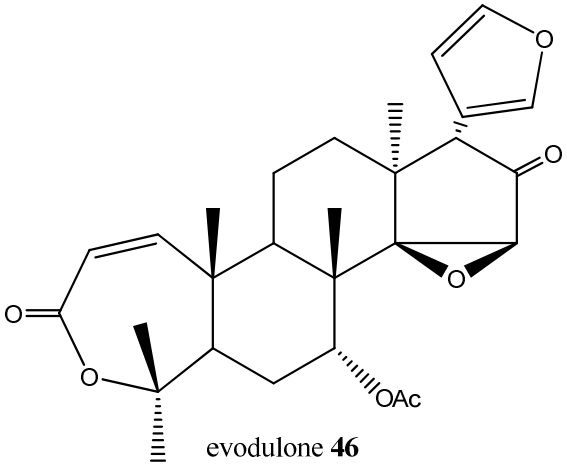

evodulone **46**

2.3.1.12 Group X Prieurianin Group (Rings A and B Opened)

Prieurianin **47** and dregeanin **48** were the first two members of this group.

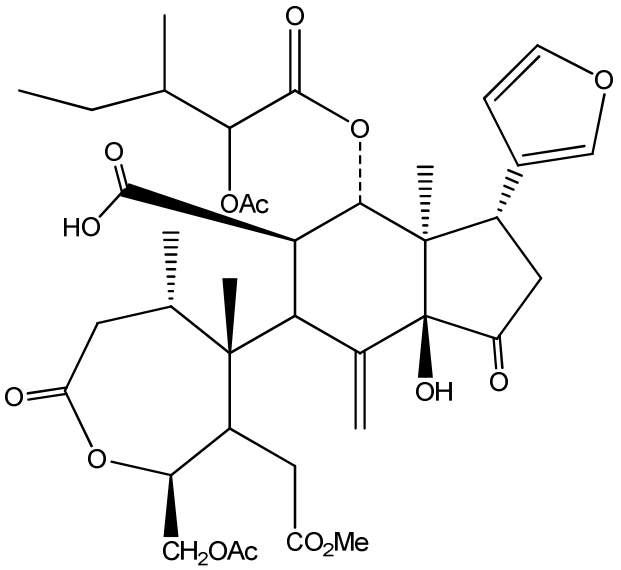

prieurianin **47**

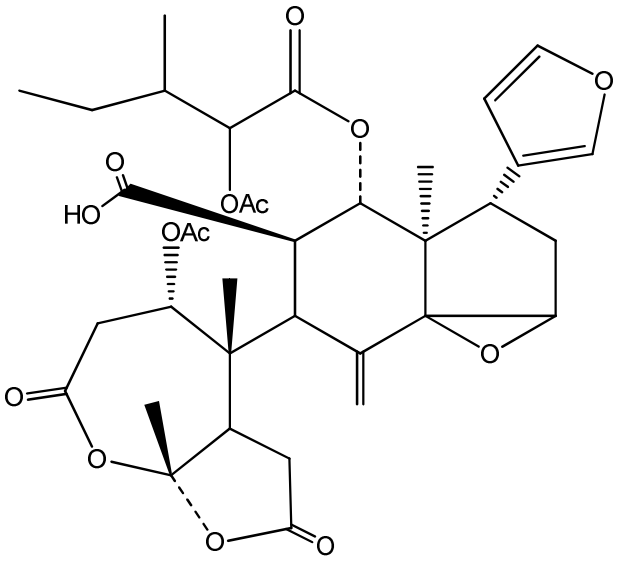

dregeanin **48**

All major classes of limonoids and their biosynthetic routes in the Meliaceae family has been summarized in the following scheme 2.11.

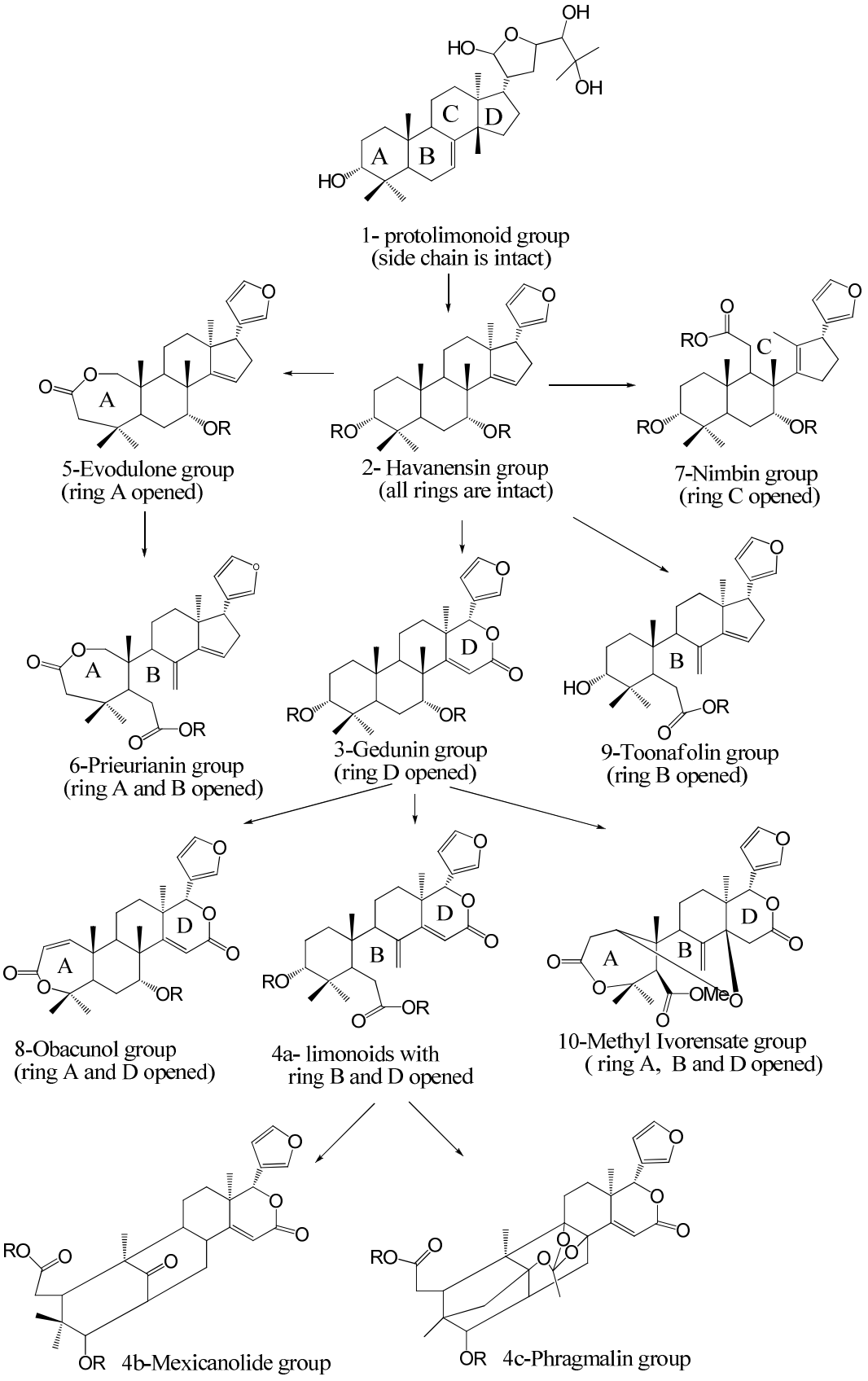

Scheme 2. 11: Major classes of limonoids and their biosynthetic routes in the Meliaceae family

2.4 Chemical Constituents of *Chisocheton* Species

Compared with some of the well-studied genera in the Meliaceae family, such as *Azadirachta* and *aglaia* species, very little research has been done on the *Chisocheton* species. Earlier phytochemical studies on the bark extracts of *Chisocheton ceramicus* had identified four new limonoids [36-37], while no investigation has been found on *Chisocheton tomentosus.* See Table 2.3.

Table 2.3 : Occurrence of some selected chemicals in species of *Chisocheton*

No.	*Chisocheton* pecies	Type of compounds	example	Ref.
1	*Chisocheton Ceramicus*	limonoid	ceramicine A **49**	[36-37]
2	*Chisocheton erythrocarpus*	limonoid	erythrocarpine A **50**	[38]
3	*Chisocheton siamensis*	limonoid	dysobinin **51**	[39]
4	*Chisocheton macrophyllus*	triterpenoid	moronic acid **52**	[40]
5	*Chisocheton microcarpus*	protolimonoid	Carda-1,14-dienolide, 7-(acetyloxy)-4,4,8-trimethyl-3-oxo-, (5*α*,7*α*,13*α*,17*α*,20S)-20,21,22,23-tetrahydro-23-oxoazadirone **53**	[41]
6	*Chisocheton paniculatus*	limonoid	chisonimbolinin A **CC4**	[42-51]
7	*Chisocheton penduliflorus*	Sesquiterpenoid,	allo-aromadendrane-10*α*,14-diol **55**	[52-53]
		triterpenoid	dammaradienone **56**	
		coumarin,	scoparone **57**	
		phenolic com.	vanilinic acid **58**	
8	*Chisocheton weinlandii*	alkaloid	chisitine **59**	[54]

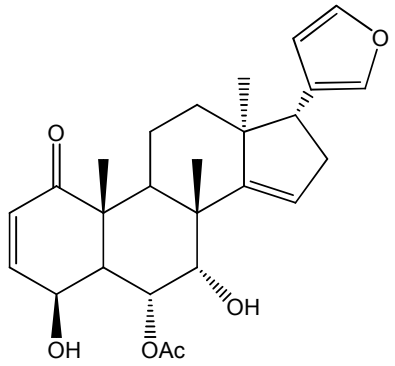

ceramicine A **49**

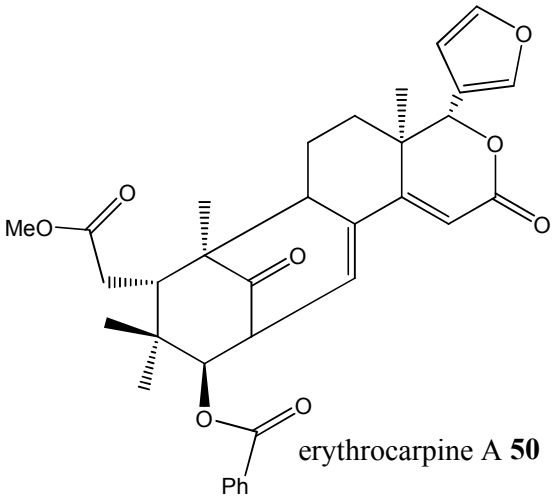

erythrocarpine A **50**

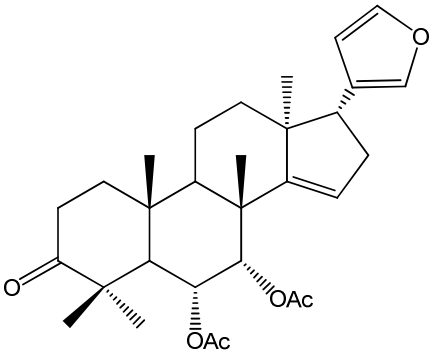

dysobinin **51**

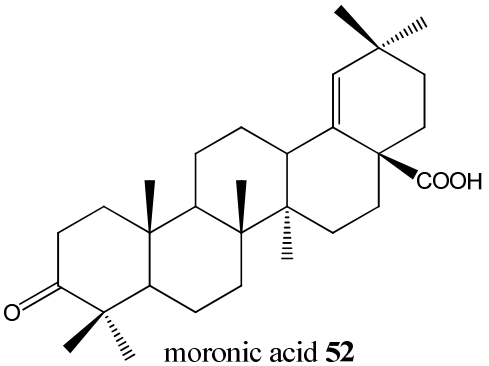

moronic acid **52**

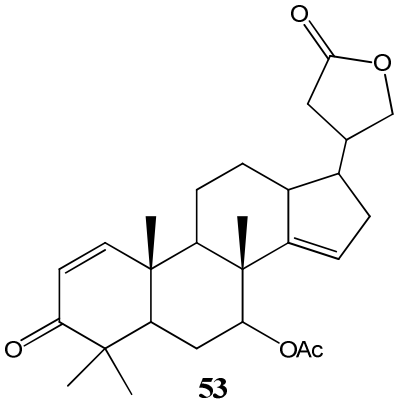

53

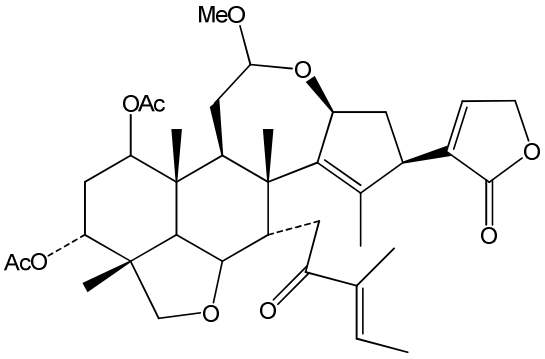

chisonimbolinin A **54**

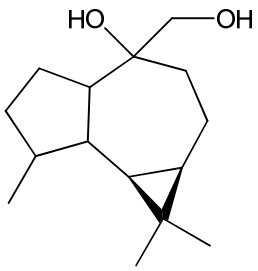

allo-aromadendrane-10,14-diol **55**

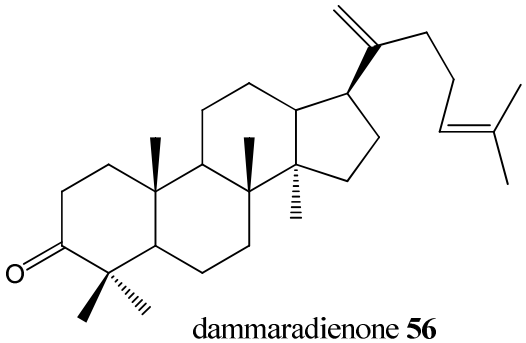

dammaradienone **56**

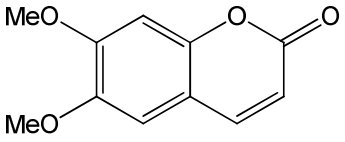

scoparone **57**

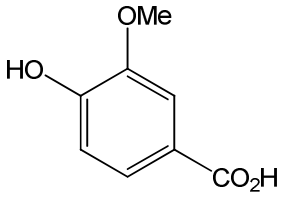

vanilinic acid **58**

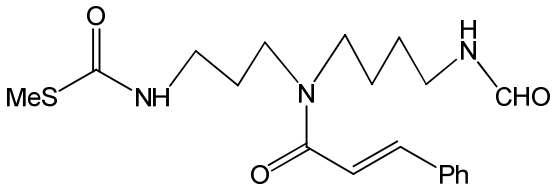

chisitine 1 **59**

2.5 Chemical Constituents of Dysoxylum Species

From our literature review we have listed in Table 2.4 some selected chemicals of *Dysoxylum* species, here again no investigation has been found on *Dysoxylum macrocarpum.*

Table 2.4 : Occurrence of some selected chemicals in species of *Dysoxylum*

No.	***Dysoxylum* pecies**	**Type of Compounds**	**Examples**	**Ref.**
1	*Dysoxylum acutangulum*	triterpenoids	acutaxyline A **60**	[55]
2	*Dysoxylum binectariferum*	chromane alkaloids	rohitukine **61**	[56-61]
3	*Dysoxylum cauliflorum*	triterpenoid	**62**	[62]
4	*Dysoxylum densiflorum*	degraded limonoids	dysodensiol A **63**	[63-64]
		sesquiterpenoids	dysodensiol D **64**	
5	*Dysoxylum hainanense*	limonoid acids	dysoxylumic acid A **65**	[65-74]
		diterpenoid	**66**	
		triterpenoid	**67**	
6	*Dysoxylum gillespie*	biflavonoid	**68**	[75]
7	*Dysoxylum kuskusense*	diterpenoids	dysokusone A **69**	[76-79]
8	*Dysoxylum macranthum*	triterpenoids	dymacrin B **70**	[80]
9	*Dysoxylum malabaricum*	steroids	**71**	[81-85]
10	*Dysoxylum muellerii*	protolimonoid	cabraleone **72**	[86-87]
11.	*Dysoxylum richii*	sulfuric comp.	dysoxysulfone **73**	[88-92]
		limonoids	dysoxylin **74**	
		triterpenoids	richenone **75**	
12.	*Dysoxylum schiffneri*	sesquiterpenoids	schiffnerone **76**	[93]
13	*Dysoxylum spectabile*	limonoids	methyl ivorensate **77**	[94-95]
		lriterpenoids	isopimara-8(14),15-diene **78**	

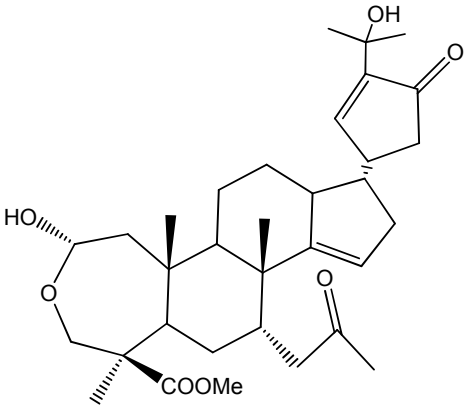

acutaxyline A **60**

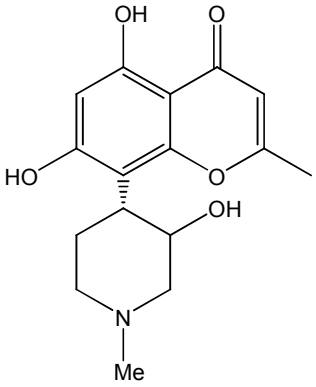

rohitukine **61**

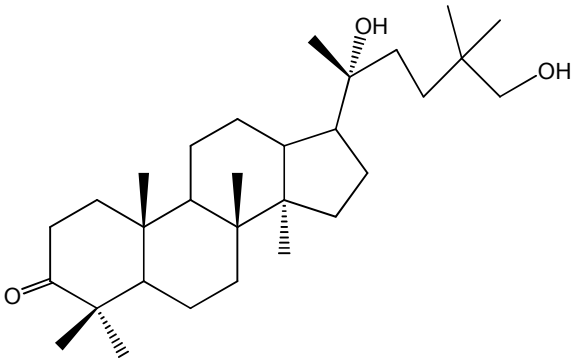

(20R)-23(24→25)abeo-20,24
-dihydroxydammaran-3-one **62**

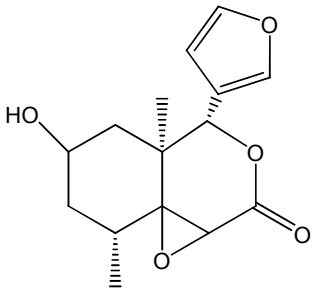

dysodensiol A **63**

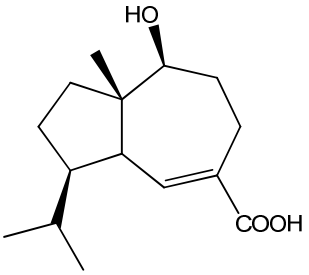

dysodensiol D **64**

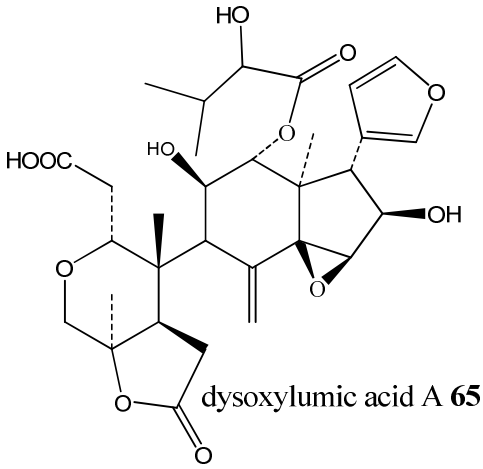

dysoxylumic acid A **65**

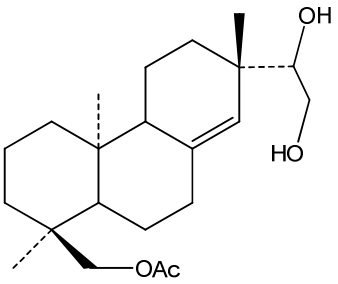

ent-18-acetoxy-8-(14)-pimarene-15S,16-diol **66**

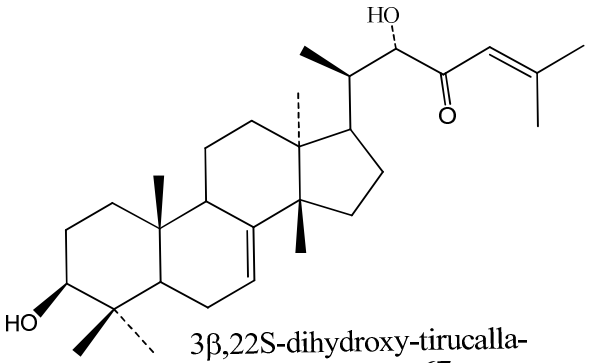

3β,22S-dihydroxy-tirucalla-7,24-dien-23-one **67**

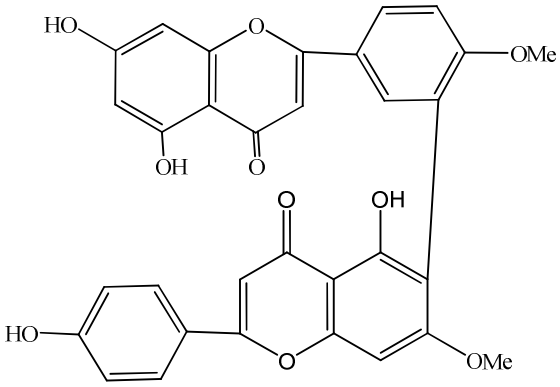

rubustaflavone 4′,7″-dimethyl ether **68**

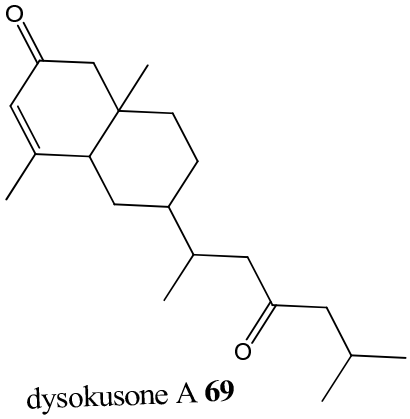

dysokusone A **69**

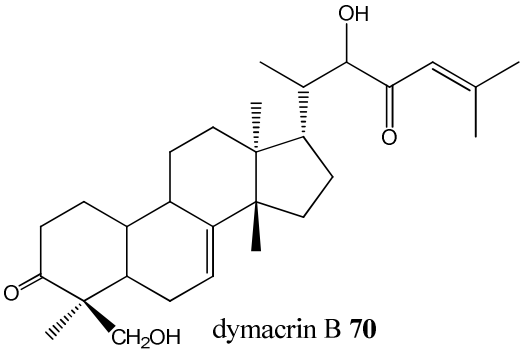

dymacrin B **70**

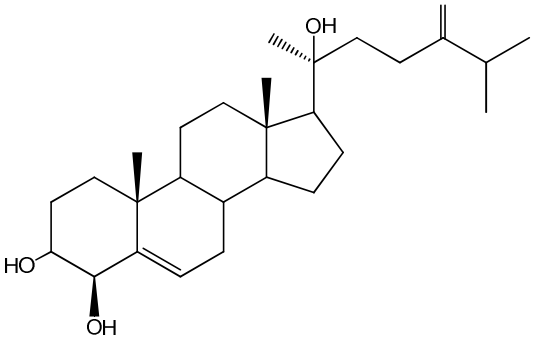

ergosta-5,24(24′)-diene-3β,4β,20*S*-triol**71**

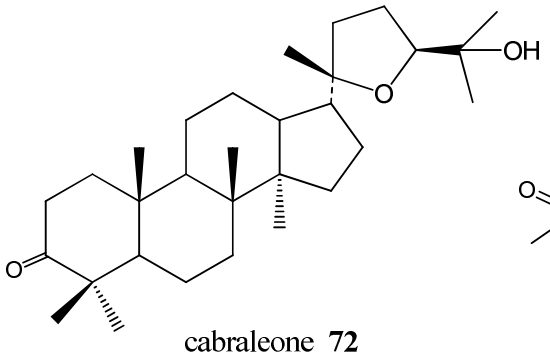

cabraleone **72**

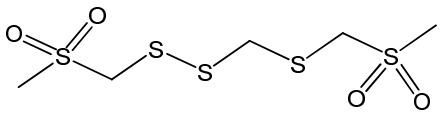

dysoxysulfone **73**

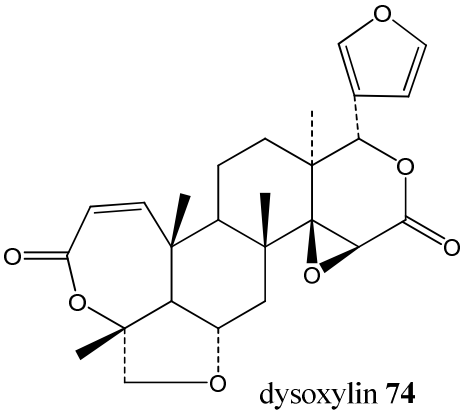

dysoxylin **74**

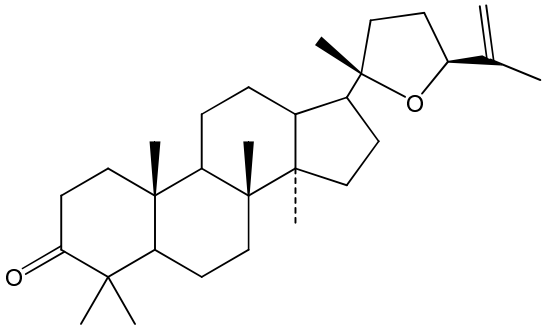

richenone **75**

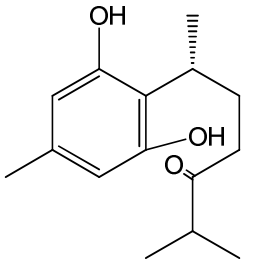

schiffnerone A**76**

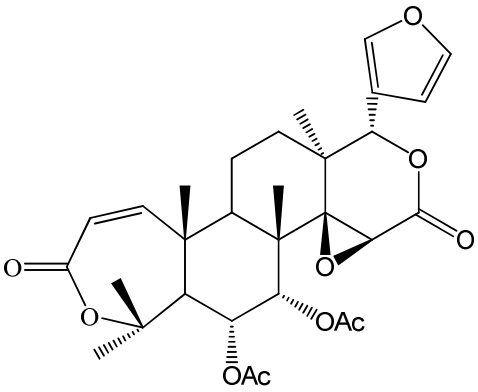

methyl ivorensate **77**

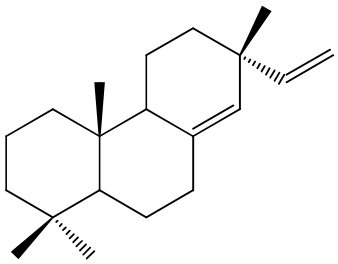

Isopimara-8(14),15-diene **78**

2.6 Biological Activities of Meliaceous Plants

Early, humankind recognized their dependence on nature in both health and illness, the use of traditional medicine and medicinal plants in most developing countries has been widely observed. In general, herbal drugs are constituting a substantial proportion of global drug market [96], Numerous investigations have demonstrated that certain tropical plants such as Meliaceous plants produce phytochemicals with potent medicinal and pesticidal properties.

Plants from Meliaceae are largely used for the treatment of ailment in traditional medicine in tropical countries [97], including the fever of malaria [98], malaria ranks as the single most important condition treated with herbal remedies. Due to either limited availability or affordability of pharmaceutical medicines in many tropical countries, about 80% of the rural population in Africa depends on traditional herbal remedies [99]. Limonoids such as anthotechol **79** derived from *Khaya anthotheca* showed potent antimalarial activity against malaria parasites [100] as well as limonoid disobinin **51** has been isolated as a major component from the seeds of *Chisocheton siamensis*, this compound was effective against malaria parasite. [39]

Some of Meliaceous limonoids, predominantly those with a 14,15-epoxy D ring and a 19/28 lactol bridge high activity against the murine P388 leukemia cell lines [101]. Further studies in 2008 (Mohamad et. al.) and in 2007 (Awang et. al.) showed that the limonoids ceramicine A, walsogyne A and erythrocarpines A–E have cytotoxicity against the same leukemia cells [36, 38]

Beside cancer associated activities, other medicinal properties of meliaceaous plants have been recognized as antifungal [102], antibacterial agents [39], antiviral [103] anti-inflammatory [104] agents, Antiplasmodial [37], and anti-oxidant [105-106] as well as some other beneficial health effects, such as blood sugar lowering properties, anti-parasitic, anti-ulcer and hepatoprotective effects [107].

2.6.1 Insecticidal Activities of Meliaceous Plants

As mentioned above, more recently this family has also proven to be a profitable source in the research of botanical insecticides; limonoids and the related triterpenoids are believed to be responsible for all activities observed. The neem tree, *Azadirachta indica*, is the most intensively studied species of the family [108], more than 300 natural products have been isolated and characterized from this tree, Among these compounds, limonoids form the major group and most of them showed measurable bioactivity against insects, at least as antifeedants. [109]. In addition to azadirachtin **80** and its derivatives, a large number of other limonoids from neem and other Meliaceous plants have been isolated, and their biological activities toward insects have been tested [32, 110-111].

It is worth mentioning that these types of limonoids with the side chain intact, the apo-euphol type, with a 14,15-epoxide and either a 19/28 lactol bridge or a cyclohexenone (3-oxo-l-ene) A ring are highly toxic toward insects, [101, 109] and, unfortunately, are also toxic towards mammals [112]. So far, no clear conclusions can be drawn regarding limonoid evolution and their bioactivities against insects, and more research is needed to study further the interactions between limonoids and insect herbivory.

Along with limonoids, some steroidal compounds, such as 3-hydroxy-pregnane-2,16-dione **81** and 2-hydroxy-androsta-1,4-diene-3,16-dione **82**, have been isolated from the insecticidal fractions from Meliaceous plants [113]. A series of potent benzofurans, including the known anti-leukemic agent, rocaglamide **83**, have been isolated from extract of Aglaia odorata [114], rocaglamide has been shown to be as active as azadirachtin as an antifeedant and insect growth reducing agent [115].

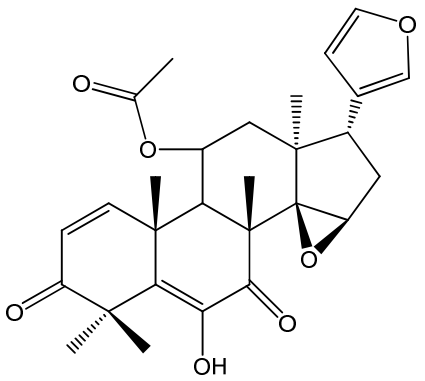

anthotechol
79

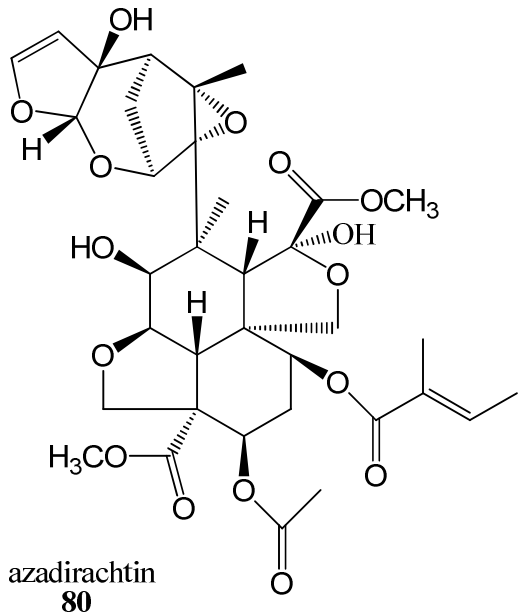

azadirachtin
80

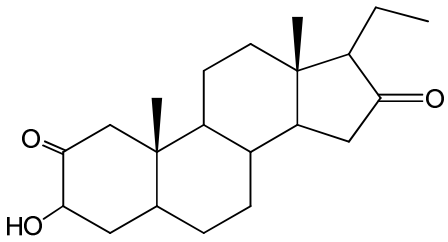

3-hydroxypregnane-2-16-dione
81

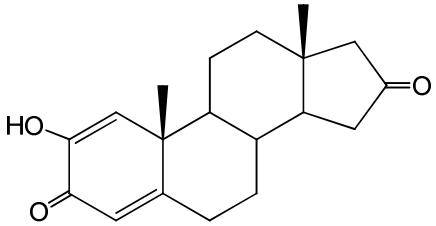

2-hydroxyandrosta-1,4-diene-3,16-diene
82

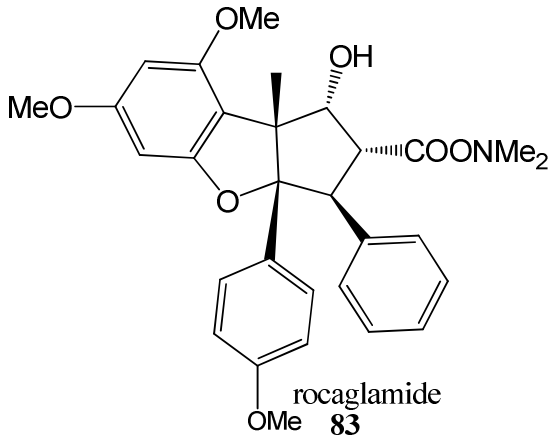

rocaglamide
83

CHAPTER THREE

RESULTS AND DISCUSSION

3.0 Introduction

Three Malaysian plants from Meliaceae family have been studied for chemical constituents. They were *Chisocheton ceramicus, Chisocheton tomentosus*, and *Dysoxylum macrocarpum*. The bark and leaves of the plants were investigated. The isolation techniques were carried out using the conventional methods, i.e. column chromatography (CC), preparative thin layer chromatography (PTLC), and high performance liquid chromatography (HPLC).

The structural elucidation was established through several spectroscopic methods; UV, IR, MS (GCMS, LCMS, and HRMS), 1D (^{1}H-NMR, ^{13}C-NMR, and DEPT), 2D-NMR (COSY, HMQC, HMBC, and NOESY), as well as X-ray reflection technique. The known compounds are identified by comparison of their spectral data with those described in the literature.

3.1 limonoids from the bark of *Chisocheton ceramicus*

The bark of *Chisocheton ceramicus* was first extracted with methanol and the methanol extract was partitioned with ethyl acetate. The ethyl acteate extract were subjected to column chromatography followed by HPLC to yield 7 limonoids, five of them were new limonoids; chisomicine A **CC1**, chisomicine B **CC2**, chisomicine C **CC3**, chisomicine D **CC4**, and chisomicine E **CC5**, and 14-deoxyxyloccensin K **CC6** which has not been isolated from any plant samples but it was established through synthesis, and one known limonoid is called proceranolide **CC7**. The percentage yielded of the isolated limonoids is shown in Table 3.1.

Table 3.1 : Chemical constituents of *Chisocheton ceramicus* (bark)

Compounds	Type Of Limonoid	%Yield
Chisomicine A **CC1**	A2,B,D-Seco	2.5
Chisomicine B **CC2**	Phragmalin	0.25
Chisomicine C **CC3**	Oxidized Phragmalin	0.16
Chisomicine D **CC4**	Phragmalin	0.033
Chisomicine E **CC5**	Phragmalin	0.033
14-Deoxyxyloccensin K **CC6**	Mexicanolide	0.19
Proceranolide **CC7**	Mexicanolide	0.15

3.1.1 Chisomicine A CC1

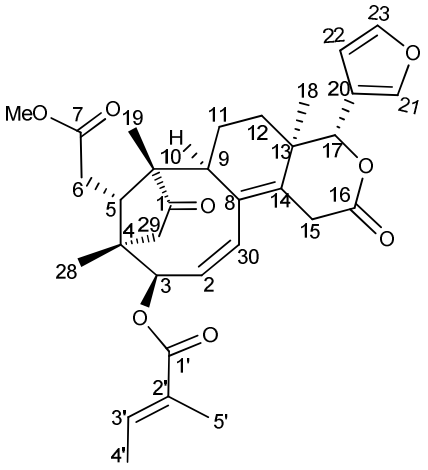

Chisomicine A **CC1** was obtained as a white amorphous solid with $[\alpha]_D^{25} = -125°$ (c= 0.7, MeOH). The UV spectrum showed absorption bands at λ_{max} 202 and 214 nm for the presence of alkene and carbonyl groups. The IR spectrum showed strongly the presence of carbonyl groups at ν_{max} 1734 cm^{-1}. An $[M+Na]^+$ ion peak at m/z 573.2464 (573.629 calculated) was detected in its HRESIMS spectrum which was associated the molecular formula $C_{32}H_{38}O_8Na$.

The ^{1}H-NMR spectrum of chisomicine A **CC1** (Table 3.2 and Figure 3.1) displayed signals for four tertiary methyls and one sec-methyls at δ_H 1.09, 0.97, 1.13, 1.76, and

1.70 assigned to H_3-18, H_3-19, H_3-28, H_3-5`, and $H_3$-4`, respectively as well as one methoxy at δ_H 3.72. Two further downfield signals appeared as doublet and singlet indicated the presence of oxygen functionality at δ_H 4.79, and 5.44 assigned to H-3 and H-17, respectively. Furthermore, two olefinic protons H-2 and H-30 resonated at δ_H 5.85 and 5.83, respectively. All naturally occurring limonoids contain a furan ring attached to the D-ring at C-17 [116]. In **CC1**, the signature mono-substituted furan moiety had characteristic chemical shifts at δ_H 6.46, 7.39, and 7.54 attributed to H-22, H-23, and H-21, respectively.

The ^{13}C-NMR spectrum (Table 3.2 and Figure 3.2) of chisomicine A **CC1** revealed thirty two carbon atoms in the molecule. DEPT spectra exhibited six methyls among them one oxygenated (δ_C 52.0), five sp^3 methylenes, four sp^3 methines among them two oxygenated exhibited at δ_C 76.8 (C-3) and 80.2 (C-17) , and six sp^2 methines two of them were oxygenated and appeared at δ_C 141.7 (C-21) and at δ_C 142.8 (C-23), while the remaining eleven carbons were quaternary carbons among them two esters at δ_C 174.1 (C-7) and 167.1 (C-1`), one lactone at 169.2 (C-16), one ketone at 220.6 (C-1) four sp^2 quaternary carbons, and three sp^3 quaternary carbons.

For further confirmation, HMQC spectrum was used to show all protonated carbon atoms (Table 3.2, Figure 3.3).

Five partial structures **a** (C-2, C-3, and C-30), **b** (from C-5 to C-6), **c** (from C-9 to C-12), **d** (from C-22 to C-23), and **e** (from C-3` to C-4`) were deduced from ^{1}H-^{1}H COSY analysis of **CC1** in $CDCl_3$ (Table 3.2, Figure 3.4). The presence of a bicyclo[5.2.1]dec-3-en-8-one unit containing the partial structure **a** was supported by HMBC correlations as shown in (Figure 3.5). HMBC correlations for H-3, H-5, H_3-28, H_2-29 of C-4 (δ_C 43.3) gave rise to the connectivity of the partial structures **a** and **b** through C-4 atom. The presence of a cyclopentanone ring connected with the partial structure **b** was assigned by the HMBC correlations for H_2-29 of C-1 (δ_C 220.6), C-5

(δ_C 40.5), and C-10 (δ_C 54.2), and for H-5 of C-1 and C-10. Connection among partial structures **a**, **b**, and **c** could be assigned through HMBC correlations for H_3-19 of C-5, C-9 (δ_C 44.4), and C-10, and for H-9 of C-8 (δ_C 131.0) and C-10. The presence of a methoxy ester group connected to the partial structure **b** was supported by the HMBC correlations for H_2-6 and H_3-OMe of C-7 (δ_C 174.1). Partial structure **e** constructing (*E*)-2-methylbut-2-enoic acid was attached at C-3 by the HMBC correlations for H-3 and H-3` of C-1` (δ_C 167.1). The presence of a *β*-furyl ring at C-17 was also assigned by the HMBC correlations. In addition, the HMBC correlations for H_3-18 of C-12 (δ_C 28.5), C-13 (δ_C 37.8), C-14 (δ_C 131.6), and C-17 (δ_C 80.2), and for H-15 of C-8, C-13, C-14, and C-16 (δ_C 169.2) indicated the presence of an isochromenone containing the partial structure **c** and a tetrahydropyran-2-one ring. Thus, chisomicine A **CC1** was concluded to be an unique limonoid possessing a bicyclo[5.2.1]dec-3-en-8-one ring system, an isochromenone, and a *β*-furyl ring at C-17.

NOESY correlations (Figure 3.6) among H-2, H-3, and H-29b indicated that the ester at C-3 and Me-28 at C-4 took a β-configuration. Furthermore, the relative configurations at C-5, C-13, and C-17 were deduced from NOESY correlations among H-5, H-12a, and H-17 as shown in the computer-generated 3D drawing as depicted in (Figure 3.6). The relative configurations at C-9 and C-10 could be assigned by NOESY correlations of H-9/H-30 and H_3-19, and of H-30/H_2-15.

The absolute stereochemistry for **CC1** could be assigned by comparing their experimental CD spectra with the calculated CD spectra (CD calculations were performed by Turbomole 6.1 [117] using RI-TD-DFT-BP86/aug-cc-pVDZ level of theory on RI-DFT-BP86/SVP [118-121] optimized geometries). The calculated CD spectrum of the 3*R*, 4*R*, 5*S*, 9*S*, 10*R*, 13*R*, 17*R* isomer of **CC1** showed similar CD patterns to those of the experimental spectrum as shown in (Figure 3.7). Therefore, the absolute stereochemistry for **CC1** was proposed as shown in the structure.

Table 3.2 : 1D (^{1}H and ^{13}C) and 2D (COSY, HMQC, and HMBC) NMR spectral data of chisomicine A **CC1**

Po.	δ_H (int.; mult.; J(Hz))	δ_C	COSY	HMQC	HMBC
1		220.6			
2	5.85 (1H, dd, 11.6, 6.4)	135.5	H-3, H-30	H-C2	3, 8
3	4.79 (1H, dd, 6.4, 1.6)	76.8	H-2	H-C3	2, 4, 5, 28, 30
4		43.3			
5	3.82 (1H, brd, 12.0)	40.5	H-6a&b	H-C5	1, 4, 5, 7, 9, 10
6a	2.52 (1H, dd, 16.0, 12.8)	33.8	H-6b, H-5	H_a-C6	4, 5, 7, 10
6b	2.35 (1H, m)		H-6a, H-5	H_b-C6	4, 5, 7
7		174.1			
8		131.0			
9	2.66 (1H, brd, 6.0)	44.4	H-11b	H-C9	5, 8, 10, 11, 12, 14
10		54.2			
11a	1.87 (1H, brd, 14.4)	19.1	H-11b	H_a-C11	13
11b	1.63 (1H, m)		H-9, H-11a, H-12a	H_b-C11	10, 13
12a	1.30 (1H, m)	28.5	H-12b, H-11b	H_a-C12	
12b	1.04 (1H, m)		H-12a	H_b-C12	9, 13, 14
13		37.8			
14		131.6			
15	3.07 (2H, brs)	33.0		H_2-C15	8, 13, 14, 16
16		169.2			
17	5.44 (1H, s)	80.2		H-C17	12, 13, 14,18, 20, 21, 22
18	1.09 (3H, s)	16.4		H_3-C18	12, 13, 14, 17
19	0.97 (3H, s)	22.9		H_3-C19	5, 9, 10
20		120.7			
21	7.54 (1H, s)	141.7		H-C21	17, 20, 22, 23
22	6.46 (1H, d, 1.2)	109.9	H-23	H-C22	17, 20, 21, 23
23	7.39 (1H, brs)	142.8	H-22	H-C23	20, 21, 22
28	1.13 (3H, s)	22.6		H_3-C28	4, 5, 29
29a	2.40 (1H, d, 17.6)	46.4	H-29b	H_a-C29	1, 3, 4, 28
29b	2.05 (1H, d, 17.6)		H-29a	H_b-C29	1, 3, 4, 5, 10
30	5.83 (1H, brd, 11.6)	129.1	H-2	H-C30	2, 3, 8
MeO	3.72 (3H, s)	52.0		H_3-MeO	7
1’		167.1			
2’		127.9			
3’	7.29 (1H, qd, 7.0, 1.6)	139.5	H-4`	H-C3`	1’, 4’, 5’
4’	1.70 (3H, d, 7.0)	14.3	H-3`	H-C4`	1’, 2’, 3’
5’	1.76 (3H, brs)	12.0		H-C5`	2’, 3’

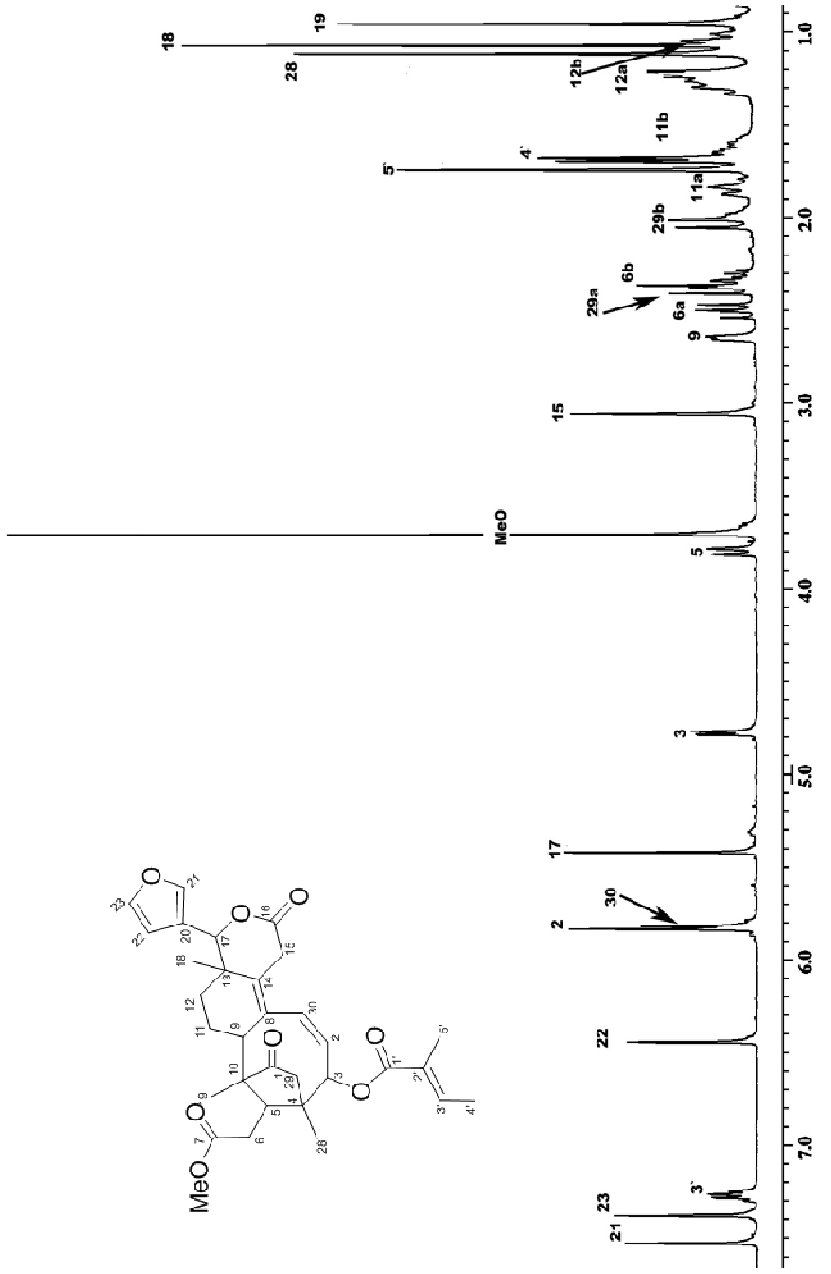

Figure 3.1 : ^{1}H-NMR spectrum of chisomicine A **CC1**

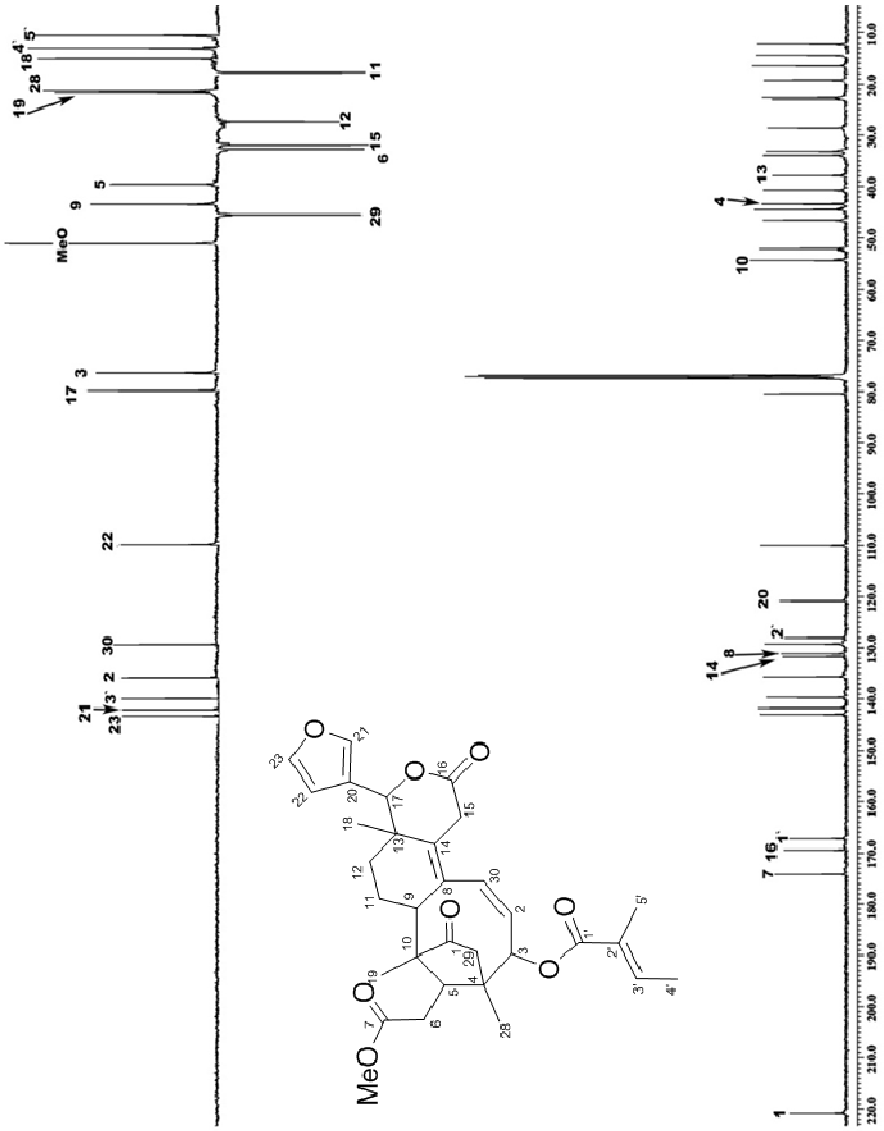

Figure 3.2 : ^{13}C-NMR and DEPT spectra of chisomicine A **CC1**

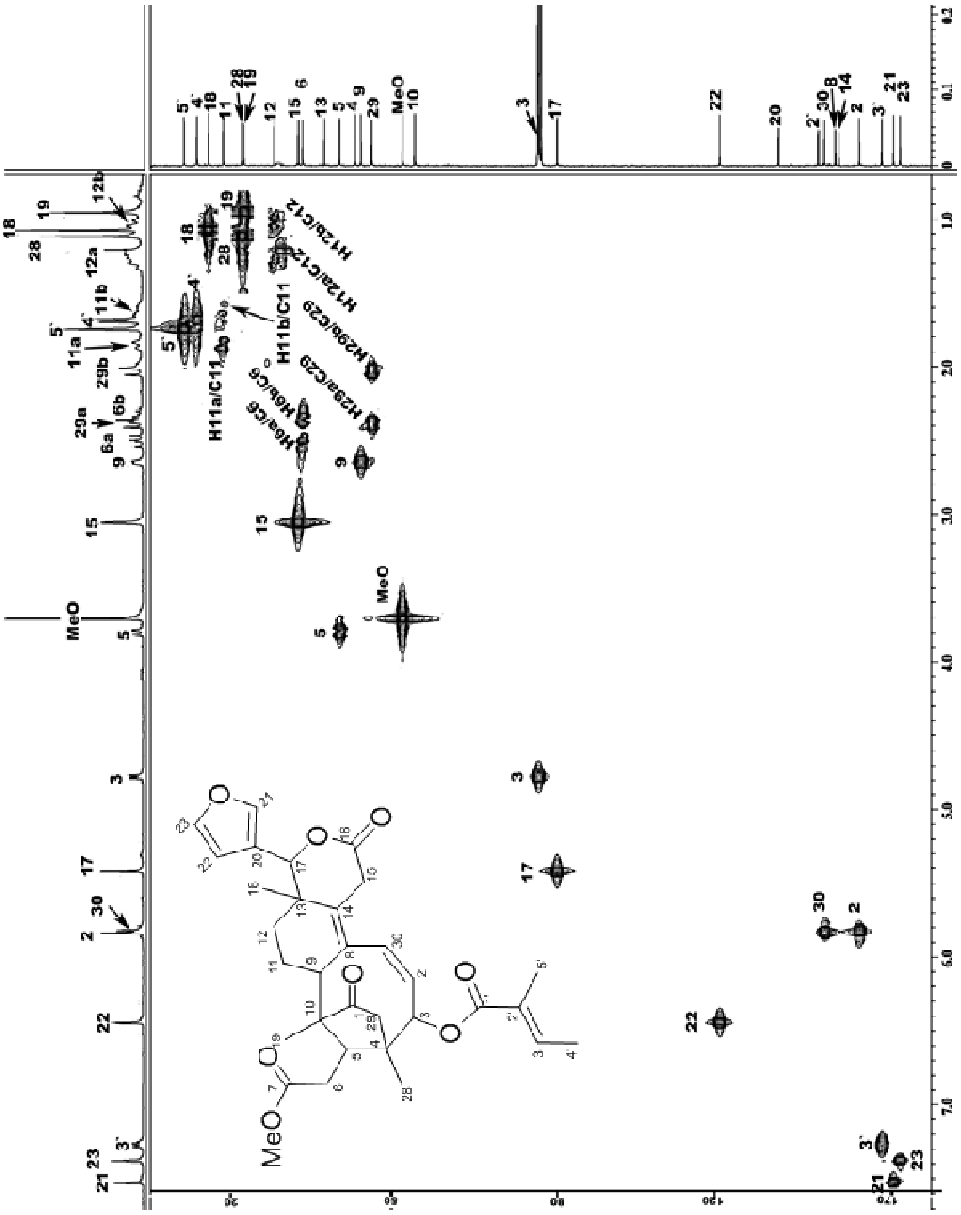

Figure 3.3 : HMQC spectrum of chisomicine A **CC1**

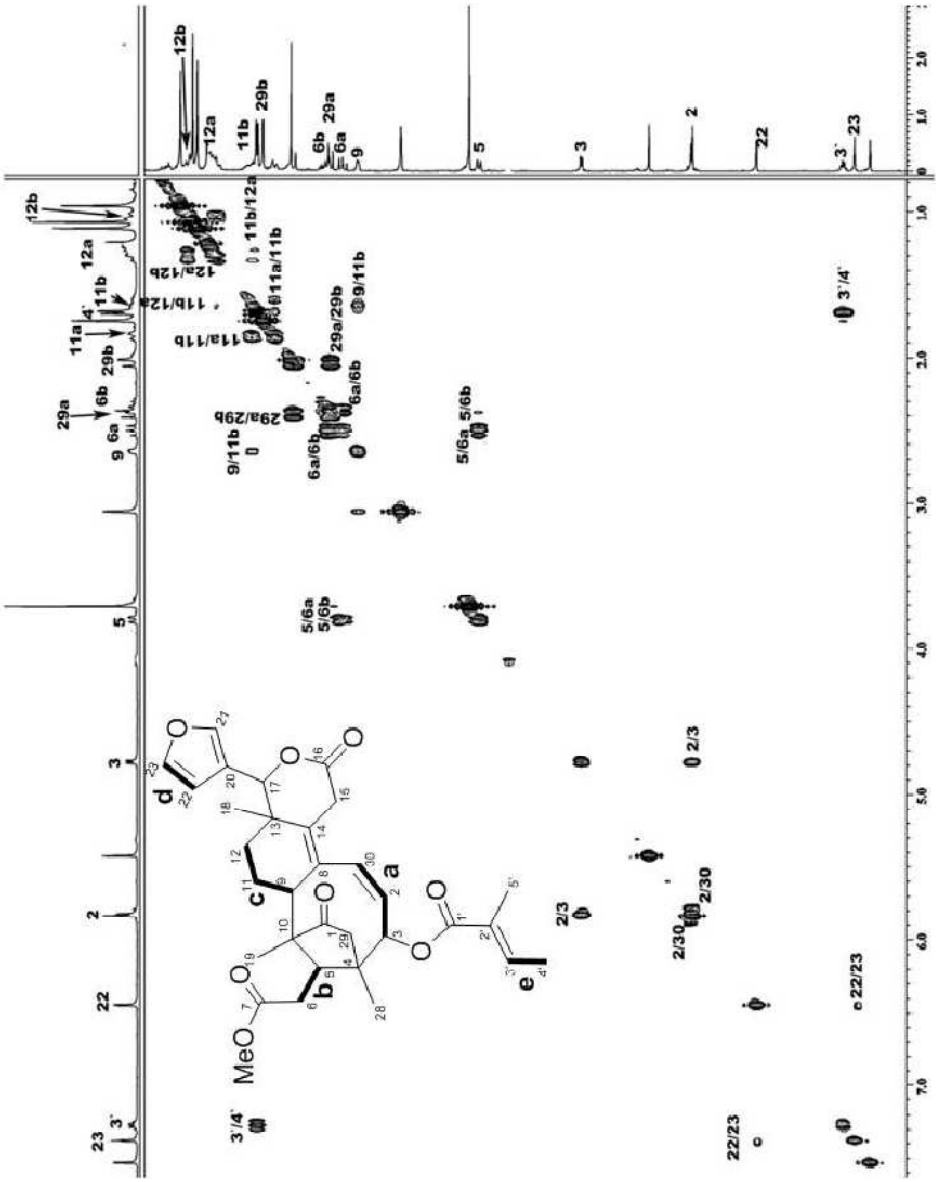

Figure 3.4 : COSY spectrum of chisomicine A **CC1**

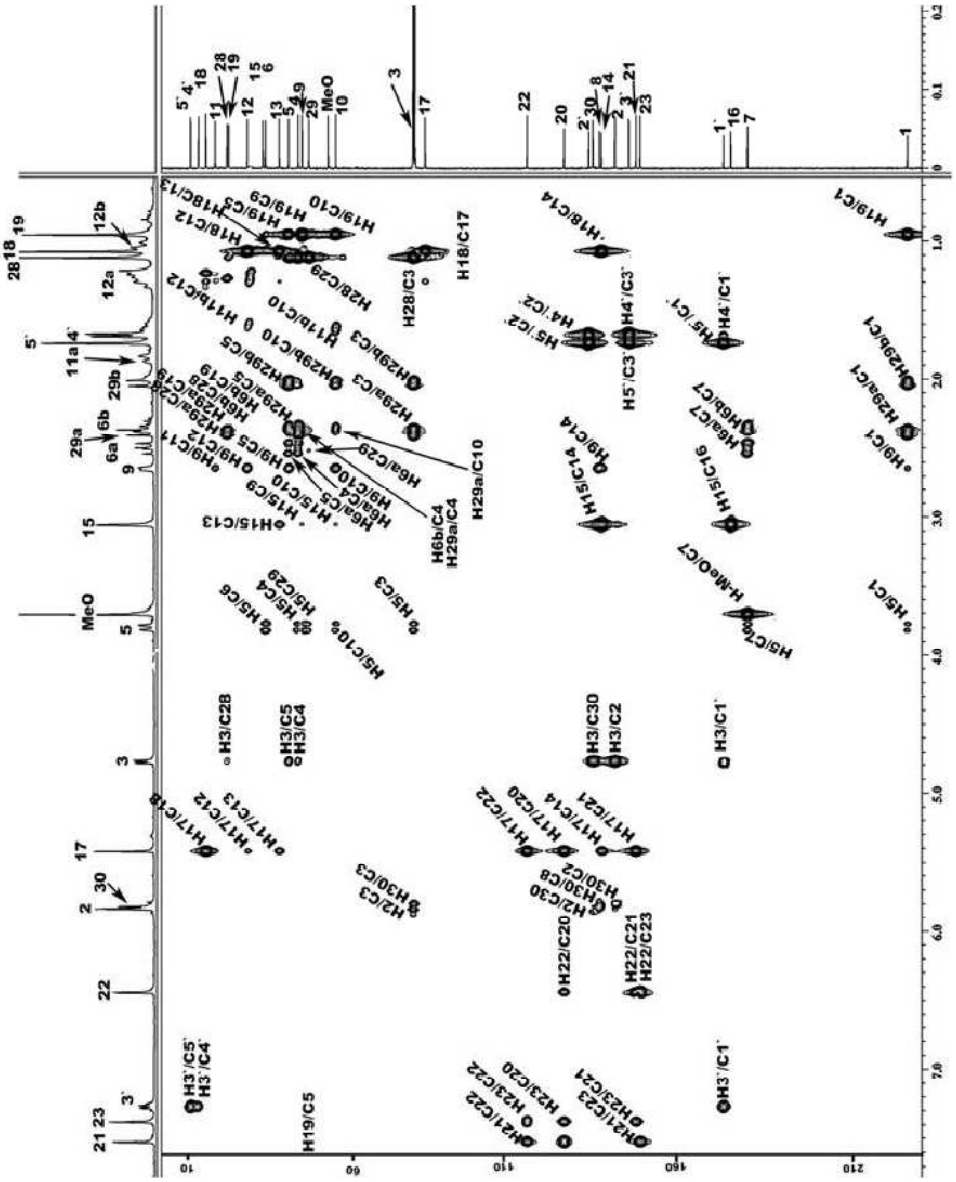

Figure 3.5 : HMBC spectrum of chisomicine A **CC1**

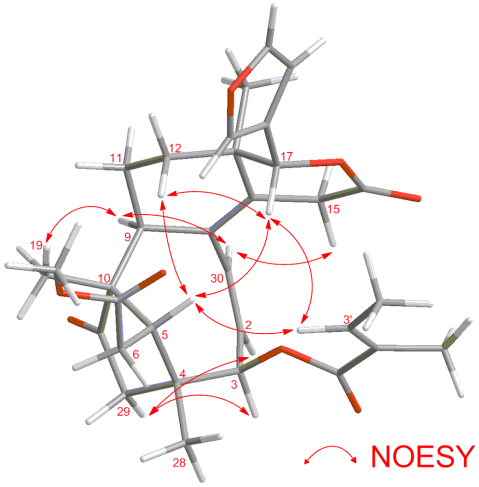

Figure 3.6 : Selected NOESY Correlations for of chisomicine A **CC1**

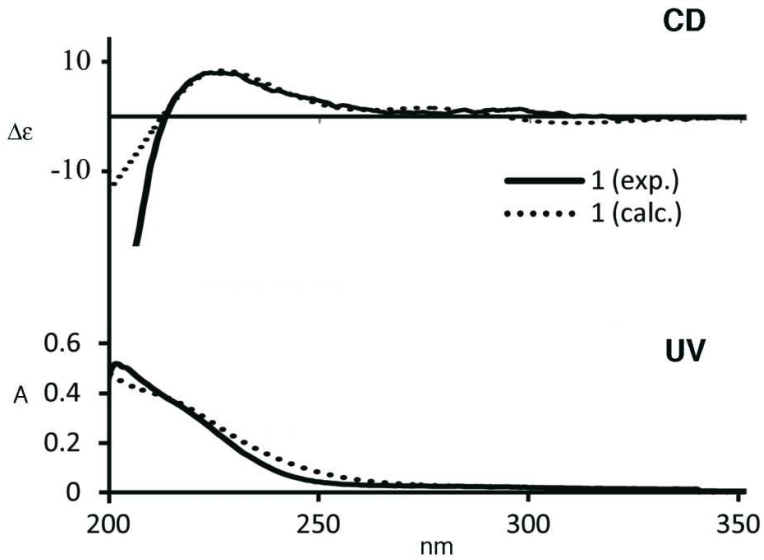

Figure 3.7 : Experimental and Calculated CD and UV Spectra of **CC1**

3.1.2 Chisomicine B CC2

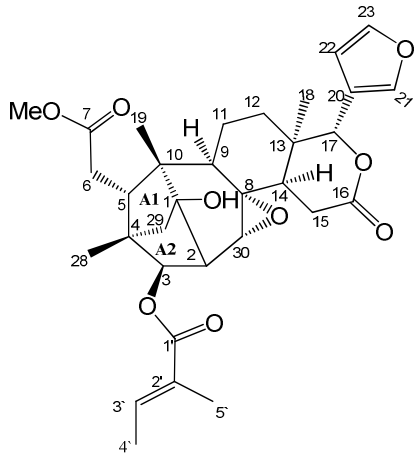

Chisomicine B **CC2** was obtained as colourless needles (m.p 176-178 ^{o}C); $[\alpha]_D^{27}$ -66° (*c* 1.0, MeOH). The UV spectrum showed absorption bands at λ_{max} 216 nm. The compound is chiral and therefore we obtained a CD spectrum, in which six bands appeared at 205, 209, 213, 223, 236 and 245. The IR spectrum exhibited the presence of OH functionality at ν_{max} 3391 and carbonyl groups at 1735 cm^{-1}. The mass spectrum exhibited a molecular ion peak $[M+H]^+$ at m/z 569.2706 (569.663 calculated) suggesting a molecular formula of $C_{32}H_{40}O_9+H^+$.

The ^{1}H-NMR spectrum (Table 3.3, Figure 3.8) of **CC2** displayed signals for four tertiary methyls and one sec-methyls at δ_H 1.0, 1.0, 0.86, 1.8, 1.3 assigned to H_3-18, H_3-19, H_3-28, H_3-5`, and $H_3$-4` , respectively as well as one methoxy at δ_H 3.69. Three further downfield signals appeared as singlet and doublet indicated the presence of oxygen functionality at δ_H 4.8, 5.4, and 3.25 assigned to H-3, H-17 and, H-30, respectively. The diagnostic downfield signals of furan moiety could obviously be assigned due to their typical proton chemical shifts at δ_H 6.4, 7.4, and 7.7 attributed to H-22, H-23, and H-21, respectively.

The broadband decoupled ^{13}C-NMR spectrum of **CC2** (Table 3.3, Figure 3.9) revealed thirty-two carbon atoms in the molecule. DEPT spectrum (Figure 3.9) exhibited six methyls, five sp^3 methylenes, and seven sp^3 methines among them three were oxygenated exhibited at δ_C 78.6 (C-3), and 77.6 (C-17) , 59.6 (C-30) and four sp^2

methines two of them were oxygenated appeared at δ_C 141.4 (C-21) and at 143.1 (C-23). While the remaining ten carbons were quaternary carbons among them two esters at δ_C 173.8 (C-7) and 168.4 (C-1`), one lactone at 169.4 (C-16), one sp^2 carbon of furan ring at 120.8, and two oxygenated carbons at δ_C 80.0 (C-1) and 61.3 (C-8).

The ^{1}H- and ^{13}C-NMR spectra along with UV, IR, and MS spectroscopic data indicated that compound **CC2** has a limonoid skeleton, saturated six-membered lactone, two ester functionality, furan ring, and six methyls.

These preliminary findings indicated that compound **CC2** has a phragmalin-type limonoid structure that was further confirmed by two-dimensional NMR spectroscopic techniques. The structure of **CC2** was deduced by combination of 1D- and 2D-NMR techniques. The main structural fragments were deduced from ^{1}H-^{1}H COSY (Table 3.3, Figure 3.10), HMQC (Table 3.3, Figure 3.11) and HMBC (Figure 3.12) spectra. The ^{1}H-^{1}H COSY spectrum of CC2 revealed the presence of six main spin systems. The spin system '**a**' was traced out starting from sp^3 methine proton of C-2, which showed COSY connectivities with both of C-3 as well as with C-30 methine protons, The spin system '**b**' was traced out with geminally coupled C-6 methylene protons showed ^{1}H-^{1}H COSY interactions with C-5 methine proton. Furthermore, an interesting connectivity could be observed in fragment '**c**' between H-9 and H_2-11, by that we could find the next cross peaks and distinguish between H_2-11 and H_2-12. Spin system'**d**' started with geminally coupled C-15 methylene protons and their partner could again be found via the ^{1}H-^{1}H COSY peak which therefore belongs to H-14. The ^{1}H-^{1}H COSY spectrum showed the signals of olefinic protons H-22 and H-23 in the fragment '**e**'. The lack of further connectivities of all fragments' protons indicated that their attachment either to the quaternary carbons or to oxygen atoms at all ends. The spin system '**f**' was identified by ^{1}H-^{1}H COSY in which C-3` methine proton couples with C-4` methyl protons.

The different structural fragments which have been identified by ^{1}H-^{1}H COSY correlations were joined together on the basis of HMBC connectivities to provide a present structure for compound **CC2**. H-2, H-3, H-5, H_3-28, and H_2-29 exhibited ^{2}J and ^{3}J couplings with C-1 (δ_C 80.0) and C-4 (δ_C 44.8) atoms. These observations helped in joining the fragments '**a**' and '**b**' together. The presence of a cyclopentanol ring (**A1**) connected with the fragment **b** was assigned by the HMBC correlations for H_2-29 with C-1 (δ_C 80.0), C-5 (δ_C 39.4), and C-10 (δ_C 45.1), and for H-5 with C-1 and C-10. The presence of a methoxy carbonyl group connected to the fragment '**b'** was supported by the HMBC correlations for H_2-6 and H_3-OMe of C-7 (δ_C 173.8). The HMBC interaction of the H-2, H-3, and H-29 with C-1 and C-4 supported the existence of cyclopentanol ring (**A2**) which implying the partial fragment '**a**'. The joining of fragments '**a**', '**c**', and '**d**' was done by the help of HMBC correlations exhibited by H-2, H-30 in fragment '**a**' , and H-9 and H-11 in the fragment '**c**' and all the protons of fragment '**d**' were connected in the epoxy ring junction at C-8. Therefore, based on the HRESIMS data, ^{1}H/^{13}C-NMR, ^{1}H-^{1}H COSY, HMBC and the published data for a structurally related compound; **CC2** was assumed to have an C-8,C-30-epoxy ring [122] The presence of a *β*-furyl ring at C-17 was also assigned by the HMBC correlations as shown in (fig. 3.1.2.5). In addition, the HMBC correlations for H_3-18 of C-12 (δ_C 33.7), C-13 (δ_C 36.0), C-14 (δ_C 44.8), and C-17 (δ_C 77.6), and for H-15 of C-8, C-13, C-14, and C-16 (δ_C 169.4) indicated the presence of an isochromenone containing the fragment '**c**' and '**d**' and a tetrahydropyran-2-one ring. In other hand, H-17 correlated with fragments '**c**', '**d**', and '**e**' through C-12, C-14, and C-22. Fragment '**f'** constructing tiglic acid was attached at C-3 by the HMBC correlations for H-3, H-2`, H-3`, and H-4` to C-1` (δ_C 168.4).

Analysis of the 2D NMR data revealed that **CC2** has similar skeleton to that of **CC1** except for the connection between C-1 and C-2. The connection between C-1 and C-2 was suggested by the HMBC correlation of H-30 to C-1 (δ_C 80.0).

Therfore, chisomicine B **CC2** was concluded to be an phragmalin-type limonoid possessing an isochromenone, a *β*-furyl ring at C-17, δ-lactone, epoxy rings, and α-methyl crotonate. The relative structure and the presence of the C-8–C-30 epoxy ring of **CC2** were confirmed by X-ray crystallography as shown in (Figure 3.13).

Table 3.3 : 1D (^{1}H and ^{13}C) and 2D (COSY, HMQC, and HMBC) NMR spectral data of chisomicine B **CC2**

Po.	δ_H (int.; mult.; J(Hz))	δ_C	COSY	HMQC	HMBC
1		80			
2	2.94 (1H, dd, 10.9, 3.4)	43.9	H-3, H-30	H-C2	1, 3,8, 29, 30
3	4.8 (1H, d, 10.9)	78.6	H-2	H-C3	1, 2, 5, 28, 30, 1`
4		44.8			
5	3.03 (1H, dd, 11.0, 2. 3)	39.4	H-6a & b	H-C5	3, 4, 6, 7, 9, 10, 19
6a	2.33 (1H, dd, 17.2, 2.3)	34.2	H-6b, H-5	H_a-C6	4, 5, 7, 10
6b	2.27 (1H, m)		H-6a, H-5	H_b-C6	4, 5, 7, 10
7		173.8			
8		61.3			
9	1.8 (1H, m)	41.6	H-11a & b	H-C9	5, 8, 10, 11, 12, 14
10		45.1			
11a	1.9 (1H, brd, 11.1)	21.5	H-11b	H_a-C11	10, 13
11b	1.81 (1H, m)		H-11a, H-12a	H_b-C11	10, 13
12a	1.62 (1H, m)	33.7	H-12b, H-11b	H_a-C12	9, 13, 14
12b	1.34 (1H, d, 11.1)		H-12a	H_b-C12	9, 13, 14
13		36.0			
14	2.04 (1H, dd, 6, 1.2)	44.8		H-C14	
15a	2.5 (1H, dd, 18.4, 7.3)	27.3		H_a-C15	8, 13, 14, 16
15b	2.3 (1H, dd, 18.4, 1.8)			H_b-C15	8, 13, 14, 16
16		169.4			
17	5.4 (1H, s)	77.6		H-C17	12, 13, 14, 18, 20, 21, 22
18	1.0 (3H, s)	22.0		H_3-C18	12, 13, 14, 17
19	1.0 (3H, s)	18.8		H_3-C19	1, 9, 10, 29
20		120.8			
21	7.7 (1H, s)	141.4		H-C21	17, 20, 22, 23
22	6.4 (1H, d, 1.2)	109.7	H-23	H-C22	20, 21, 23
23	7.4 (1H, s)	143.1	H-22	H-C23	20, 21, 23
28	0.86 (3H, s)	15.0		H_3-C28	3, 4, 5, 29
29a	2.0 (1H, d, 11.0)	43.3	H-29b	H-C29	1, 3, 4, 28
29b	1.33 (1H, dd, 11.0, 1.5)		H-29a	H-C29	1, 3, 4, 5, 10
30	3.25 (1H, d, 3.2)	59.6	H-2	H-C30	1, 2, 3, 8
MeO	3.69 (3H, s)	52.0		H_3-MeO	7
1’		168.4			
2’		128.0			
3’	6.97 (1H, qd, 9.0, 1.6)	139.3	H-4`	H-C3`	1`, 5`
4’	1.3 (3H, d, 9.0)	14.2	H-3`	H_3-C4`	1`, 2`, 3`
5’	1.8 (3H, brs)	12.1		H_3-C5`	1`, 2`, 3

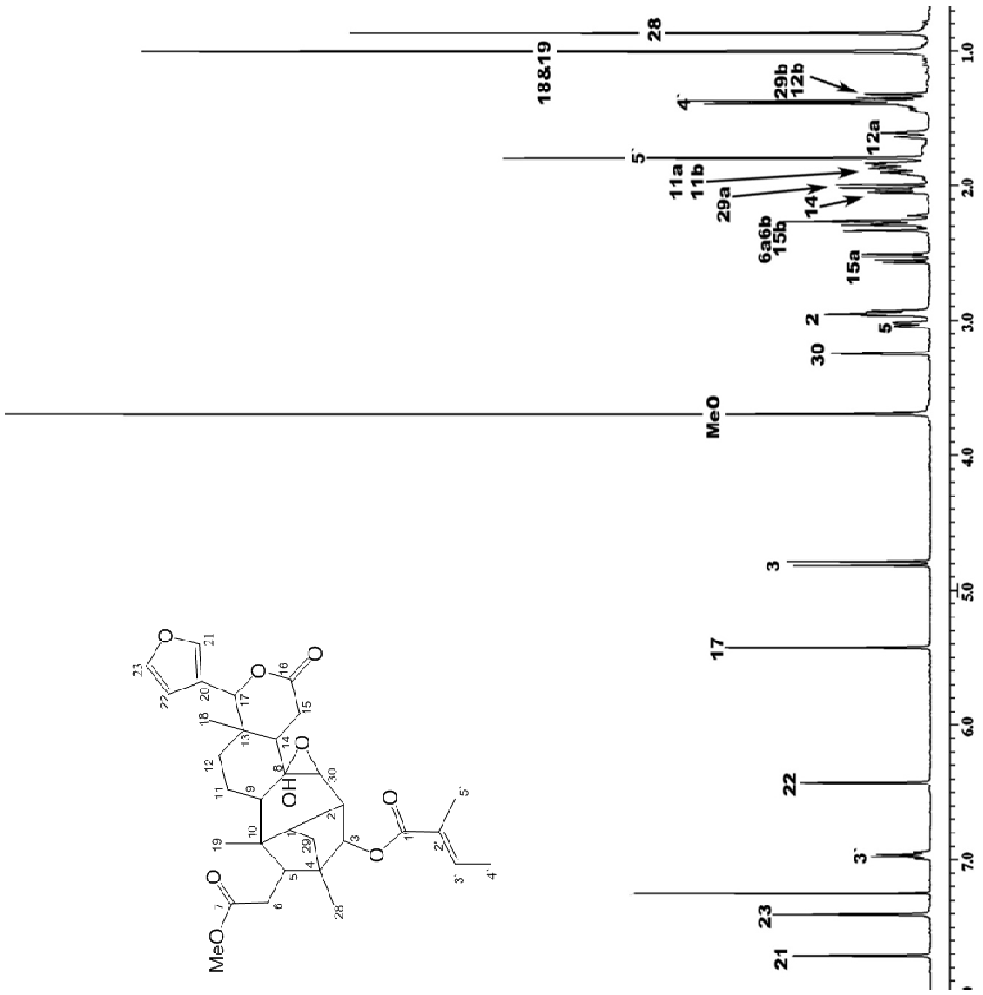

Figure 3.8 : ^{1}H-NMR spectrum of chisomicine B **CC2**

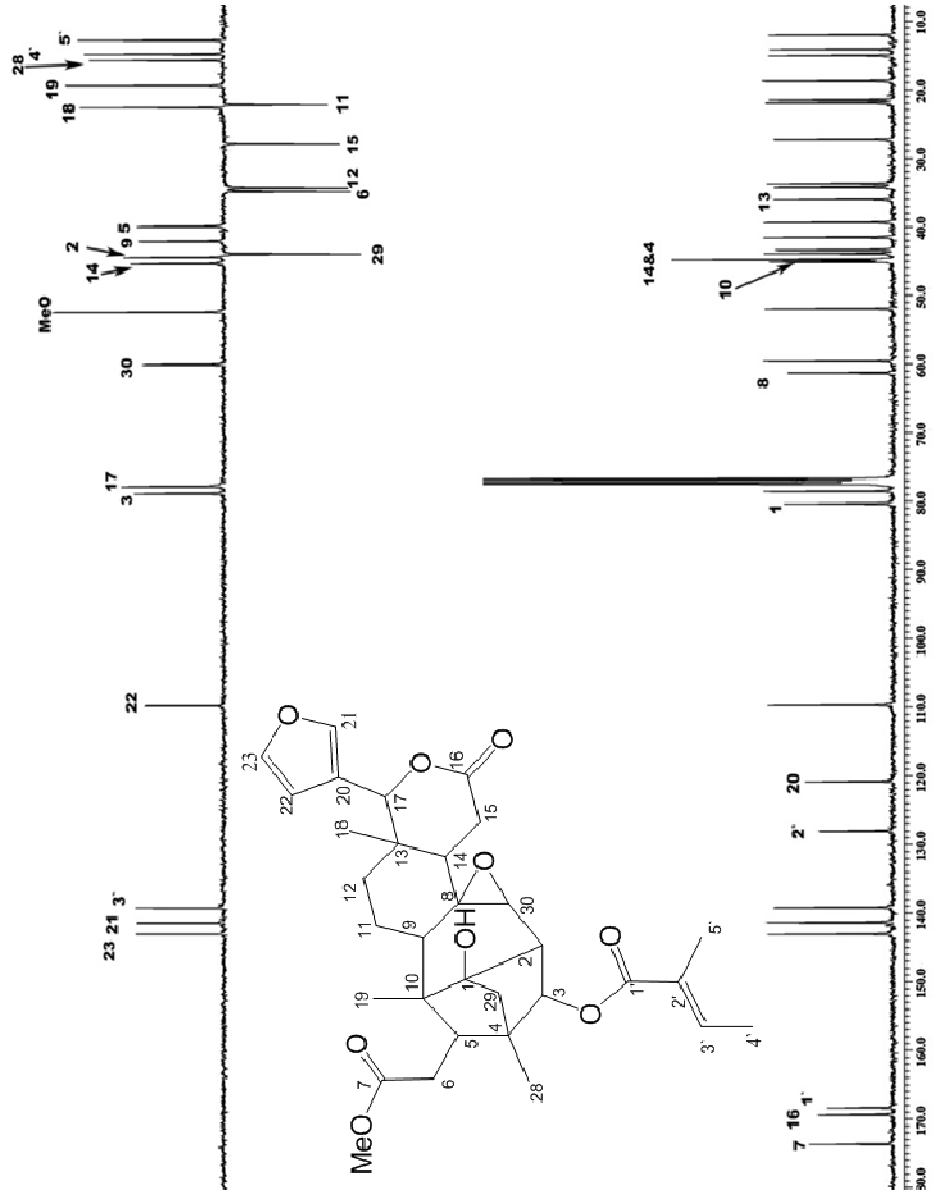

Figure 3.9 : ^{13}C-NMR and DEPT spectra of chisomicine B **CC2**

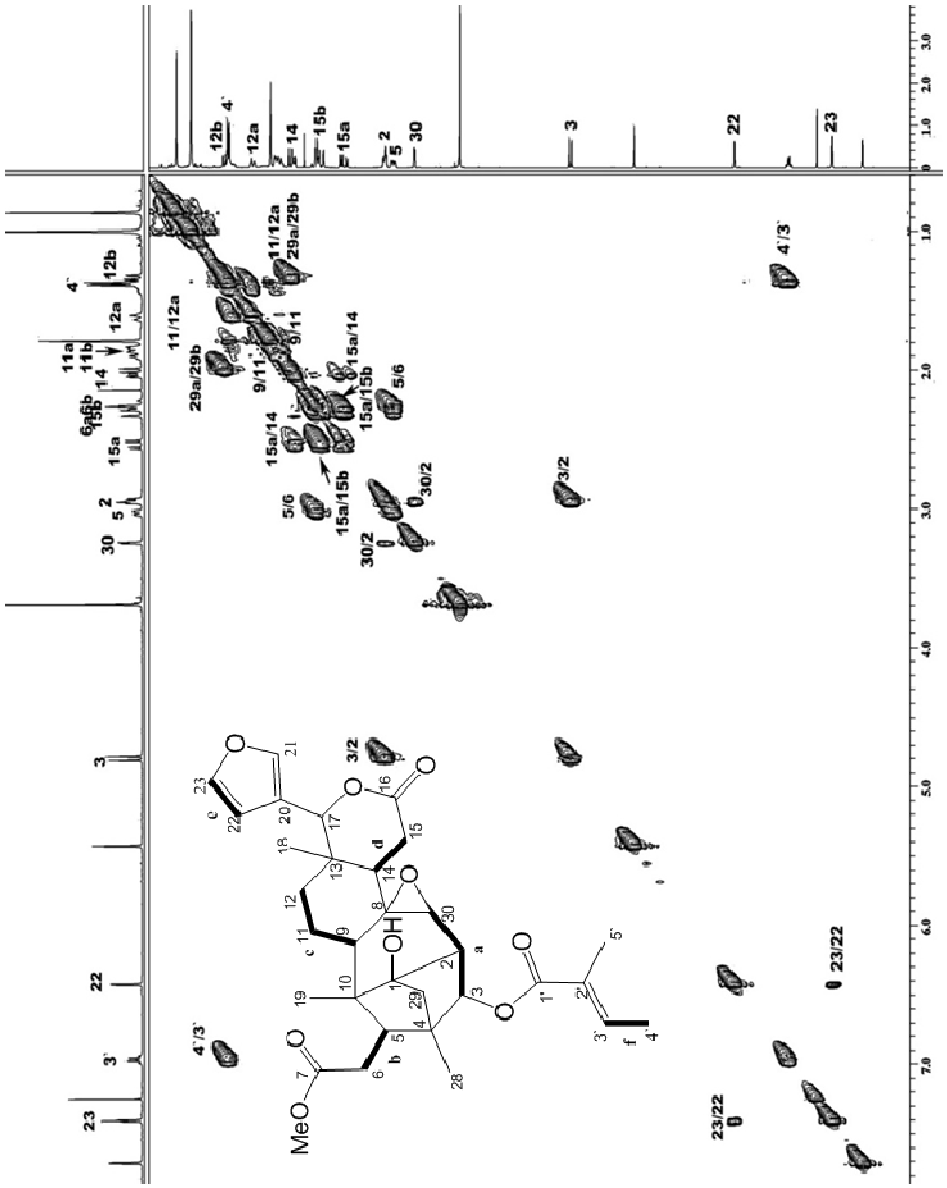

Figure 3.10 : COSY spectrum of chisomicine B **CC2**

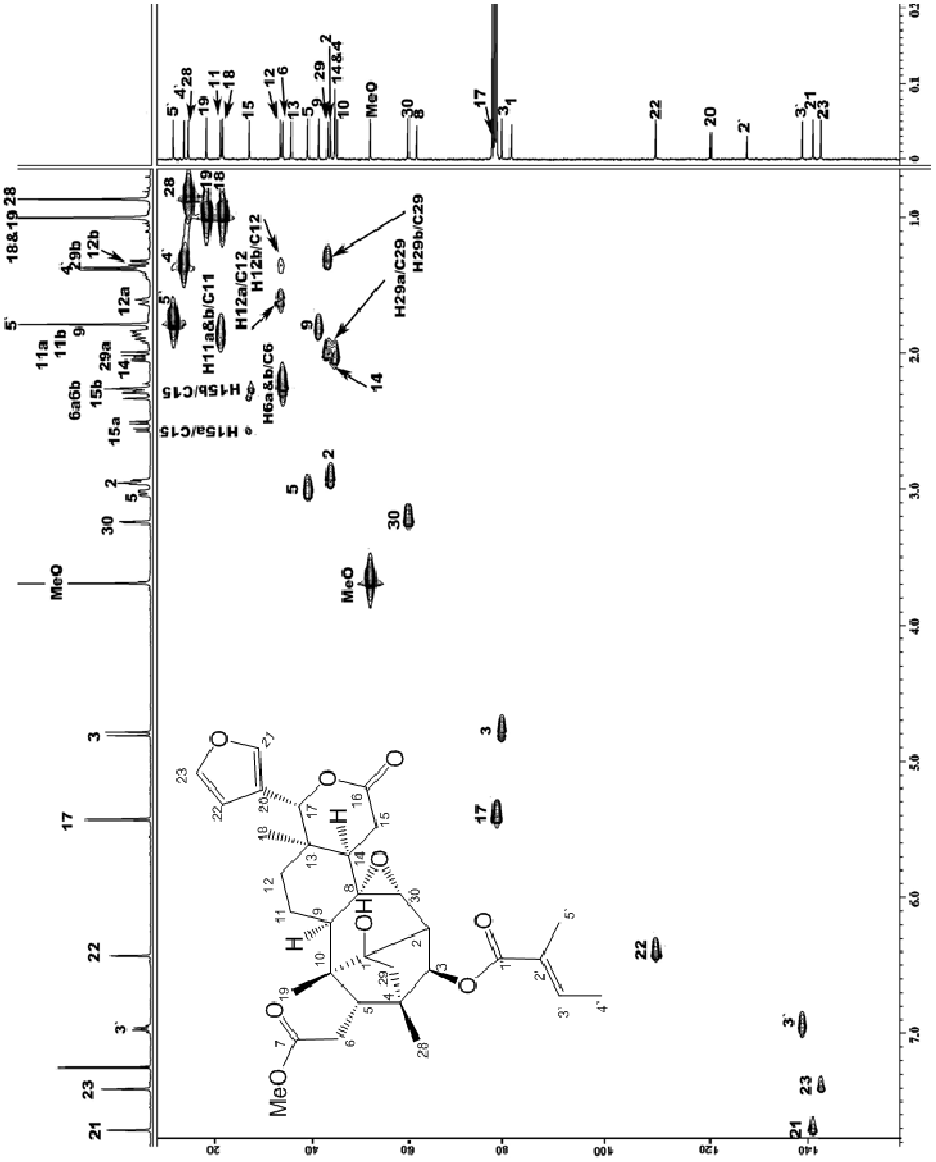

Figure 3.11 : HMQC spectrum of chisomicine B **CC2**

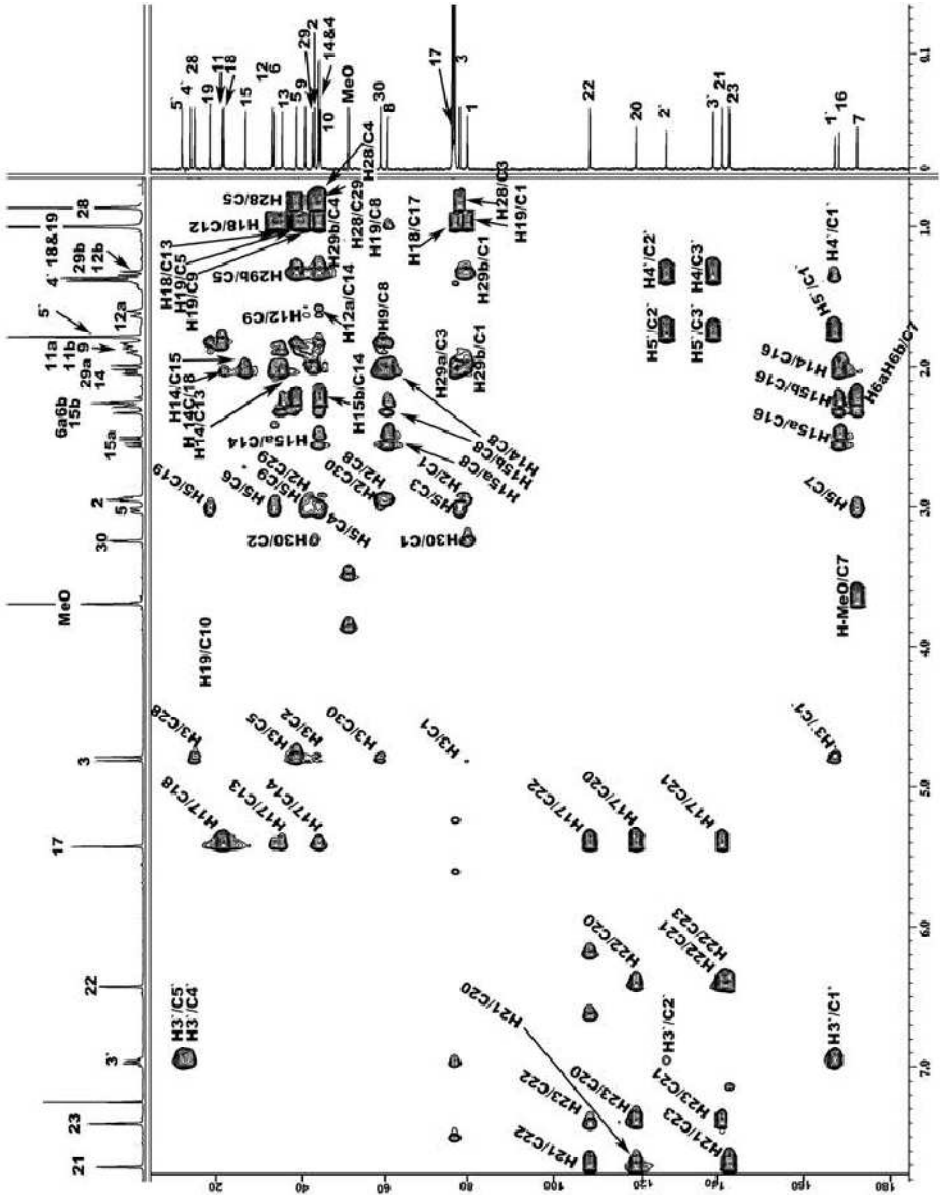

Figure 3.12 : HMBC spectrum of chisomicine B **CC2**

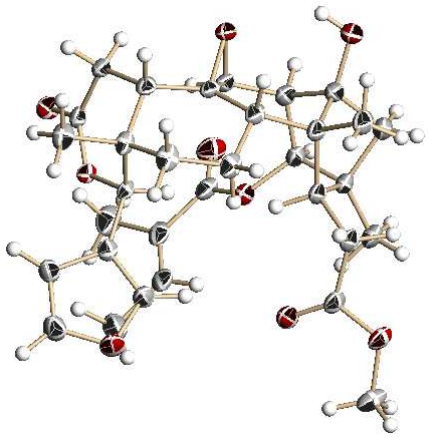

Figure 3.13 : X-ray Crystallographic Structure of **CC2**

3.1.3 Chisomicine C CC3

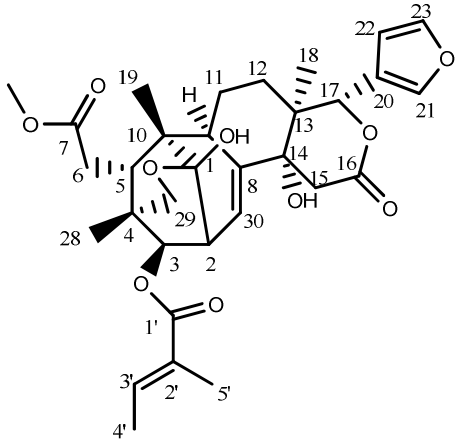

Chisomicine C **CC3** was afforded as white amorphous solid; $[\alpha]_D^{27}$ -86° (*c* 1.0, MeOH). The IR (KBr) spectrum showed absorption band at ν_{max} 3441 cm^{-1} (OH) and 1732 cm^{-1} (C=O). The UV spectrum displayed one distinct maximum at λ_{max} 206 and the CD spectrum showed bands at λ_{max} 201, 208, 211, 217, 221, 227, 235, and 263 nm. The HRESIMS measurement revealed a pseudomolecular ion peak at *m/z* 607.2512 (607.644 calculated) for $C_{32}H_{40}O_{10}Na$.

The ^{1}H-NMR spectrum (Table 3.4, Figure 3.14) showed the presence of *β*-mono-substituted furan moiety by characteristic chemical shifts of H-21 singlet at δ_H 7.78, H-22 as a broad singlet at δ_H 6.46, and H-23 at δ_H 7.39. Additionally, four down field sp^3

proton signals appeared at δ_H 4.80 (H-3), 5.38 (H-17), 3.93 (H-29a), and 3.48 (H29b), which therefore indicated the presence of oxygen functionality, it was in the agreement of 1D NMR data [123]. Additionally, four methyl singlets signals were detected at δ_H 1.01 (Me-18), 1.01 (Me-19), 0.63 (Me-28), and 1.77 (Me-5`), meanwhile, one methyl doublet signals (Me-4`) detected at δ_H 1.60 and a methoxy singlet at (δ_H 3.69). Two sp^2 proton signals, were detected at δ_H 6.92 as multiplet and at 5.48 belong to H-3`and H-30, respectively.

The ^{13}C/DEPT NMR spectra (Table 3.4, Figure 3.15) revealed thirty two carbon resonances due to, five methyls, one methoxy appeared at δ_C 52.2, five sp^3 methylenes among them one was oxygenated, appeared δ_C 67.9 (C-29), five sp^3 methines among them two were oxygenated, appeared at δ_C 75.3 (C-3), 76.9 (C-17), five sp^2 methines among them two oxygenated belong to furan ring at δ_C 142.1 (C-21) and 143.1 (C-23), the remaining were quaternary carbons; two for ester at δ_C 167.7 (C-1′) and δ_C 174 (C-7) and one for lactone (C-16) at δ_C (169.3), three sp^2 quaternary carbons, five sp^3 quaternary carbons among them two were ascribed to those bearing an oxygen atom at δ_C 97.3 (C-1) and δ_C 72.9 (C-14). According to the ^{13}C-NMR spectral data, C-1 (δ_C 97.3) could be an acetal or hemiacetal carbon. For correlation between protons and their carbons, see (Table 3.4, Figure 3.16)

^{1}H–^{1}H COSY cross signals observed between (H-2/H-3 and H-2/H-30), (H-5/H_2-6), (H-9/H_2-11, H_2-11/H_2-12), (H-22/H-23), and (H-3′/H_3-4′) were shown in (Table 3.4, Figure 3.17) as fragments a, b, c, d, e.

Figure 3.18 shows selected HMBC correlations and its spectrum (Figure 3.19) for **CC3**. HMBC correlations of H-17 to C- 20, C-21, and C-22 indicated the presence of a *β*-furyl ring at C-17. The presence of a α-methyl crotonate at C-3 was confirmed based on the HMBC correlation of H-3 (δ_H 4.8) to C-1′ δ_C 167.7). Additionally, the HMBC correlations of the H_3-MeO, H-5, and H_2-6 to C-7 suggested that the methoxy group was

attached to C-7 and methyl acetate substituent attached to C-5. In the δ-lactone ring (ring-D), the geminal proton of H_2-15 showed the HMBC correlations to carbons of C-8 (δ_C 140.9), C-14 (δ_C 72.9), and C-16 (δ_C 169.3). Three methyls of C-18, C-19 and C-28 were attached to C-13, C-10, and C-4 , respectively by HMBC correlations of (H_3-18 to C-12, C-13, C-14 and C-17), (H_3-19 to C-1, C-5, C-9, and C-10), and (H_3-28 to C-3, C-4, C-5 and C-29).

Based on the analysis of both 1D and 2D NMR data of **CC3**, the structure was deduced to be an oxidized-phragmalin type limonoid with a rare C-1–C-29 oxygen bridge similar to granaxylocarpin C [123]. The presence of the C-8–C-30 double bond was confirmed by the ^{1}H-^{1}H COSY correlation of H-2/H-30, and by the HMBC correlation of H-2/C-8. The relative structure of **CC3** was assumed to be similar to **CC2** and granaxylocarpin C, and was confirmed by the observed NOESY correlations as shown in Figure 3.20). The configuration of a hydroxyl at C-14 was deduced by the NOESY correlations of H-5/H-17 and H-17/H-3'. Thus, the relative structure of **CC3** was elucidated to be as shown in the structure.

Table 3.4 : 1D (^{1}H and ^{13}C) and 2D (COSY, HMQC, and HMBC) NMR spectral data of chisomicine C **CC3**

Po.	δ_H (int.; mult.; J(Hz))	δ_C	COSY	HMQC	HMBC
1		97.3			
2	2.96 (1H, m)	45.2	H-3, H-30	H-C2	1, 3, 4, 8,10, 30
3	4.80 (1H, d, 10.0)	75.3	H-2	H-C3	4, 1`
4		36.2			
5	2.90 (1H, dd, 12.0, 10.0)	34.8	H-6a & b	H-C5	10
6a	2.37 (1H, d, 11.3)	31.8	H-6b, H-5	H_a-C6	4, 5, 7
6b	2.30 (1H, d, 11.3)		H-6a, H-5	H_b-C6	4, 5, 7
7		174.0			
8		140,9			
9	2.44 (1H, dd, 5.5, 4.5)	43.8	H-11a & b	H-C9	
10		41.4			
11a	1.66 (1H, brd, 14.0)	19.1	H-11b, H-12b, H-9	H_a-C11	
11b	1.51 (1H, m)		H-11a, H-12a, H-9	H_a-C11	
12a	2.00 (1H, m)	28.6	H-12b, H-11b	H_a-C12	
12b	1.17 (1H, m)		H-12a	H_b-C12	
13		41.2			
14		72.9			
15a	2,94 (1H, d, 18.7)	39.3	H-15b	H_a-C15	8, 14, 16
15b	2,79 (1H, d, 18.7)		H-15a	H_b-C15	8, 14, 16
16		169.3			
17	5.38 (1H, s)	76.9		H-C17	13, 14, 18, 20, 21, 22
18	1.01 (3H, s)	15.5		H_3-C18	12, 13, 14, 17
19	1.01 (3H, s)	14.7		H_3-C19	1, 5, 9, 10
20		120.0			
21	7.78 (1H, s)	142.1		H-C21	20, 22, 23
22	6.46 (1H, brs)	109.9	H-23	H-C22	20, 21, 23
23	7.39 (1H, brs)	143.0	H-22	H-C23	20, 21, 22
28	0.63 (3H, s)	14.9		H_3-C28	3, 4, 5, 29
29a	3.93 (1H, d, 9.6)	67.9	H-29b	H_a-C29	3
29b	3.48 (1H, d, 9.6)		H-29a	H_b-C29	1, 3, 5
30	5.48 (1H, d, 6.2)	121.8	H-2	H-C30	1,2, 14
MeO	3.69 (3H, s)	52.2		H_3-MeO	7
1`		167.7			
2`		127.3			
3`	6.92 (1H, qd, 7.0, 1.5)	140	H-4`	H-C3`	1′, 4′, 5′
4`	1.60 (3H, d, 7.0)	14.7	H-3`	H_3-C4`	1`, 2′, 3′
5`	1.77 (3H, brs)	11.8		H_3-C5`	1′, 2′, 3′, 4`

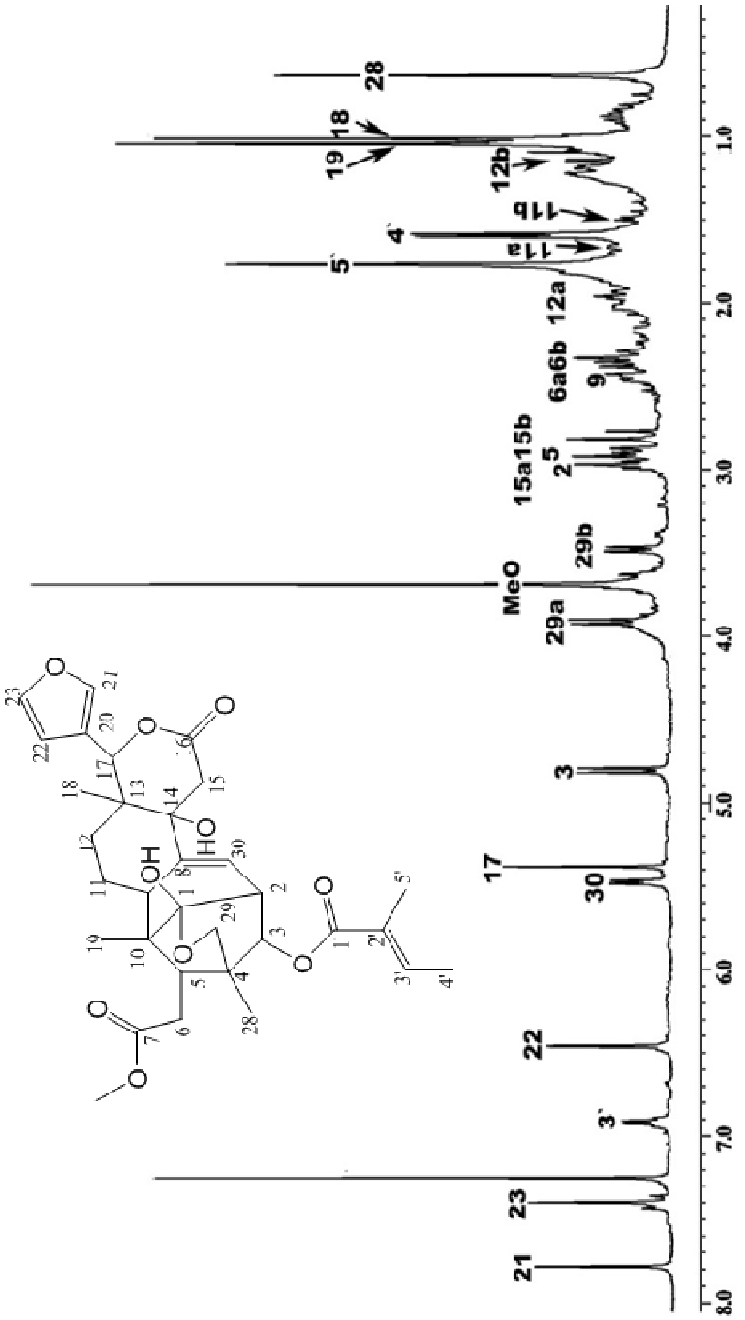

Figure 3.14 : ^{1}H-NMR spectrum of chisomicine C **CC3**

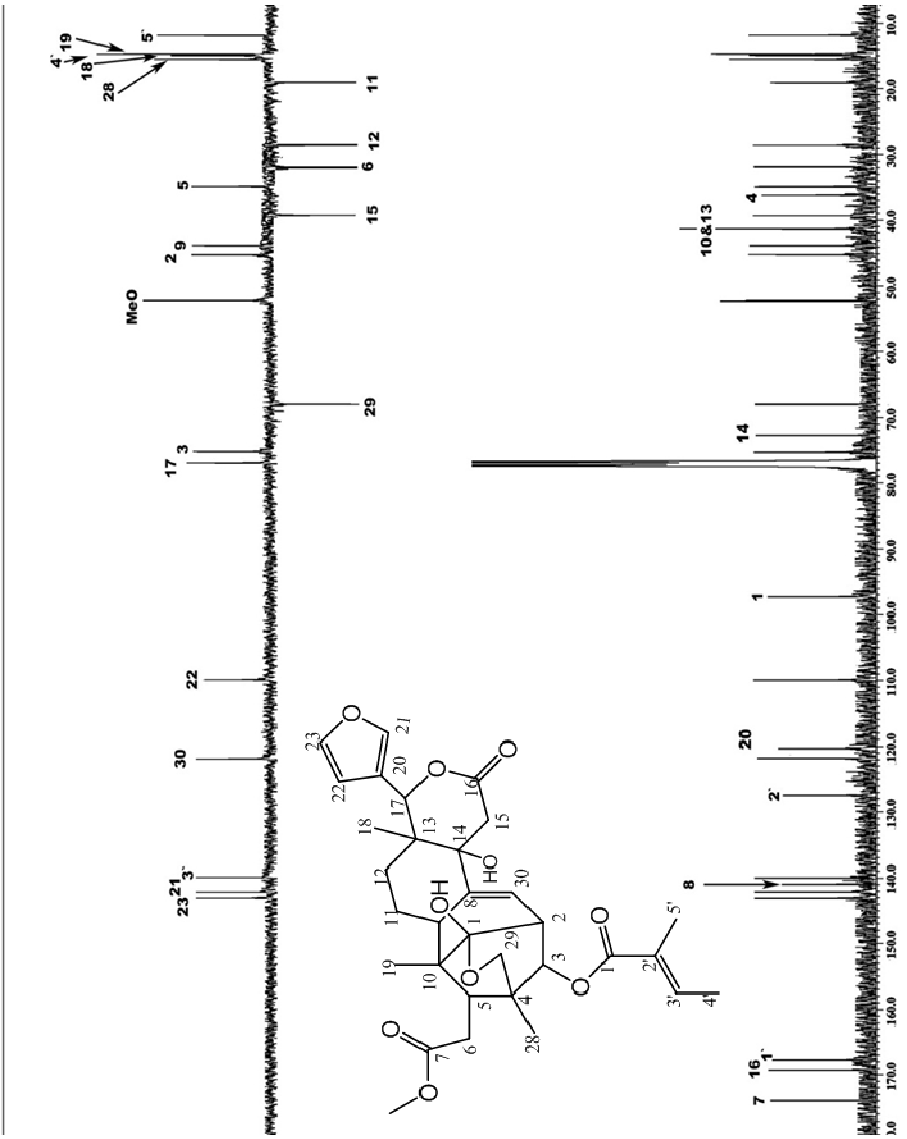

Figure 3.15 : ^{13}C-NMR and DEPT spectra of chisomicine C **CC3**

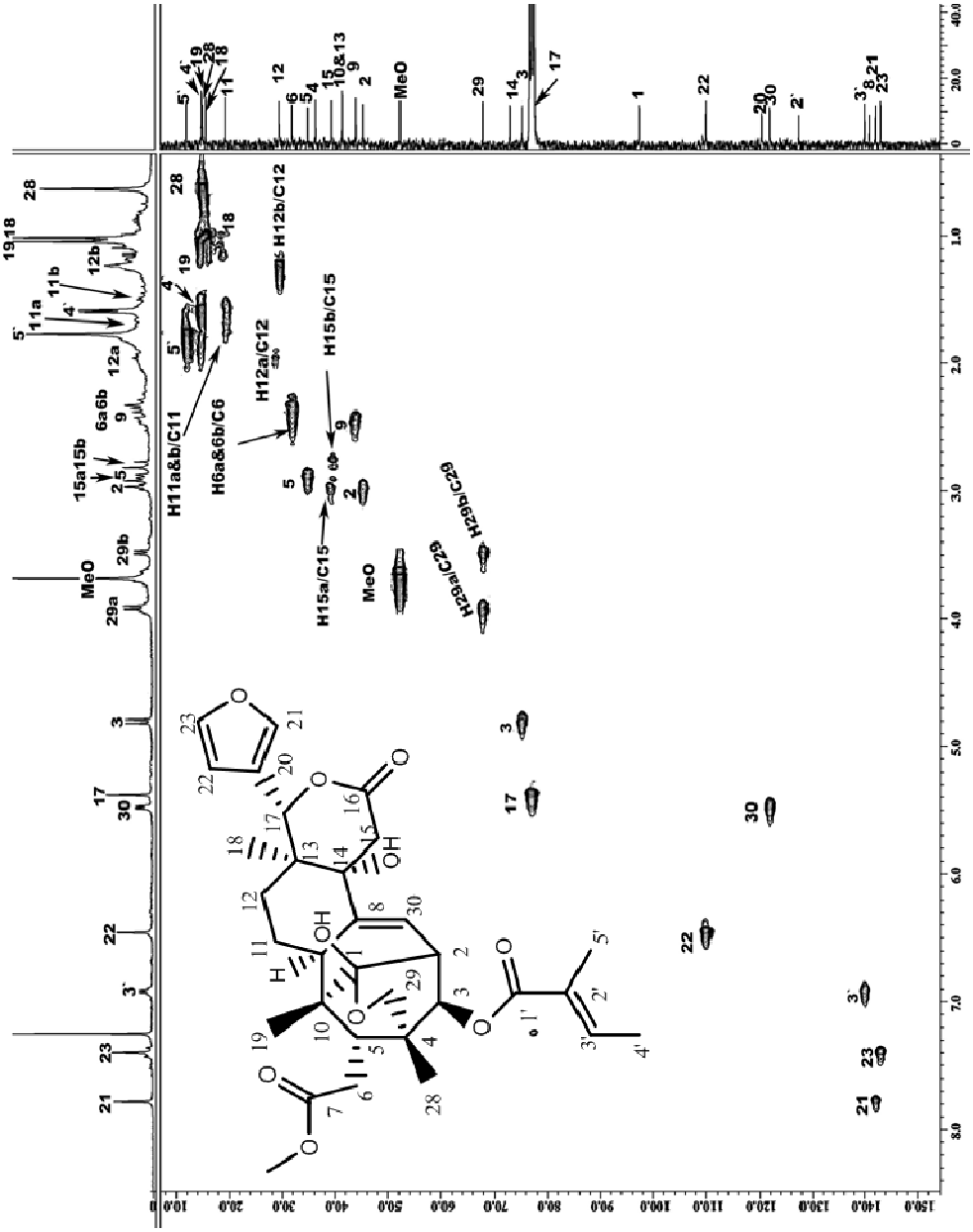

Figure 3.16 : HMQC spectrum of chisomicine C **CC3**

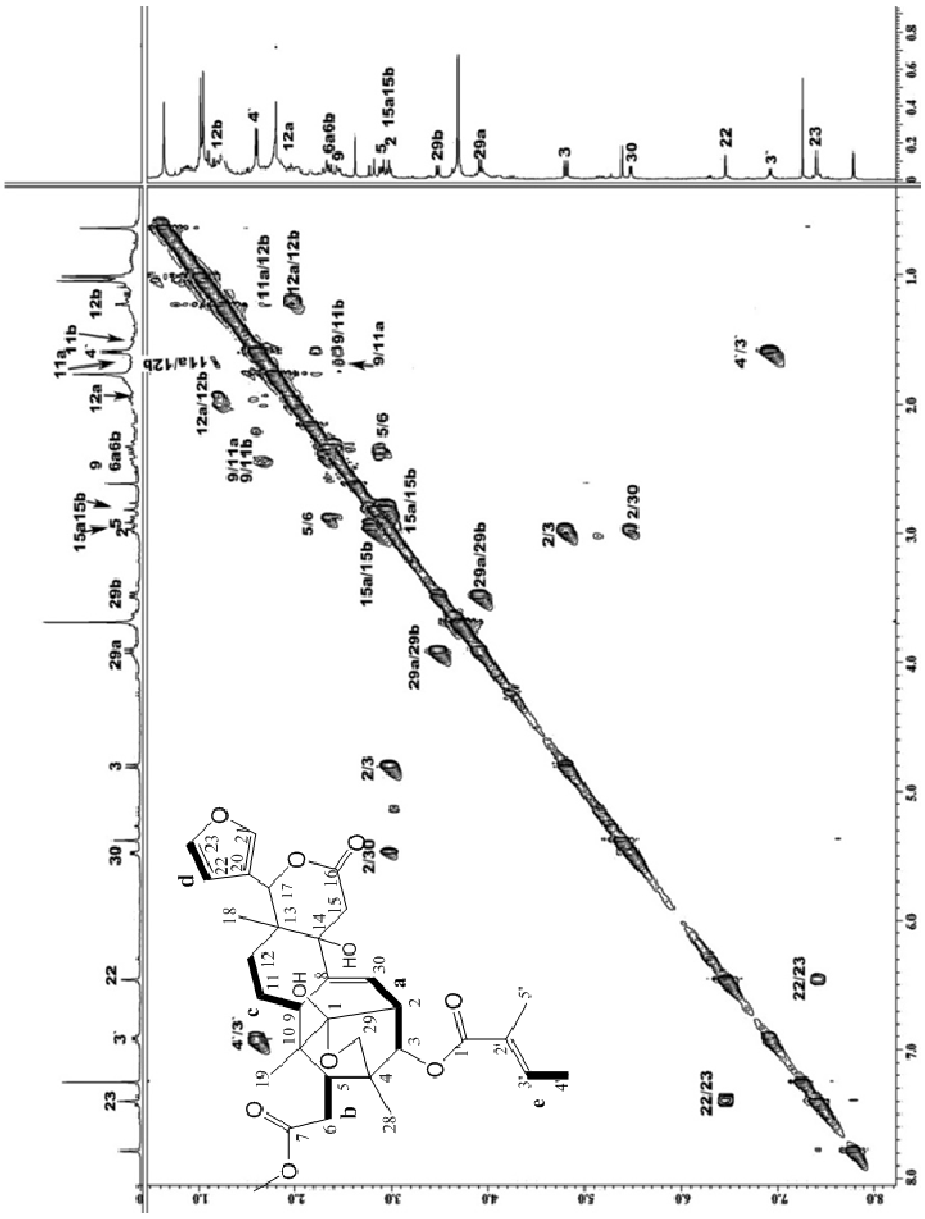

Figure 3.17 : COSY spectrum of chisomicine C **CC3**

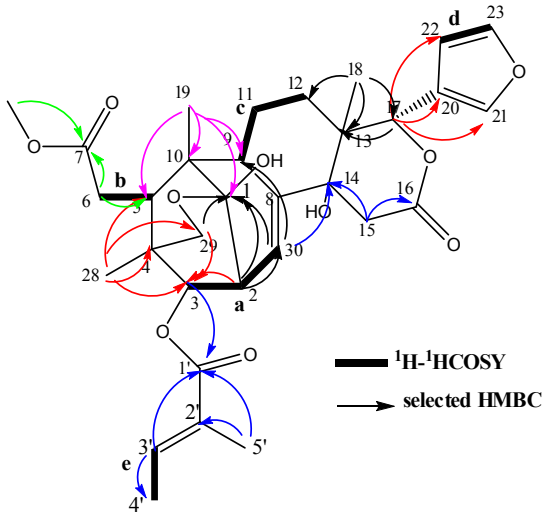

Figure 3.18 : Selected 2D NMR correlations of Chisomicine C **CC3**

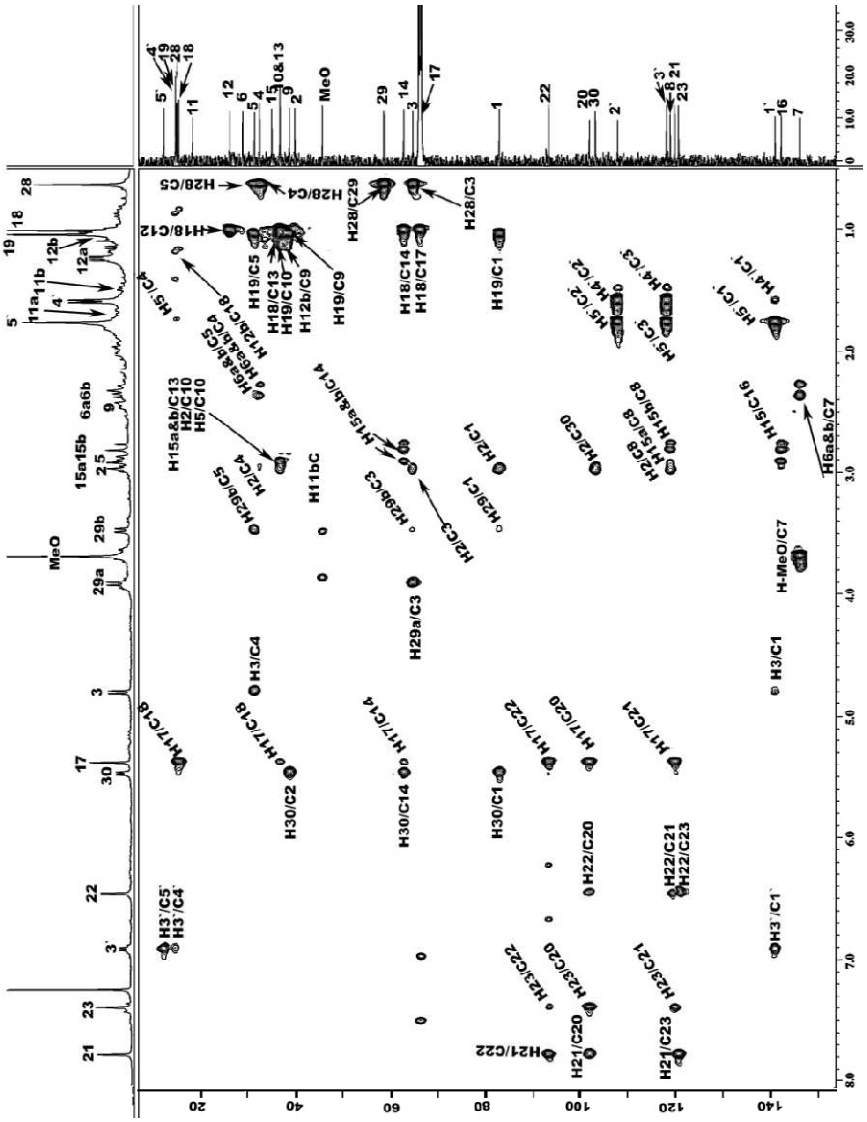

Figure 3.19 : HMBC spectrum of chisomicine C **CC3**

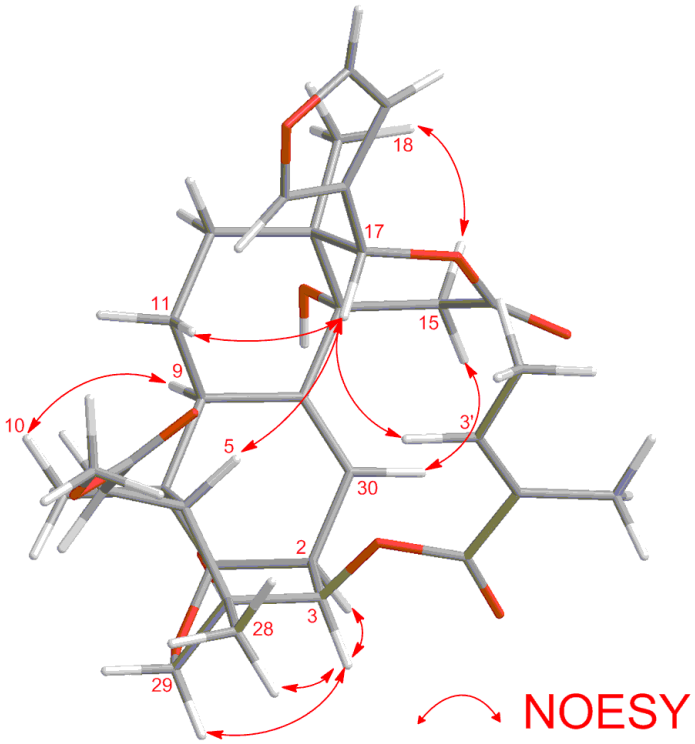

Figure 3.20 : Selected NOESY Correlations for **CC3.**

3.1.4 Chisomicine D CC4

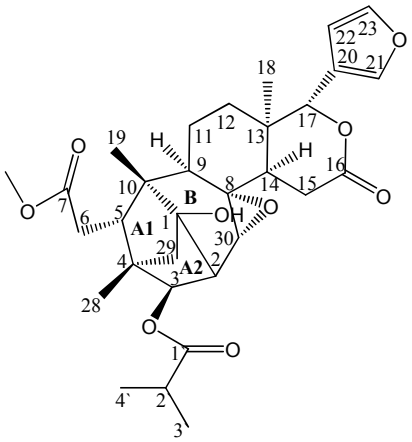

Chisomicine D **CC4** was obtained as white amorphous powder with $[\alpha]_D^{20}$ 23° (*c* 1.0, $CDCl_3$). The UV spectrum showed absorption bands at λ_{max} 202 nm. The IR spectrum showed absorptions at ν_{max} 3391 and 1735 cm^{-1} indicated the presence of OH and carbonyl functionality respectively. The HRESIMS displayed an $[M+H]^+$ ion peak

at ion peak at 557.2693 (557.6518 calculated) $[M+H]^+$ corresponding to the molecular formula of $C_{31}H_{40}O9+H$.

At first, we expected that chisomicine D **CC4** and Chisomicine E **CC5** are dimer based on NMR data, but, finally we realized that they were a mixture of an equal quantity of two compounds. These two compounds have been separated successfully by RP-HPLC using chiral column.

The ^{1}H-NMR spectrum ($CDCl_3$ 400MHz) (Table 3.5, Figure 3.21, Figure 3. 22) of **CC4** displayed signals for three tertiary methyls and two sec-methyls at δ_H 1.11, 1.03, 0.85, 1.12, 1.05 assigned to H_3-18, H_3-19, H_3-28, H_3-3`, and $H_3$-4` , respectively as well as one methoxy at δ_H 3.67. Three further downfield signals appeared as a singlet and two doublets indicated the presence of oxygen functionality at δ_H 5.7, 5.18 and 3.31 assigned to H-17 and H-3, H-30, respectively. The diagnostic downfield signals of furan moiety could obviously be assigned due to their typical proton chemical shifts at δ_H 6.51, 7.44, and 7.85 attributed to H-22, H-23, and H-21 respectively.

The broad band decoupled ^{13}C NMR spectrum (Table 3.5, Figure 3. 24) of **CC4** revealed thirty one carbon atoms in the molecule; six methyls, five sp^3 methylenes, eight sp^3 methines among them three oxygenated exhibited at δ_C 76.7 (C-3), 59.9 (C-30), and 77.7 (C-17), and three sp^2 methines two of them were oxygenated appeared at δ_C 141.8 (C-21) and at 143.3 (C-23), while the remaining nine carbons were quaternary carbons among them two esters at δ_C 173.6 (C-7) and 177.7 (C-1`), one lactone at 169.8 (C-16), one sp^2 carbon of furan ring at 120.4, and two oxygenated carbons at δ_C 80.2 (C-1) and 61.32 (C-8).

^{1}H- and ^{13}C-NMR spectra of along with UV, IR, and MS spectroscopic observations indicated that the compound **CC4** has limonoid skeleton, six-membered saturated lactone, two ketone functionality, and furan ring, epoxy at C-8 and C-30 , and six methyls.

These preliminary findings indicated that compound **CC4** has a limonoid structure, which was further confirmed by two-dimensional NMR spectroscopic techniques.

The structure of **CC4** was deduced by combination of 1D- and 2D-NMR techniques. The main structural fragments were deduced from ^{1}H-^{1}H COSY (Table 3.5**,** Figure 3.25), HMQC (Table 3.5, Figure 3.26) and HMBC (Figure 3.27, Figure 3.28) spectra. The ^{1}H-^{1}H COSY spectrum of **CC4** in $CDCl_3$ revealed the presence of six main spin systems. The spin system '**a**' was traced out starting from sp^3 methine proton of C-2, which showed COSY connectivities with both of C-3 as well as with C-30 methine protons, The spin system '**b**' was traced out with geminally coupled C-6 methylene protons showed ^{1}H-^{1}H COSY interactions with C-5 methine proton. Furthermore, an interesting connectivity could be observed in fragment '**c**' between H-9 and H_2-11, by that we could find the next cross peaks and distinguish between H_2-11 and H_2-12. Spin system'**d**' started with geminally coupled C-15 methylene protons and their partner could again be found via the ^{1}H-^{1}H COSY peak which therefore belongs to H-14. The ^{1}H-^{1}H COSY spectrum showed the signals of olefinic protons H-22 and H-23 in the fragment '**e**'. The lack of further connectivities of all fragments' protons indicated that their attachment either to the quaternary carbons or to oxygen atoms at all ends. Since the spin system '**f**' was identified by ^{1}H-^{1}H COSY couplings of C-2` methine proton with two methyl protons at δ_H 1.12 and at δ_H 1.05.

The different structural fragments which have been identified by ^{1}H-^{1}H COSY correlations were joined together on the basis of HMBC connectivities to provide a present structure for compound **CC4**. H-2, H-3, H-5, H_3-28, and H_2-29 exhibited *J* couplings with C-1 (δ_C 80.2) and C-4 (δ_C 46.0) atoms. These observations helped in joining the fragments '**a**' and '**b**' together. The presence of a cyclopentanol ring (**A1**) connected with the fragment **b** was assigned by the HMBC correlations for H_2-29 with

C-1 (δ_C 80.2), C-5 (δ_C 39.3), and C-10 (δ_C 44.8), and for H-5 with C-1 and C-10. The presence of a methyl ester group connected to the fragment '**b'** was supported by the HMBC correlations for H_2-6 and H_3-OMe with C-7 (δ_C 173.6). The HMBC interaction of the H-2, H-3, and H-29 with C-1 and C-4 supported the existence of cyclopentanol ring (**A2**) which implying the partial fragment '**a**'. The joining of fragments '**a**', '**c**', and '**d**' was done by the help of HMBC correlations exhibited by H-2, H-30 in fragment '**a**' , and H-9 and H-11 in the fragment '**c**' and all the protons of fragment '**d**' were connected in the epoxy ring junction at C-8. Therefore, according to $^1H/^{13}C$-NMR, ^1H-^1H COSY, HMBC and the published data for a structurally related compound; an α-C-8,C-30-epoxy was suggested [122]. The presence of a *β*-furyl ring at C-17 was also assigned by the HMBC correlations. In addition, the HMBC correlations for H_3-18 with C-12 (δ_C 33.6), C-13 (δ_C 36.1), C-14 (δ_C 45.1), and C-17 (δ_C 77.7), and for H-15 with C-8, C-13, C-14, and C-16 (δ_C 169.8) indicated the presence of an isochromenone containing the fragment '**c**' and '**d**' and a tetrahydropyran-2-one ring. In other hand, H-17 correlated with fragments '**c**', '**d**', and '**e**' through C-12, C-14, and C-22. Fragment '**f'** constructing isobutyric acid was attached at C-3 by the HMBC correlations for H-3, H-2`, H-3`, and H-4` to C-1` (δ_C 177.7).

Thus, chisomicine D **CC4** was concluded to be a phragmalin-type limonoid possessing an isochromenone, δ-lactone, and a *β*-furyl and epoxy rings and isobutyrate.

Table 3.5 : 1D (^{1}H and ^{13}C) and 2D (COSY, HMQC, and HMBC) NMR spectral data of chisomicine D **CC4**

Po.	δ_H (int.; mult.; J(Hz))	δ_C	COSY	HMQC	HMBC
1		80.2			
2	2.88 (1H, dd, 11.0, 3.3)	43.1	H-3, H-30	H-C2	1, 3,30
3	5.18 (1H, d, 11.0)	76.7	H-2	H-C3	1, 2, 4, 5, 28, 30, 1`,2`
4		46.0			
5	2.95 (1H, dd, 11.0, 2.4)	39.3	H-6	H-C5	1, 4, 5, 7, 9, 10
6	2.28 (1H, m)	34.1	H-5	H-C6	4, 5, 7, 10
7		173.6			
8		61.2			
9	1.90 (1H, m)	41.4	H-11a&b	H-C9	5, 8, 10, 11, 12, 14
10		44.8			
11a	1.90 (1H, m)	21.5	H-9, H-11b, H-12b	H_a-C11	10, 13
11b	1.88 (1H, m)		H-9, H-11a, H-12a,	H_a-C11,	10, 13
12a	1.7 (1H, m)	33.6	H-12bH-11b	H_a-C12	9, 13, 14
12b	1.48 (1H, d, 11.0)		H-12a	H_b-C12	
13		36.1			
14	2.18 (1H, dd, 6.2, 1.3)	45.1		H-C14	
15a	2.67 (1H, dd, 18.6, 7.2)	27.4	H-15b	H_a-C15	8, 13, 14, 16
15b	2.38 (1H, dd, 18.6, 1.9)		H-15a	H_b-C15	
16		169.8			
17	5.7 (1H, s)	77.7		H-C17	12, 13, 14, 18, 20, 21, 22
18	1.11 (3H, s)	22.1		H_3-C18	12, 13, 14, 17
19	1.03 (3H, s)	18.3		H_3-C19	
20		120.4			
21	7.85 (1H, s)	141.8		H-C21	17, 20, 22, 23
22	6.51 (1H, s)	109.6	H-23	H-C22	20, 21, 23
23	7.44 (1H, s)	143.3	H-22	H-C23	20, 21, 22
28	0.85 (3H, s)	15.1		H_3-C28	4, 5, 29
29a	2.04 (1H, d, 11.0)	43.3	H-29b	H_a-C29	1, 3, 4, 28
29b	1.4 (1H, dd, 11.0, 1,7)		H-29a	H_b-C29	1, 3, 4, 5, 10
30	3.31 (1H, d, 3.0)	59.9	H-2	H-C30	1, 2, 3, 8
MeO	3.67 (3H, s)	51.9		H_3-MeO	7
1`		177.7			
2`	2.65 (1H, m)	33.7	H-3`, H-4`	H-C2`	1`, 3`, 4`
3`	1.12 (3H, bs)	18.8	H-4`	H_3-C3`	1`, 2`, 4`
4`	1.05 (3H, bs)	19.8	H-3`	H_3-C4`	1`, 2`, 3`

3.1.5 Chisomicine E CC5

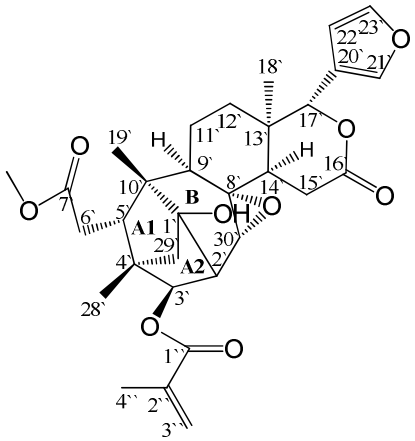

Chisomicine E **CC5** was obtained as white amorphous powder with $[\alpha]_D^{20}$ -23° (*c* 1.0, $CDCl_3$). The UV spectrum showed absorption band at λ_{max} 202 nm. The IR spectrum showed absorptions at ν_{max} 3390 and 1733 cm^{-1} indicated the presence of OH and carbonyl functionality respectively and the HRESIMS displayed a pseudo molecular ion peak $[M+H]^+$ ion peak at 555.2551 (555.6360 calculated) corresponding to the molecular formula of $C_{31}H_{38}O_9$+H.

The $^1H/^{13}C$-NMR spectra ($CDCl_3$ 400MHz) (Table 3.6, Figure 3.21, Figure 3. 23, Figure 3. **24**) of **CC5** displayed signals as same as chisomicine D **CC4** except the lack of one methyl group and one sp^3 methine group, meanwhile one sp^2 methylene group at (δ_C 127.1 and δ_{Ha} 6.30 and δ_{Hb} 5.40) and one sp^2 quaternary carbon atom at (δ_C 135.3) have been increased indicated the elimination of two protons in the isobutanoic substituent to be converted into isobutenoic acid.

The planar structure elucidation of **CC5** was similar skeleton to that of **CC4** except the '**f**' fragment, fragment **f** has not been found in ^1H-^1H COSY (Table 3.6, Figure 3.25) and it has been replaced by α- and *β*- protons of sp^2 methylene which correlated in HMBC (Table 3.6, Figure 3.27) with their carbonyl C-1``, C-4``, and sp^2 quaternary carbon C-2`` as shown in (Figure 3.29).

Table 3.6 : 1D (^{1}H and ^{13}C) and 2D (COSY, HMQC, and HMBC) NMR spectral data of chisomicine E **CC5**

Po.	δ_H (int.; mult.; J(Hz))	δ_C	COSY	HMQC	HMBC
1`		80.4			
2`	2.99(1H, dd, 11.0, 3.3)	43.6	H-3`, H-30`	H-C2`	1`, 3`,30`
3`	4.85 (1H, d, 11.0)	78.7	H-2`	H-C3`	1`, 2`, 4`, 5`, 28`, 30`, 1``,2``
4`		45.1			
5`	3.05(1H, dd, 11.0, 2.4)	39.2	H-6`	H-C5`	1`, 4`, 5`, 7`, 9`, 10`
6`	2.28 (1H, m)	34.1	H-5`	H-C6`	4`, 5`, 7`, 10`
7`		173.7			
8`		61.3			
9`	1.88 (1H, m)	41.6	H-11a` & b`	H-C9`	5`, 8`, 10`, 11`, 12`,14`
10`		44.7			
11a`	1.90 (1H, m)	21.5	H-9`, H-11b`, H-12b`	H_a-C11`	10`, 13`
11b`	1.88 (1H, m)		H-9`,H-11a`, H-12a`	H_a-C11`	10`, 13`
12a`	1.70 (1H, m)	33.5	H-12b`, H-11b`	H_a-C12`	9`, 13`, 14`
12b`	1.48 (1H, d, 11.0)		H-12a`	H_b-C12`	
13`		36.0			
14`	2.08 (1H, dd, 6.2, 1.3)	44.9		H-C14`	
15a`	2.58 (1H, dd, 18.6, 2)	27.3	H-15b`	H_a-C15`	8`, 13`, 14`, 16`
15b`	2.37 (1H, dd, 18.6,1.9)		H-15a`	H_b-C15`	
16`		169.5			
17`	5.46 (1H, s)	77.7		H-C17`	12`, 13`, 14`, 18`, 20`, 21`,22`
18`	1.14 (3H, s)	22.2		H_3-C18`	12`, 13`, 14`, 17`
19`	1.02 (3H, s)	18.1		H_3-C19`	
20`		120.7			
21`	7.70 (1H, s)	141.3		H-C21`	17`, 20`, 22`, 23`
22`	6.45 (1H, s)	109.6	H-23`	H-C22`	20`, 21`, 23`
23`	7.42 (1H, s)	143.1	H-22`	H-C23`	20`, 21`, 22`
28`	0.90 (3H, s)	15.0		H_3-C28`	4`, 5`, 29`
29a`	2.04 (1H, d, 11.0)	43.4	H-29b`	H_a-C29`	1`, 3`, 4`, 28`
29b`	1.40(1H, dd, 11.0, 1,7)		H-29a`	H_b-C29`	1`, 3`, 4`, 5`, 10`
30`	3.28 (1H, d, 3.0)	59.5	H-2`	H-C30`	
MeO`	3.71 (3H, s)	52.0		H_3-MeO`	7`
1``		167.8			
2``		135.3			1``, 3``, 4``
3`a	6.30 (1H, s)	127.1		H_a-C3``	1``, 2``, 4``
3`b	5.40 (1H, s)			H_b-C3``	1``, 2``, 4``
4`	1.95 (3H, s)	21.5		H_3-C4``	1``, 2``, 3``

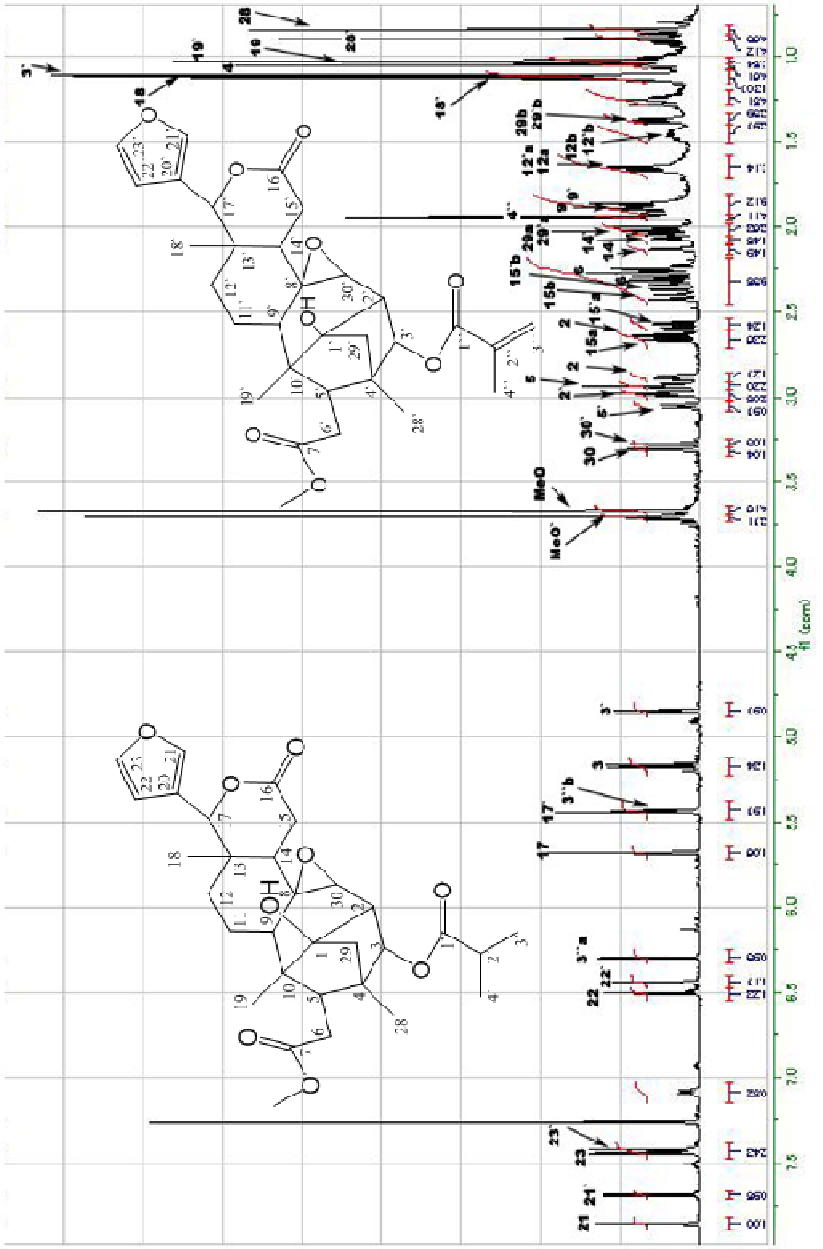

Figure 3.21 : ^{1}H-NMR spectrum of a mixture of chisomicines D **CC4** & E **CC5**

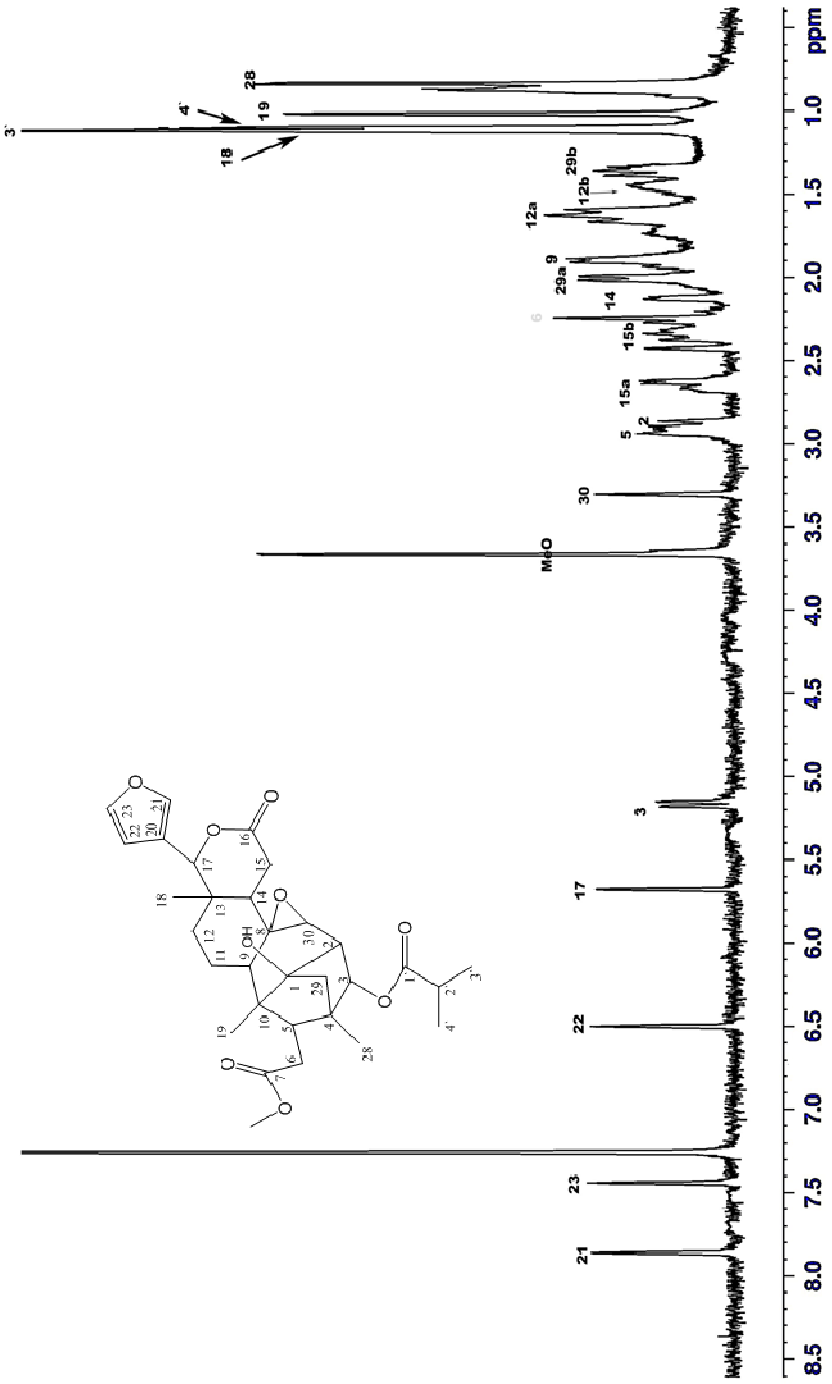

Figure 3. 22 : ^{1}H-NMR spectrum of chisomicine D **CC4**

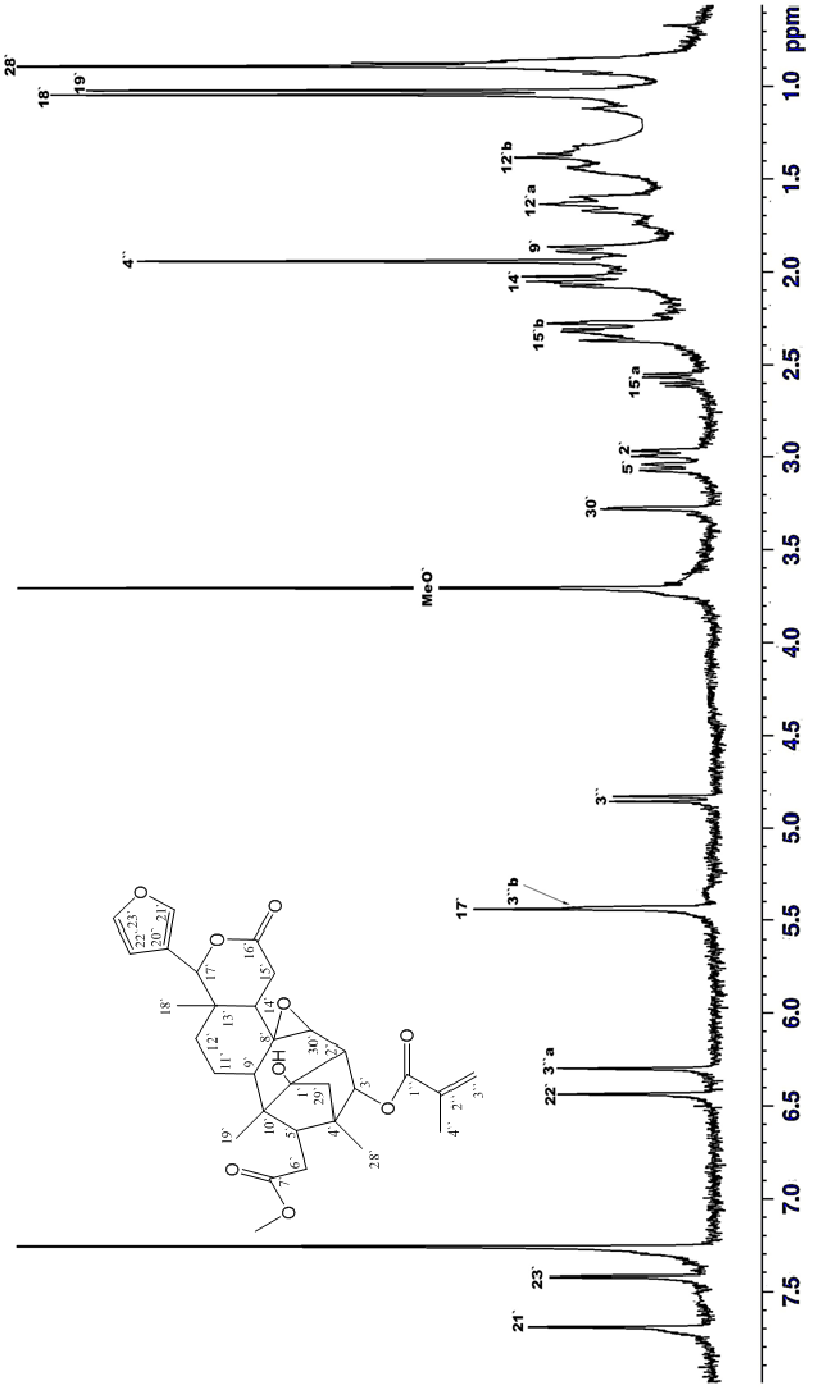

Figure 3. 23 : ^{1}H-NMR spectrum of chisomicine **E CC5**

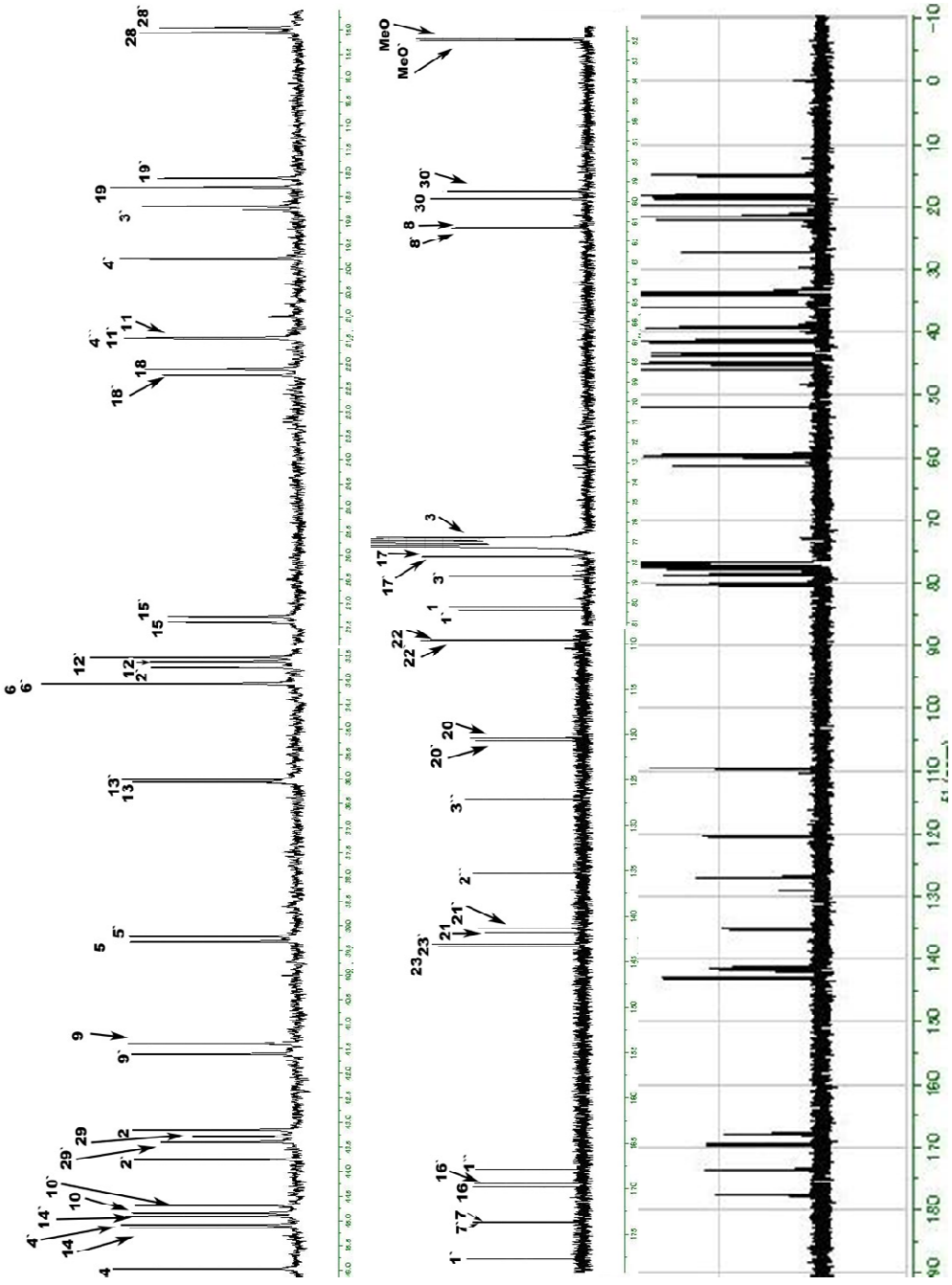

Figure 3. 24 : ^{13}C-NMR spectra of chisomicine D **CC4** & E **CC5**

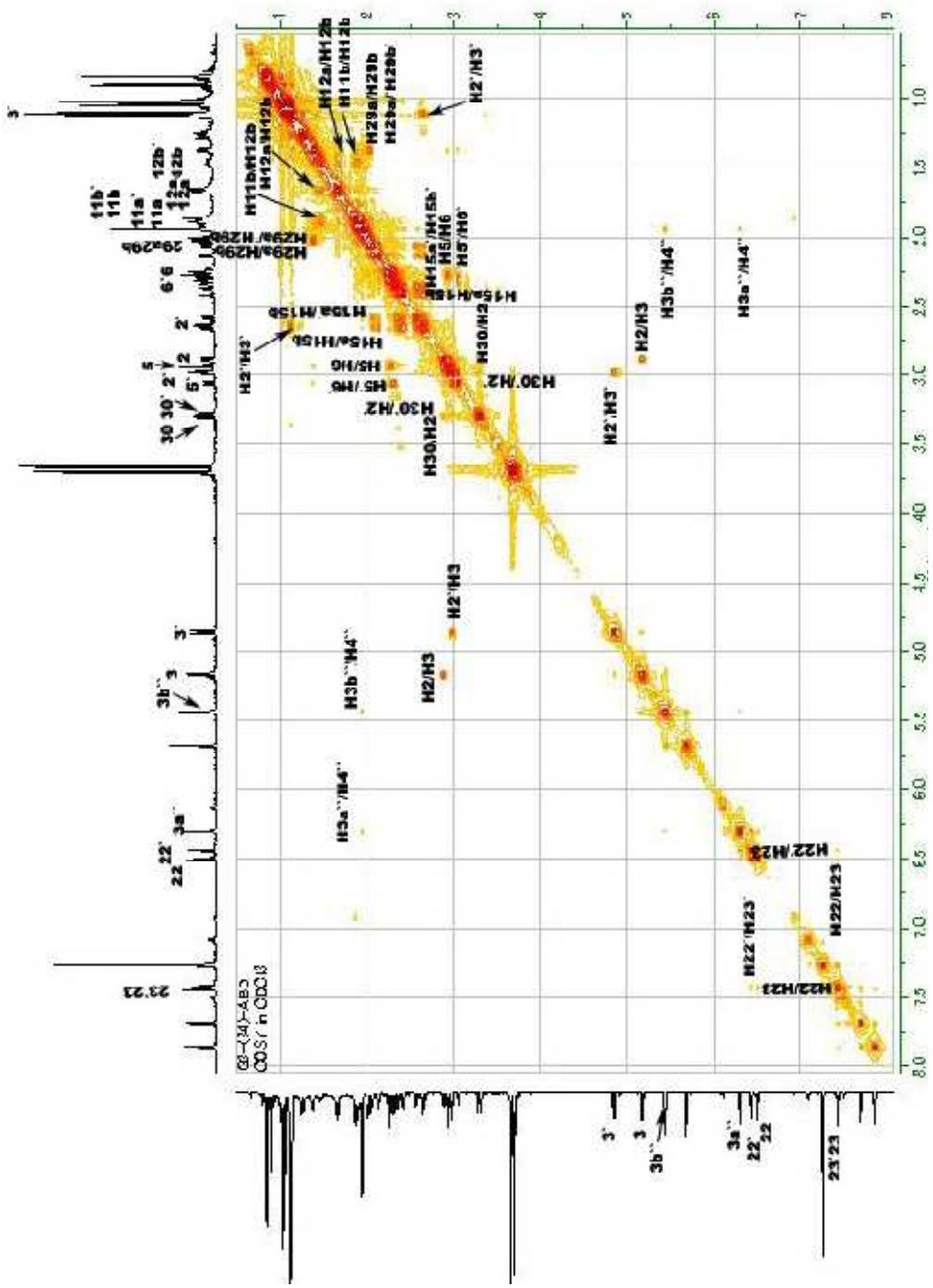

Figure 3.25 : COSY spectrum of chisomicine D **CC4** & E **CC5**

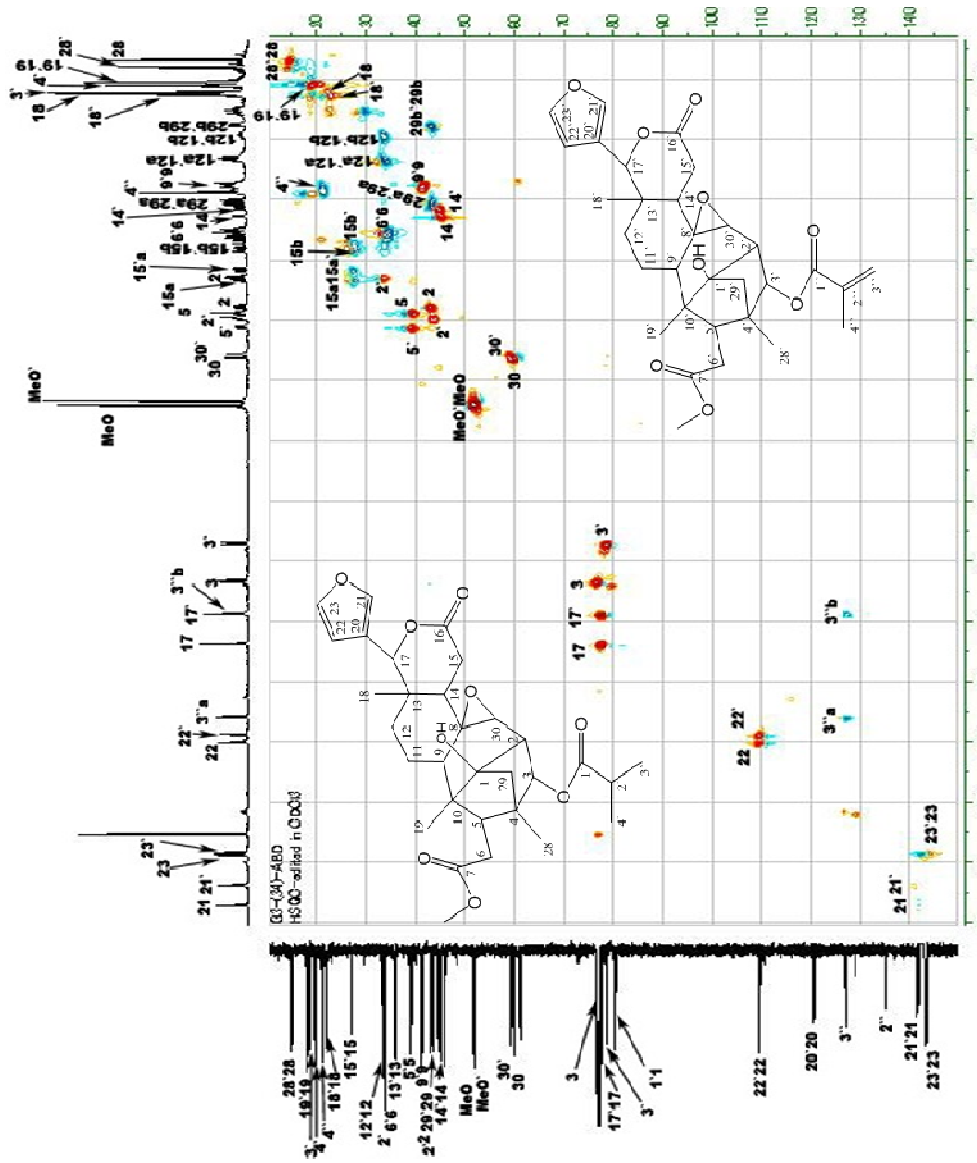

Figure 3.26 : HMQC spectrum of chisomicine D **CC4** & E **CC5**

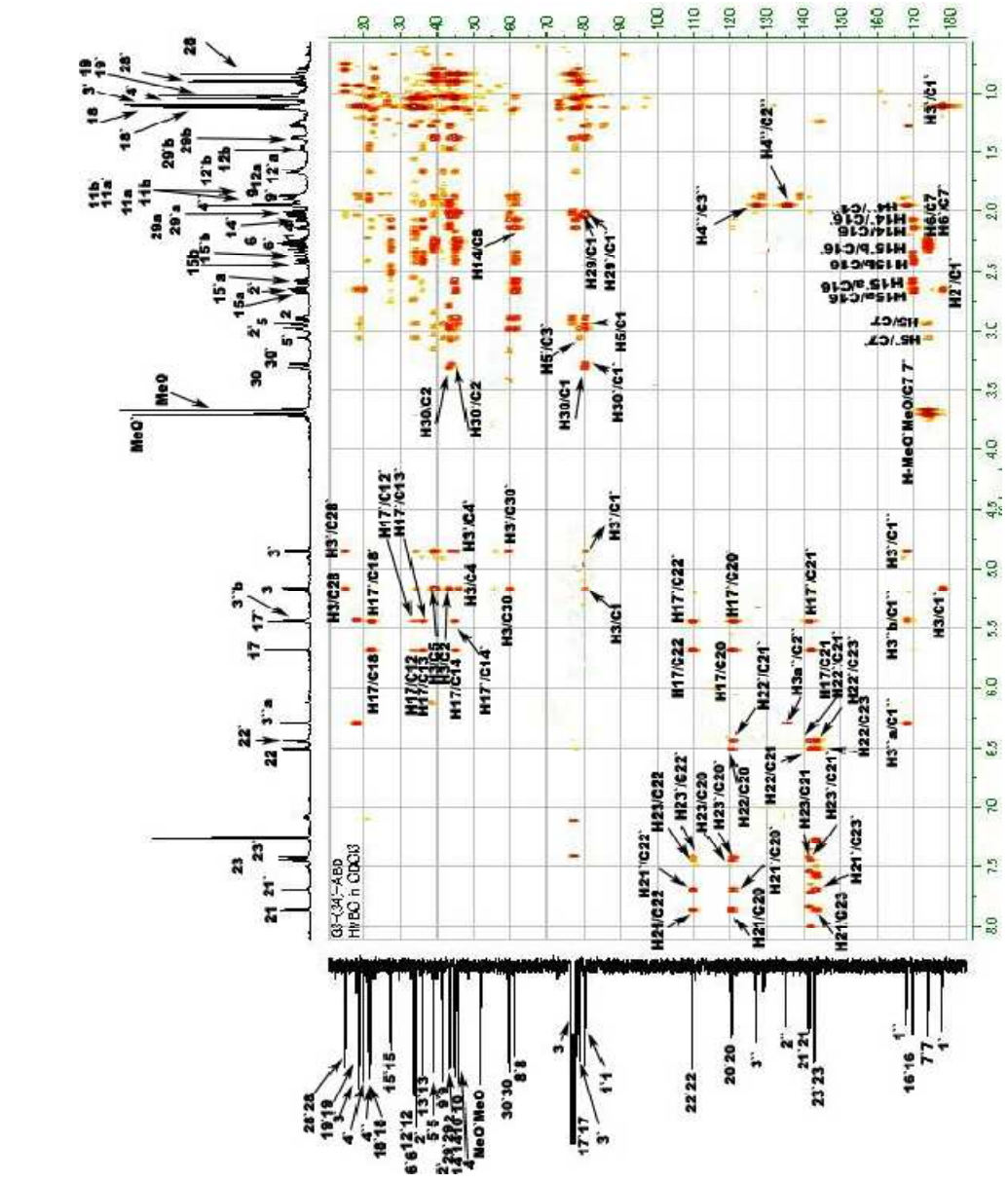

Figure 3.27 : HMBC spectrum of chisomicine D **CC4** & E **CC5**

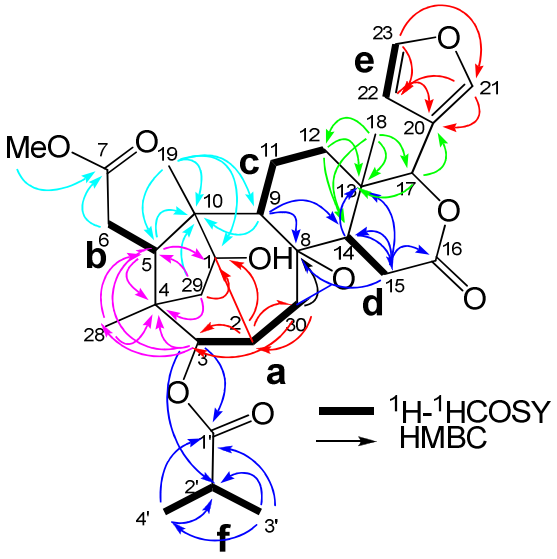

Figure 3.28 : Selected 2D NMR correlations of chisomicine D **CC4**

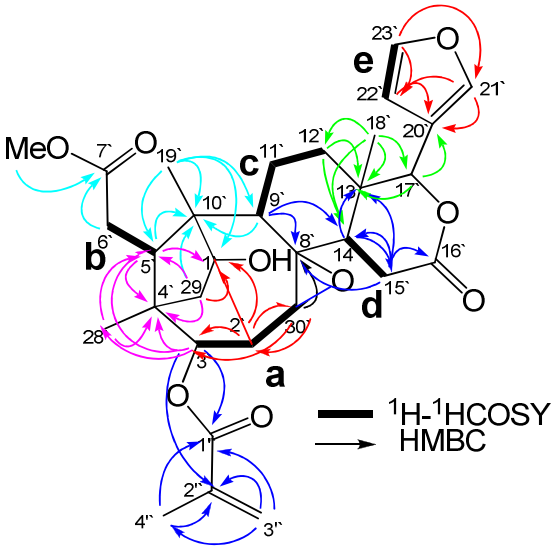

Figure 3.29 : Selected 2D NMR correlations of chisomicine E **CC5**

3.1.6 14-Deoxyxyloccensin K CC6

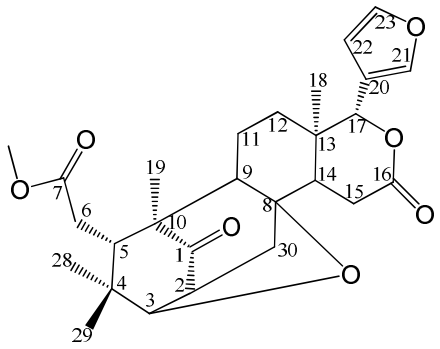

Limonoid **CC6** was isolated as colorless needle crystal, mp 207-208 °C. The UV spectrum showed absorption bands at λ_{max} 200, 283, and 291nm. The IR spectrum showed the presence of carbonyl group at 1733cm^{-1} . The LCMS displayed a pseudomolecular ion peak at *m/z* 471.1822 (471.5626 calculated) $[M+H]^+$, gave the possible molecular formula of ($C_{27}H_{34}O_7$ +H).

The ^{1}H NMR data (Table 3.7, Figure 3.30) of **CC6** displayed the characteristic chemical shifts of furan ring at δ_H 6.43 (1H, br s H-22), 7.41 (1H, brs, H-23), 7.48 (1H, brs, H-21). The ^{1}H-NMR spectrum of **CC6** showed further signals due to four tertiary methyl groups (18, 19, 28, and 29), one methoxy, and two downfield CH groups at δ_H 4.14 and 6.04 which were attributable to proton H-3 and H-17 respectively.

The ^{13}C/DEPT NMR spectra (Table 3.7, Figure 3.31) revealed twenty seven carbon resonances due to three carbonyls (one ester, lactone, and one ketone), one sp^2 quaternary carbons, four sp^3 quaternary carbons, three sp^2 methines, six sp^3 methines, five sp^3 methylenes, and five methyls. Among them, two sp^3 methines δ_C 90.9 (C-3) and 77.4 (C-17), one methyl (52.1), one sp^3 quaternary 82.0 (C-8) and two sp^2 methines δ_C 140.8 (C-21) and 143.0 (C-23) were ascribed to those bearing an oxygen atom. All protons have been correlated with their carbons through HMQC (Table 3.7, Figure 3.32).

Figure 3.33 shows HMBC correlations for **CC6**. Three carbon atoms C- 20, C-21, and C-22 could be reached via H-17, indicated the presence of a β -furyl ring at C-17. Additionally, the HMBC correlations of H-5, H_2-6, and methoxy to C-7 suggested that the methoxy group was attached to C-7 and the whole group (methyl acetate substituent) attached to C-5. It was interesting to observe two downfield carbon signals at the positions of 3 and 8. Therefore, they should be oxygenated in the form of epoxy, that was confirmed by comparing with the literature data [122, 124] and HMBC correlations of H-2 to C-3, C-8 , and C-30; H-30 to C-2 and C-1; and H-3 to C-30. That was supported by COSY (Table 3.7, Figure 3.34) H-2/H-3 and H-2/H-30. Furthermore, the geminal protons of H_2-15 showed the HMBC correlations to C-8, C-14, and C-16.

Finally, the linkages between different methyl groups of the molecule could be easily observed, where there is a cross peak between H_3-18 with C-13, H_3-19 with C10, while the proton signals of H_3-28 and H_3-29, both show HMBC correlations to C-3, C-5, and quaternary carbon C-4, and also H_3-28 could see C-29 and H_3-29 could see C-28 confirming that the two methyl groups should be attached to the same position C-4.

Therefore, compound **CC6** was determined to be a new natural product in its occurrence as 14-deoxyxyloccensin K, and further confirmed by X-Ray refractrometery [125] as shown in (Figure 3.35).

Table 3.7 : 1D (^{1}H and ^{13}C) and 2D (COSY, HMQC, and HMBC) NMR spectral data of 14-deoxyxyloccensin K **CC6**

Po.	δ_H (int.; mult.; J(Hz))	δ_C	COSY	HMQC	HMBC
1		215.4			
2	2.90 (1H, dd, 6.0, 6.0)	49.6	H-3, H-30a	H-C2	1, 8, 30, 10, 3
3	4.14 (1H, d, 11.0)	90.9	H-2	H-C3	1, 5, 8, 28, 30
4		37.3			
5	3.03 (1H, dd, 11.0, 2.0)	43.2	H-6	H-C5	1, 4, 6, 7, 8, 9, 28, 29
6	2.14 (2H,dd, 17.3, 2.2)	32.8	H-5	H-C6	4, 5, 7, 10
7		174.5			
8		82.0			
9	1.53 (1H, m)	56.6	H-11a & b	H-C9	
10		51.6			
11a	2.10 (1H, m)	18.3	H-9, H-11b, H-12b	H_a-C11	
11b	1.48 (1H, m)		H-9, H-11a, H-12a	H_a-C11,	
12a	1.77 (1H, m)	34.2	H-12b, H-11b	H_a-C12	
12b	1.19 (1H, m)		H-12a	H_b-C12	
13		35.2			
14	1.85 (1H, m)	44.0	H-15	H-C14	13, 15, 16, 17
15	2.77 (2H, m)	27.9	H-14	H-C15	8, 14, 16
16		171.2			
17	6.04 (1H, s)	77.4		H-C17	8, 13, 14, 20, 21, 22
18	0.97 (3H, s)	22.3		H_3-C18	12, 13, 14, 17
19	0.90 (3H, s)	17.0		H_3-C19	1, 5, 9, 10
20		121.3			
21	7.48 (1H, brs)	140.8		H-C21	20, 22, 23
22	6.43 (1H, brs)	109.9	H-23	H-C22	20, 21, 23
23	7.41 (1H, brs)	143.0	H-22	H-C23	20, 21, 22
28	1.10 (3H, s)	29.2		H_3-C28	3, 4, 5, 29
29	0.63 (3H, s)	20.4		H_3-C29	3, 4, 5, 28
30a	2.44 (1H,dd, 11.9, 6.0)	44.5	H-30b, H-2	H_a-C30	1, 2, 8, 9
30b	1.70 (1H,dd, 11.9, 6)		H-30a	H_b-C30	1, 3
MeO	3.67 (3H, s)	52.1		H_3-MeO	7

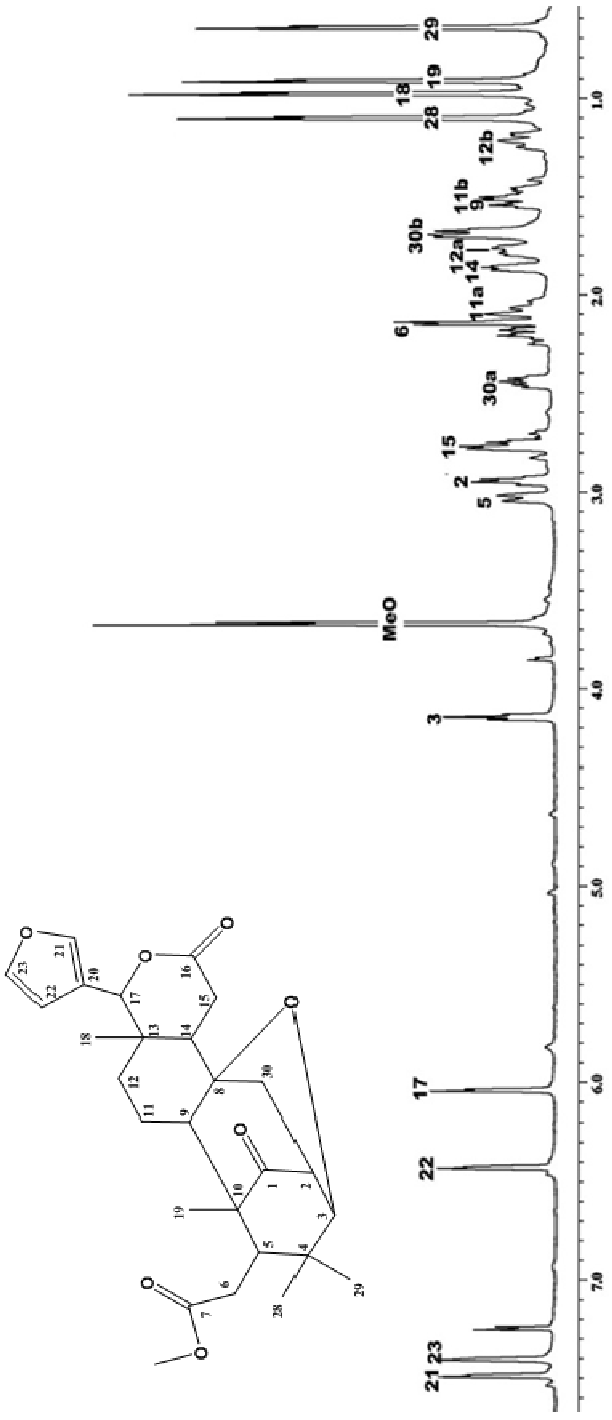

Figure 3.30 : ^{1}H-NMR Spectrum of 14-deoxyxyloccensin K **CC6**

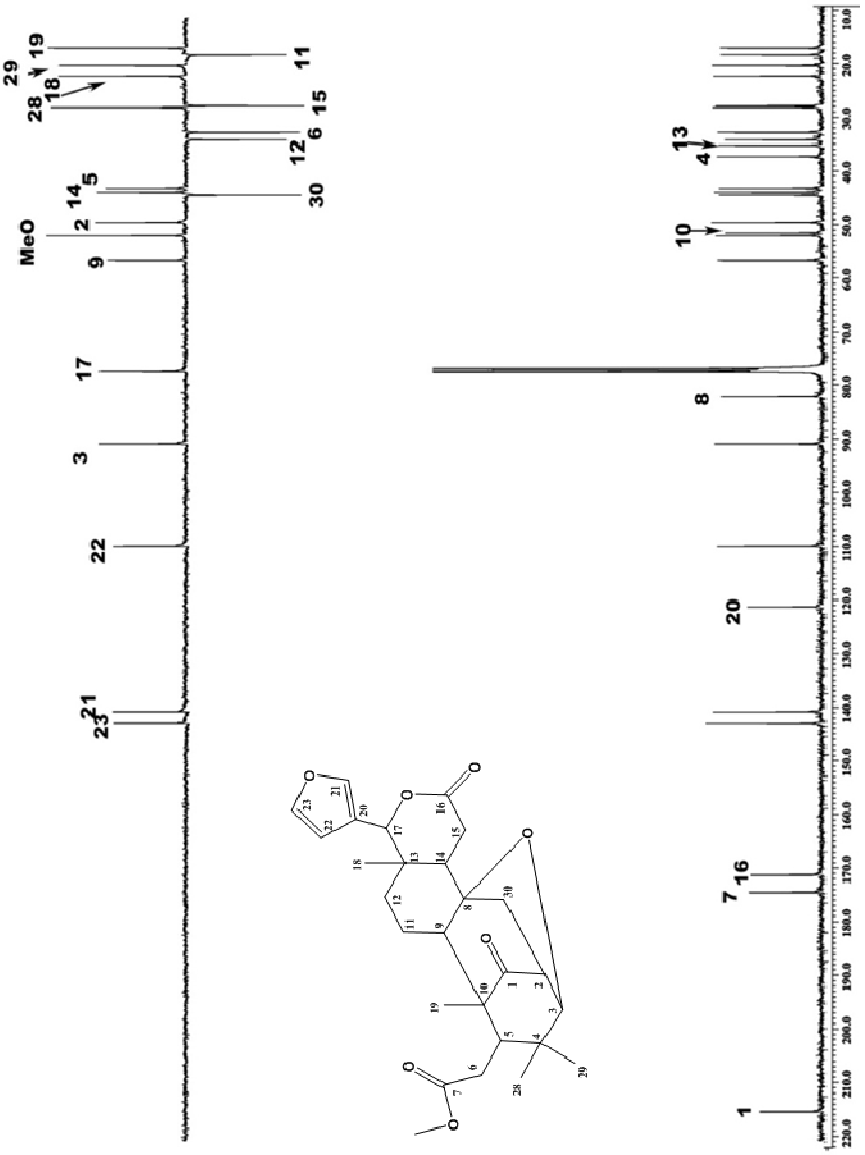

Figure 3.31 : ^{13}C/DEPT Spectra of 14-deoxyxyloccensin K **CC6**

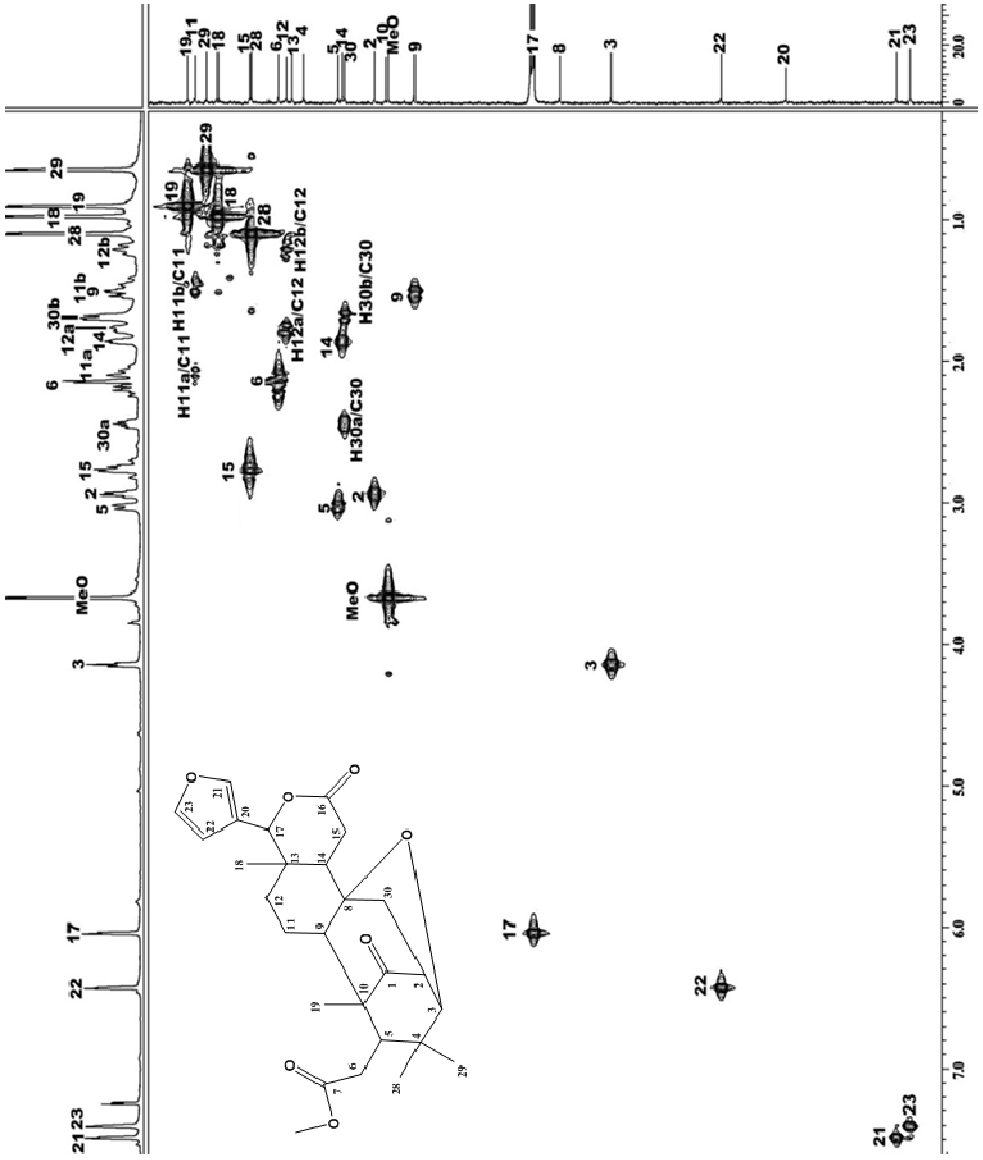

Figure 3.32 : HMQC spectrum of 14-deoxyxyloccensin K **CC6**

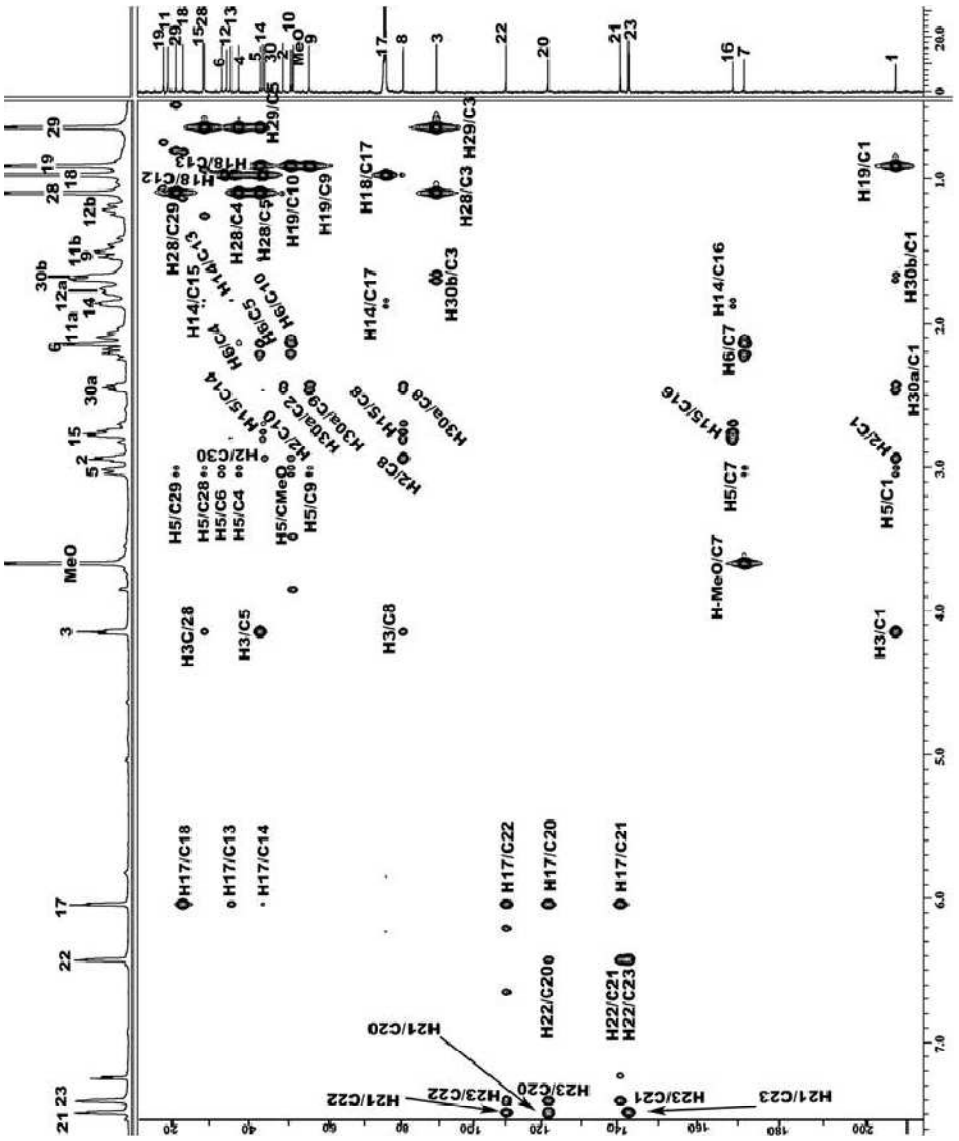

Figure 3.33 : HMBC spectrum of 14-deoxyxvloccensin **K CC6**

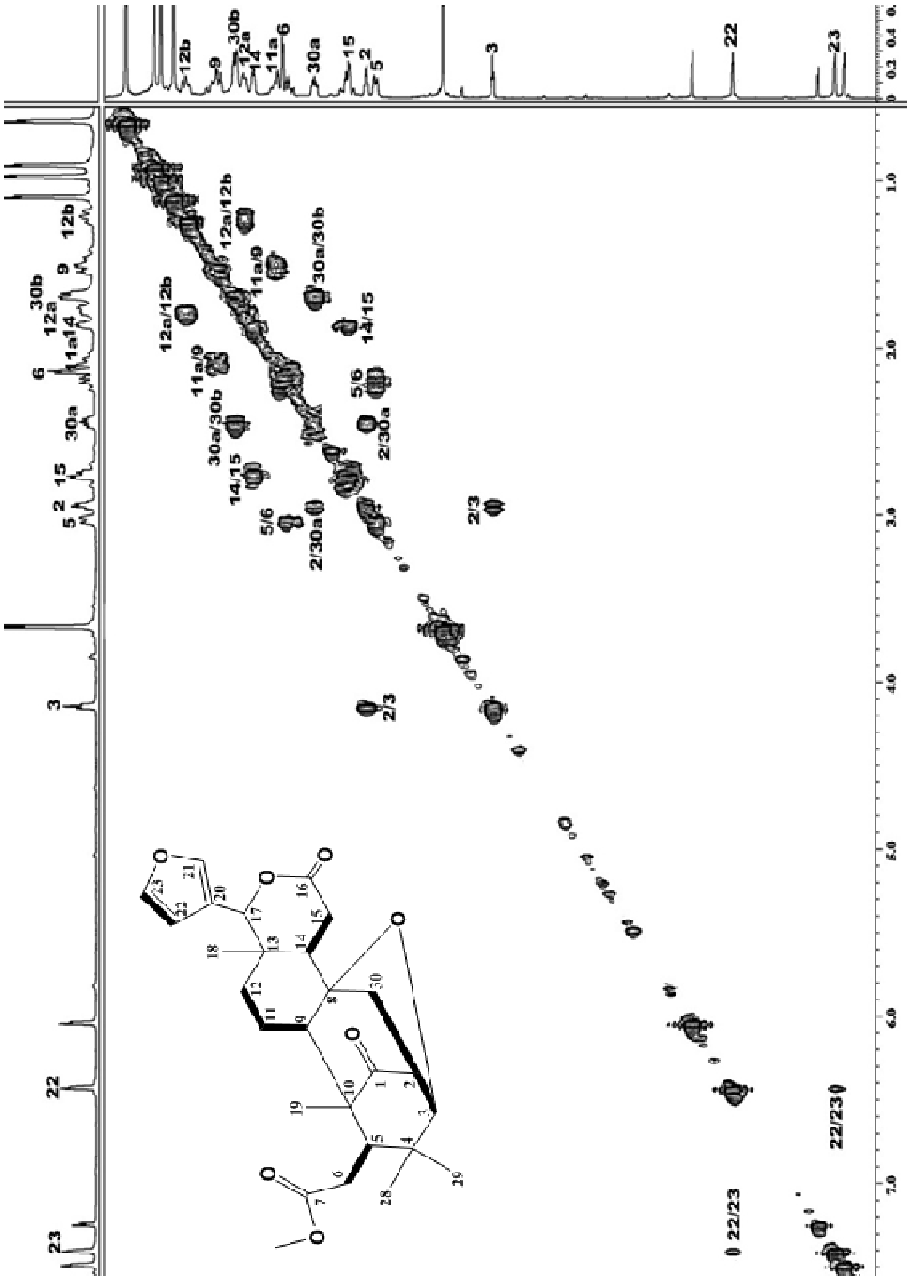

Figure 3.34 : ^{1}H-^{1}HCOSY spectrum of 14-deoxvxvloccensin K **CC6**

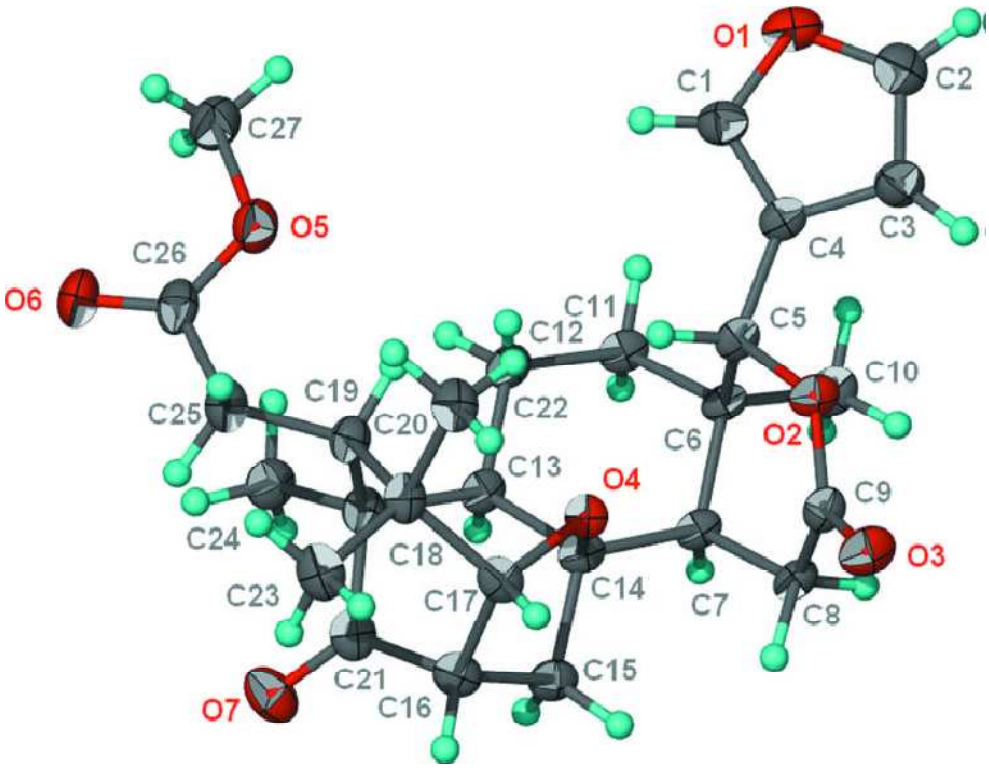

Figure 3.35 : X-Ray structure of 14-deoxyxyloccensin K **CC6**

3.1.7 Proceranoloide CC7

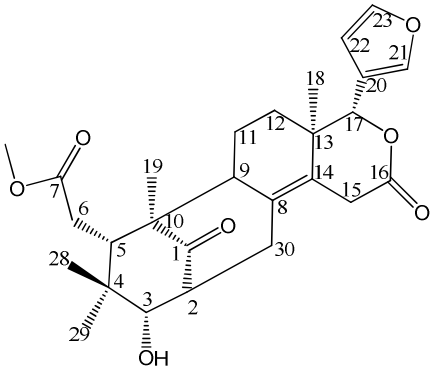

Limonoid **CC7** was isolated as yellow pale oil. The UV absorption showed maxima at λ 200 and 281 nm The IR spectrum exhibited the presence OH at ν_{max} 3435 cm^{-1} and carbonyl group at ν_{max} 1732 cm^{-1} and The LCMS displayed an $[M+H]^+$ ion

peak at *m/z* 471.1882, corresponding to the elemental formula of ($C_{27}H_{34}O_7$+H). IR, UV, and mass closely matched those of **CC6**.

The ^{1}H-NMR spectrum (Table 3.8, Figure 3.36) of **CC7** showed considerable similarity with that of 14-deoxyxyloxccensin K indicating that the two structures are closely related. The most significant difference was the appearance of the double of doublet H-15 signal being shifted in downfield area which caused by extra double bond in the positions of 8 and 14.

The ^{13}C /DEPT NMR spectra (Table 3.8, Figure 3.37) confirmed that **CC7** has three carbonyls, three sp^2 quaternary carbons rather than two in comparison with previous compound, three sp^3 quaternary carbons, three sp^2 methines, five sp^3 methines, five sp^3 methylenes, and five methyls. Among them, two sp^3 methines (δ_C 80.3 and 77.3), one sp^3 methyl (52.1), and two sp^2 methines (δ_C 142.7 and 141.8) were ascribed to those bearing an oxygen atom. So above deduction and further indicated the presence of one extra double bond.

^{1}H-NMR and ^{13}C-NMR data suggested that **CC7** has the same structure of proceranoloide [126]. ^{1}H-^{1}H COSY spectrum (Table 3.8, Figure 3.38) of proceranoloide **CC7** has found the same spin system of the former compound except the COSY connection of H14/H15, where there is no COSY cross peaks between them, that is another approve of the double bond between C-8 and C-14, the compound further approved by HMQC (Table 3.8, Figure 3.39) and HMBC (Figure 3.40).

Table 3.8 : 1D (^{1}H and ^{13}C) and 2D (COSY, HMQC, and HMBC) NMR spectral data of proceranoloide **CC7**

Po.	δ_H (int.; mult.; J(Hz))	δ_C	COSY	HMQC	HMBC
1		220.5			
2	3.04 (1H, m)	50.1	H-3, H-30b	H-C2	1, 8
3	3.73 (1H, d, 10.1)	77.3	H-2	H-C3	5
4		39.4			
5	3.23 (1H, dd, 9.4, 3.1)	39.3	H-6	H-C5	1, 7, 10
6	3.37 (2H, m)	33.6	H-5	H-C6	5, 7, 10
7		174.4			
8		128.3			
9	1.97 (1H, m)	51.9	H-11	H-C9	
10		53.7			
11	1.77 (2H, m)	18.8	H-9, H-11, H-12a	H_a-C11	8
12a	1.7 (1H, m)	28.7	H-11, H-12b	H_a-C12	11, 17
12b	1.01 (1H, m)		H-12a	H_b-C12	
13		38.0			
14		131.6			
15a	4.04 (1H, d, 21.3)	33.4	H-15b	H-C15a	8, 14, 16
15b	3.46 (1H, 21.0, 3.0)		H-15a	H-C15b	8, 14, 16
16		171.4			
17	5.57 (1H, s)	80.3		H-C17	13, 14, 18, 20, 21, 22
18	1.02 (3H, s)	17.6		H_3-C18	12, 13, 14, 17
19	1.12 (3H, s)	17.0		H_3-C19	5, 10,
20		120.9			
21	7.55 (1H, d, 0.8)	141.8		H-C21	20, 22, 23
22	6.48 (1H, d, 0.8)	110.2	H-23	H-C22	20, 21
23	7.37 (1H, dd, 1.6, 1.4)	142.7	H-22	H-C23	20, 21, 22
28	0.72 (3H, s)	20.2		H_3-C28	3, 5, 29
29	0.80 (3H, s)	23.9		H_3-C29	3, 5, 28
30a	3.2 (1H, dd, 16.2, 2.0)	33.2	H-30b	H_a-C30	8, 14
30b	1.97 (1H, m)		H-30a, H-2	H_b-C30	3, 8, 14
MeO	3.68 (3H, s)	52.1		H_3-MeO	7

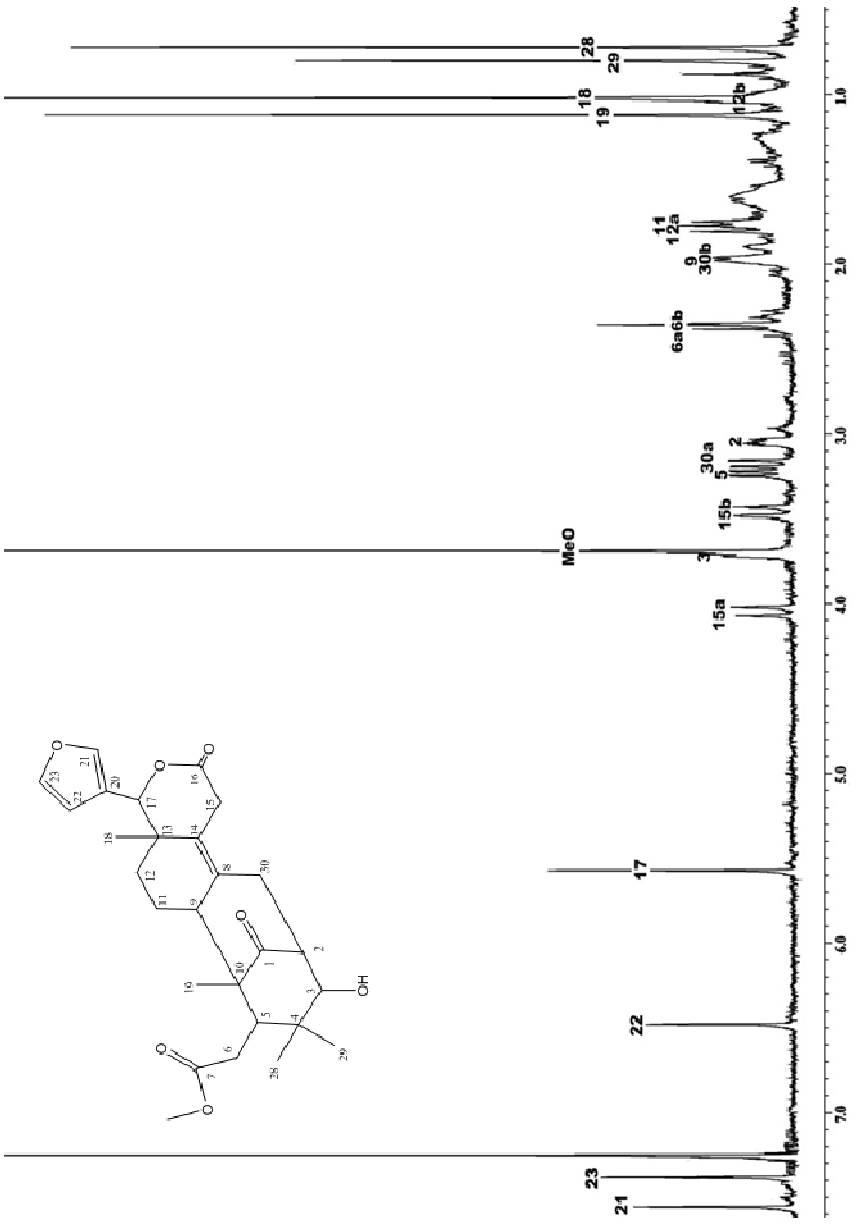

Figure 3.36 : ^{1}H-NMR spectrum of proceranoloide **CC7**

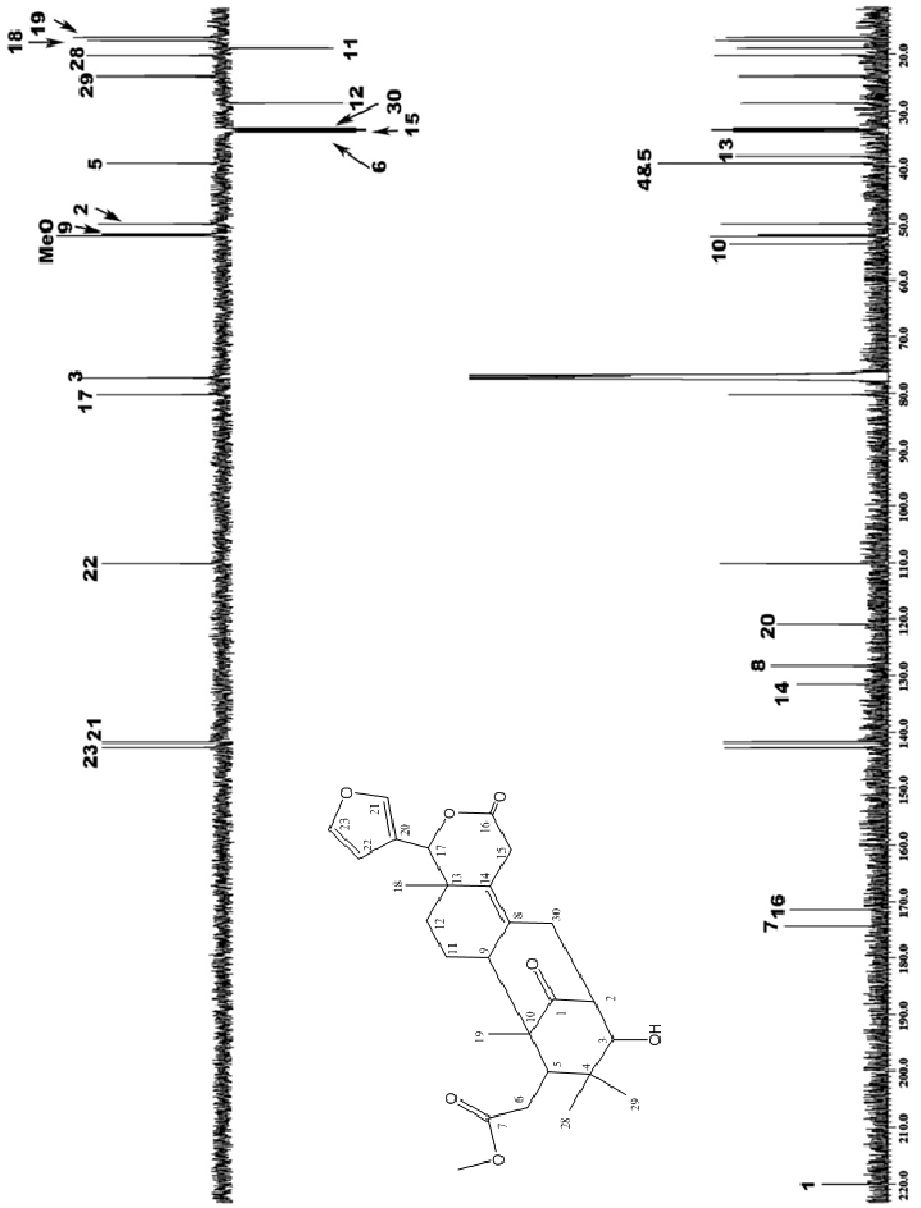

Figure 3.37 : ^{13}C -NMR and DEPT spectra of proceranoloide **CC7**

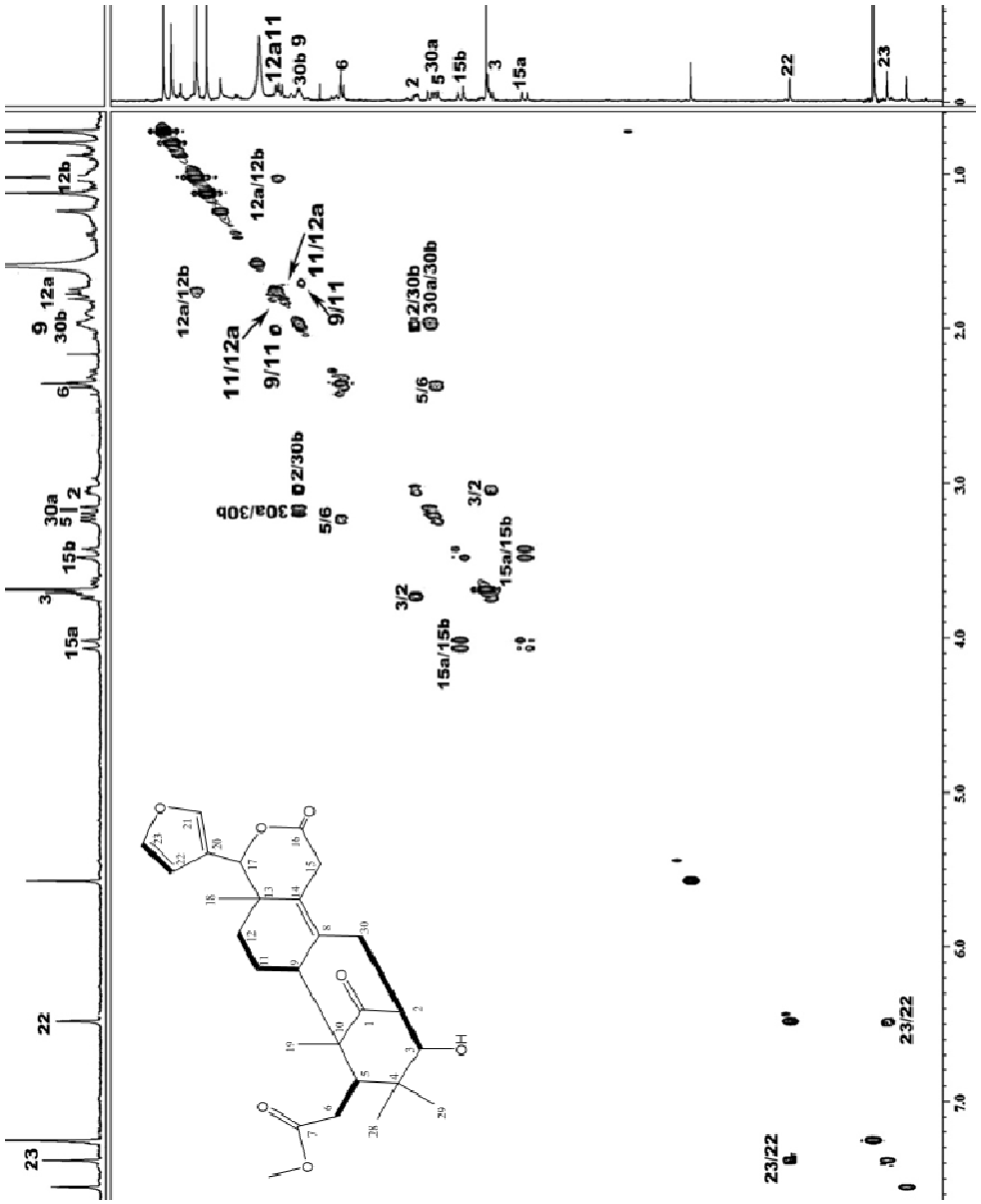

Figure 3.38 : ^{1}H - ^{1}H COSY spectrum of proceranoloide **CC7**

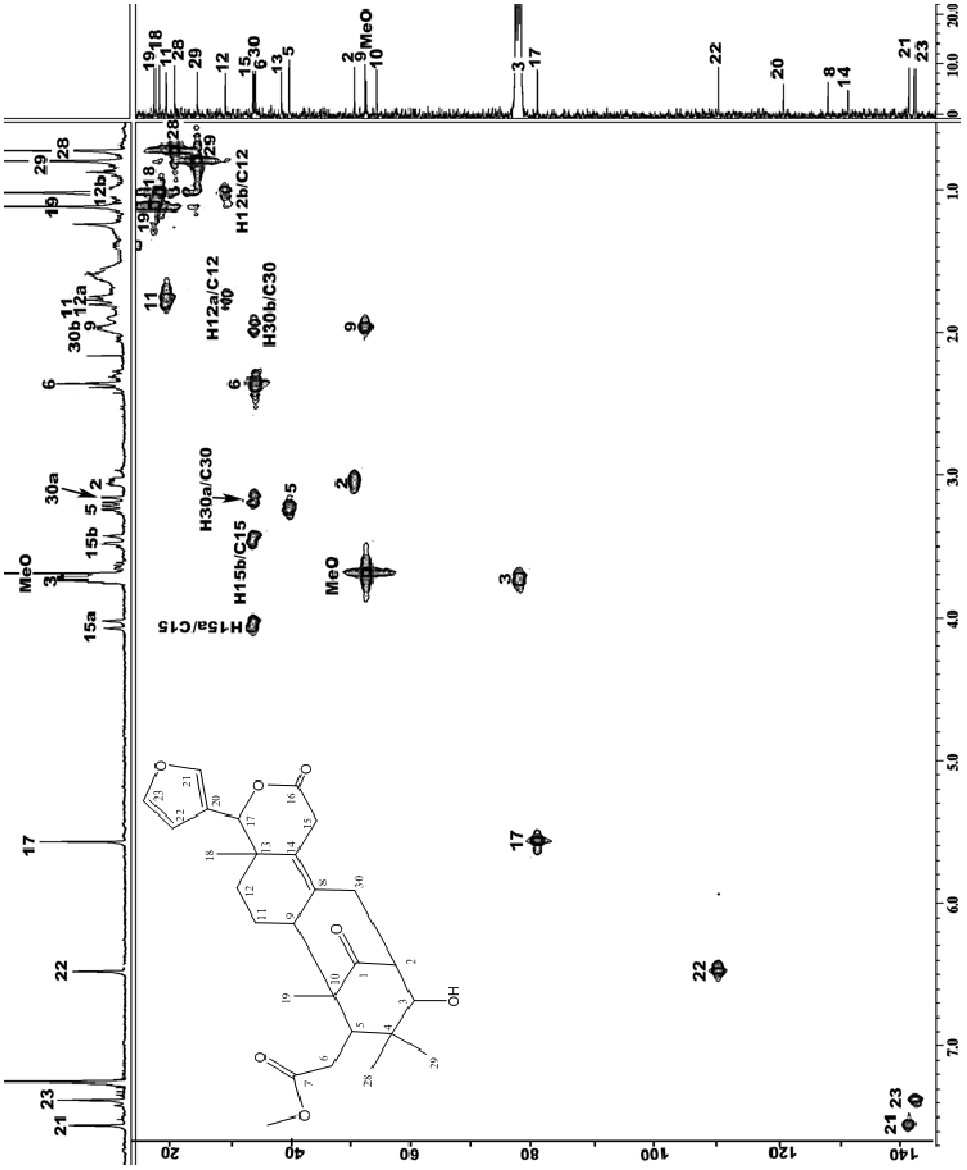

Figure 3.39 : HMQC spectrum of proceranoloide **CC7**

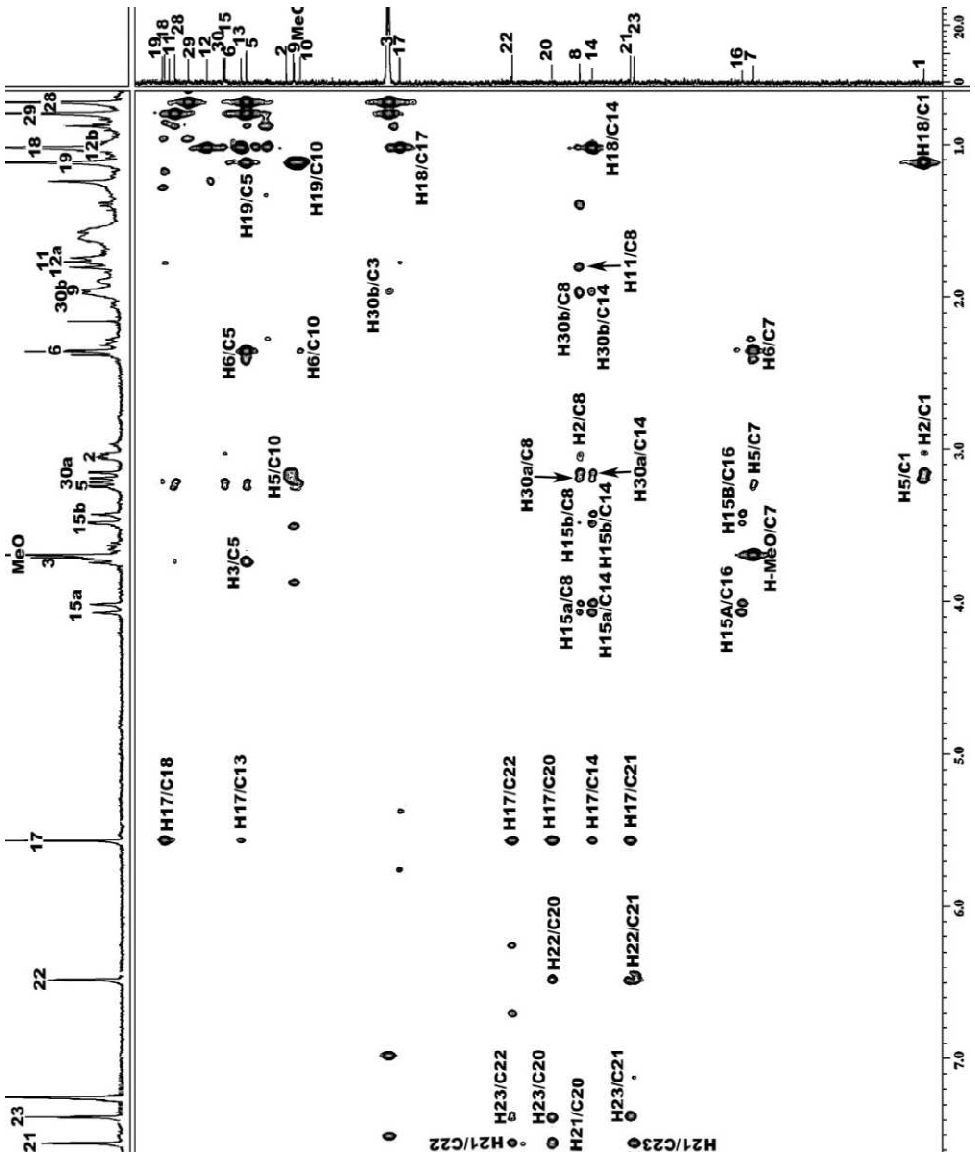

Figure 3.40 : HMBC spectrum of proceranoloide **CC7**

A plausible biogenetic pathway for limonoids (**CC1**–**CC7**), which might be derived from andirobin skeleton by Michael cyclization and further oxidation proposed to form mexicanolide skeleton **CC6** and **CC7**, as shown in Scheme 3.1. While chisomicine B, D, and E (**CC2, CC4**, and **CC5** respectively), with a phragmalin skeleton could be biosynthesized from the coupling of C-1 – C-29 of a mexicanolide skeleton, and an oxidative cleavage of C-1 – C-2 bond in chisomicine B, D, and E (**CC2**, **CC4**, and **CC5**) followed by dehydroxylation would yield chisomicine A **CC1**. Whereas chisomicine C **CC3** might be biosynthesized from a mexicanolide skeleton after oxidation at C-29 followed by formation of hemiketal linkage.

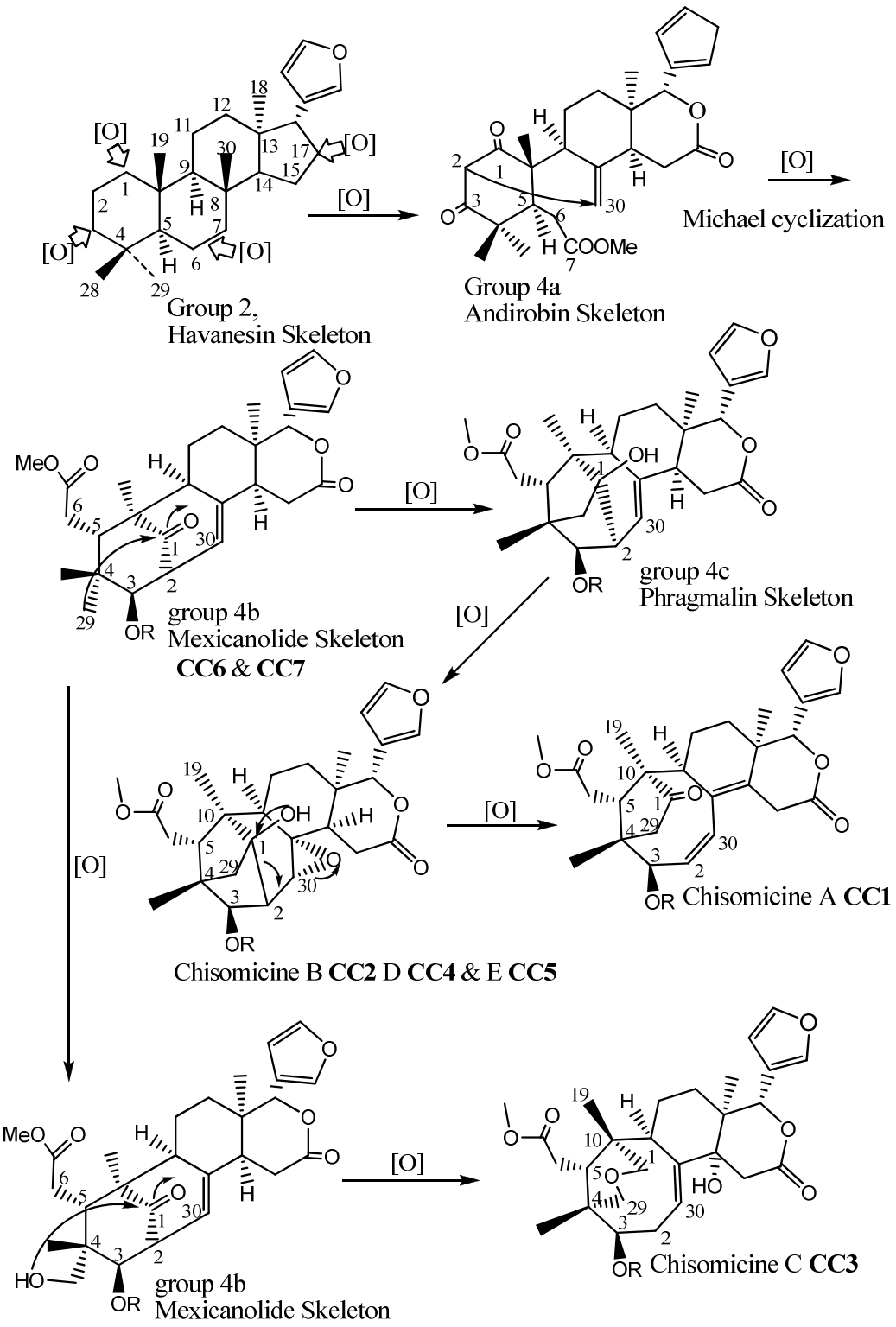

Scheme 3.1 : Plausible biogenetic path way for chisomicines A–E (**CC1–CC7**).

3.2 Steroids and phenolic compounds from the bark of *Chisocheton tomentosus*

The bark of *Chisocheton tomentosus* yielded thirty eight compounds among them fifteen were new and one new as crystal, they were four steroids; 7*α*-Hydroxy-*β*-sitosterol **CT1** (new as crystal form), stigmasta-4,6-diene-3-one **CT2**, stigmasterol **CT3** and sitosterol **CT4,** and thirty two phenolic compounds; hydroxy acid derivatives of ferulate **CT5A-P** among them **CT5A, CT5C, CT5D, CT5K, CT5L, CT5M, CT5N, CT5O,** and **CT5P** were new, *E*-alkyl-*p*-coumarate **CT6A-O** among them **CT6B**, **CT6C, CT6L**, **CT6M**, **CT6N**, and **CT6O** were new, ferulaldehyde **CT7**, vanillin **CT8** and the last one was styryl lactone (goniothalamin) **CT9**. The percentage yielded of the isolated steroids, as shown in Table 3.9.

Table 3.9 : Chemical constituents of *Chisocheton tomentosus*

Compounds	Type of compounds	%yield
7*α*-Hydroxy-*β*-sitosterol **CT1**	steroid	2
stigmasta-4,6-diene-3-one **CT2**	steroid	0.05
stigmasterol **CT3** and sitosterol **CT4**	steroid	2.1
hydroxy acid derivatives of ferulate **CT5A-O**	phenolic	0.5
E-alkyl-*p*-coumarate **CT6A-O**	phenolic	0.09
ferulaldehyde **CT7**	phenolic	0.35
vanillin **CT8**	phenolic	0.26
goniothalamin **CT9**	styryl lactone	0.5

3.2.1 7*α*-Hydroxy-*β*-sitosterol CT1

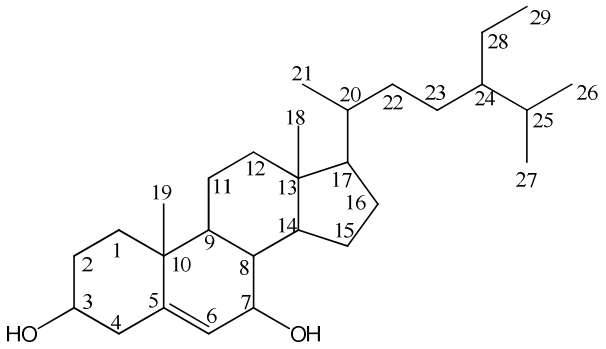

The compound was isolated as a colorless crystal mp 138-140 °C, the UV spectrum showed absorption at λ_{max} 302 nm and 254nm. The IR spectrum indicated the presence of hydroxyl group by the absorption band at ν_{max} 3430 cm^{-1}; the GCMS spectrum revealed a molecular ion peak $[M]^+$ at m/z 430, Corresponding for molecular formula $C_{29}H_{50}O_2$.

The ^{1}H-NMR spectrum (Table 3.10, Figure 3.41) of **CT1** showed six methyl groups resonated as singlets, doublets and triplet in the region of δ_H 0.65-0.95. A characteristic doublet for H-6 methine proton appeared at δ_H 5.55 indicating the presence of double bond functionality between C-5 and C-6, two downfield signals at δ 3.81 and 3.54 were assigned to the H-7 and H-3 respectively, indicating to the presence of oxygen functionality at their carbons.

The broadband decoupled ^{13}C- NMR spectrum (Table 3.10, Figure 3.42) of **CT1** displayed twenty-nine carbon atoms in the molecule, the DEPT spectra exhibited six methyl, ten methylene and ten methine carbons, while the remaining three carbons were quaternary as deduced from broadband spectrum. No signals was observed beyond δ_C 146.3 and, therefore, it was concluded that no ketonic function in this molecule in comparison with the next compound. The downfield signals at δ_C 146.3 was attributed to olefinic quaternary carbon, the C-6 olefinic methine carbon appeared at δ_C 123.8, two more signals for oxygen-bearing carbons at δ_C 71.3 and 65.4 were ascribed to C-3 and C-7 respectively.

The COSY spectrum (Figure 3.43) indicated the presence of two major spin systems, spin system "**a**" and spin sysyem "**b**", spin system "**a**" started with the couplings of C-3 proton with the C-4 methylene protons, meanwhile, spin system "**b**" the olefinic proton of C-6 showed vicinal connectivity with C-7 methine proton.

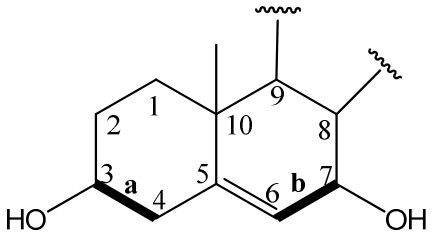

All protons of methyl, methylene, sp^3 methine, and sp^2 methine were approved by HMQC (Table 3.10, Figure 3.44). The HMBC spectrum of **CT1** (Table 3.10, Figure 3.45) showed long range correlation of C-19 proton with quaternary carbon of C-10, similarly C-18 methyl protons showed HMBC connectivity with quaternary C-13, so they show that the methyl group (19 and 18) should be attached directly with C-10 and C-13 respectively, and the long chain substituent should be attached in the position of C-17 according to their correlations by HMBC.

Based on UV, IR, GC-MS (Figure 3.46), $^{1}H/^{13}C$ NMR, and comparing with literature review, it was concluded that the molecule should be 7α-Hydroxy-β-sitosterol [127-130]. This was further supported by X-Ray reflection technique (Figure 3.47) [131].

Table 3.10 : 1D (^{1}H and ^{13}C) and 2D (HMQC, and HMBC) NMR spectral data of of 7*α*-hydroxy-*β*-sitosterol **CT1**

Position	δ_H (int.; mult.; J(Hz))	δ_C	HMQC	HMBC
1a	1.80 (1H, m)	37.08	H_a-C1	1,3,5,10
1b	1.01 (1H,m)		H_b-C1	1,3,5,10
2a	1.80 (1H, m)	31.3	H_a-C2	1, 3
2b	1.47 (1H, m)		H_b-C2	1, 3
3	3.54 (1H, m)	71.3	H-C3	
4	2.29 (2H, d, 5)	42.0	H_2-C4	2,5,6,10
5		146.3		
6	5.55 (1H, d, 5.0)	123.8	H-C6	4,7,8,10
7	3.81 (1H, brs)	65.4	H-C7	5,6,9
8	1.43 (1H, m)	37.5	H-C8	14,10,4,13,9
9	1.15 (1H, m)	42.3	H-C9	8,10,11,12,19
10		37.4		
11	1.49 (2H, m)	20.7	H_2-C11	9,10,12,13
12a	1.97 (1H, m)	39.2	H_a-C12	9,13,14
12b	1.12 (1H, m)		H_b-C12	9,13,14
13		42.2		
14	1.41 (1H, m)	49.4	H-C14	15,16,17,18
15a	1.66 (1H, m)	24.3	H_a-C15	
15b	1.08 (1H, m)		H_a-C15	
16a	1.83 (1H, m)	28.3	H_a-C16	13,20,21
16b	1.22 (1H, m)		H_a-C16	13,20,21
17	1.14 (1H, m)	55.7	H-C17	18, 21, 15,16
18	0.65 (3H, s)	11.7	H_3-C18	12,13, 14, 17
19	0.95 (3H, s)	19.2	H_3-C19	1, 2, 9, 10, 11
20	1.33 (1H, m)	36.1	H-C20	17, 18, 23, 24
21	0.89 (3H, d, 6.4)	18.3	H_3-C21	17, 20, 22
22	2.24 (2H, m)	33.8	H_2-C22	
23	1.22 (2H, m)	29.8	H_2-C23	22, 24, 25
24	0.93 (1H, m)	49.4	H-C24	29, 26, 27
25	1.64 (1H, m)	29.0	H-C25	24, 26, 27, 28
26	0.81 (3H, m)	19.9	H_3-C26	24, 28
27	0.77 (3H, m)	18.9	H_3-C27	24, 25, 26
28	1.22 (2H, m)	23.1	H_2-C28	23,24, 25, 27, 29
29	0.83 (3H, m)	12.1	H_3-C29	23, 24, 25, 28

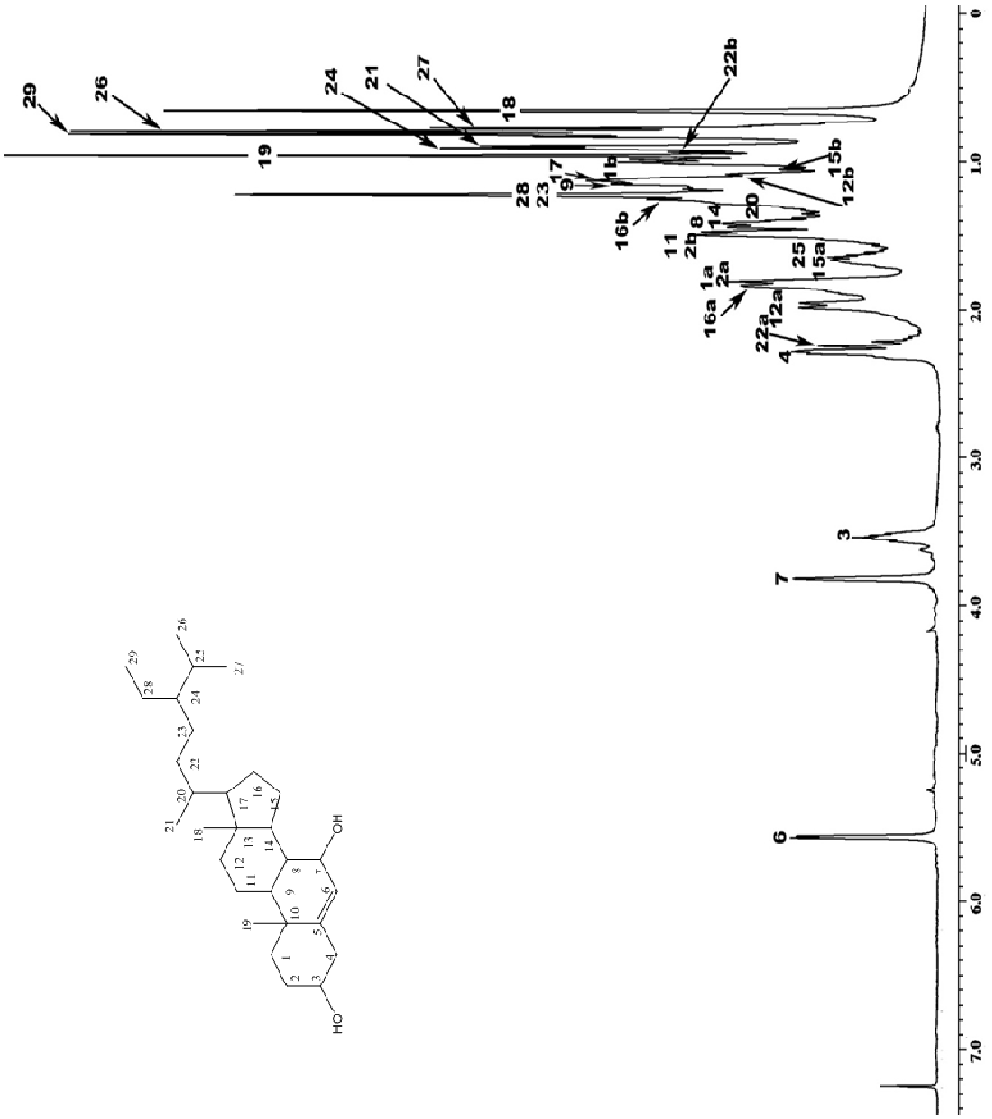

Figure 3.41 : ^{1}H-NMR spectrum of 7α-hydroxy-β-sitosterol **CT1**

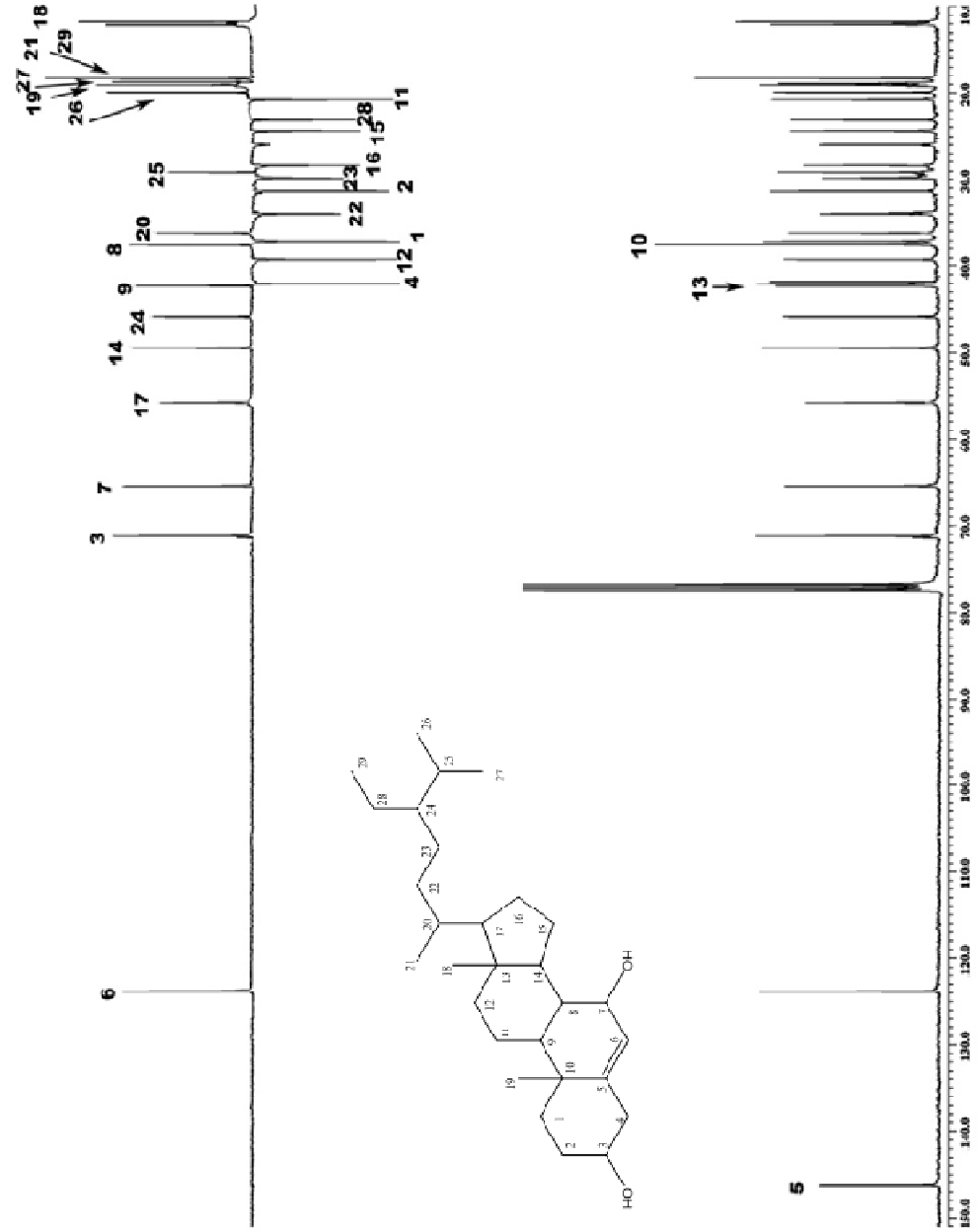

Figure 3.42 : ^{13}C-DEPT NMR spectra of 7 α -hydroxy-β-sitosterol **CT1**

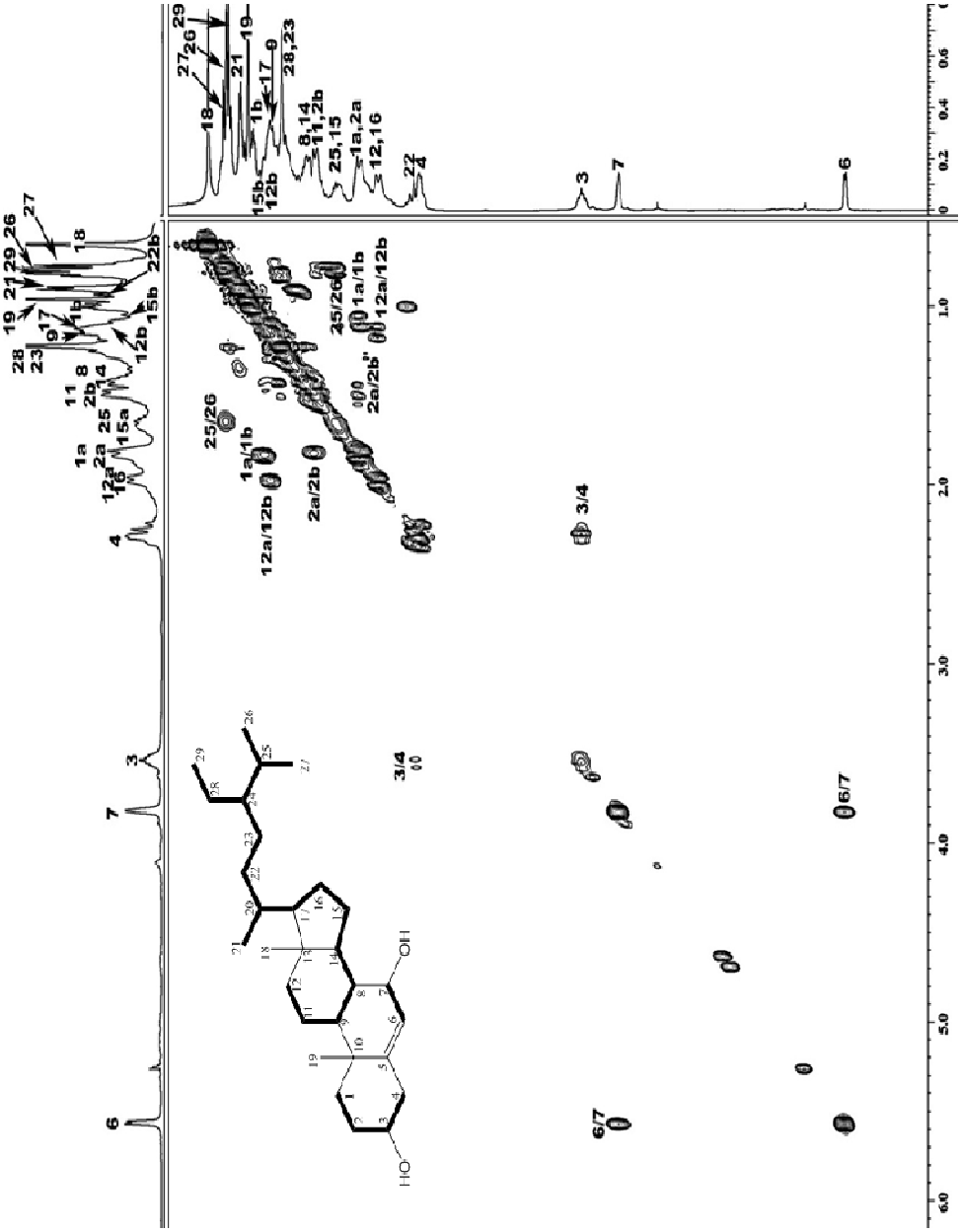

Figure 3.43 : ^{1}H-^{1}H COSY spectrum of 7 α -hydroxy-β-sitosterol **CT1**

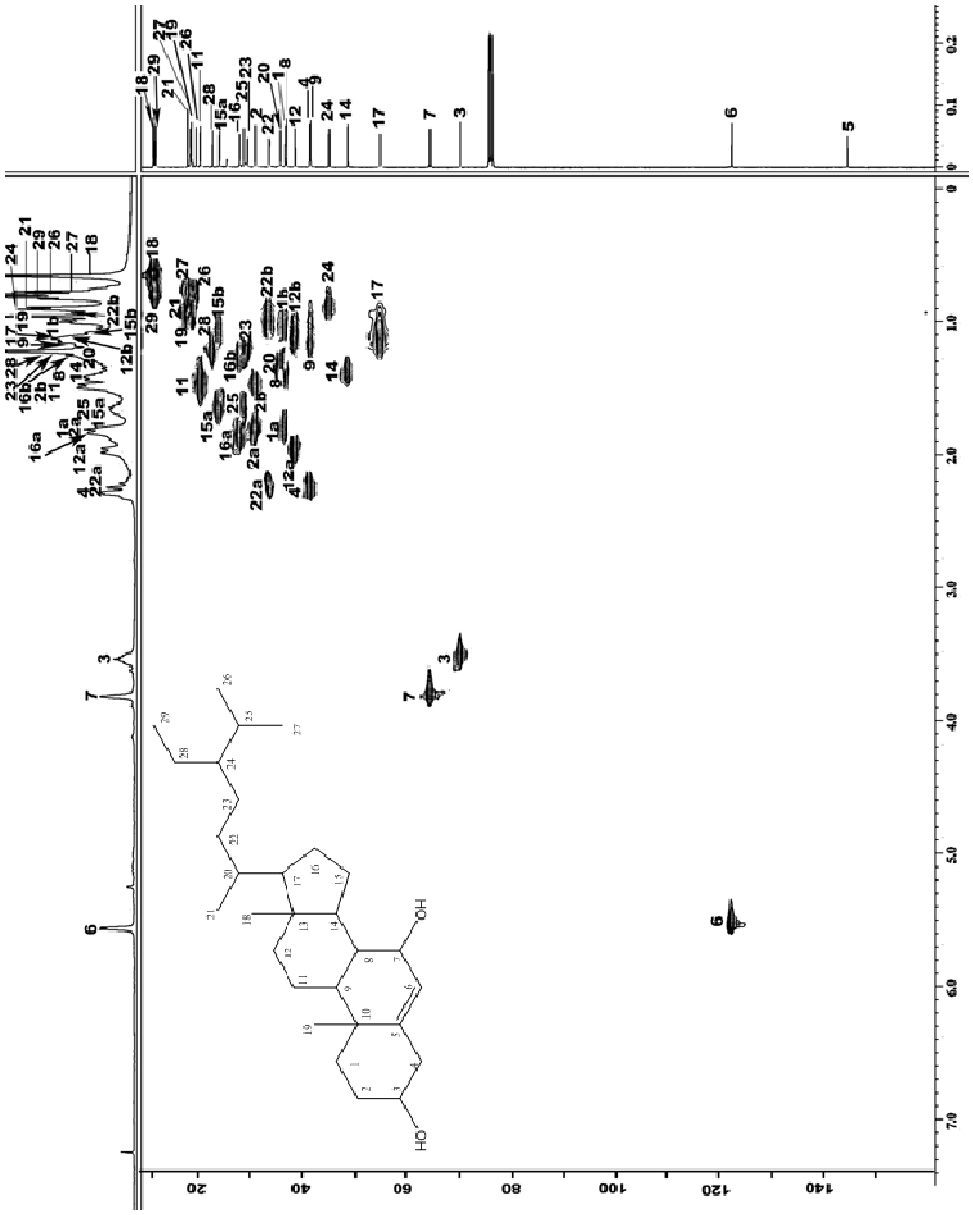

Figure 3.44 : HMQC spectrum of 7 ***α*** -hydroxy-*β*-sitosterol **CT1**

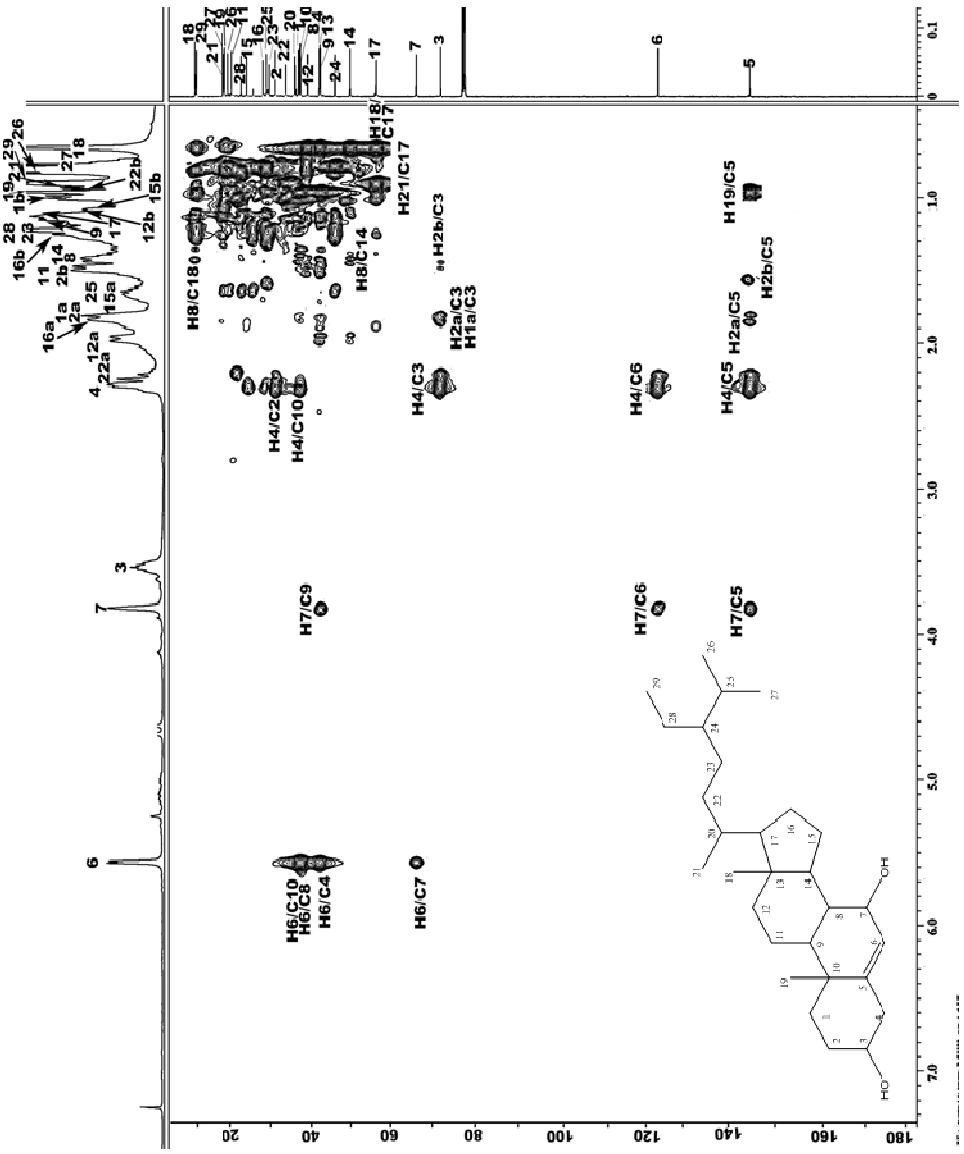

Figure 3.45 : HMBC spectrum of 7 α -hydroxy-β-sitosterol **CT1**

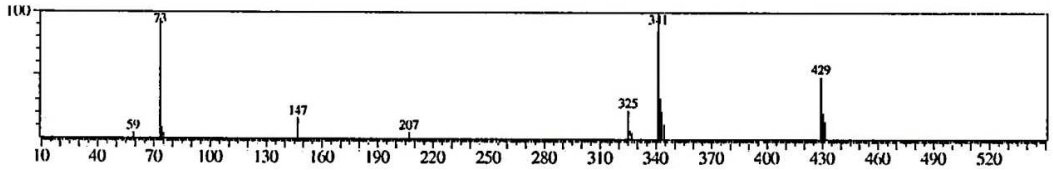

Figure 3.46 : GCMS of 7*α*-hydroxy-*β*-sitosterol **CT1**

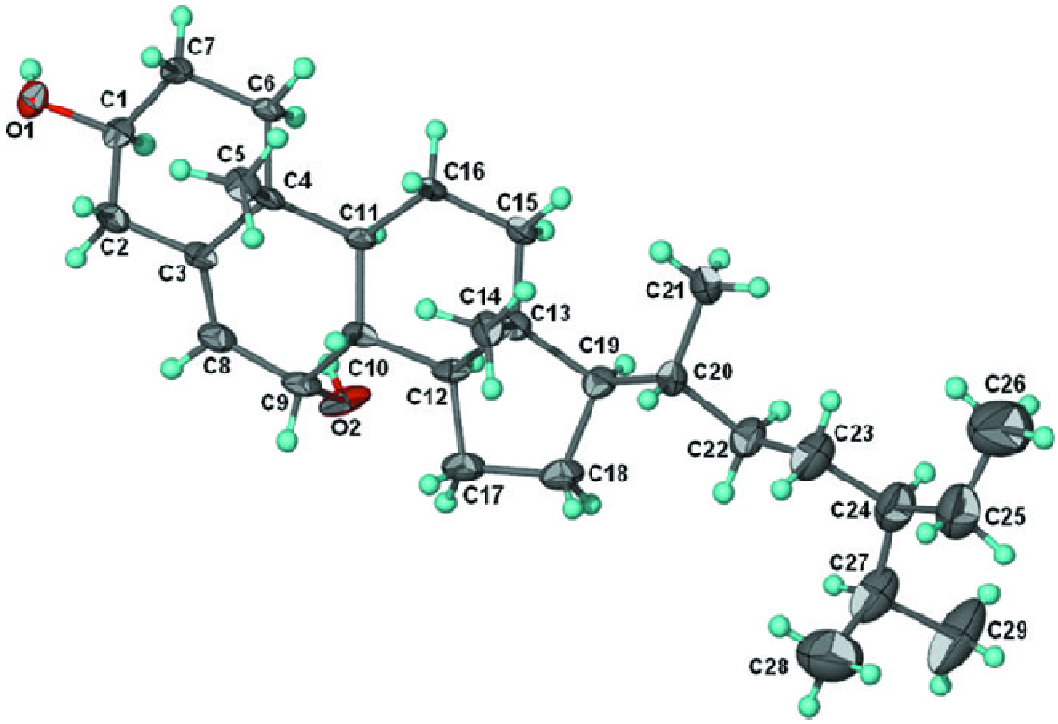

Figure 3.47 : X-Ray structure of 7*α*-hydroxy-*β*-sitosterol **CT1**

3.2.2 4,6-stigmastadiene-3-one CT2

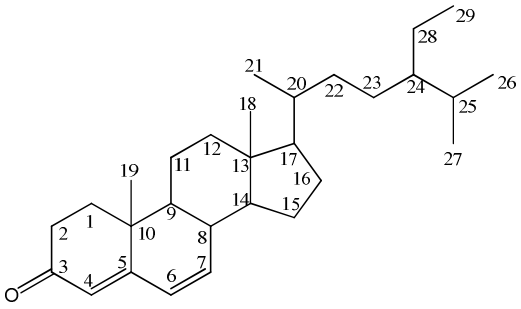

Compound **CT2** was isolated as white amorphous, UV spectrum showed absorption at λ_{max} 282 nm. The IR spectrum indicated the presence of conjugated ketone at ν_{max} 1670cm^{-1} , 1620, 1588, and 875 (conjugated diene); the LCMS spectrum revealed a molecular ion peaks $[M]^+$ at m/z 410 corresponding to molecular formula $C_{29}H_{46}O$.

The ^{1}H-NMR spectrum (Figure 3.48, Table 3.11) of **CT2** was closely resemble with compound **CT1** (7-hydroxy *β*-sitosterol), it showed six methyl groups resonated as singlets, doublets and triplet in the region of δ_H 0.74-1.09. A diagnostic downfield signals at δ_H 5.64 (singlet), 6.06 (dd, $J_{6,7}$=10 Hz, $J_{6,4}$= 2.5), and 6.09 (triplet, $J_{7,6}$ and $J_{7,8}$= 10) were ascribed to C-4, C-6, C-7 olefinic protons, respectively. Downfield multiplet signals at δ_H 2.55 and 2.42 were attributed to two geminal protons of C-2 vicinal to ketone, the multiplicity signals of C-2 protons again indicated the presence of carbonyl at vicinal C-3. This indicating the presence of 4,6-diene-3-oxo system in the rings A and B.

The ^{13}C-NMR spectrum (Figure 3.49, Table 3.11) of **CT2** displayed twenty-nine carbon signals; the DEPT spectra indicated the presence of six methyl, nine methylene and ten methine carbons, while the remaining four carbons were quaternary as deduced from broadband spectrum. The downfield signals at δ_C 199.8 was assigned to the 3-oxo-carbon, the signals at δ_C 123.5, 164.2, 127.8, and 141.8 were ascribed to the olefinic C-

4, C-5, C-6, C-7 respectively. By comparison of its data with the reported data, the compound **CT2** was identified as a known stigmasta-4,6-diene-3-one [132-133]. This was further supported by two-dimentional NMR spectroscopy HMQC (Figure 3.50, Table 3.11).

The COSY spectrum (Figure 3.51) indicated the presence of two major selected fragments, spin system in the fragment "**a**" and spin system in the fragment "b", spin system "**a**" started with the couplings of C-1 protons with the C-2 methylene protons, meanwhile, spin system "b" started with the couplings of olefinic proton of C-6 with C-7 methine proton which in turn showed couplings with C-8 methine proton and so on. These homonuclear couplings helped in the construction of the double bond in the fragment "**b**" which conjugated with the double bond of C-4 and C-5

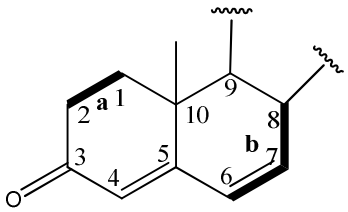

selected ^{1}H-^{1}H COSY

The C-19 methyl protons at junction of rings A and B showed HMBC connectivity (Figure 3. **52**, Table 3.11) with sp^3 quaternary carbon of C-10, sp^2 quaternary carbon of C-5, methylene of C-1 and methine carbon of C-9. Similarly, C-2 methyene protons showed HMBC correlations with ketonic carbon at C-3 and methylene carbon of C-1, indicating that the ketone should be at the position C-3.

By comparing the spectral data and LCMS (Figure 3.53) of **CT2** with reported data [132-133]; the compound **CT2** was identified as stigmasta-4,6-diene-3-one.

Table 3.11 : 1D (^{1}H and ^{13}C) and 2D (HMQC, and HMBC) NMR spectral data of 4,6-stigmastadiene-3-one **CT2**

Position	δ_H (int.; mult.; J(Hz))	δ_C	HMQC	HMBC
1a	1.96 (1H, m)	39.9	H_a-C1	2, 10, 19, 5
1b	1.70 (1H, m)		H_b-C1	2, 10, 19
2a	2.55 (1H, m)	34.0	H_a-C2	1, 3
2b	2.42 (1H, m)		H_b-C2	10, 3
3		199.8	H-C3	
4	5.64 (1H, s)	123.5	H_2-C4	2, 6, 19, 20
5		164.2		
6	6.06 (1H, dd, 10.0, 2.5)	127.8	H-C6	4, 5, 8
7	6,09 (1H, t, 10.0)	141.8	H-C7	5,8,9,14
8	2.18 (1H, m)	37.8	H-C8	6, 7, 9, 14
9	1.18 (1H, m)	50.7	H-C9	12, 14
10		36.1		
11a	1.57 (1H, m)	20.7	H_a-C11	12
11b	1.42 (1H, m)		H_b-C11	12
12a	2.05 (1H, m)	39.6	H_a-C12	9, 11, 14
12b	1.24 (1H, m)		H_b-C12	13, 18
13		43.5		
14	1.25 (1H, m)	53.4	H-C14	16, 18
15a	1.77 (1H, m)	23.8	H_a-C15	
15b	1.25 (1H, m)		H_a-C15	
16	1.14 (2H, m)	26.1	H-C16	
17	1.14 (1H, m)	56.0	H-C17	13, 18, 20
18	0.74 (3H, s)	11.9	H_3-C18	12, 13, 14, 17
19	1.09 (3H, s)	16.4	H_3-C19	1, 5, 9, 10
20	1.36 (1H, m)	36.2	H-C20	21
21	0.90 (3H, m)	18.7	H_3-C21	
22a	1.36 (1H, m)	39.9	H_a-C22	
22b	1.02 (1H, m)		H_b-C22	
23a	1.90 (1H, m)	28.3	H_a-C23	
23b	1.30 (1H, m)		H_b-C23	
24	0.90 (1H, m)	45.9	H-C24	26, 27, 29
25	1.66 (1H, m)	29.1	H-C25	24, 26, 27, 28
26	0.81 (3H, m)	19.9	H_3-C26	24, 28
27	0.77 (3H, m)	19.0	H_3-C27	24, 25, 26
28	1.22 (2H, m)	23.1	H_2-C28	23,24, 25, 27, 29
29	0.83 (3H, m)	12.0	H_3-C29	23, 24, 25, 28

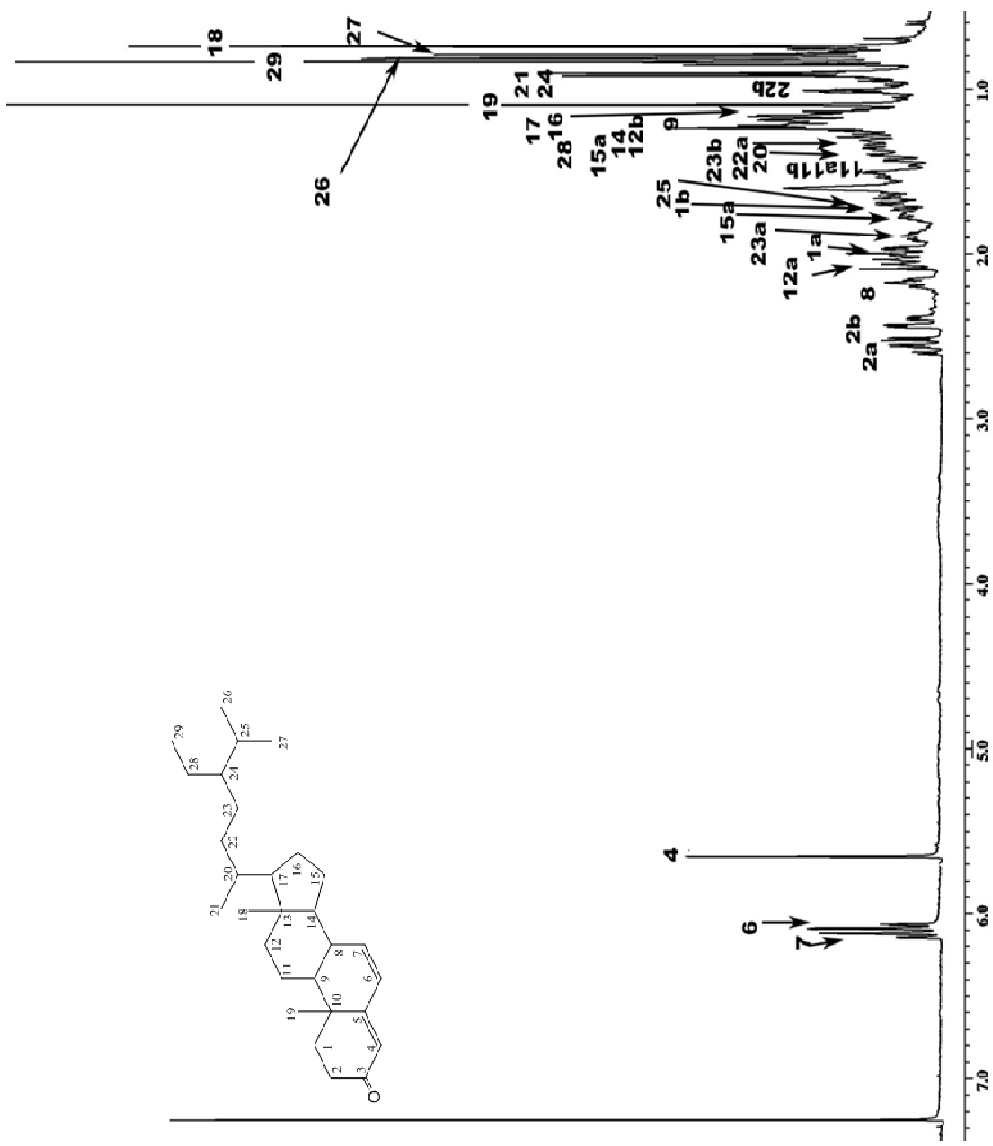

Figure 3.48 : ^{1}H-NMR spectrum of stigmasta-4,6-diene-3-one **CT2**

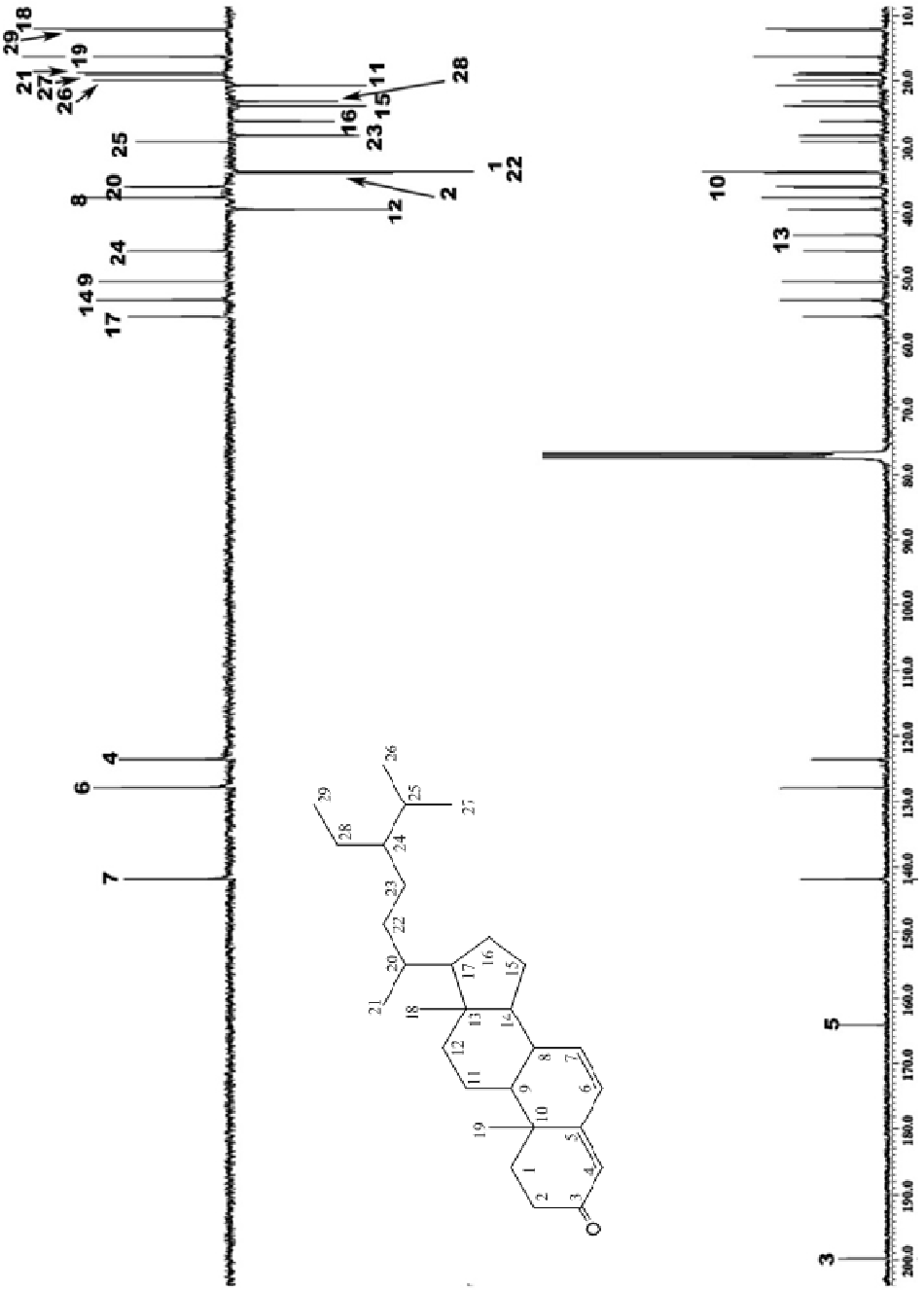

Figure 3.49 : ^{13}C/DEPT NMR spectra of stigmasta-4,6-diene-3-one **CT2**

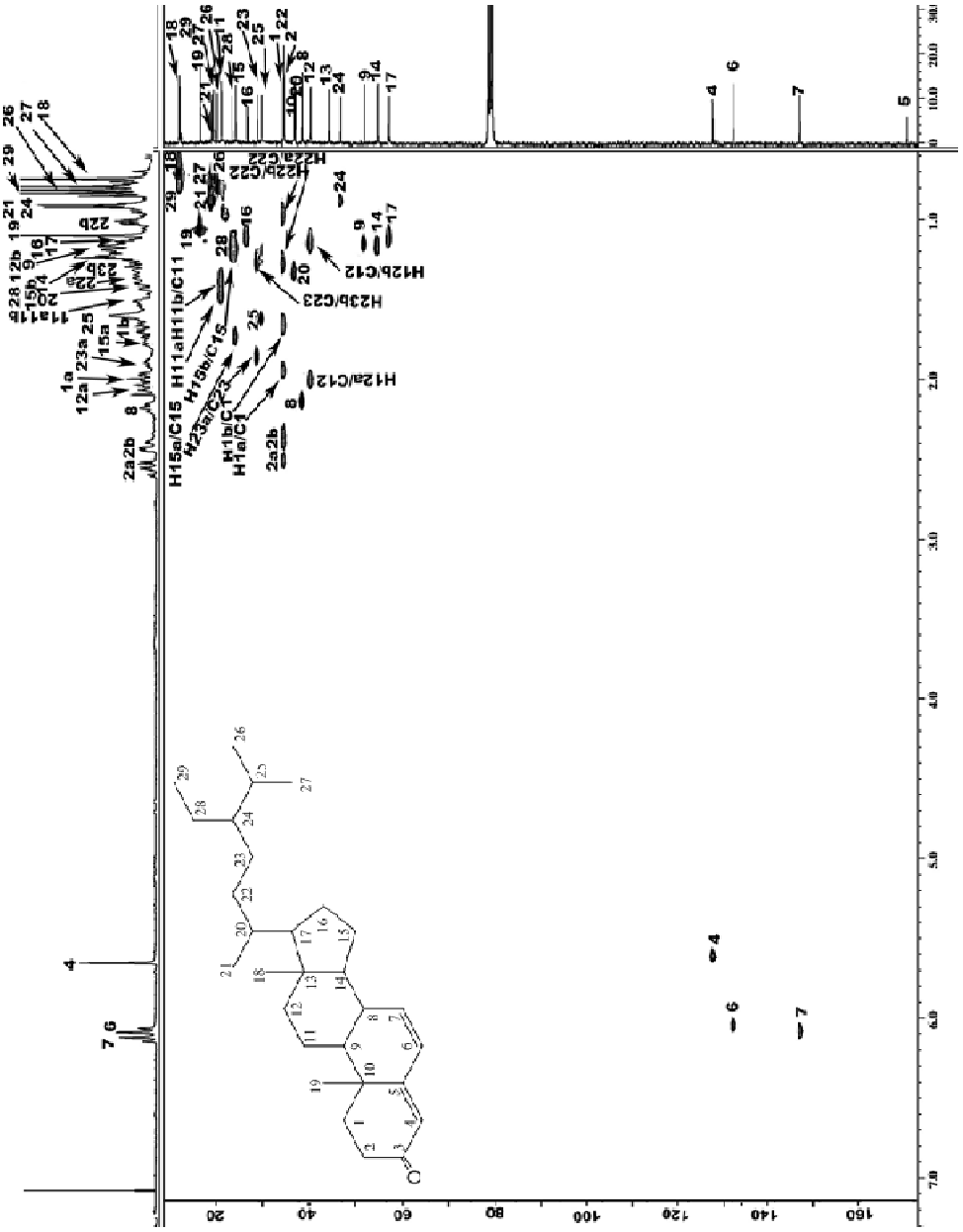

Figure 3.50 : HMQC spectrum of stigmasta-4,6-diene-3-one **CT2**

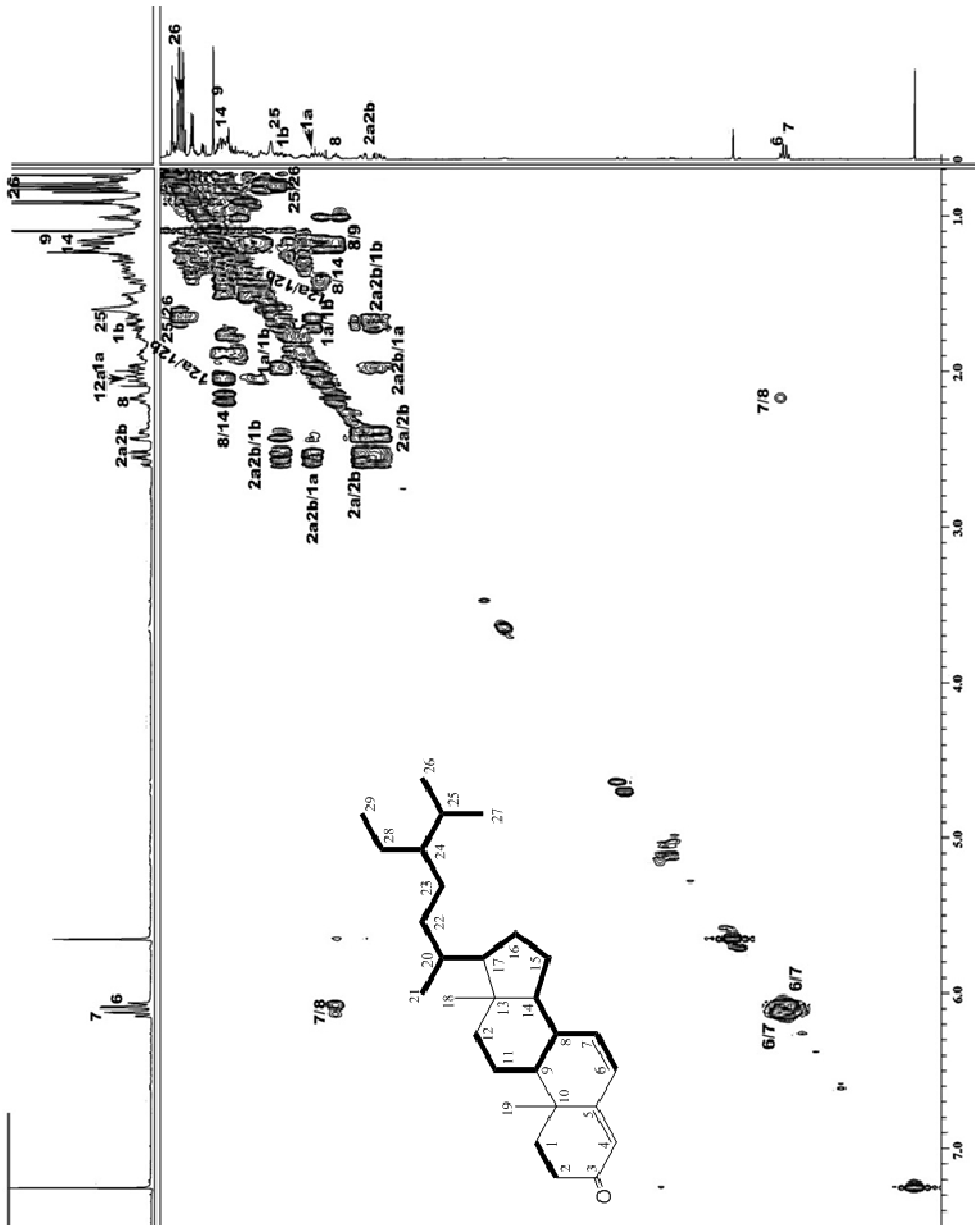

Figure 3.51 : ^{1}H-^{1}H COSY spectrum of stigmasta-4,6-diene-3-one **CT2**

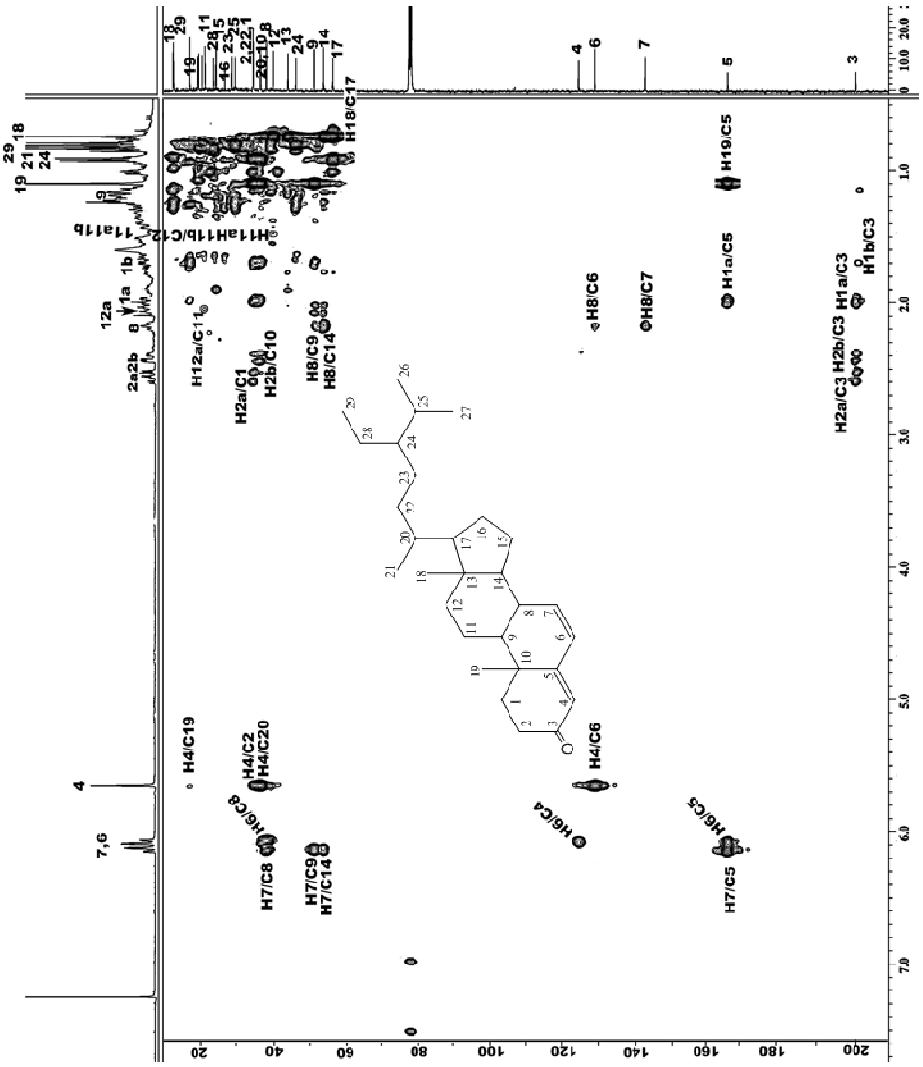

Figure 3. 52 : HMBC spectrum of stigmasta-4,6-diene-3-one **CT2**

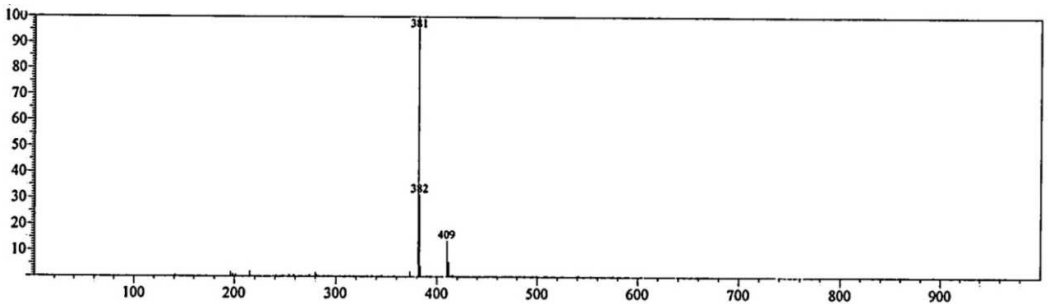

Figure 3.53 : LCMS of stigmasta-4,6-diene-3-one **CT2**

3.2.3 Stigmasterol CT3 and *β*-sitosterol CT4

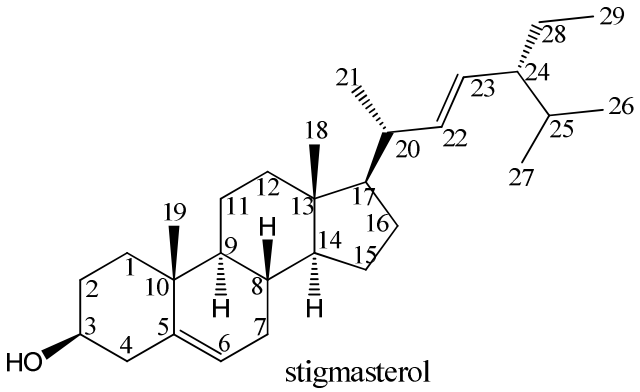

stigmasterol

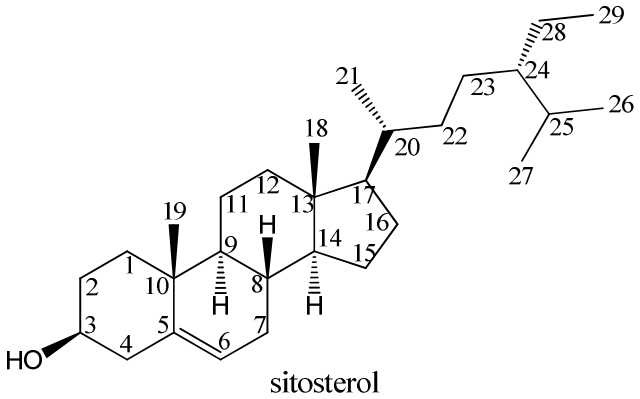

sitosterol

Compound **CT3** and **CT4** were isolated as a mixture of a white solid with the same R_f values. The UV spectrum showed absorption bands at λ_{max} 302 and 254 nm. The infrared (IR) spectrum indicated the presence of hydroxyl group by the absorption bands at ν_{max} 3430 cm^{-1}. The presence of stigmasterol **CT3** was confirmed by the LCMS (Figure 3.56) showing a molecular peak $[M+H]^+$ at *m/z* 413 and 415, corresponding to the molecular formula $C_{29}H_{49}O$ and $C_{29}H_{51}O$ respectively.

Sterols with an ethyl group at C-24, such as stigmasterol and *β*-sitosterol are by far the most abundant compounds in most plants.

The mixture of these two compounds was analyzed by ^1H and ^{13}C-NMR spectroscopy. The ^1H-NMR spectrum (Table 3.12, Figure 3.54) of this mixture showed twelve methyl groups (six methyl groups for each compound) resonated as singlets, doublets and triplets in the region of δ_H 0.65-1.00. In the ^1H-NMR spectrum, the signal

a methine proton attached to C-6 of both compounds resonated further downfield as a doublet at δ_H 5.32, the most significant differences on the ^{1}H-NMR chemical shift of these two molecules were the proton signals of C-22 and C-23. In the compound **CT3,** the presence of a double bond at position C-22 gave rise to two-doublet of a doublet signals at δ_H 4.96 and 5.09 which were belong to H-23, and H-22, respectively. In compound **CT4**, the protons of two ethylene groups C-22 and C-23, gave rise as multiplets in the region of δ_H 0.90- 2.00. The rest of the protons resonated as multiplets in the region of δ_H 0.7-3.5.

The integration of H-6, H-22 and H-23 appeared to be in the ratio of 1:0.25:0.25. Therefore, it could be deduced that the mixture of isolated stigmasterol and *β*-sitosterol was in the ratio of approximately 1:2.

Since compound **CT3** and **CT4** have an identical sterol skeleton, the ^{13}C/DEPT spectra (Table 3.12, Figure 3.55) of this mixture showed quite similar chemical shifts. The most significant differences on the chemical shift of these two molecules were the signals of C-22 and C-23. For compound **CT3**, the sp^2 carbons; C-22 and C-23 resonated at δ_C 138.3 and 129.2, respectively. The presence of the double bond also moved C-20, C-21, C-24, C-25 and C-28 further downfield at δ_C 40.5, 21.2, 51.2, 31.9 and 25.4 respectively, as compared to that of compound **CT4**, which showed the signals at δ_C 36.1, 18.8, 45.8, 29.1 and 23.1 for C-20, C-21, C-24, C-25 and C-28, respectively.

By comparing the NMR spectra data with the literature value [134-140], it was confirmed that compound **CT3** was a stigmasterol and compound **CT4** was a *β*-sitosterol.

Table 3.12 : 1D (^{1}H and ^{13}C) and 2D (HMBC) NMR Spectral Data of **CT3** and **CT4**

Position	**δ_H (int.; mult.; J(Hz))**	**δ_C**	**δ_H (int.; mult.; J(Hz))**	**δ_C**
1a	1.81 (1H, m)	37.2	1.81 (1H, m)	37.2
1b	1.04 (1H, m)		1.04 (1H, m)	
2a	1.79 (1H, m)	29.7	1.79 (1H, m)	31.6
2b	1.50 (1H, m)		1.50 (1H, m)	
3	3.51 (1H, m)	71.8	3.46 (1H, m)	71.8
4	2.27 (1H, m)	42.3	2.27 (1H, m)	39.8
5		140.7		140.7
6	5.32 (1H, m)	121.7	5.32 (1H, m)	121.7
7	1.93 (1H, m)	31.9	1.93 (1H, m)	31.9
	1.50 (1H, m)		1.50 (1H, m)	
8	1.45 (1H, m)	31.9	1.45 (1H, m)	31.9
9	0.92 (1H, m)	50.1	0.92 (1H, m)	50.1
10		36.5		36.5
11	1.50 (2H, m)	21.1	1.50 (2H, m)	21.1
12	1.95 (1H, m)	39.7	1.95 (1H, m)	42.3
	1.17(1H, m)		1.17 (1H, m)	
13		42.2		42.3
14	1.00 (1H, m)	56.8	1.00 (1H, m)	56.7
15	1.54 (1H, m)	24.3	1.54 (1H, m)	24.3
	1.04 (1H, m)		1.04 (1H, m)	
16	1.65 (1H, m)	28.9	1.65 (1H, m)	28.2
17	1.12 (1H, m)	55.9	1.12 (1H, m)	56.0
18	0.67 (3H, s)	12.0	0.65 (3H,s)	11.8
19	1.00 (3H, s)	19.4	1.00 (3H, s)	19.4
20	2.00 (1H, m)	40.5	1.95 (1H, m)	36.1
21	0.98 (3H, m)	21.2	0.98 (3H, m)	18.8
22	5.09 (1H, *d*, 15.1)	138.3	0.93 (1H, m)	33.9
			1.99 (1H, m)	
23	4.96 (1H, *d*, 15.1)	129.2	1.04 (1H, m)	26.0
24	1.52 (1H, m)	51.2	1.47 (1H, m)	45.8
25	1.53 (1H, m)	31.9	1.47 (1H, m)	29.1
26	0.83 (3H,m)	21.1	0.80 (3H, m)	19.8
27	0.80 (3H, m)	19.9	0.78 (3H, m)	19.0
28	1.43 (1H, m)	25.4	1.21 (1H, m)	23.0
	1.17 (1H, m)		1.11 (1H, m)	
29	0.81 (3H, t)	12.2	0.89 (3H, m)	12.0

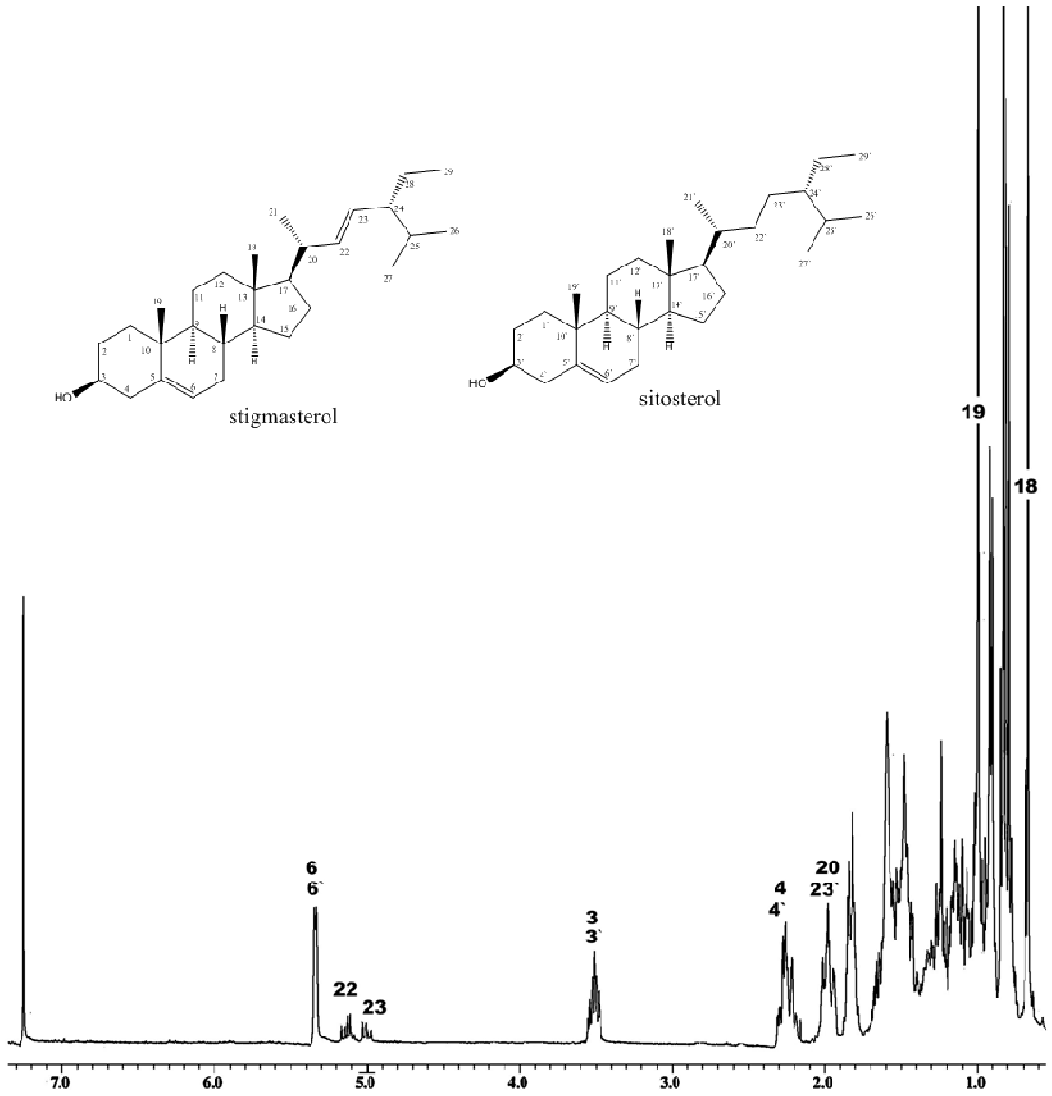

Figure 3.54 : ^{1}H-NMR spectrum of a mixture of stigmasterol **CT3** and *β*-sitosterol **CT4**

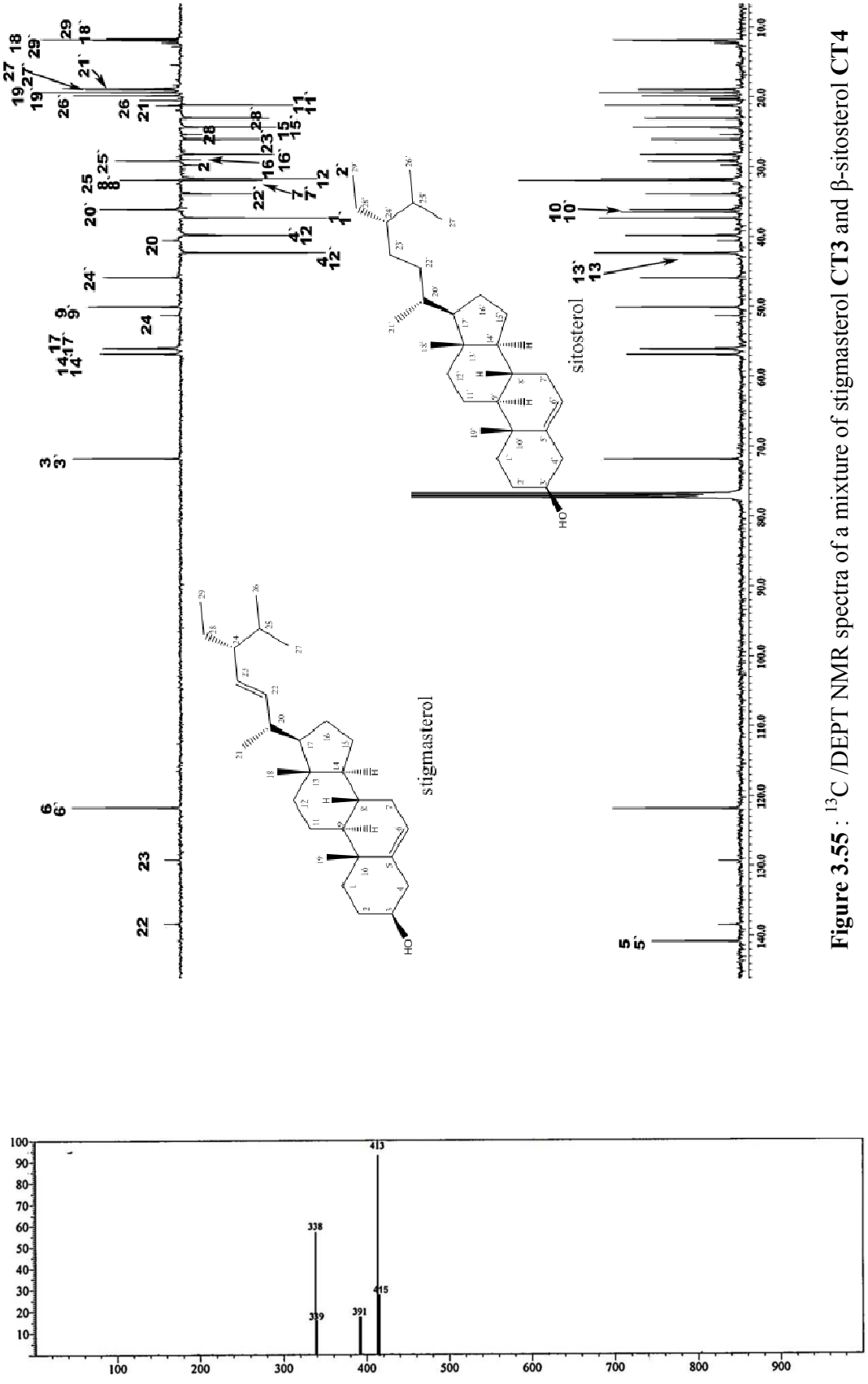

Figure 3.55 : ^{13}C /DEPT NMR spectra of a mixture of stigmasterol **CT3** and β-sitosterol **CT4**

Figure 3.56 : LCMS of stigmasterol **CT3** and *β*-sitosterol **CT4**

3.2.4 Hydroxy Acid Derivatives of Ferulate CT5A-P

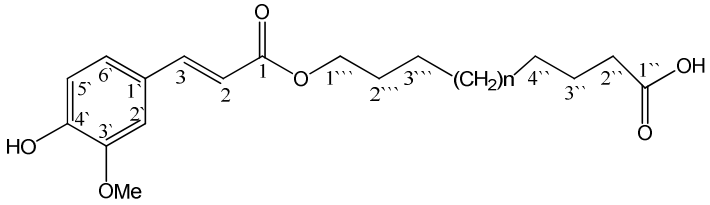

Compounds of hydroxy acid derivatives of ferulate with (CH_2)n, n=8-10, 12-13, 15-17, 19, 21, 25, 27, 28, 30, 31, 33 were isolated as white powder in different fractions, (n=8, 10, 25, 27, 28, 30, 31,and 33 were new compounds). The UV spectrum showed λ_{max} at 324, 236 nm. The IR spectrum showed for conjugated and non-conjugated C=O with α, β C=C at ν_{max} 1736-1709 cm $^{-1}$, aromatic C=C 1515-1513 cm^{-1}, C=C stretch of acryl part at 1678-1673cm^{-1}, phenolic- OH at ν_{max} 3583-3592 cm^{-1}, while carboxylic acid OH group had broad peak at ν_{max} 3200-2800 which overlapped with sp^3 C-H stretch at ν_{max} 2926- 2917cm^{-1} and finally for methylene groups had characteristic bending absorption of approximately at ν_{max} 1465 cm^{-1}. While the LCMS (Figure 3.62-Figure 3.77) showed molecular ion peak $[M+Na]^+$ peak at m/z [457, 471, 485, 513, 527, 555, 569, 583, 611, 637, 693, 723, 737, 765, 779, 807] corresponding to hydroxy acid derivatives of *E*-ferulate (CH_2)n, n=8-10,12-13,15-17, 19, 21, 25, 27, 28, 30, 31, 33 respectively. It is worthy to mention that molecular ion peak $[M+Na]^+$ peak at 583 (n=17) was the most abundant mass, meanwhile, several major peaks were observed with most of them at m/z 194 which maybe showed the ion of ferulic acid. The last single peak found at m/z 144, which could show the ions of octanoic acid.

^{1}H-NMR spectra (Table 3.13, Figure 3.57) of the above compounds displayed one tall and broad singlet peak at δ_H 1.25 corresponding to (CH_2)n ,n= 8-10, 12-13, 15-17, 19, 21, 25, 27, 28, 30, 31, 33 and showed two singlet peaks at δ_H 3.91, and 5.50 corresponding to methoxy and C-4`-OH group respectively. In addition of that, ^{1}H-NMR spectrum showed four doublet peaks at δ_H 7.02 with *J*=1.7, at δ_H 6.89 with *J*= 8.3

Hz, and at δ_H 6.27 and 7.59 with the same *J*= 16.0 Hz, corresponding to H-2`, H-5`, H-2 and H-3, respectively. Protons in the positions H-2 and H-3 should be in the trans position according to the *J* value =16.0 Hz, one double of doublet peak at δ_H 7.05 with *J*= 8.3, 1.8 Hz corresponding of H-6`. Meanwhile ^{1}H-NMR spectrum showed two deshielded triplet peaks at δ_H 4.2 with *J* = 6.6 Hz and at δ_H 2.33 with *J*= 7.54 Hz corresponding to two of CH_2 in the positions of H-1``` and H-2`` respectively. While two multiplet less downfielded peaks appeared at $\delta_H$ 1.69 and at $\delta_H$ 1.69 corresponding to two other $CH_2$ of the positions H-3``, H-2``` respectively.

The ^{13}C-NMR and DEPT spectra (Table 3.13, Figure 3.58) of compounds **CT5A-CT5P** displayed a high peak due to overlapping of many CH_2 together at δ_C 29.7, five quaternary carbons at δ_C 127.1, 147.9, 146.8, 167.6, and 178.7 due to C-1`, C-4`, C-3`, C-1, and C-1" respectively. Three aromatic CH carbons appeared at $\delta_C$ 109.3, 114.8, 123.1 of positions C-2`, C-5`, C-6` respectively, and two olefinic CH carbons at δ_C 115.7 δ 144.8 for C-2 and C-3 respectively. A very clear CH_2-O displayed at δ_C 64.7, one CH_2CO appeared at δ_C 33.9, and one OCH_3 at δ_C 56 and no CH_3 found in all of them.

Regarding NMR spectra no differences have been found between the above compounds in the positions of ^{1}H-NMR and ^{13}C-NMR, except in the integration of ^{1}H-NMR and the length of ^{13}C-NMR peaks of $(CH_2)_n$.

The structure has been further approved by COSY (Figure 3.59, HMQC (Table 3.13, Figure 3.60, and HMBC (Figure 3.61). Based on the spectral data and comparison with literature [141-145], the above compounds were assigned as hydroxy acid derivatives of ferulate.

3.13:1D (^{1}H and ^{13}C) and 2D (HMQC and HMBC) NMR Spectral Data of **CT5A-P**

Position	δ_H (int.; mult.; J(Hz))	δ_C	HMQC	HMBC
1	…….	167.6		……..
2	6.27 (1H, d, 16.0)	115.7	H-C1	1, 1'
3	7.59 (1H, d, 16.0)	144.8	H-C2	1, 2, 2`, 6`
1`	……..	127.1		…….
2`	7.02 (1H, d, 1.7)	109.4	H-C2`	3, 4`, 6`
3`	…….	146.8		…….
4`		147.9		…….
5`	6.89 (1H, d, 8.3)	114.8	H-C5`	1`, 3`
6`	7.05 (1H, dd, 8.3, 1.8)	123.1	H-C6`	2`, 3, 4`
-OCH_3	3.91 (3H, s)	56		3`
4`-OH	5.5			
1"	……	178.7		……
2"	2.33 (2H, t, 6.6)	33.9	H_2-C2``	1``, 3``, 4``
3"	1.60 (2H, m)	24. 8	H_2-C3``	1``,2``, 4``
4``	1.25 (2H, brs)	29.1	H_2-C4``	All overlapped
(CH2)n-6	1.25 (nH, brs)	29.7		All overlapped
3```	1.25 (2H, brs)	26.0	H_2-C3```	All overlapped
2```	1.69 (2H, m)	28.8	H_2-C2```	1```,3```
1```	4.20 (2H, t, 6.6)	64.7	H_2-C1```	1, 2```, 3```

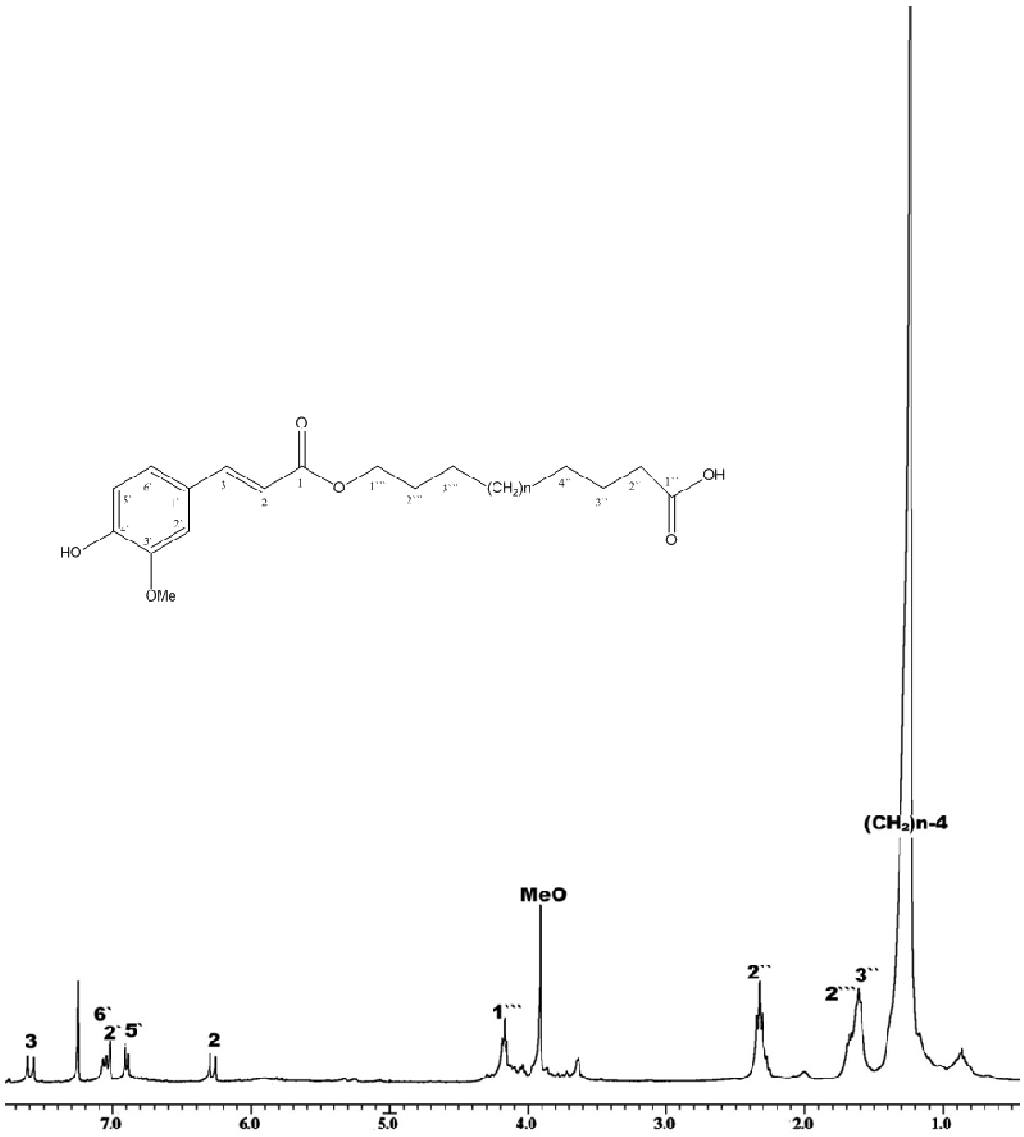

Figure 3.57 : ^{1}H-NMR spectrum of ferulate **CT5A-P**

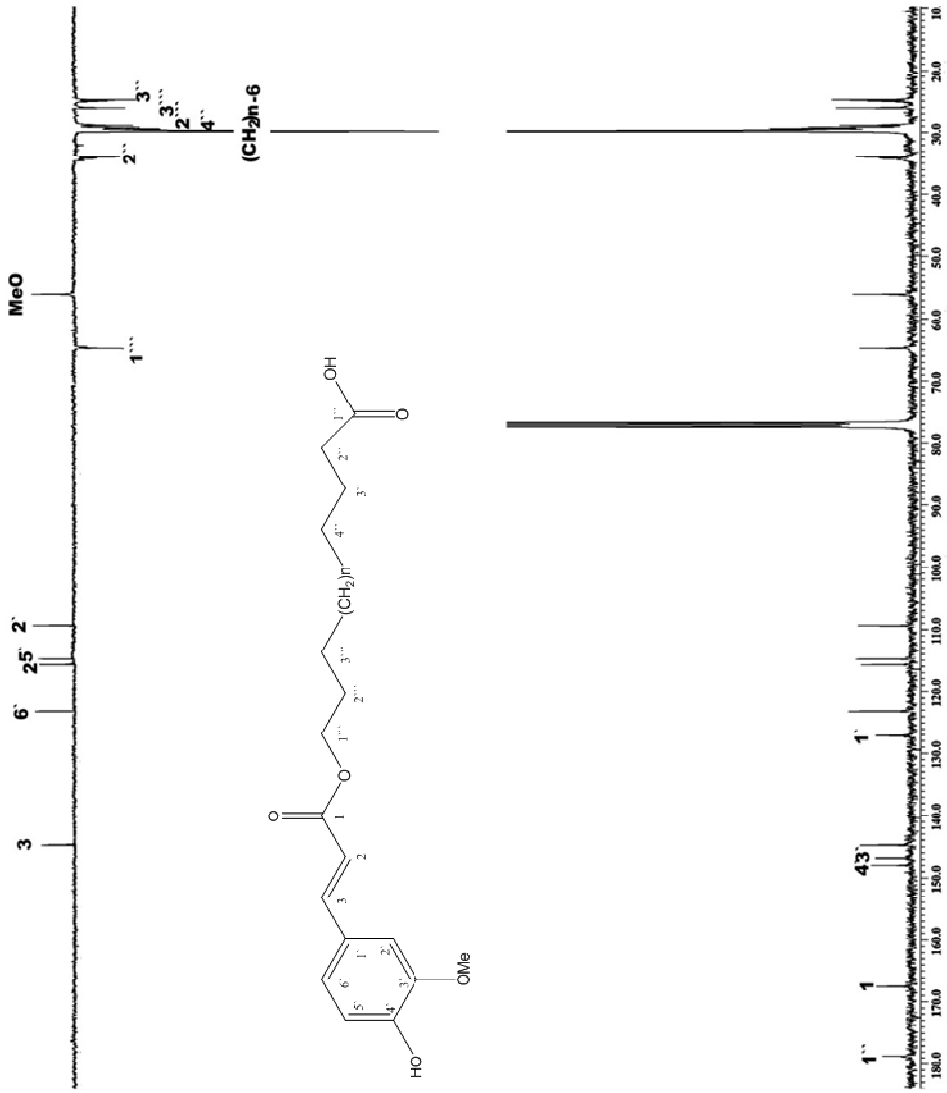

Figure 3.58 : ^{13}C/DEPT NMR spectra of **CT5A-P**

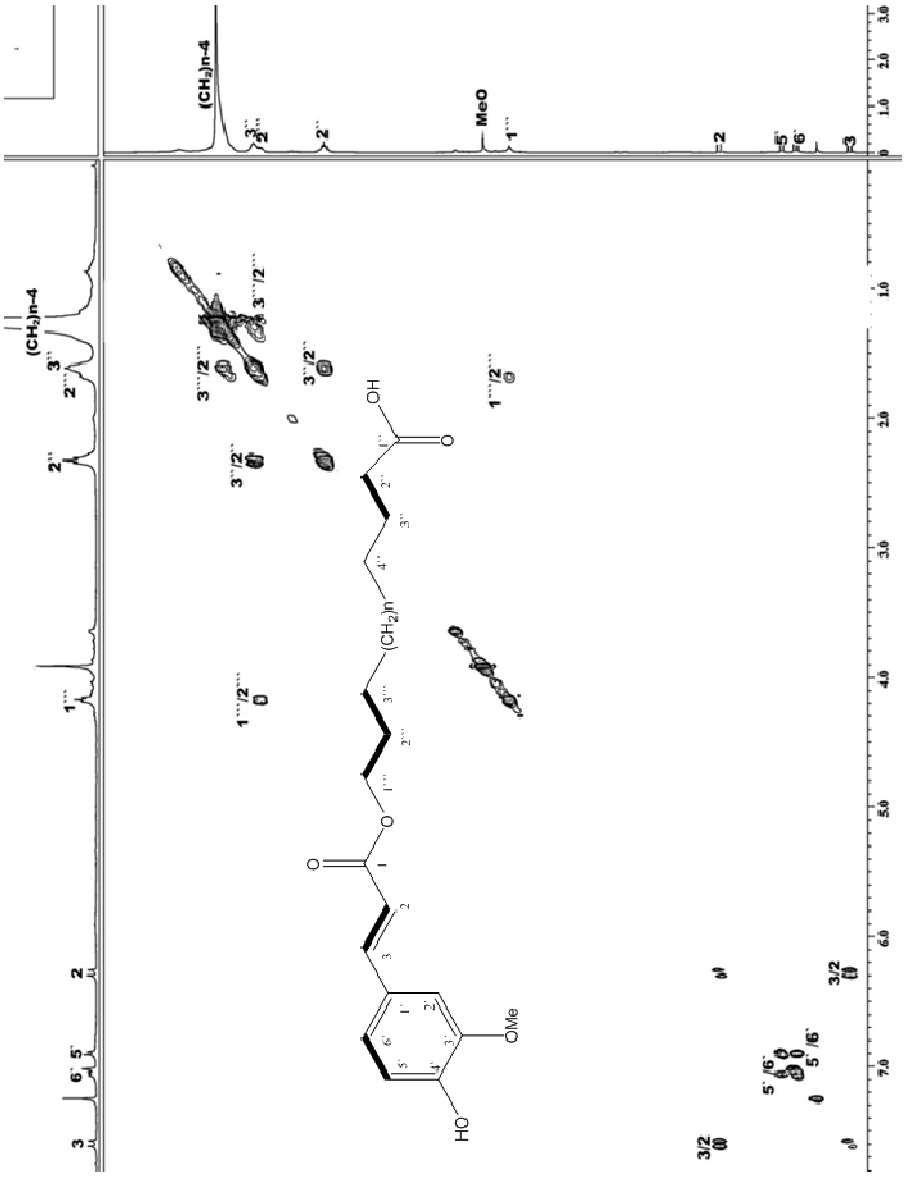

Figure 3.59 : ^{1}H-^{1}H-COSY spectrum of **CT5A-P**

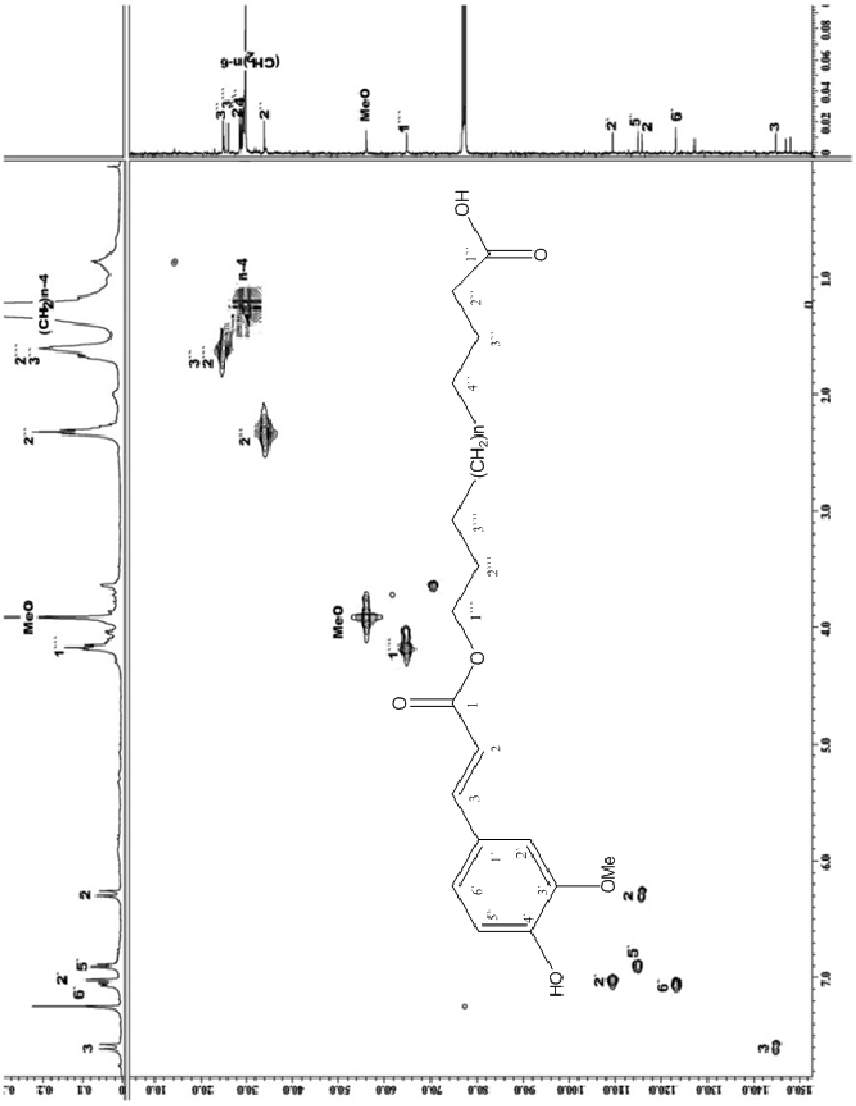

Figure 3.60 : HMQC spectrum of **CT5A-P**

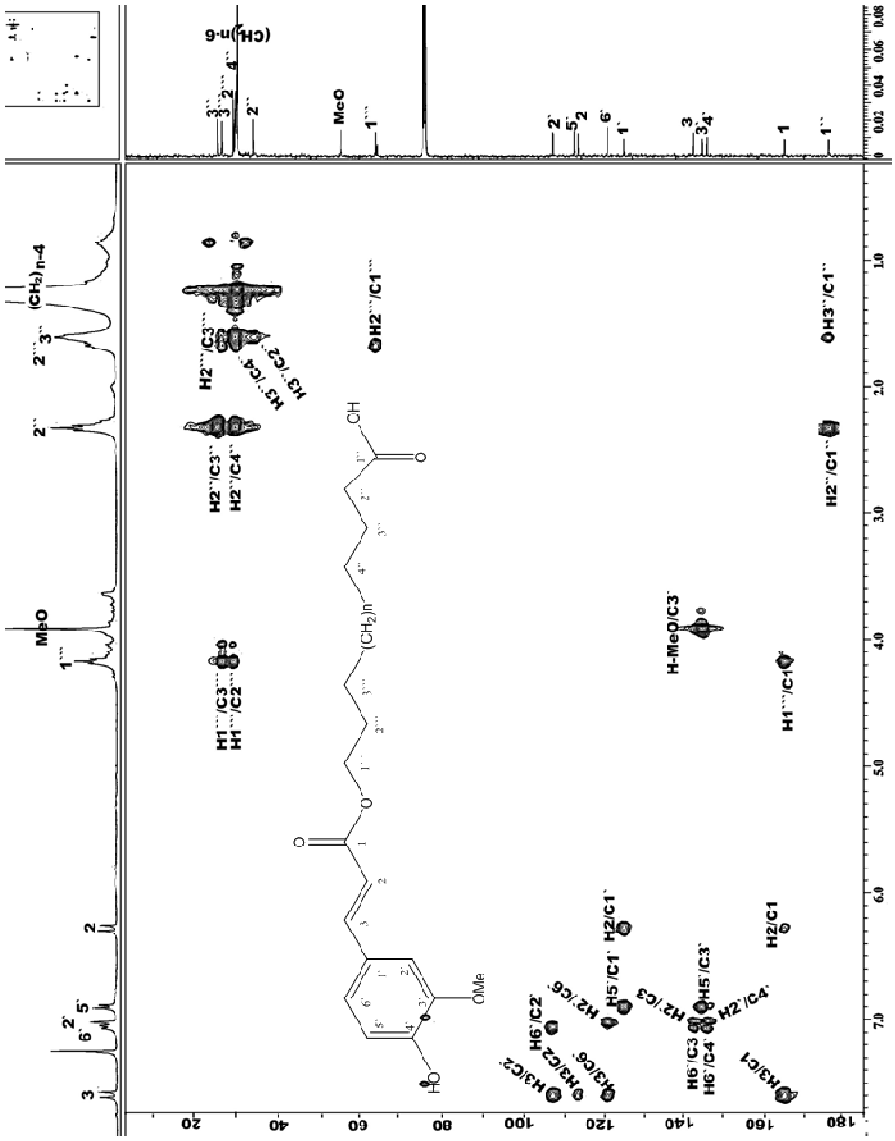

Figure 3.61 : HMBC spectrum of **CT5A-P**

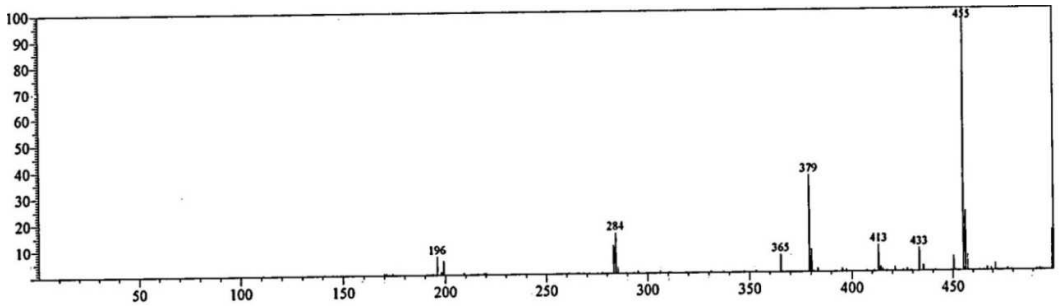

Figure 3.62 : LC-MS of **CT5A**

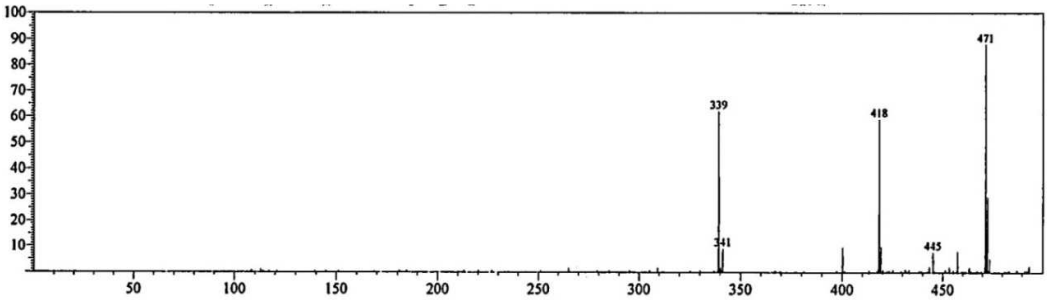

Figure 3.63 : LC-MS of **CT5B**

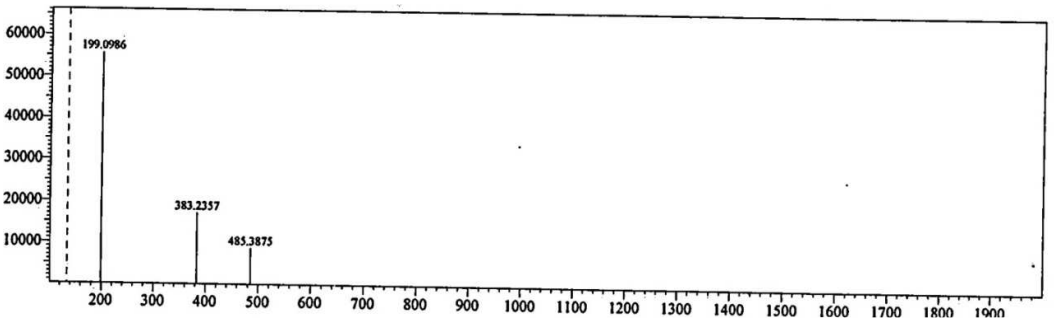

Figure 3.64 : LC-MS of **CT5C**

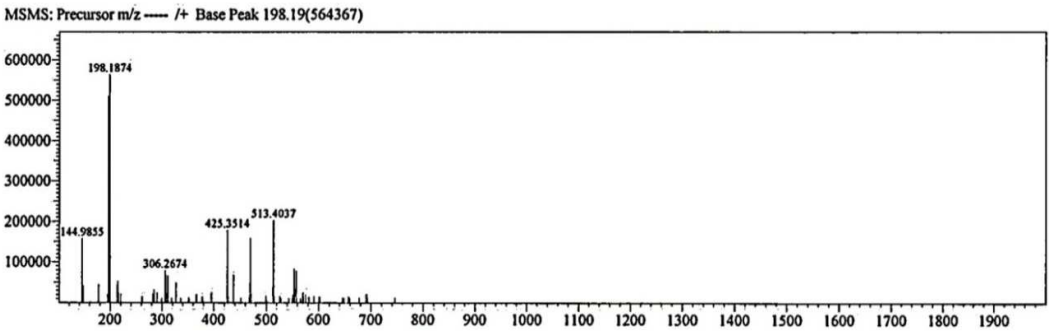

Figure 3.65 : LC-MS of **CT5D**

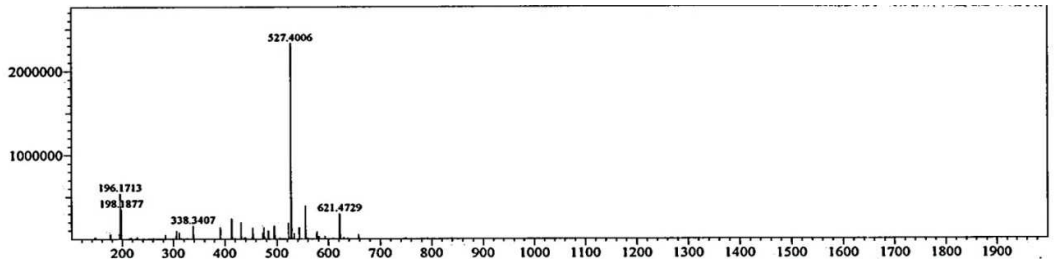

Figure 3.66 : LC-MS of **CT5E**

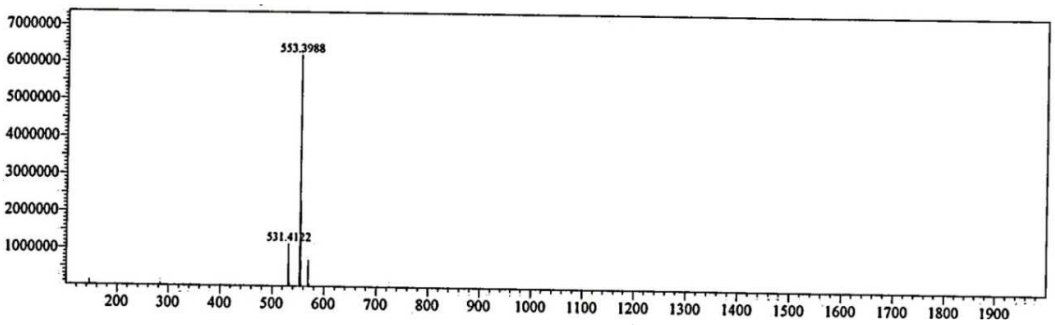

Figure 3.67 : LC-MS of **CT5F**

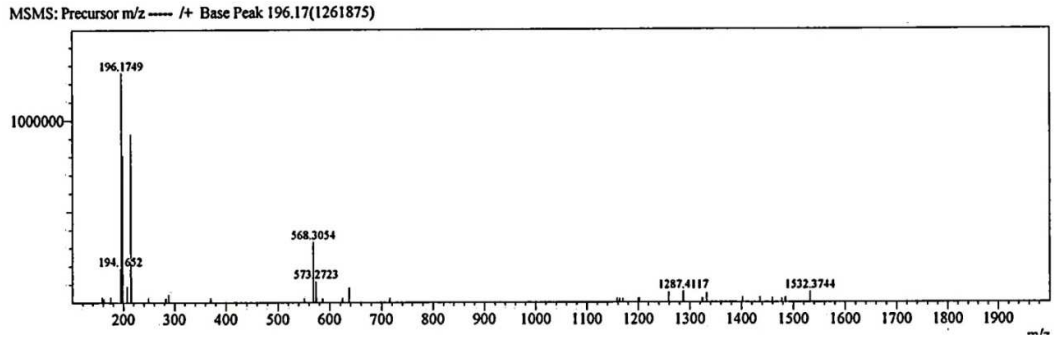

Figure 3.68 : LC-MS of **CT5G**

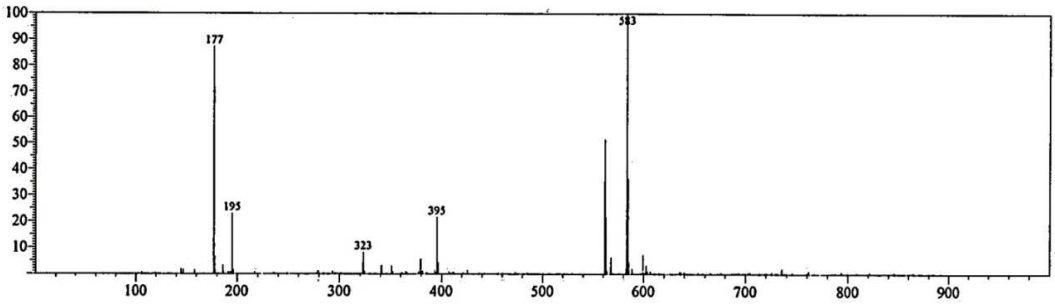

Figure 3.69 : LC-MS of **CT5H**

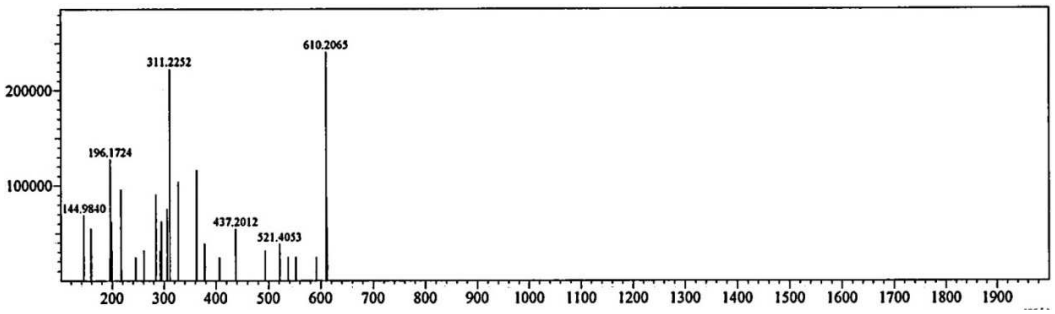

Figure 3.70 : LC-MS of **CT5I**

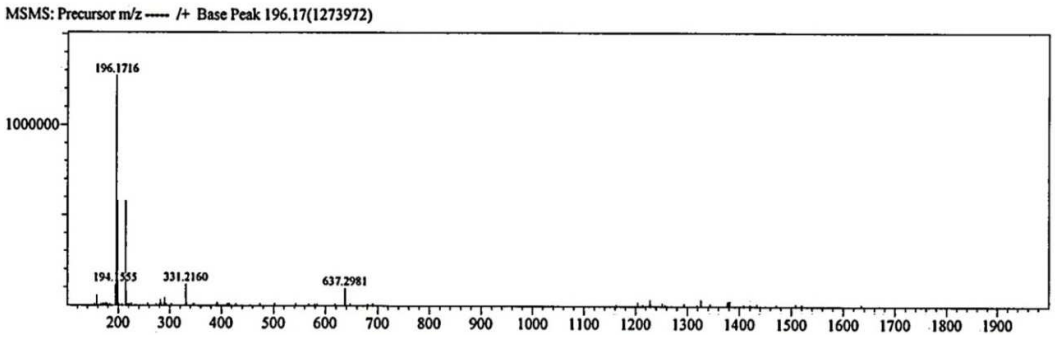

Figure 3.71 : LC-MS of **CT5J**

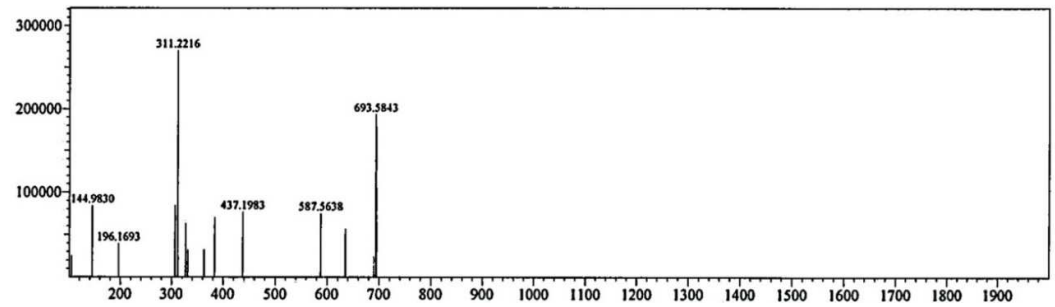

Figure 3.72 : LC-MS of **CT5K**

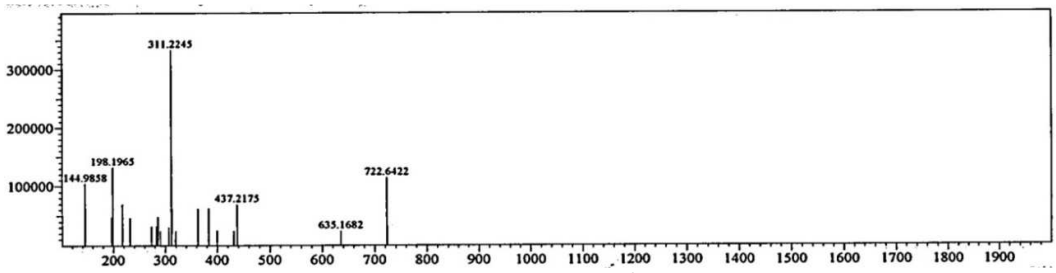

Figure 3.73 : LC-MS of **CT5L**

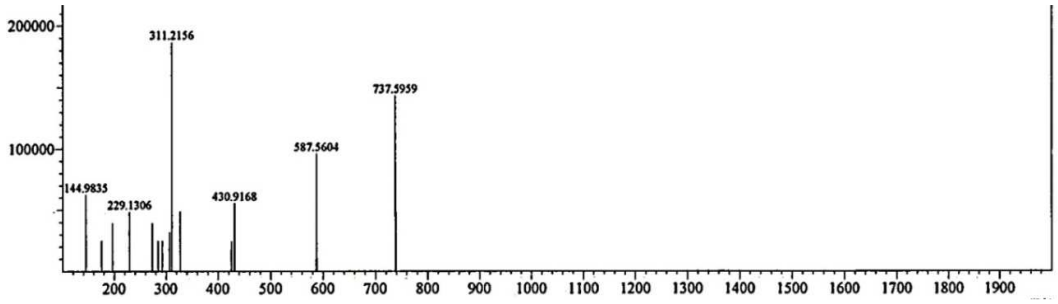

Figure 3.74 : LC-MS of **CT5M**

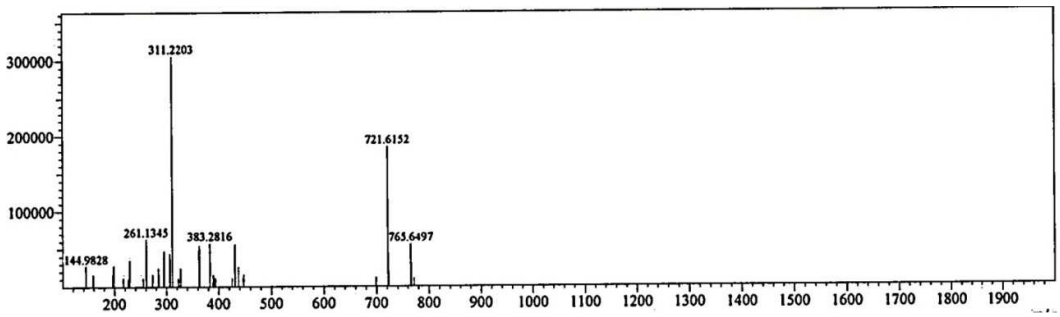

Figure 3.75 : LC-MS of **CT5N**

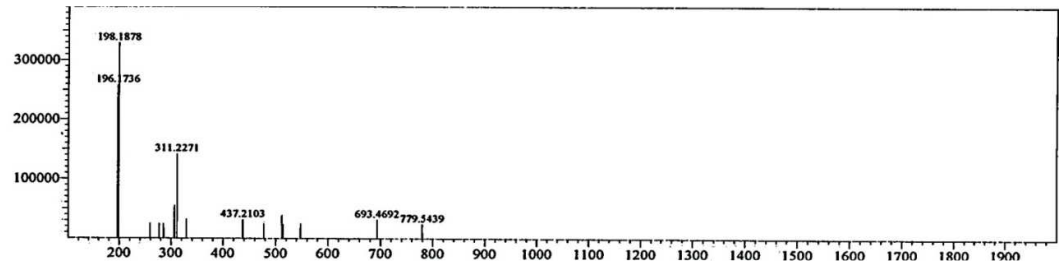

Figure 3.76 : LC-MS of **CT5O**

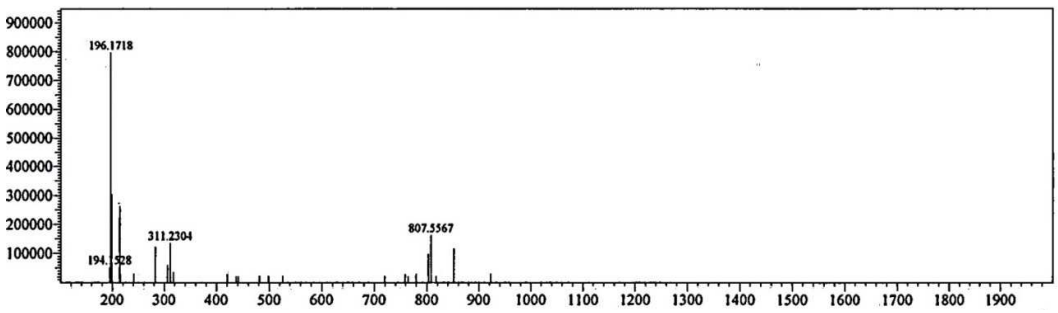

Figure 3.77 : LC-MS of **CT5P**

3.2.5 *E*-alkyl-*p*-coumarate CT6A-O

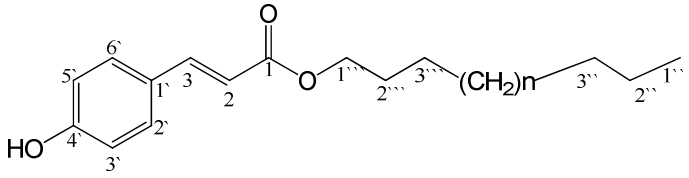

Compounds of alkyl coumarate **CT6A-O** were found as white amorphous. The UV spectrum showed λ_{max} nm 214, 230, 310, 360. IR ν_{max} 3375, 2912, 2849, 1718, 1607, 1516, 1462, 1172 and 835cm^{-1}. The LC-MS analysis (Figure 3.83-Figure 3.97) exhibited the molecular ion peak $[M-H]^+$ at m/z [331, 345, 373, 401, 443, 457, 471, 513, 527, 583, 611, 653, 695, 723, 737] which indicated that this fraction contains a mixture of 15 compounds with different $(CH_2)_n$ n=6, 7, 9, 11, 14, 15, 16, 19, 20, 24, 26, 29, 32, 34, 35 respectively. Compounds **CT6B**, **CT6C**, **CT6L**, **CT6M**, **CT6N**, and **CT6O** were new.

The ^{1}H-NMR spectrum (Table 3.14, Figure 3.78) of alkyl coumarate displayed four doublet signals in the sp^2 region, two of them were found in the form of AA`XX` pattern of para substitueted benzene ring at δ_H 7.40 and δ_H 6.81 with integration two times more than other two peaks that shows the overlapping of aromatic H in the position of (3` and 5`) and (2` and 6`), respectively. The other two peaks appeared at δ_H 7.6 and δ_H 6.27 which are typical of a trans-double bond of H-3 and H-2. With a spin coupling constant of 16.12 Hz, a triplet peak has been observed at δ_H 4.15 which referrers to the H of O-CH_2, a multiplet peak has been observed at δ_H 1.66 referred to the CH_2 in the position 2```, a high overlapped peak was seen at δ_H 1.23 which referred to the CH_2 of long chain, another triplet peak found at δ_H 0.8567 showed the terminal CH_3.

The ^{13}C-NMR (Table 3.14, Figure 3.79) spectrum of alkyl coumarate displayed in the aromatic region the overlapping peak of C-2` with C-6` at δ 129.9 and overlapping

peak of C-3` with C-5` at δ 115.9, which revealed a typical pattern of a para-substituted aromatic compound. Three quaternary carbon atoms were shown at δ_C 157.5, 127.2, and at 167.7 clearly belong to the oxygen –substituted atom C-4`, C-1`, and the carbonyl of ester C-1 respectively, which were disappeared through DEPT-135 (Figure 3.79), two peaks of sp^2 carbon appeared at δ_C 115.9 and δ_C 144.1 for both of C-2 and C-3. Meanwhile C-1``` appeared at δ_C 64.6, a high peak appeared at δ_C 29.57 referred to long chain of CH_2, the terminal carbon appeared at δ_C 14.1.

The first COSY (Figure 3.80) expansion showed connectivity for H-2 with H-3, the triplet signals at δ_H 4.16 has a COSY cross peak to one multiplet at δ_H 1.66 ppm. The COSY further revealed four protons 2` with 3` and 5` with 6`, which are strongly coupled to each other, and finally the terminal methlyl group correlated with its neighbor CH_2. The compounds are further approved by HMQC (Table 3.14, Figure 3.81) and HMBC (Figure 3.82),

Based on the spectral data and comparison with literature the above compounds were assigned as *E*-alkyl-*p*-coumarate [146-148].

Table 3.14 : 1D (^{1}H and ^{13}C) and 2D (HMQC, and HMBC) NMR spectral data of *E*-alkyl-*p*-coumarate **CT6A-O**

Position	δ_H (int.; mult.; J(Hz))	δ_C	HMQC	HMBC
1	…….	167.7		……..
2	6.27 (1H, d, 16.1)	115.9	H-C2	1, 1'
3	7.6 (1H, d, 16.1)	144.1	H-C3	1, 2, 2`, 6`
1`	……..	127.1		…….
2`	6.82 (1H, d, 8.5)	130.0	H-C2`	3, 4`, 6`
3`	7.40 (1H, d, 8.5)	115.9	H-C3`	5`, 1`, 4`
4`-OH	5.40 (1H, brs)	157.5		…….
5`	7.40 (1H, d, 8.5)	115.9	H-C5`	1`, 3`, 4`
6`	6.82 (1H, d, 8.5)	130.0	H-C6`	2`, 3, 4`
1``	0.86 (3H, t, 6.8)	14.2	H_2-C1``	2``
2``	1.23 (2H, m)	22.8	H_2-C2``	All overlapped
3``	1.23 (2H, m)	32.0	H_2-C3``	All overlapped
(CH_2)n-6	1.23 (nH, brs)	29.5		All overlapped
3```	1.23 (2H, m)	26.0	H_2-C3```	All overlapped
2```	1.66 (2H, m)	28.8	H_2-C2```	1```,3```, 4```
1```	4.16 (2H, t, 6.8)	64.5	H_2-C1```	1, 2```, 3```

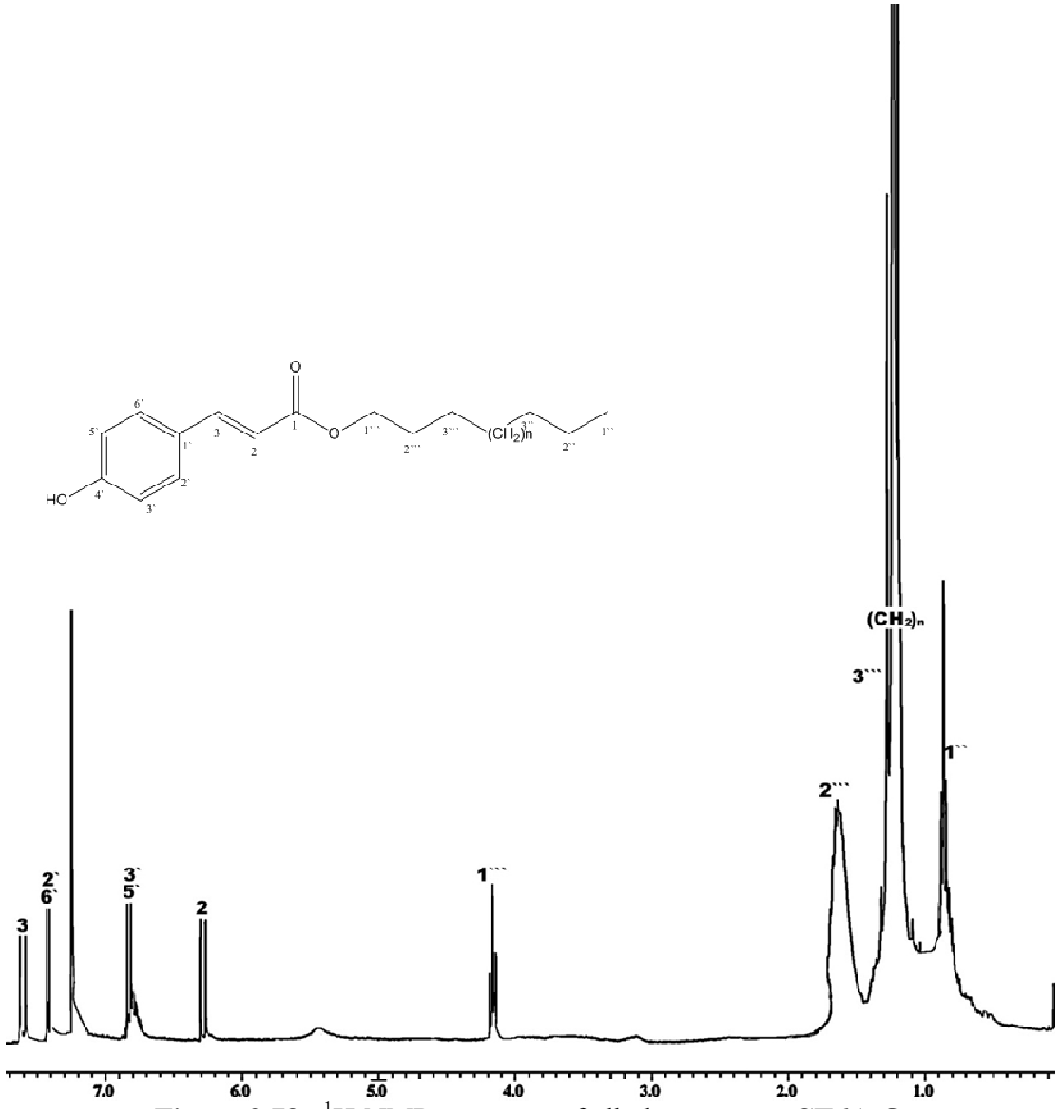

Figure 3.78 : ^{1}H-NMR spectrum of alkyl coumarate **CT6A-O**

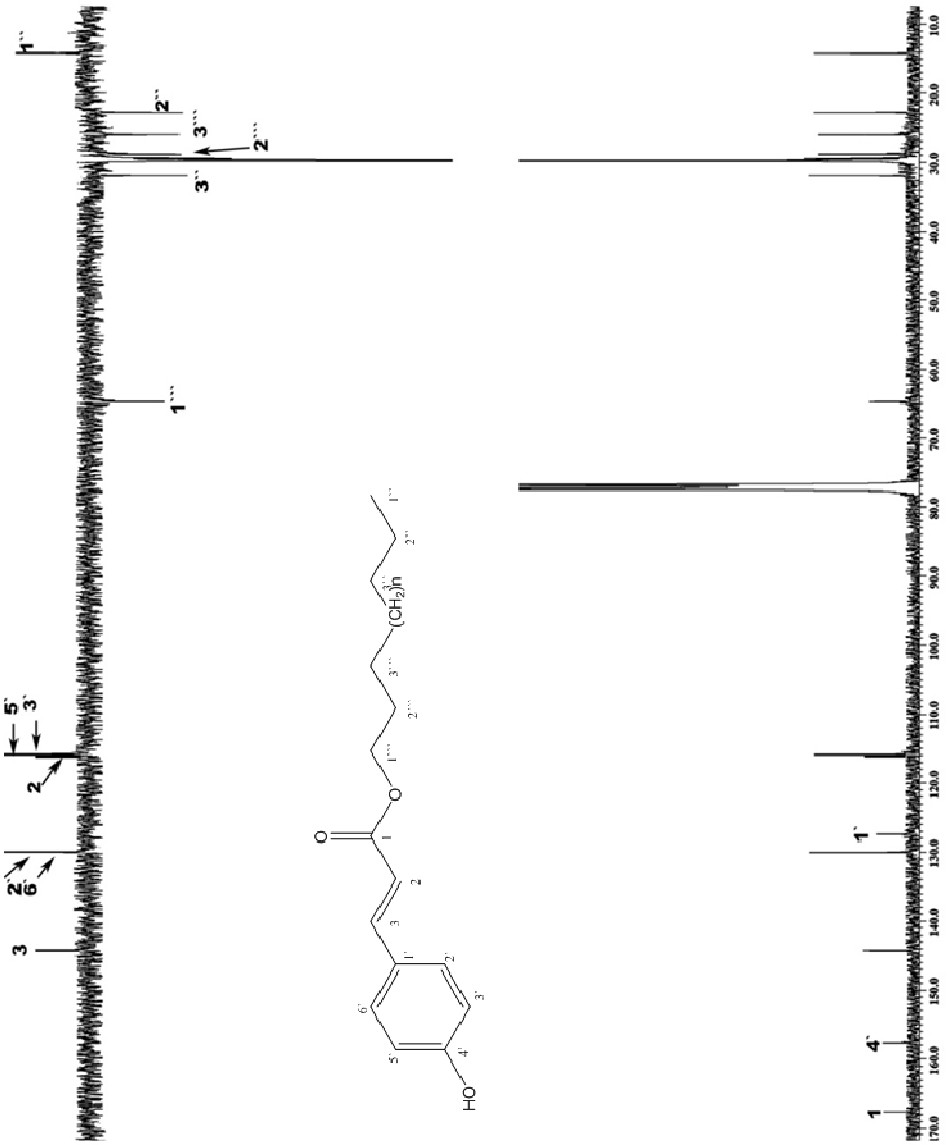

Figure 3.79 : ^{13}C/DEPT-NMR spectra of alkyl coumarate **CT6A-O**

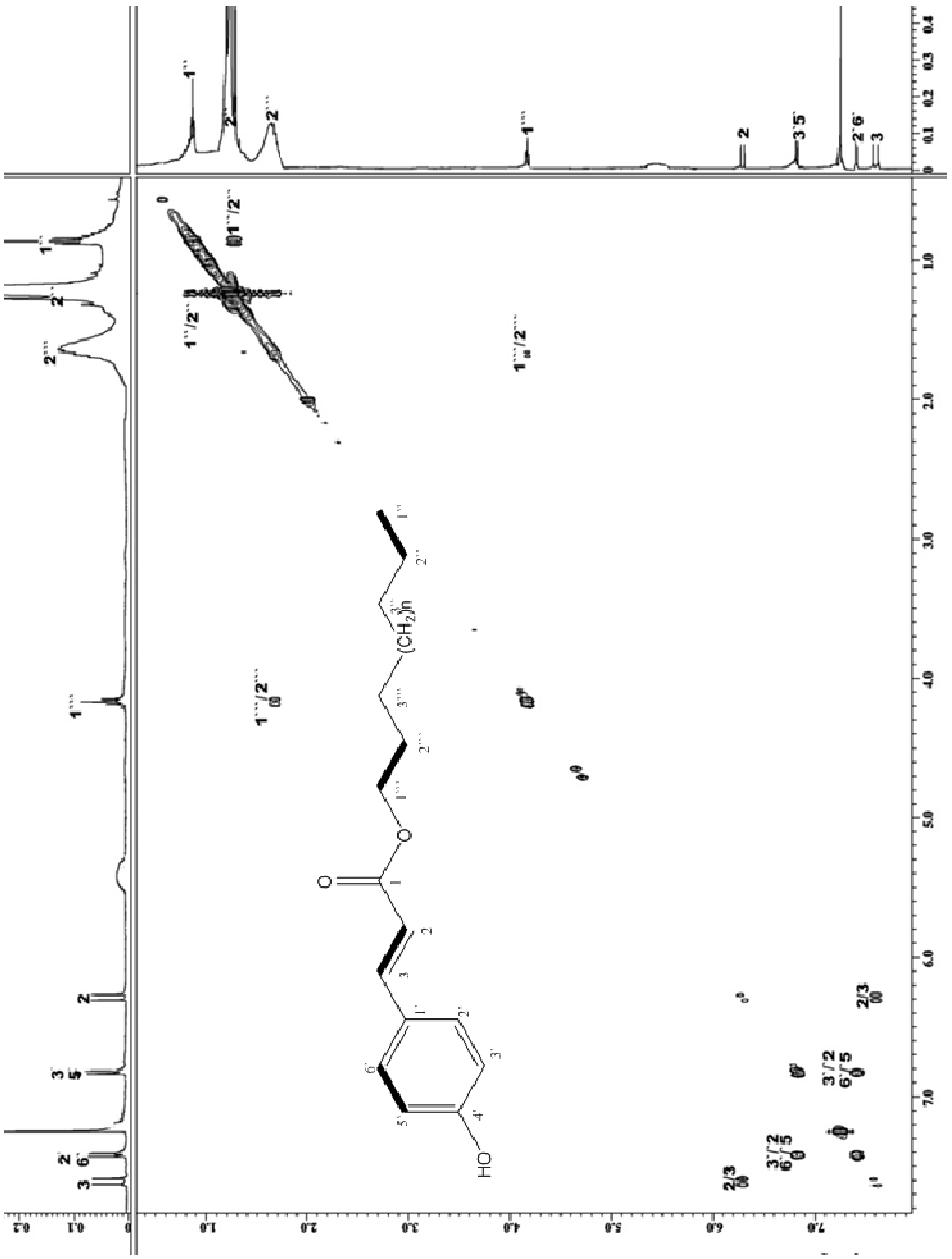

Figure 3.80 : ^{1}H-^{1}H COSY spectrum of alkyl coumarate **CT6A-O**

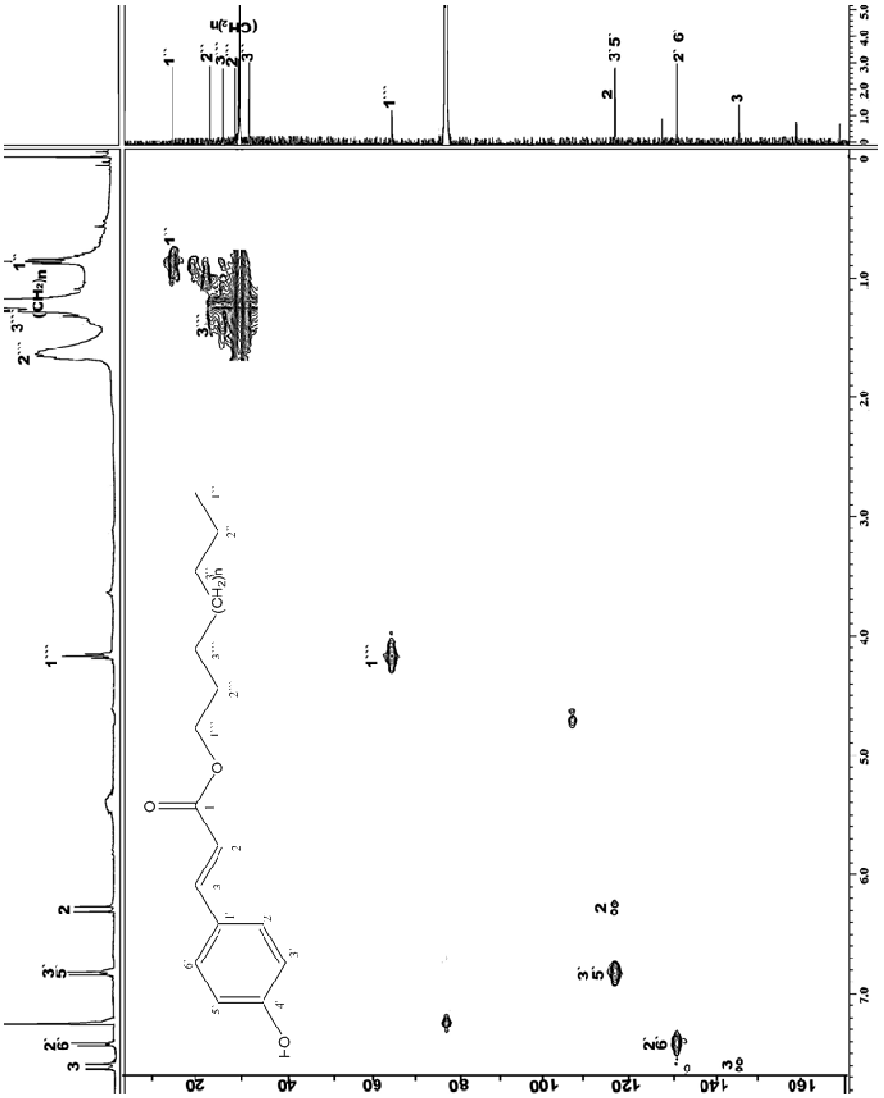

Figure 3.81 : HMQC spectrum of alkyl coumarate **CT6A-O**

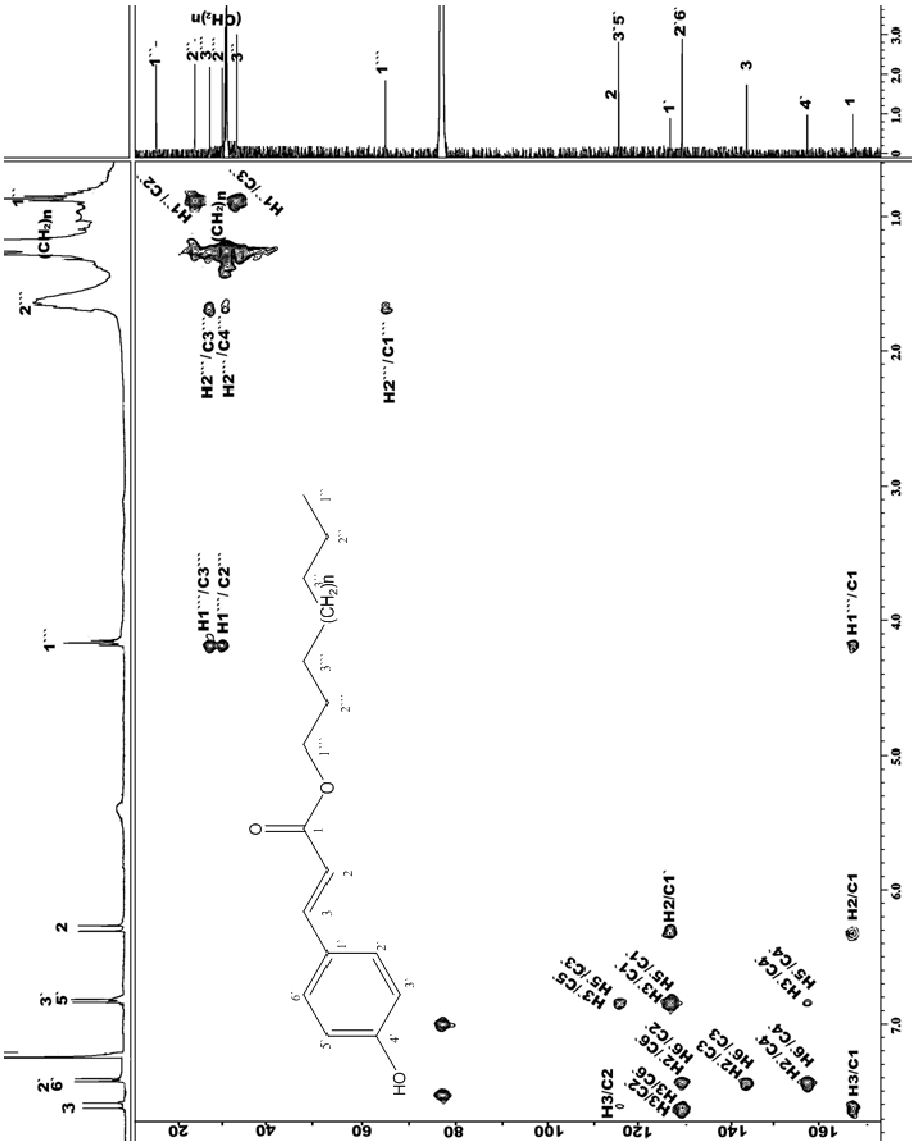

Figure 3.82 : HMBC spectrum of alkyl coumarate **CT6A-O**

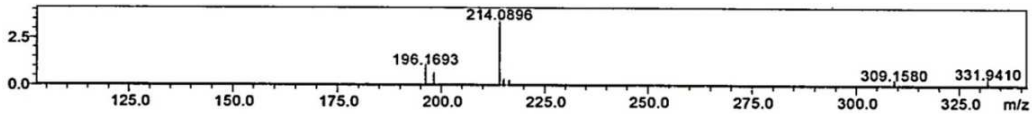

Figure 3.83 : LC-MS of alkyl coumarate **CT6A**

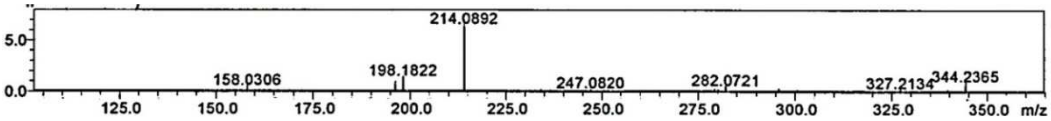

Figure 3.84 : LC-MS of alkyl coumarate **CT6B**

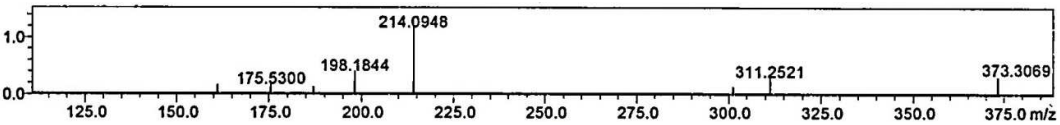

Figure 3.85 : LC-MS of alkyl coumarate **CT6C**

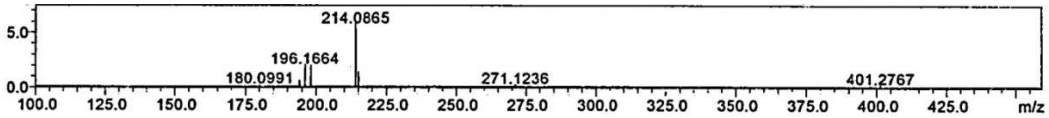

Figure 3.86 : LC-MS of alkyl coumarate **CT6D**

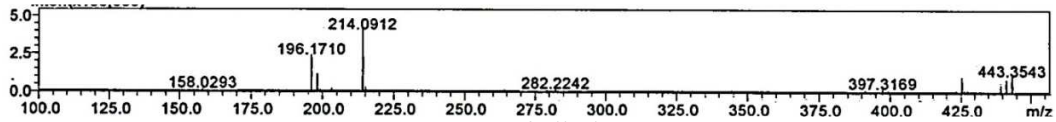

Figure 3.87 : LC-MS of alkyl coumarate **CT6E**

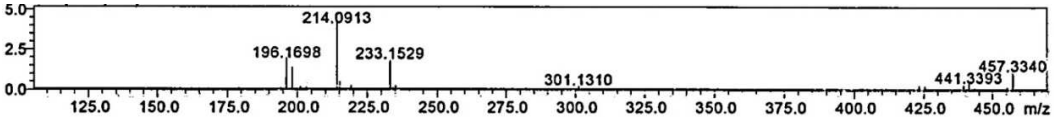

Figure 3.88 : LC-MS of alkyl coumarate **CT6F**

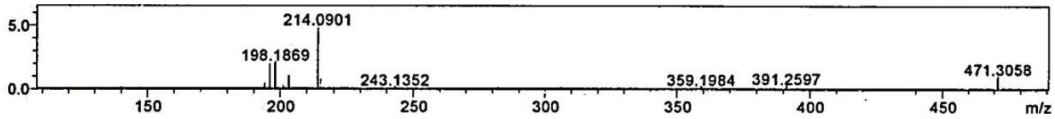

Figure 3.89 : LC-MS of alkyl coumarate **CT6G**

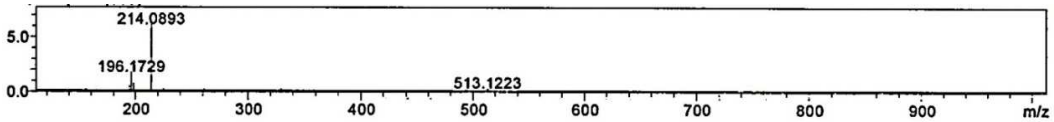

Figure 3.90: LC-MS of alkyl coumarate **CT6H**

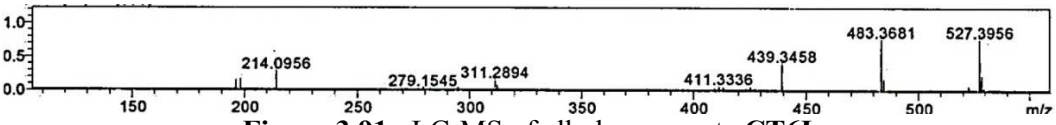

Figure 3.91 : LC-MS of alkyl coumarate **CT6I**

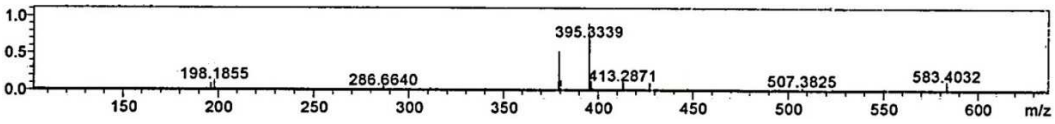

Figure 3.92 : LC-MS of alkyl coumarate **CT6J**

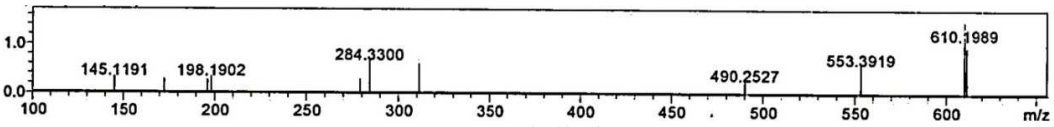

Figure 3.93 : LC-MS of alkyl coumarate **CT6K**

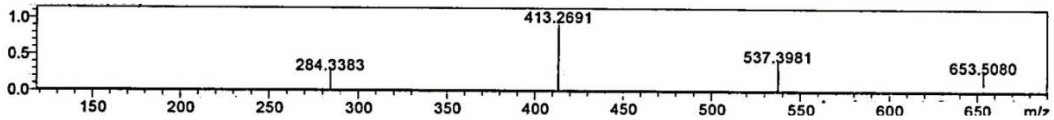

Figure 3.94 : LC-MS of alkyl coumarate **CT6L**

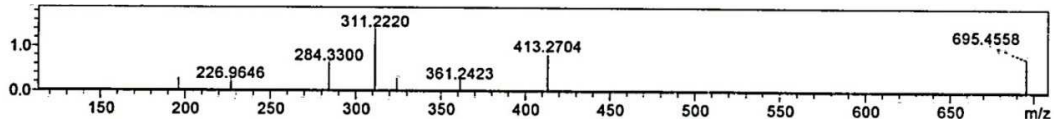

Figure 3.95 : LC-MS of alkyl coumarate **CT6M**

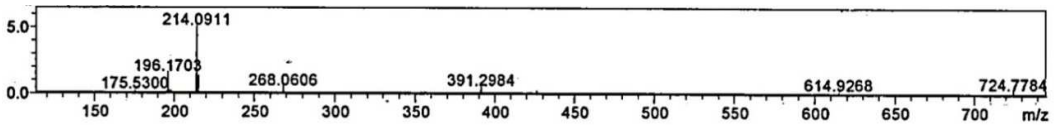

Figure 3.96 : LC-MS of alkyl coumarate **CT6N**

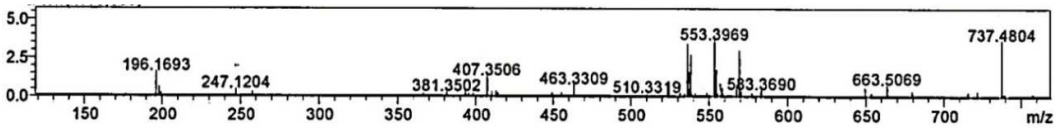

Figure 3.97 : LC-MS of alkyl coumarate **CT6O**

3.2.6 Ferulaldehyde CT7

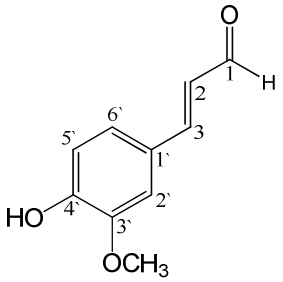

Compound **CT7** was obtained as brown oil. The UV spectrum showed absorption bands at 314 nm indicating a highly unsaturated chromophoric system, Infrared spectroscopic analysis showed the presence of phenolic group at ν_{max} 3366 cm^{-1}, conjugated carbonyl at ν_{max} 1660 cm^{-1} and C-H of aldehyde at ν_{max} 2880 cm^{-1}. The LCMS (Figure 3.103) displayed an ion peak $[M]^+$ at m/z 178, gave a molecular formula of $C_{10}H_{10}O_3$.

The ^{1}H-NMR (Table 3.15, Figure 3.98) analysis showed the existence of an aldehyde group at δ_H 9.66, a methoxy group at δ_H 3.95, a hydroxyl group at δ_H 6.09, two aromatic protons one of them as doublet and the second one as double of doublet appeared at δ_H 6.97, and δ_H 7.14 belong to 5` and 6` respectively with J= 8.2 Hz shows that they are in ortho position to each other but the one which is double of doublet with J=1.8 Hz should be affected by proton of meta position (2`). One aromatic proton at $\delta_H$ 7.08 with with the same coupling constant of 6`, it has been approved that they are meta position to each other. ^{1}H-NMR showed two olefinic protons at δ_H 6.61 and at δ_H 6.71 with J =16.0 Hz which belongs to H-2 and H-3, respectively and ascribable to trans configuration.

The ^{13}C-NMR and DEPT spectra (Table 3.15, Figure 3.99) showed 10 signals, five sp^2 CH, three sp^2 quaternary carbon atoms, one due to carbonyl of adehyde which was confirmed by the resonance at δ_C 193.8 and the last one due to methoxy group. Confirmation of the proposed structure was approved by COSY (Figure 3.100), HMQC (Table 3.15, Figure 3.101) and HMBC (Figure 3.102). According to the above data and

with comparison with the literature review [149-151] and mass, the structure of **CT7** was elucidated as IUPAC name *Z*-3-(4-hydroxy-3-methoxyphyneyl) prop-2-enal.

Table 3.15 : 1D (^{1}H and ^{13}C) and 2D (HMQC and HMBC) NMR spectral data of Ferulaldehyde **CT7** in CDCl3

Position	δ_H (int.; mult.; J(Hz))	δ_C	HMQC	HMBC
1	9.66 (1H, d, 7.7)	193.8		2
2	6.61 (1H, dd, 16.03, 7.7)	126.5	H-C2	6`
3	7.42 (1H, d, 16.0)	153.3	H-C3	1,1`, 2`, 6`
1`		126.7		
2`	7.08 (1H, d, 1.8)	109.5	H-C2`	3`, 4`, 6`
3`		147.0		
4`		149.0		
5`	6.97 (1H, d, 8.2)	115.0	H-C5`	1`, 3`
6`	7.14 (1H, dd, 8.2, 1.8)	124.2	H-C6`	2`, 3`, 4`
MeO	3.95 (1H, s)	56.1	H_3-C-MeO	
OH	6.09 (1H, bs)			

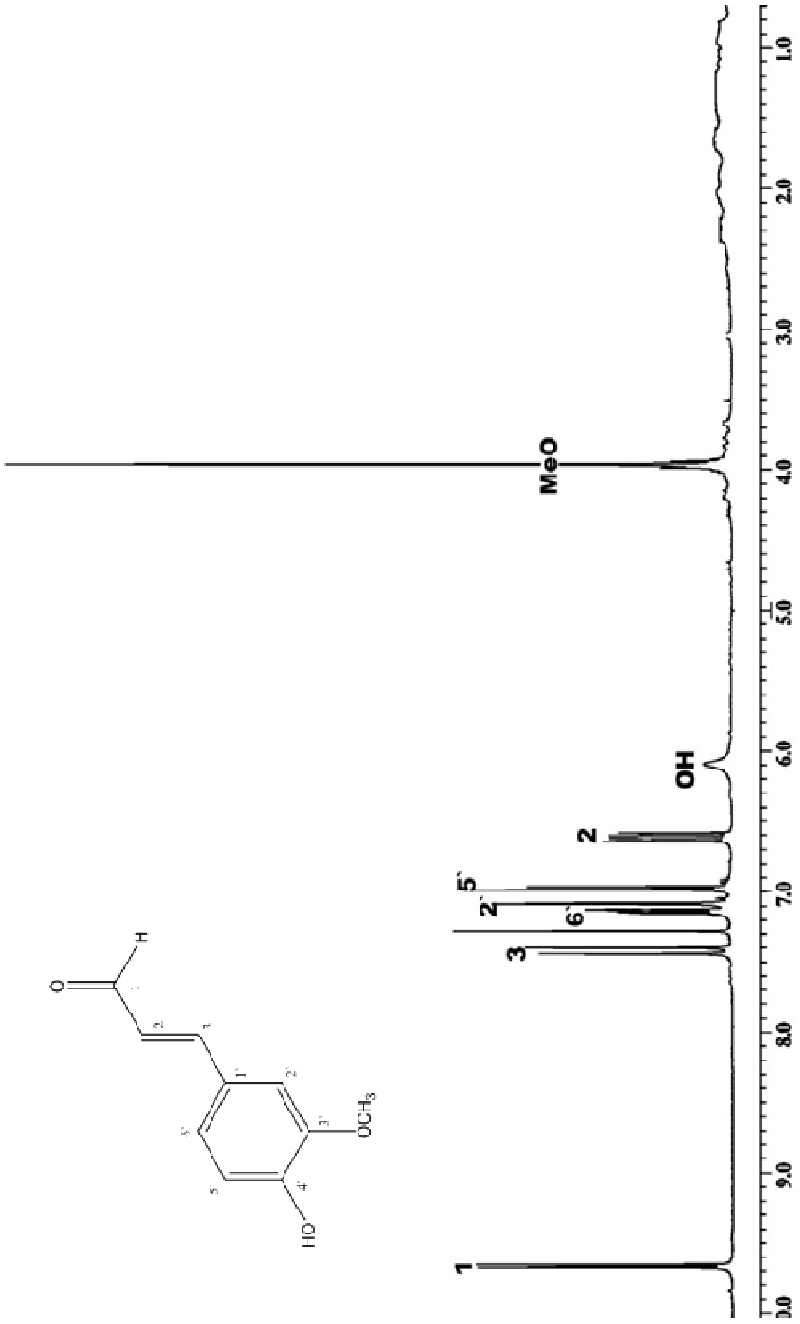

Figure 3.98 : ^{1}H-NMR spectrum of Feruladehyde **CT7**

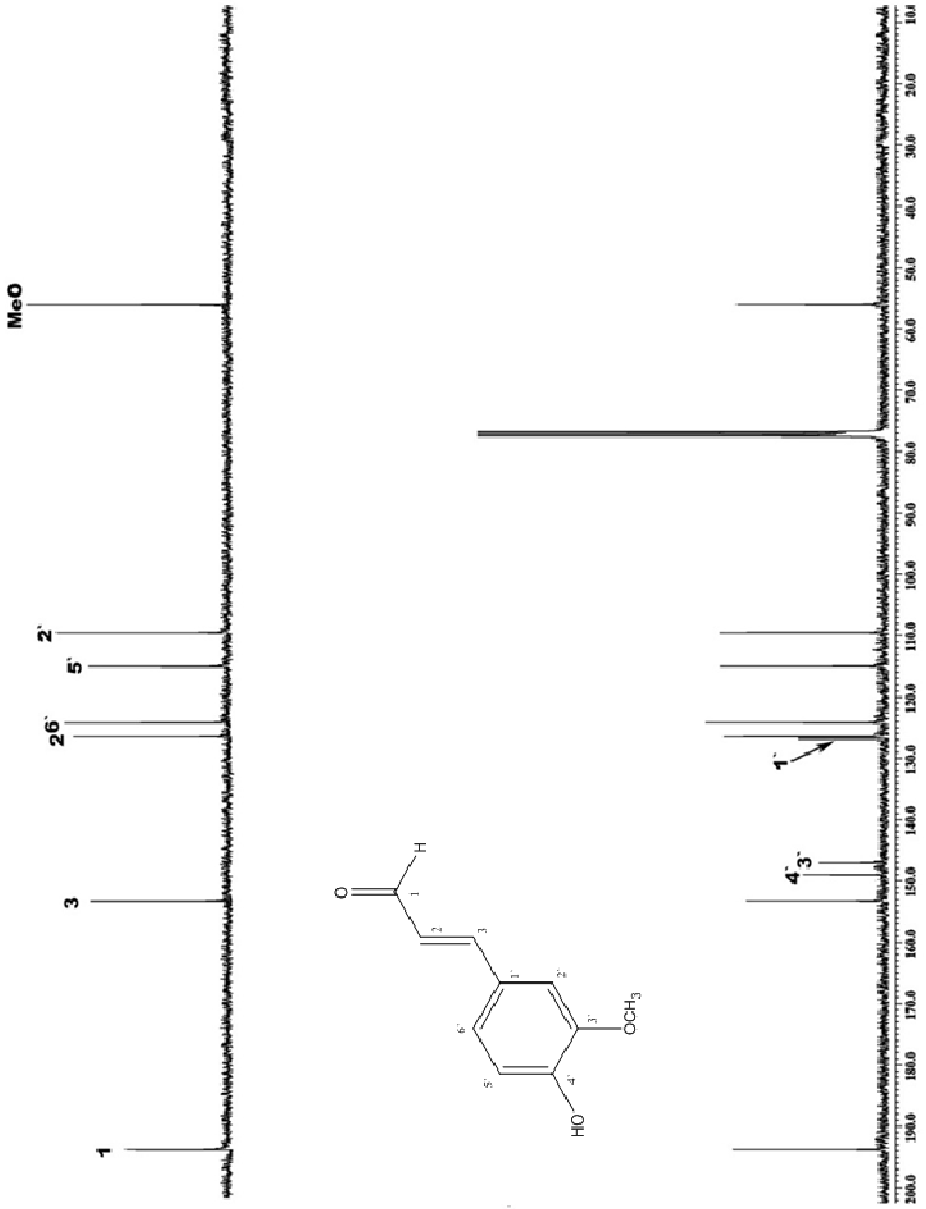

Figure 3.99 : ^{13}C/DEPT-NMR spectra of Ferulaldehyde **CT7**

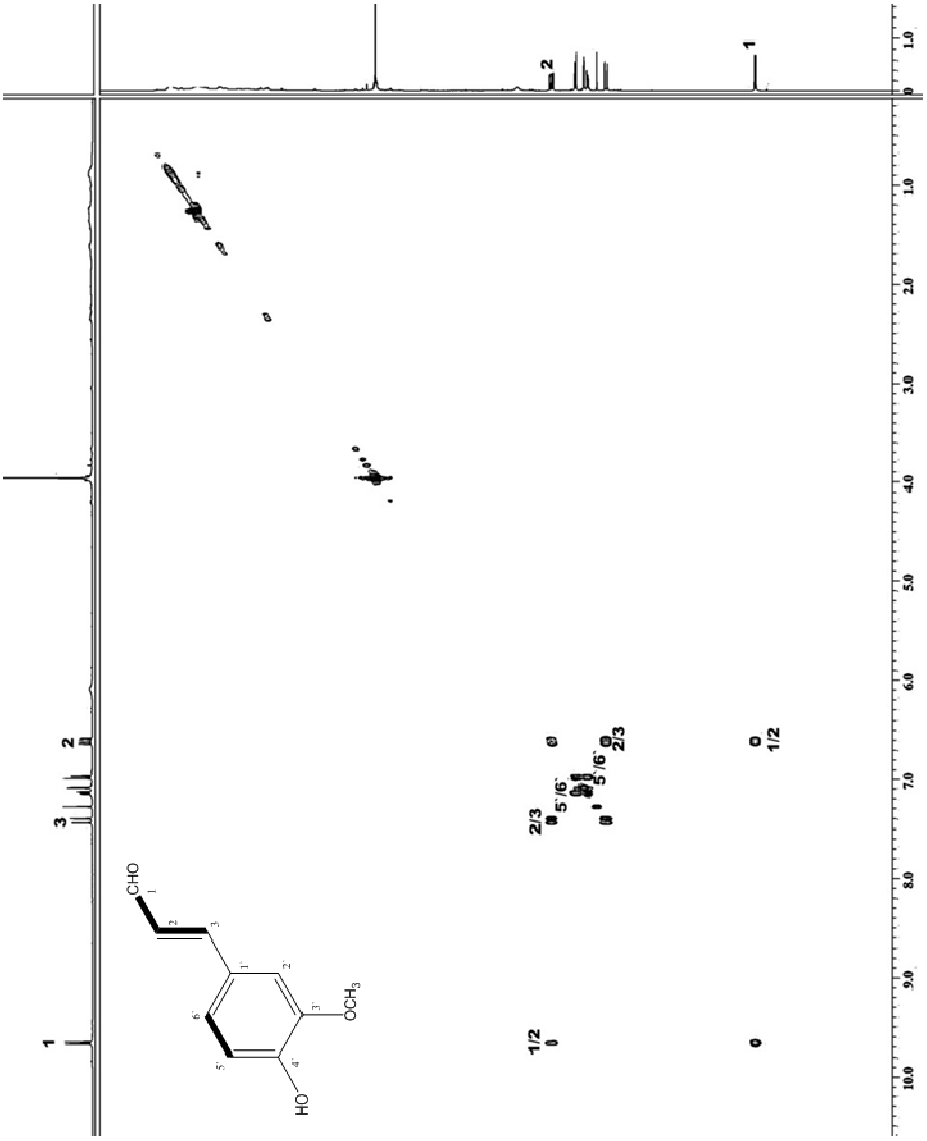

Figure 3.100 : ^{1}H - ^{1}H COSY spectrum of Feruladehyde **CT7**

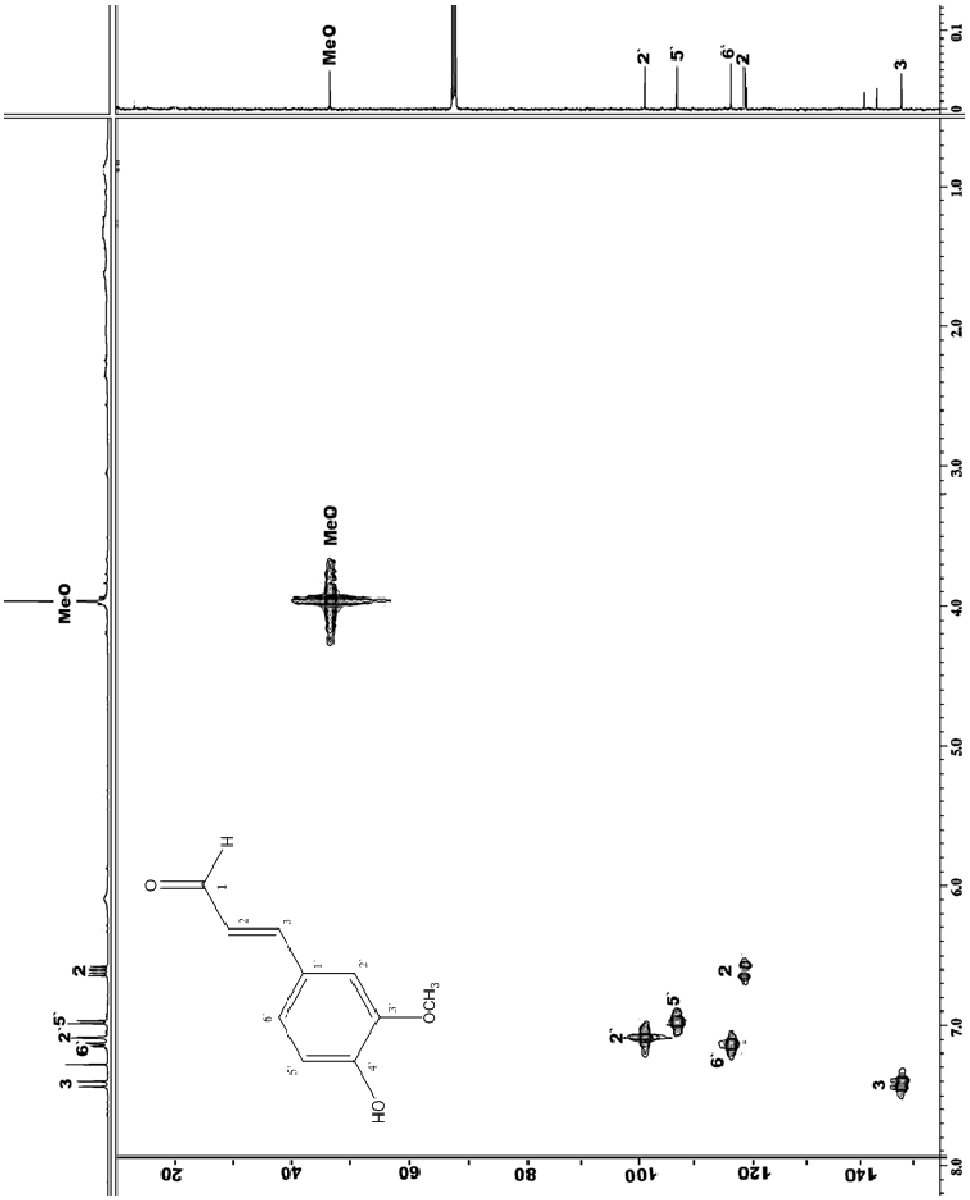

Figure 3.101 : HMQC spectrum of Ferulaldehyde **CT7**

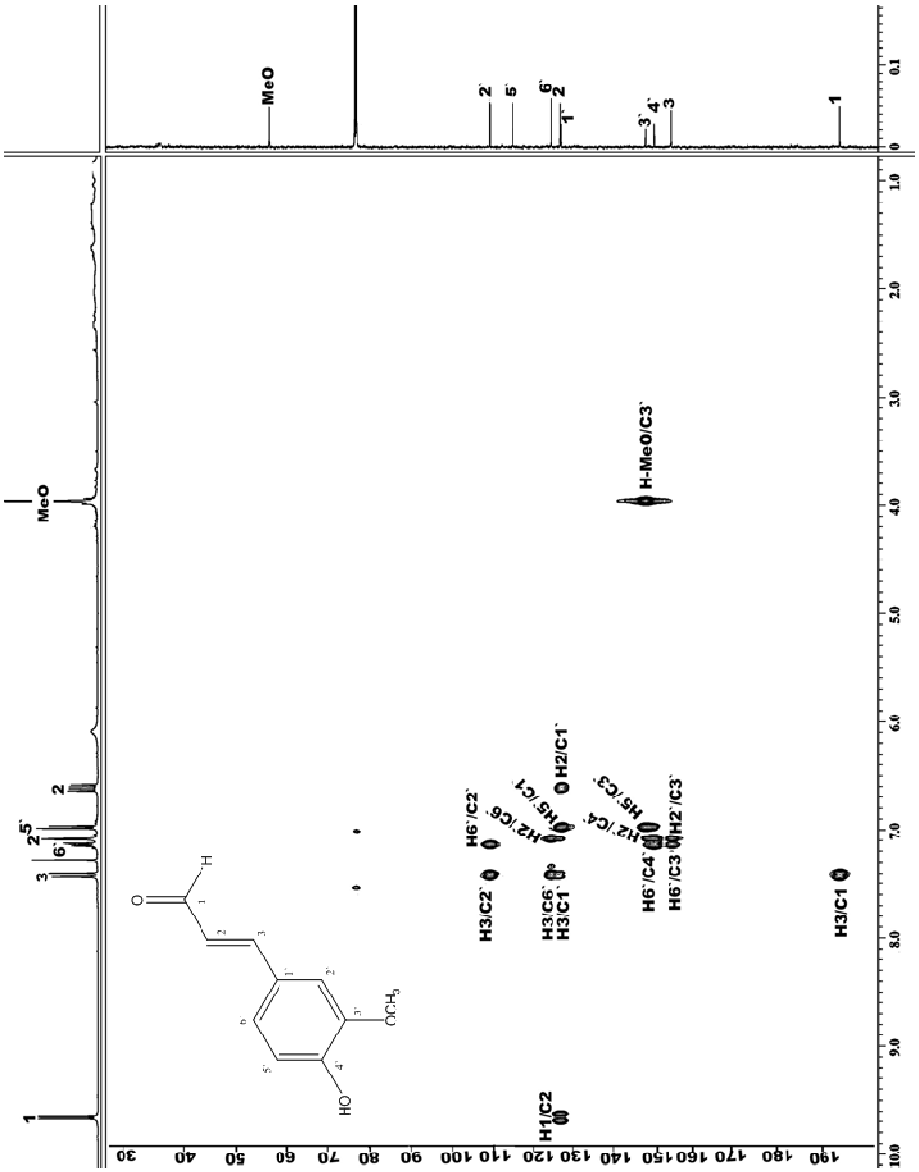

Figure 3.102 : HMBC spectrum of Ferulaldehyde **CT7**

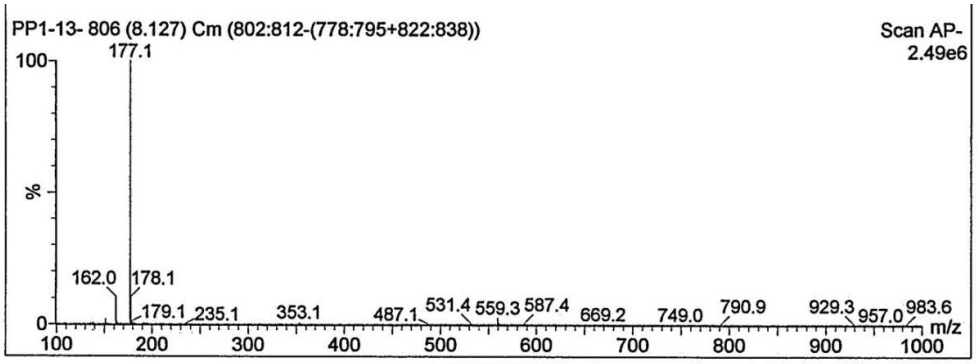

Figure 3.103 : Mass of Ferulaldehyde **CT7**

3.2.7 Vanillin CT8

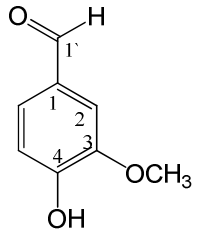

Compound **CT8** was obtained as lightly yellow needle crystals with mp 80-82 °C [152]. The UV spectrum showed absorption bands at 308 and 278 nm, Infrared spectroscopic analysis showed the presence of phenolic at ν_{max} 3600-2730 cm^{-1}, C-H of aldehyde at ν_{max} 2680 cm^{-1}, and carbonyl at ν_{max} 1690. The LCMS spectrum displayed ion peak $[M+H]^+$ at m/z 153.05, gave molecular formula of ($C_8H_8O_3$+H).

^{1}H-NMR (Table 3.16, Figure 3.104) analysis showed the existence of an aldehyde group δ_H 9.8, a methoxy group at δ_H 3.94, a hydroxyl group at δ_H 6.22, two aromatic protons overlaped at δ_H 7.40, and one aromatic proton at δ_H 7.02 with a coupling constant 8.3 Hz. It suggested ortho, para, and meta-arrangement of the three groups -OH, -CHO, and OCH_3 on the aromatic ring.

^{13}C/ DEPT NMR spectra (Table 3.16, Figure 3.105) showed 8 signals of which six due to aromatic nucleus, one due to carbonyl group and the last one due to methoxy group. Confirmation of the proposed structure was approved by COSY Figure 3.106), HMQC (Table 3.16, Figure 3.107), and HMBC (Figure 3.108) and LCMS (Figure 3.109).

Comparison of melting point and spectral data with that of commercial sample confirmed that the isolated compound is 4-hydroxy-3-methoxybenzaldehyde [152].

Table 3.16 : 1D (^{1}H and ^{13}C) and 2D (HMQC and HMBC) NMR spectral data of Vanillin **CT8** in CDCl3

Position	δ_H (int.; mult.; J(Hz))	δ_C	HMQC	HMBC
1		129.9		
2	7.40 (1H, m)	108.7	H-C2	1`,3, 4, 6
3		147.1		
4		151.6		
5	7.02 (1H, d, 8.3)	114.4	H-C5	1, 2, 3, 4, 6
6	7.40 (1H, m)	127.5	H-C6	1, 1`, 2, 4
CHO	9.80 (1H, s)	119.9		1, 2
MeO	3.94 (3H, s)	56.1	H_3-MeO	3
OH	6.22 (1H, s)			

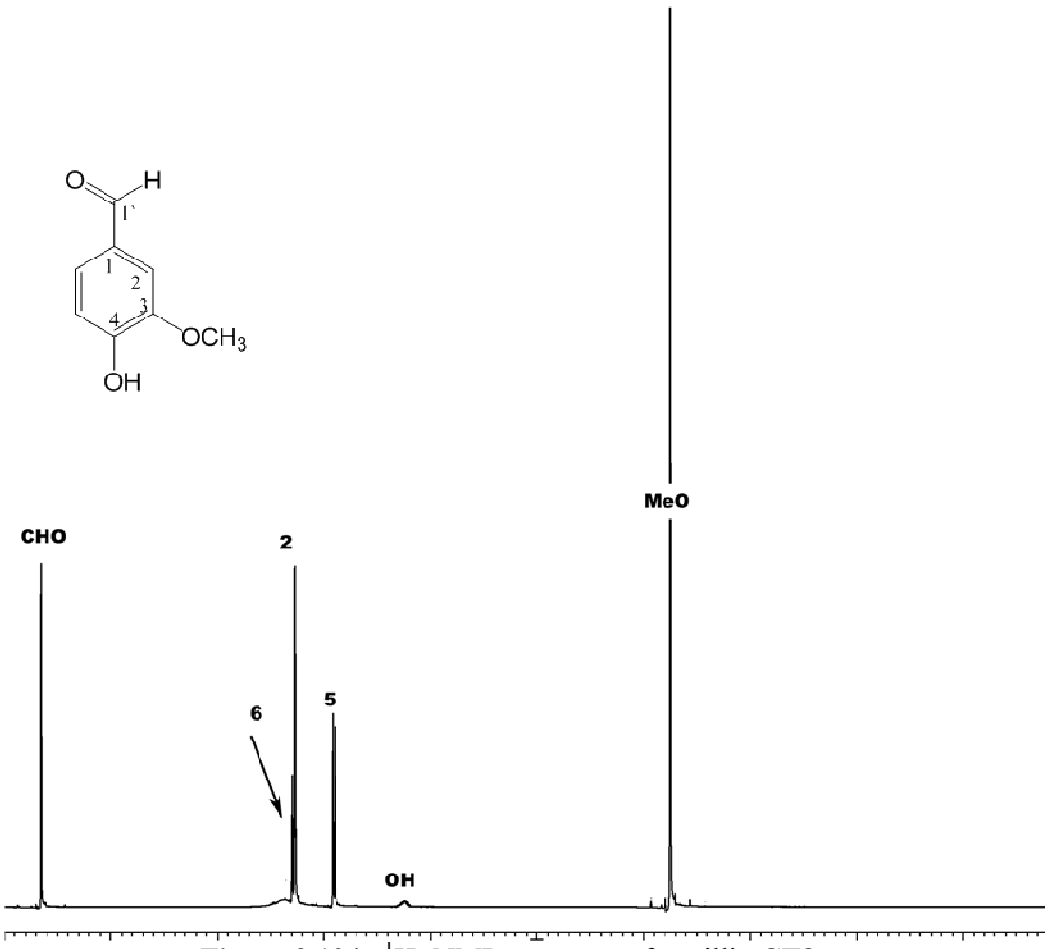

Figure 3.104 : ^{1}H -NMR spectrum of vanillin **CT8**

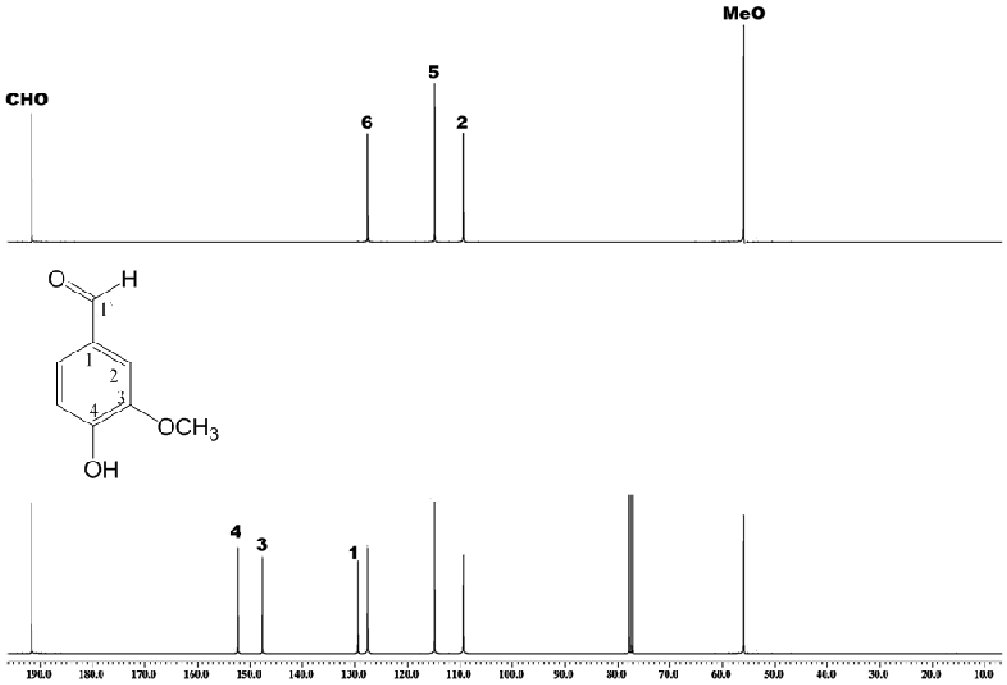

Figure 3.105 : ^{13}C/DEPT-NMR specta of vanillin **CT8**

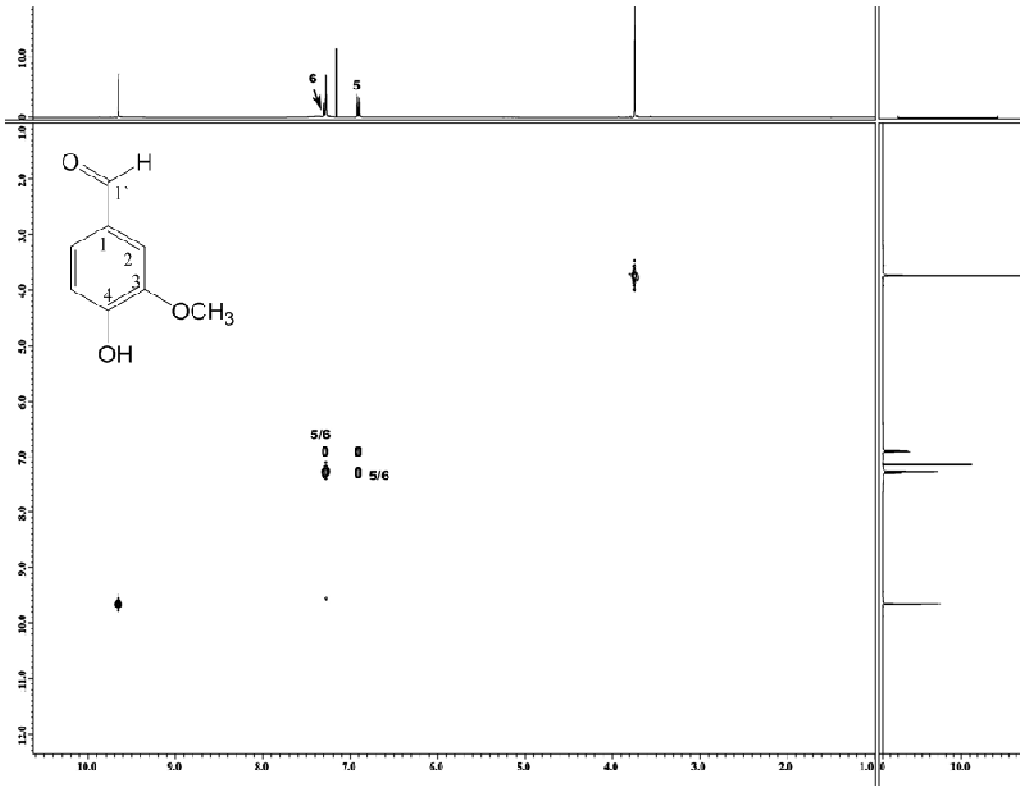

Figure 3.106 : COSY spectrumof vanillin **CT8**

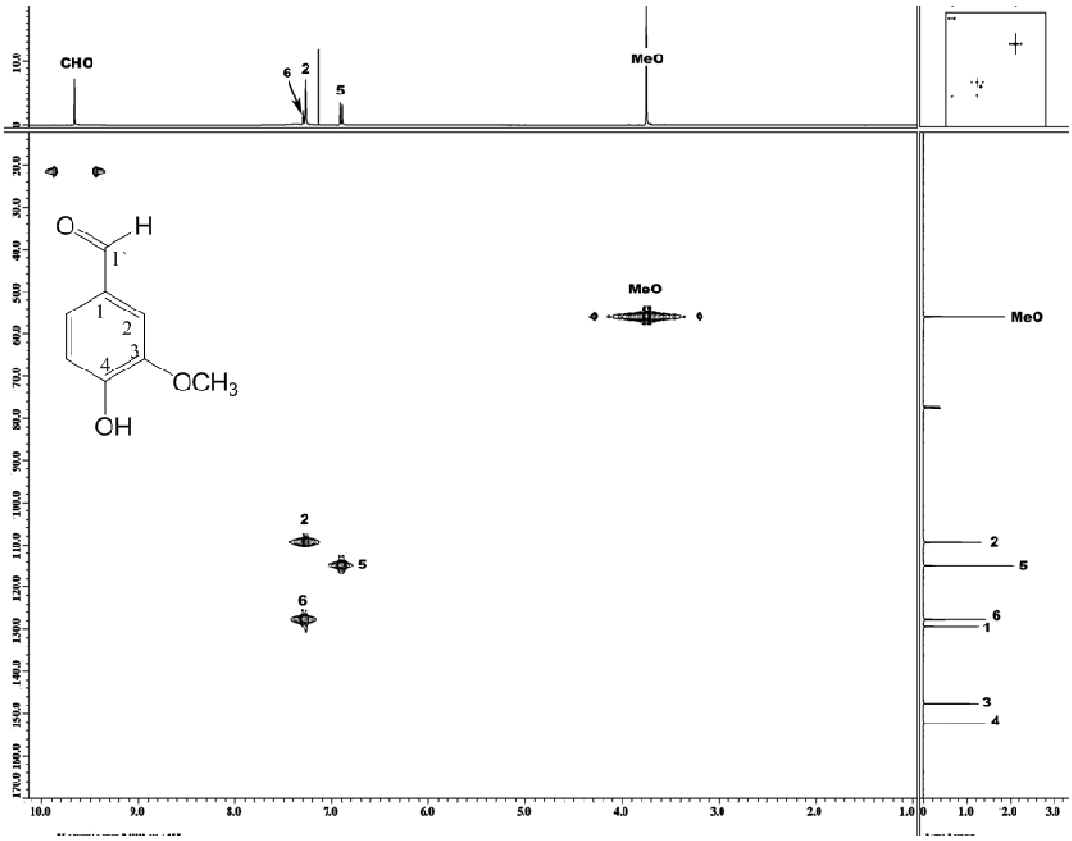

Figure 3.107 : HMQC spectrum of vanillin **CT8**

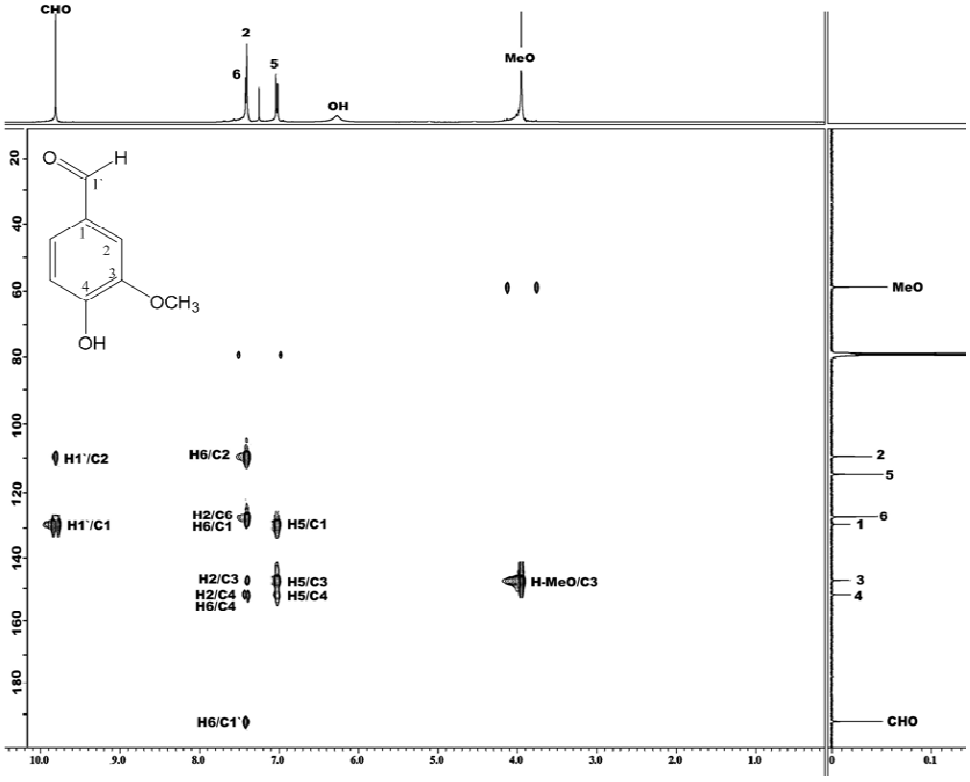

Figure 3.108 : HMBC spectrum of vanillin **CT8**

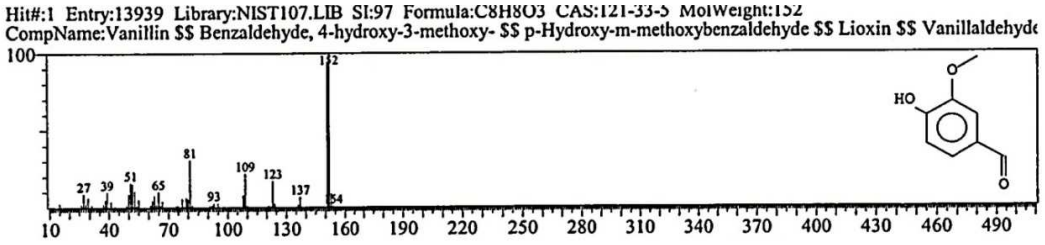

Figure 3.109 : LCMS of vanillin **CT8**

3.2.7 Goniothalamin CT9

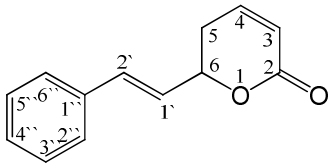

Goniothalamin was isolated as as white crystal m.p 85-87°C [153], $[\alpha]_D$ + 125.3° (c, 1.38 $CHCl_3$). The UV λ_{max} spectrum showed the absortion at 210, 258, 300 and 310 nm. The IR spectrum showed signals at ν_{max} 1718, 1244 and 750 cm^{-1} assignable to the resonance of α, *β*-unsaturated sigma-lactone moiety. GCMS showed a molecular ion peak $[M]^+$ at m/z 200 which consistent with the molecular formula $C_{13}H_{12}O_2$. The base peak was observed at m/z 68, corresponding to the ionized furan.

^{1}H-NMR (Table 3.17, Figure 3.110) showed two olefinic protons at δ_H 6.26 and at δ_H 6.71 with *J* =16.0 Hz which belongs to H-1` and H-2`, respectively ascribable to trans configuration. Resonances at δ_H 6.07 (1H, dt, 9.6, 1.8 Hz) and δ_H 6.96 (1H, dt, 9.6, 4.3 Hz) were assigned to H-3 and H-4 of α,*β*-unsaturated sigma-lactone moiety. A multiplet was observed at δ_H 2.53 corresponding to an allylic methylene (H-5) and a proton on a carbon bearing the oxygen of the lactone group appeared as a quadruple doublet at δ_H 5.08 (H-6).

^{13}C/DEPT NMR spectra (Table 3.17, Figure 3.111) of Goniothamin exhibited 11 signals corresponding to 13 carbon resonances. Signal at δ_C 164.0 was ascribable to carbonyl carbon attached to oxygen (C-2), while signal at δ_C135.8 was assigned to a quarternary carbon C-1`` Monosubstituted ring system that gave equivalent peaks at δ_C

128.8 and δ_C 126.8 were attributed to C-3``/5`` and C-2``/4``, respectively. Four olefinic carbons were observed at δ_C 125.7, 133.2, 121.7 and 144.8 corresponding to C-1`, C-2`, C-3 and C-4, respectively. The rest of the signals were assigned to a methylene carbon at δ_C 29.9 and a deshielded methine carbon at δ_C 78.6 which should be oxygenated one. The structure has been further approved by COSY (Figure 3.112), HMQC (Table 3.17, Figure 3.113), HMBC (Figure 3.114), and GCMS (Figure 3.115). Based on the spectral data and comparison with literature, compound **CT9** was assigned as goniothalamin [153].

Table 3.17 : 1D (^{1}H and ^{13}C) and 2D (HMQC and HMBC) NMR spectral data of Goniothalamin **CT9** in $CDCl_3$

Position	**δ_H (int.; mult.; J(Hz))**	**δ_C**	**HMQC**	**HMBC**
2		164.0		
3	6.07 (1H, dt, 9.6, 1.8)	121.7	H-C3	2, 5
4	6.96 (1H, dt, 9.6, 4.3)	144.8	H-C4	2, 6
5	2.53 (2H, m)	29.9	H_2-C5	1`,2,3,4,6
6	5.08 (1H, qd, 7.8, 1.8)	78.0	H-C6	2, 4, 5, 1`, 2`
1`	6.26 (1H, dd, 16.0, 6.4)	125.7	H-C1`	2`, 5, 6
2`	6.71 (1H, d, 16.0)	133.2	H-C2`	1`, 6
1``		135.8		
2``	7.38 (1H, dd, 6.8, 1.8)	126.8	H-C2``	2`, 4``
3``	7.28 (1H, qt, 6.8, 1.4)	128.8	H-C3``	2``, 6``
4``	7.33 (1H, dt, 6.8, 1.4)	128.5	H-C4``	1``, 3``, 5``
5``	7.28 (1H, qt, 6.8, 1.4)	128.8	H-C5``	2``, 6``
6``	7.38 (1H, dd, 6.8, 1.8)	126.8	H-C6``	2`, 4``

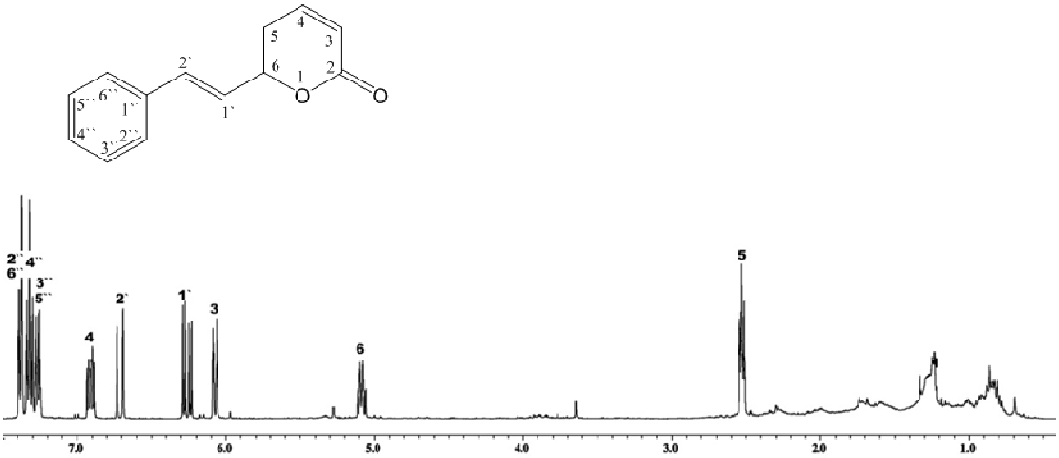

Figure 3.110 : ^{1}H-NMR spectrum for Goniothalamin **CT9**

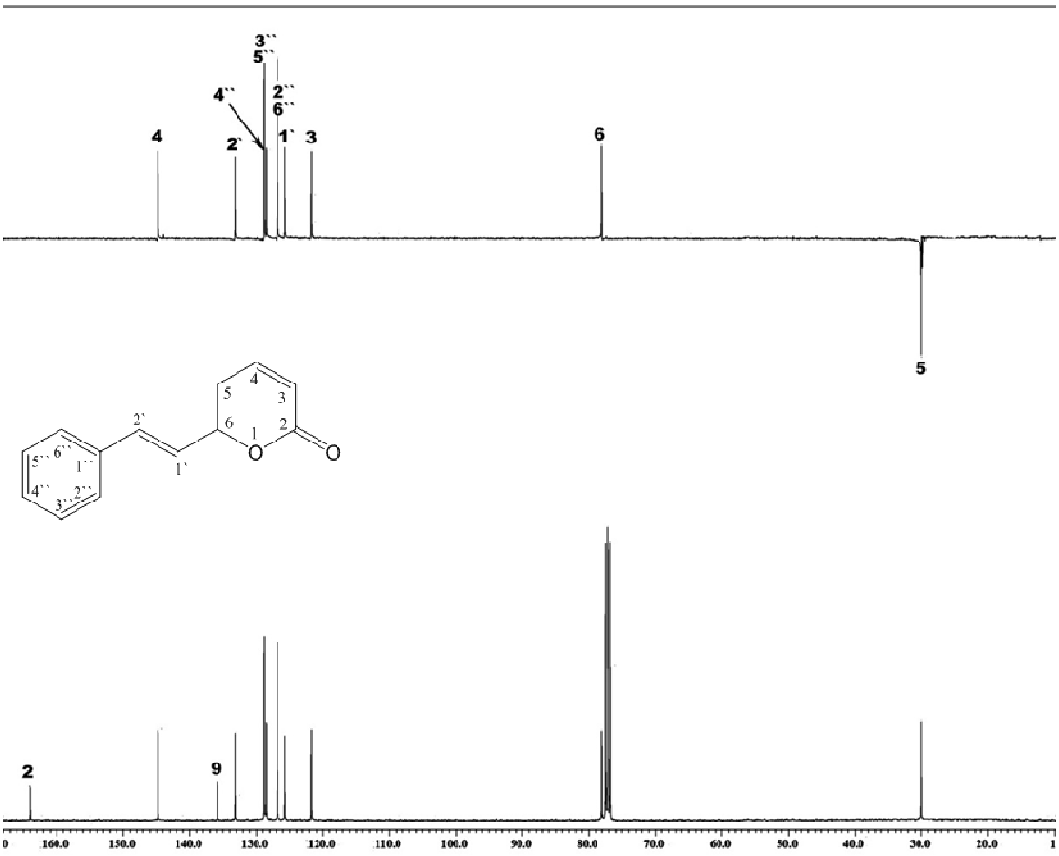

Figure 3.111 : ^{13}C/DEPT-NMR spectra for Goniothalamin **CT9**

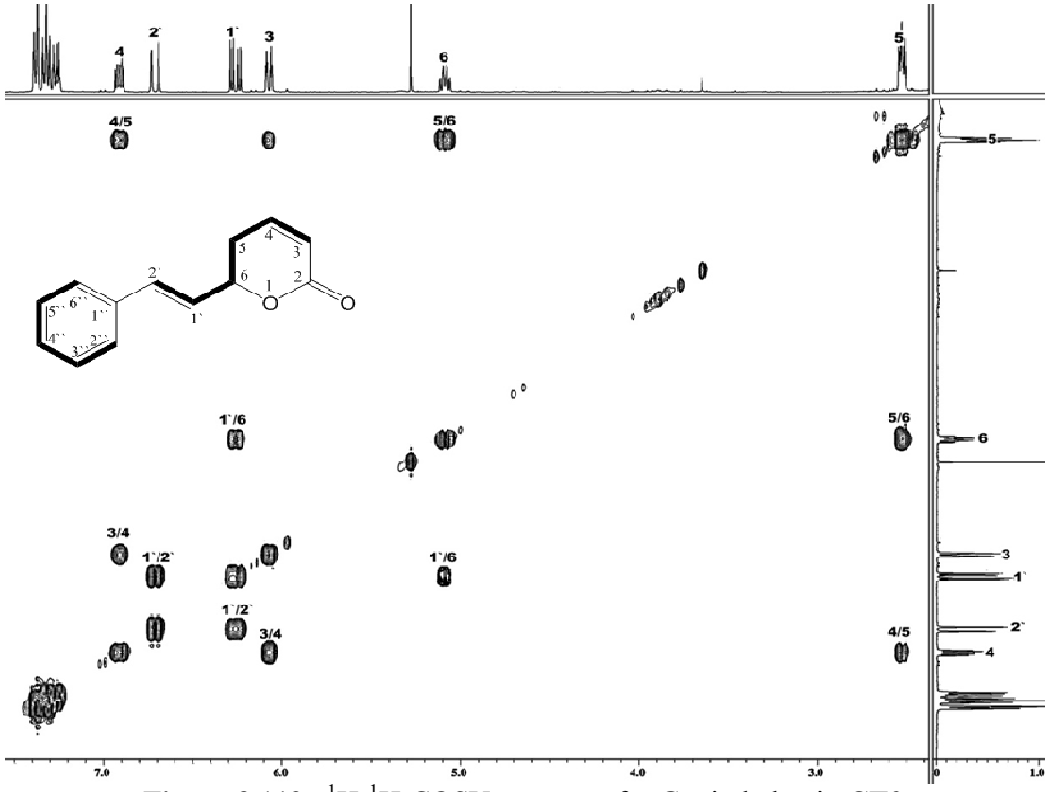

Figure 3.112 : ^{1}H-^{1}H-COSY spectrum for Goniothalamin **CT9**

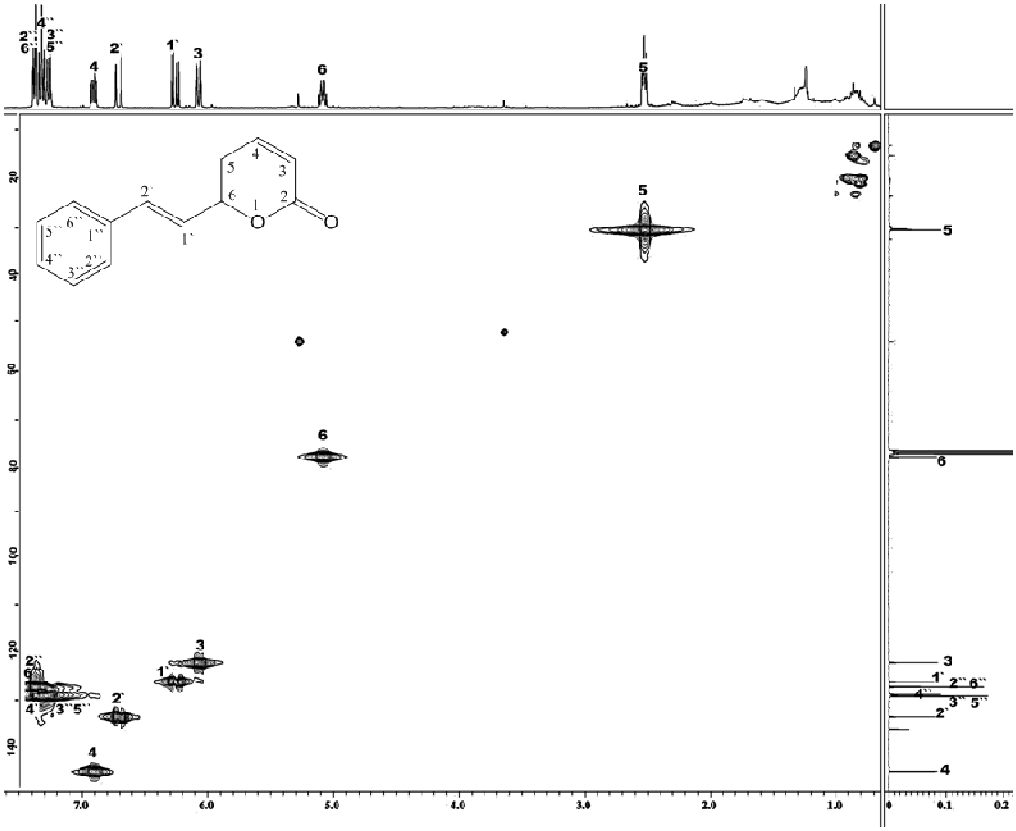

Figure 3.113 : HMQC spectrum for Goniothalamin **CT9**

Figure 3.114 : HMBC spectrum for Goniothalamin **CT9**

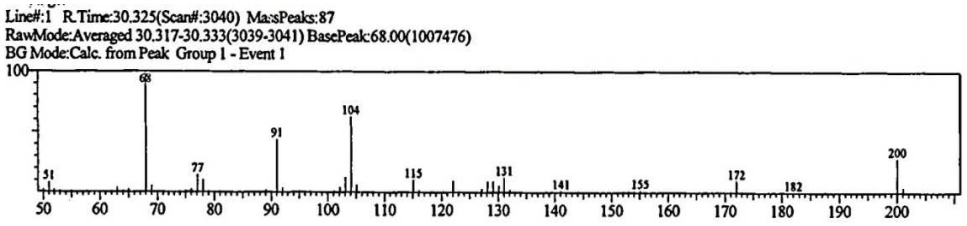

Figure 3.115 : GCMS spectrum of Goniothalamin **CT9**

3.3 Phenolic Compound, Triterpene and Steroids from the Leaves and Bark of *Dysoxylum macrocarpum*

The leaves and bark of *Dysoxylum macrocarpum* were firstly extracted with hexane followed by dichloromethane and lastly with methanol. The dichloromethane crudes were subjected to column chromatography, preparative thin layer chromatography, and high performance liquid chromatography to yield four compounds. Two compounds were isolated from the leave of *Dysoxylum macrocarpum,* which are 5-Hydroxy-7-methoxy-2-methyl-4H-chromen-4-one (Eugenin) **DM1**. This compound was new as crystal and squalene **DM2**. Two more compounds were isolated from the bark of *Dysoxylum macrocarpum*, they were stigmasterol **CT3** and sitosterol **CT4**, as shown in Table 3.18.

Table 3.18 : Chemical constituents of *Dysoxylum macrocarpum*

Compounds	Type of compounds	%yield
(Eugenin) **DM1**	phenolic	0.18
squalene **DM2**	triterpene	1.2
stigmasterol **CT3** and sitosterol **CT4**	steroids	0.23

3.3.1 5-Hydroxy-7-methoxy-2-methyl-4*H*-chromen-4-one (Eugenin) DM1

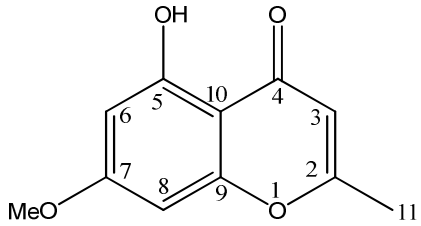

Compound **DM1** was isolated for the first time as white crystal [154] m.p118-119 °C. The UV spectrum showed λ_{max} 207, 232, 250, 256, 290 and 316 nm. The IR absorption showed a broad signal at ν_{max} 3434 cm^{-1} assignable to OH and a strong

absorption at ν_{max} 1636 cm^{-1} which was characterized for a conjugated ketone. The LCMS spectrum showed a molecular positive ion peak $[M+H]^+$ at m/z 207 which consistent with the molecular formula $C_{11}H_{10}O_4$+H.

Furthermore, in the ^{1}H-NMR spectrum (Table 3.19, Figure 3.116) of **DM1** showed three singlet peaks two of them were sharp singlet at δ_H 2.343 and 3.84 due to methyl and methoxy protons , respectively, and one singlet at exact δ_H 6.00 indicated the proton of H-3. Two doublets at δ_H 6.30 and 6.33 indicated the presence of two protons in *meta* positions of H-6 and H-8, respectively.

The ^{13}C-NMR and DEPT spectra (Table 3.19, Figure 3.117) of **DM1** exhibited 11 signals corresponding to 11 carbon resonances. Signal at δ_C 182.6 was ascribable to conjugated carbonyl carbon C-4. Furthermore five sp^2 quaternary carbons among them four were oxygenated (C-2, C-5, C-7, C-9) and appeared in more downfield in comparison with the fifth one C-10. In COSY spectrum no correlation was found. The structure has been further approved by HMQC (Table 3.19, Figure 3.118), HMBC (Figure 3.119), X-Ray (Figure 3.120), and LCMS (Figure 3.121). Based on the spectral data and comparison with literature [155], compound **DM1** was assigned as 5-Hydroxy-7-methoxy-2-methyl-4*H*-chromen-4-one.

Table 3.19 : 1D (^{1}H and ^{13}C) and 2D (HMQC and HMBC) NMR spectral data of eugenin **DM1** in $CDCl_3$

Position	δ_H (int.; mult.; J(Hz))	δ_C	HMQC	HMBC
2		166.9		
3	6.00 (1H, s)	108.8	H-C3	2, 4, 10, 11
4		182.6		
5		162.2		
6	6.30 (1H, d, 2.0)	98.0	H-C6	4, 5, 7, 8, 10
7		165.4		
8	6.33 (1H, d, 2.0)	92.5	H-C8	6, 7, 9, 10
9		158.2		
10		105.3		
11	2.34 (3H, s)	20.6	H_3-C11	2, 3
MeO	3.84 (3H, s)	55.8	H_3-MeO	7

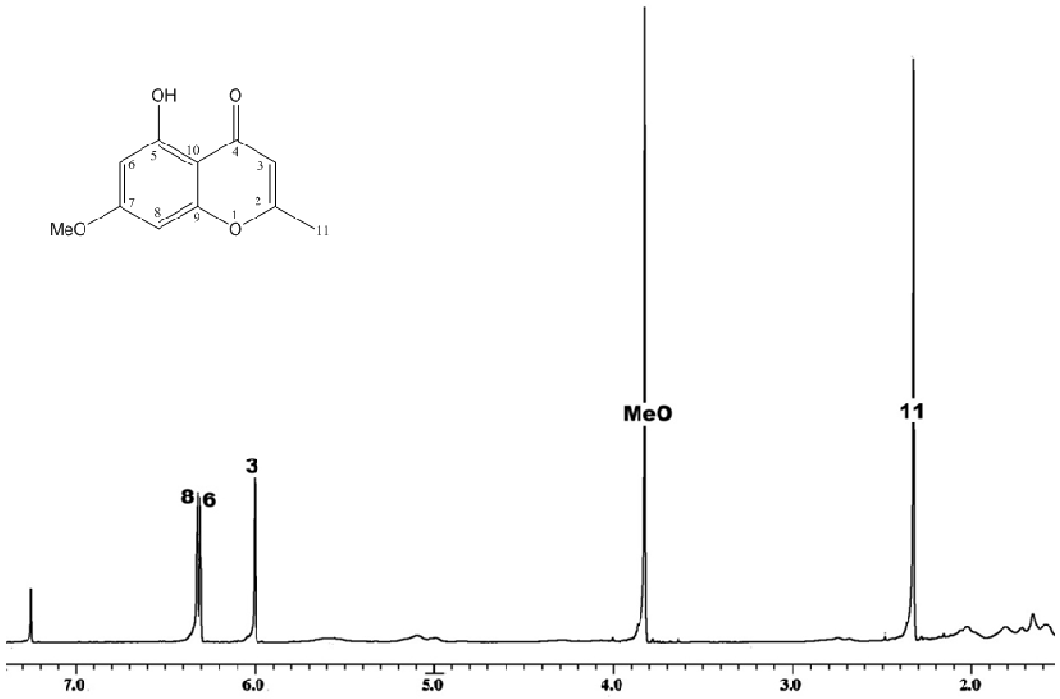

Figure 3.116 : ^{1}H-NMR spectrum of eugenin **DM1**

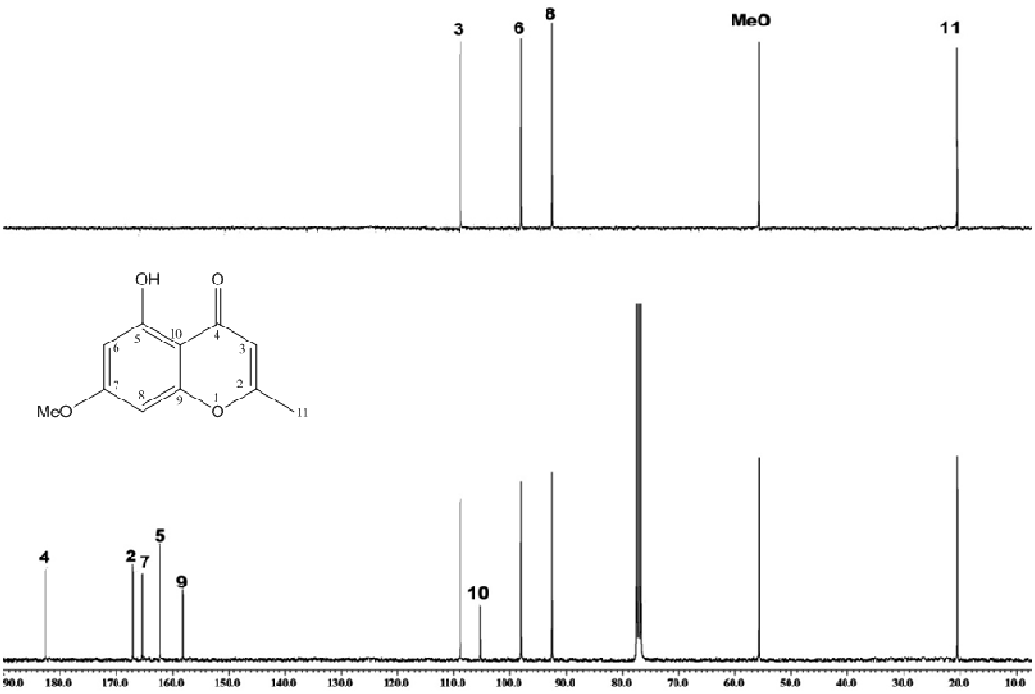

Figure 3.117 : ^{13}C/DEPT-NMR specta of eugenin **DM1**

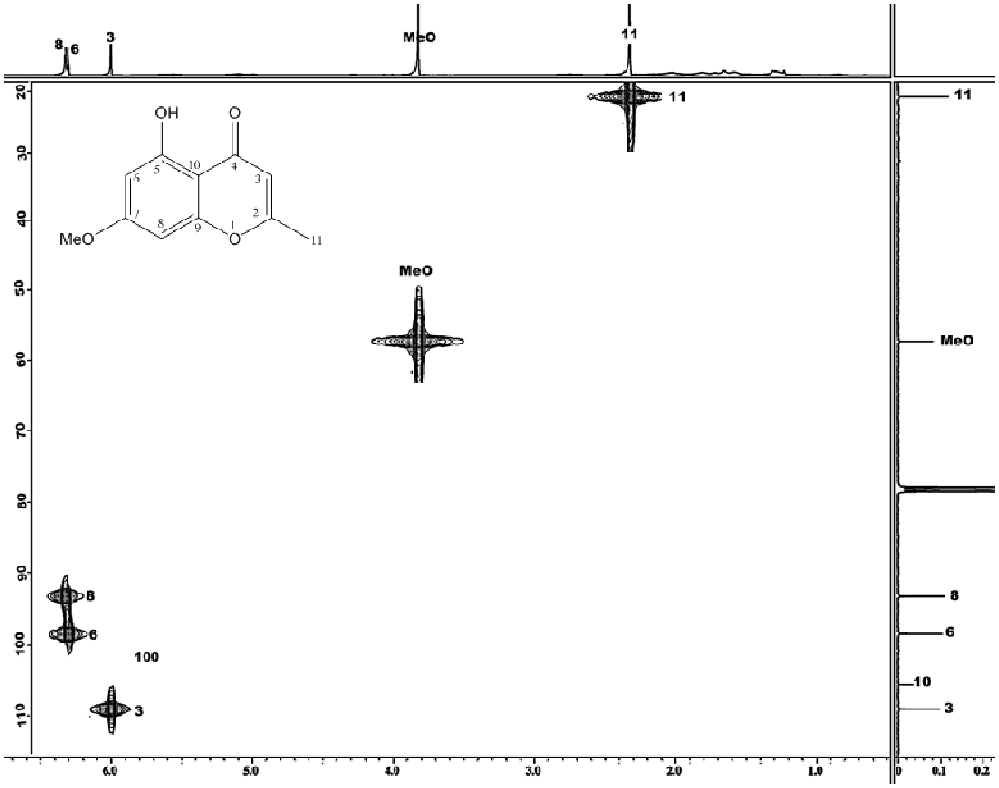

Figure 3.118 : HMQC spectrum for eugenin **DM1**

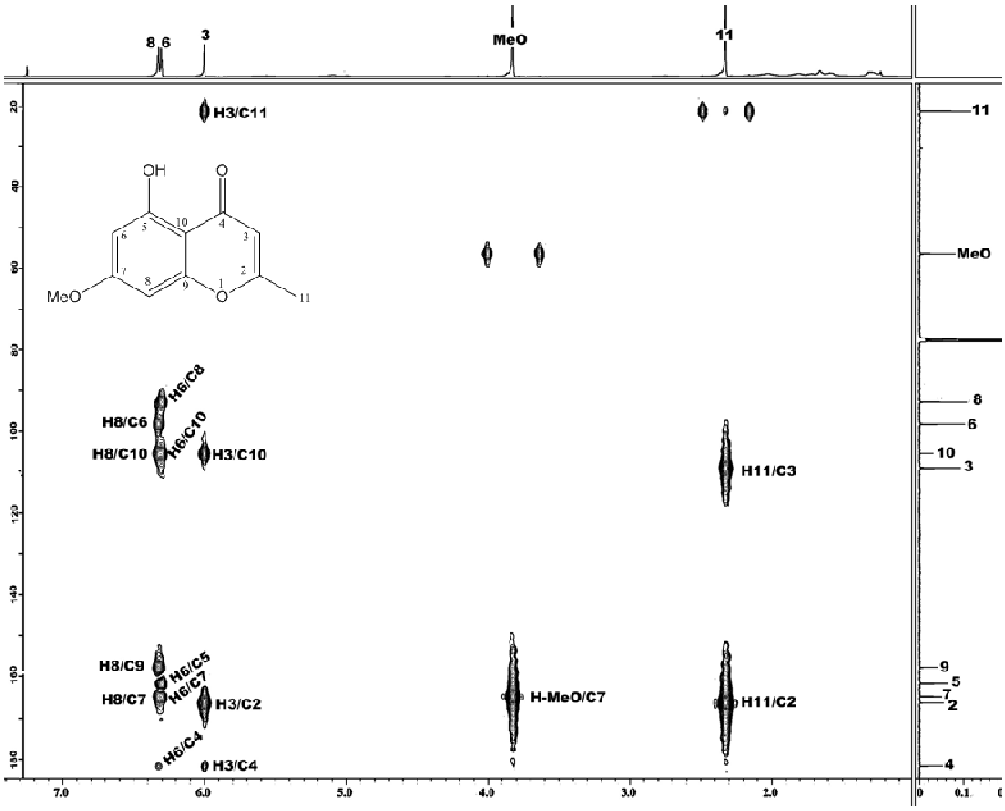

Figure 3.119 : HMBC spectrum of eugenin **DM1**

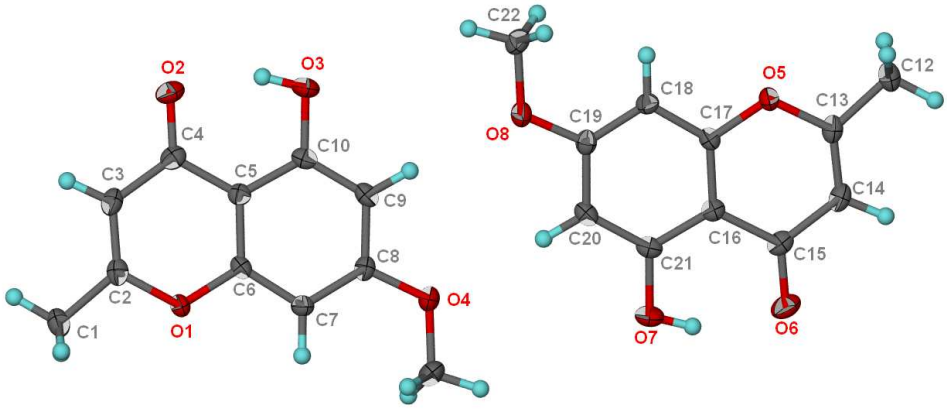

Figure 3.120 : X-Ray structure of eugenin **DM1**

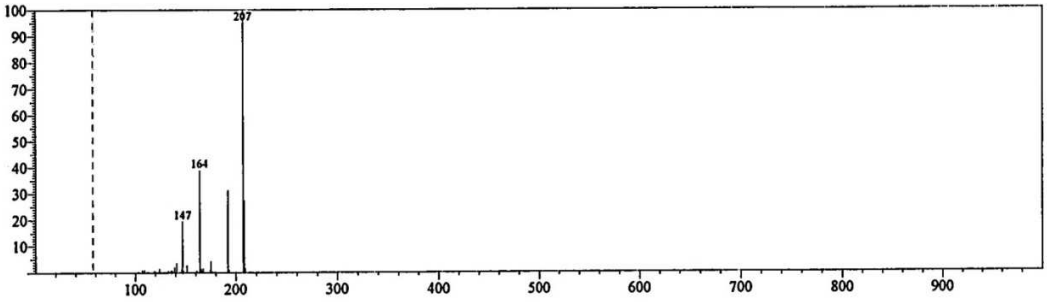

Figure 3.121 : LCMS of eugenin **DM1**

3.3.2 Squalene DM2

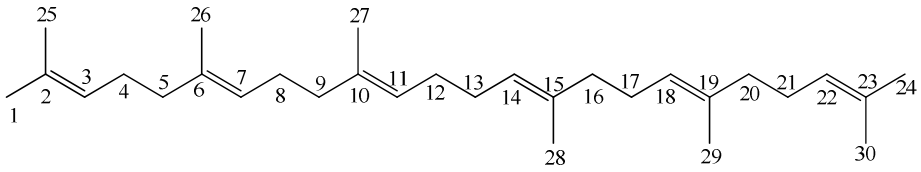

Compound **DM2** was isolated as yellow colored oil with b.p. 285°C. The UV spectrum showed λ_{max} at 344 nm. The IR spectrum showed signals at ν_{max} 2914 (C-H stretching), 2728, 1668 (alkene, non-conjugated), 1446 (alkane, CH_2), 1382 (alkane, CH_3), 1330, 1224, 1151, 1188, 964 (alkene, disubstituted trans), 835 (two adjacent hydrogen atoms). The GCMS spectrum showed the molecular ion mass $[M]^+$ at m/z 410 which consistent with the molecular formula $C_{30}H_{50}$.

The ^{1}H-NMR spectrum (Table 3.20, Figure 3.122) consists of four signal groups dispersed over the sp^3 and sp^2 chemical shift range. In the olefinic regions, six protons (H-3, H-7, H-1 1, H-14, H-18 and H-22) were found at δ_H 5.10, the signal groups of twenty protons (ten methylene) appeared at δ_H 2.05 belongs to H_2-4, H_2-5, H_2-8, H_2-9, H_2-12, H_2-13, H_2-16 H_2-17, H_2-20 and H_2-21. Meanwhile, a ^{1}H-NMR spectrum consisted a singlet at δ_H 1.66, that clearly belonged to H_3-1 and H_3-24, together with a broad singlet at δ_H 1.58 ($6H_3$) which corresponded to (H_3-25, H_3-26, H_3-27, H_3-28, H_3-29, H_3-30).

All proton signals have been further substantiated by the presence of the ^{13}C / DEPT experiments (Table 3.20,

Figure 3.123), which showed 30 resonance carbons, due to eight methyls, ten methylenes, six methines resonating at δ_C 124.20, 124.30 and 124.40, and six trisubstituted quartemary carbons. In the ^{13}C-NMR spectrum, the out-of-chain methyl groups appeared at δ_C 17.65, 16.02 and 15.98 indicated the geometry of the six trisubstitutional double bonds, while signal appeared at δ_C 25.67 (H_3-1 and H_3-24), confirmed its in-chain position. The elucidation of the structure has been approved by

2D NMR COSY (Figure 3.124), HMQC (Figure 3.125), and GCMS (Figure 3.126). These NMR spectral data were almost the same as squalene.

Based on these ^{1}H and ^{13}C-NMR spectral features and by comparison with the authentic data, compound **DM2** was identified as squalene [156-158].

Table 3.20 : ^{1}H-NMR and ^{13}C-NMR, for squalene in CDCl3

Position	**δ_H (int.; mult.; J(Hz))**	**δ_C**
1, 24	1.66 (3H, s)	25.67
2, 23		131.22
3, 22	5.10 (1H, m)	124.20
4, 21	2.05 (2H, m)	26.77
5, 20	2.05 (2H, m)	39.75
6, 19		134.88
7, 18	5.10 (1H, m)	124.40
8, 17	2.05 (2H, m)	26.66
9, 16	2.05 (2H, m)	
10, 15		135.08
11, 14	5.10 (1H, m)	124.30
12, 13	2.05 (2H, m)	28.27
25, 30	1.58 (3H, bs)	17.65
26, 29	1.58 (3H, bs)	16.02
27, 28	1.58 (3H, bs)	15.98

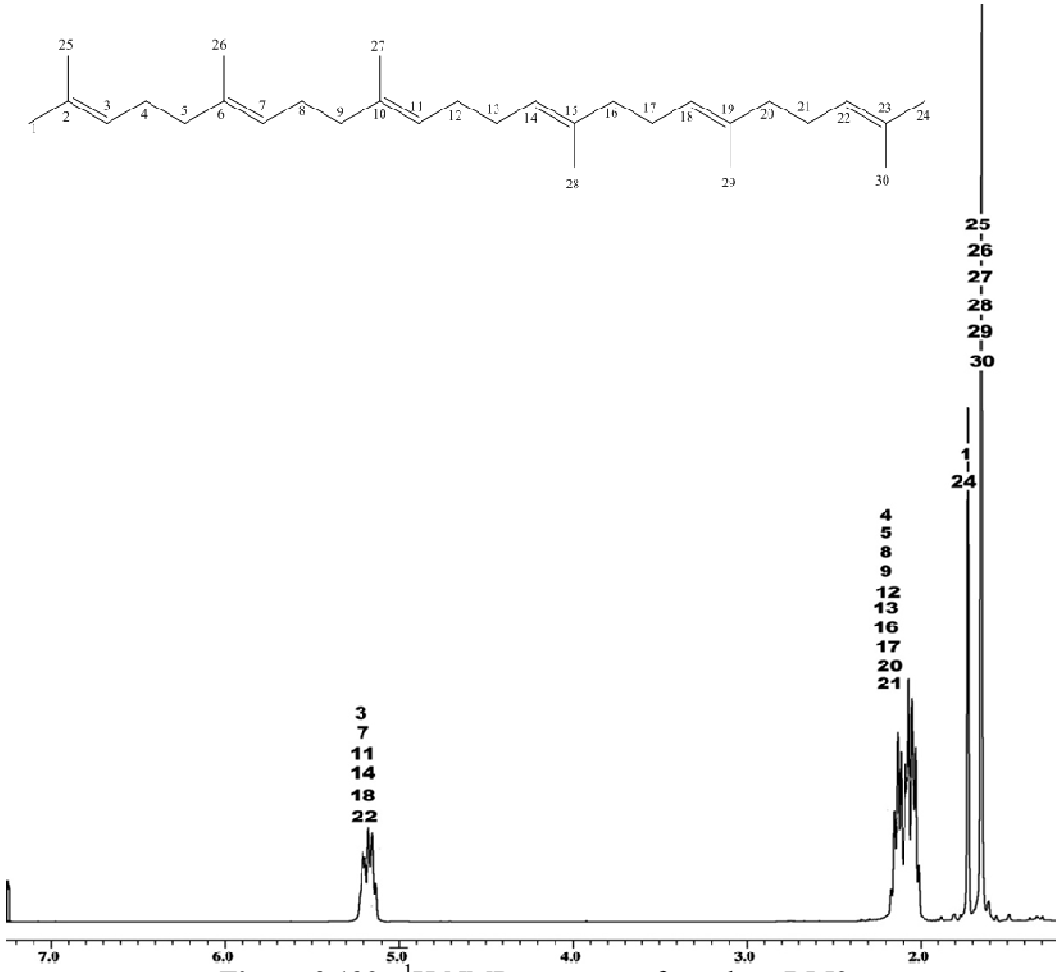

Figure 3.122 : ^{1}H-NMR spectrum of squalene **DM2**

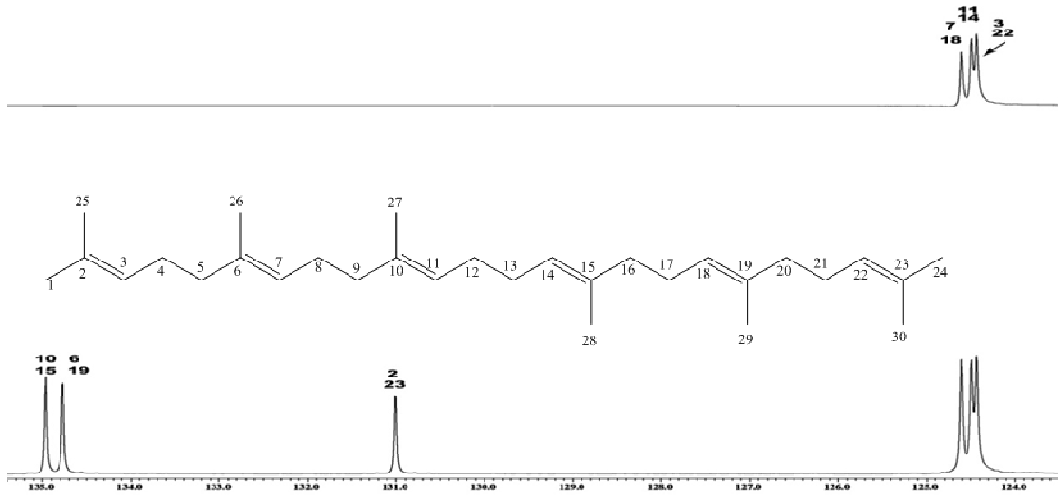

Expansion of the ^{13}C/DEPT spectrum in the sp^2 region

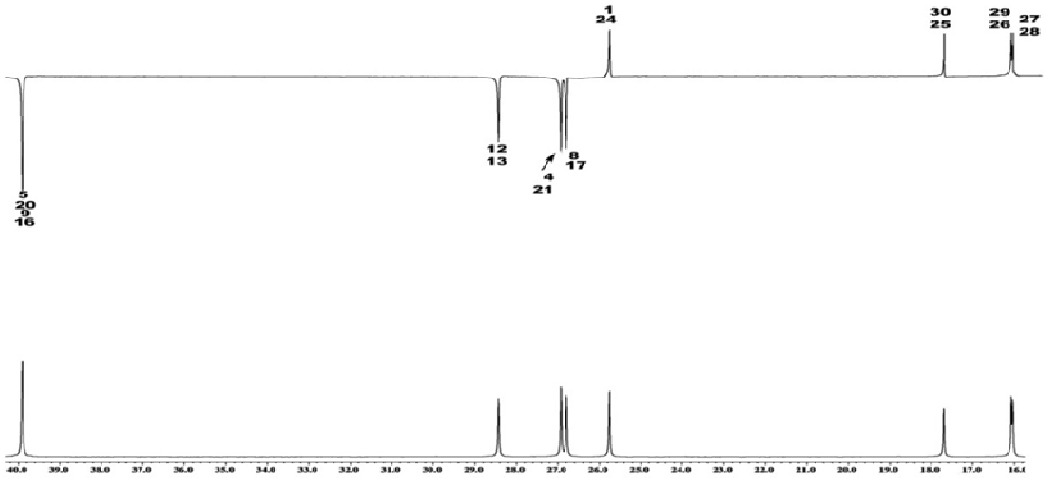

Expansion of the ^{13}C/DEPT spectrum in the sp^3 region

Figure 3.123: ^{13}C/DEPT spectra of squalene **DM2**

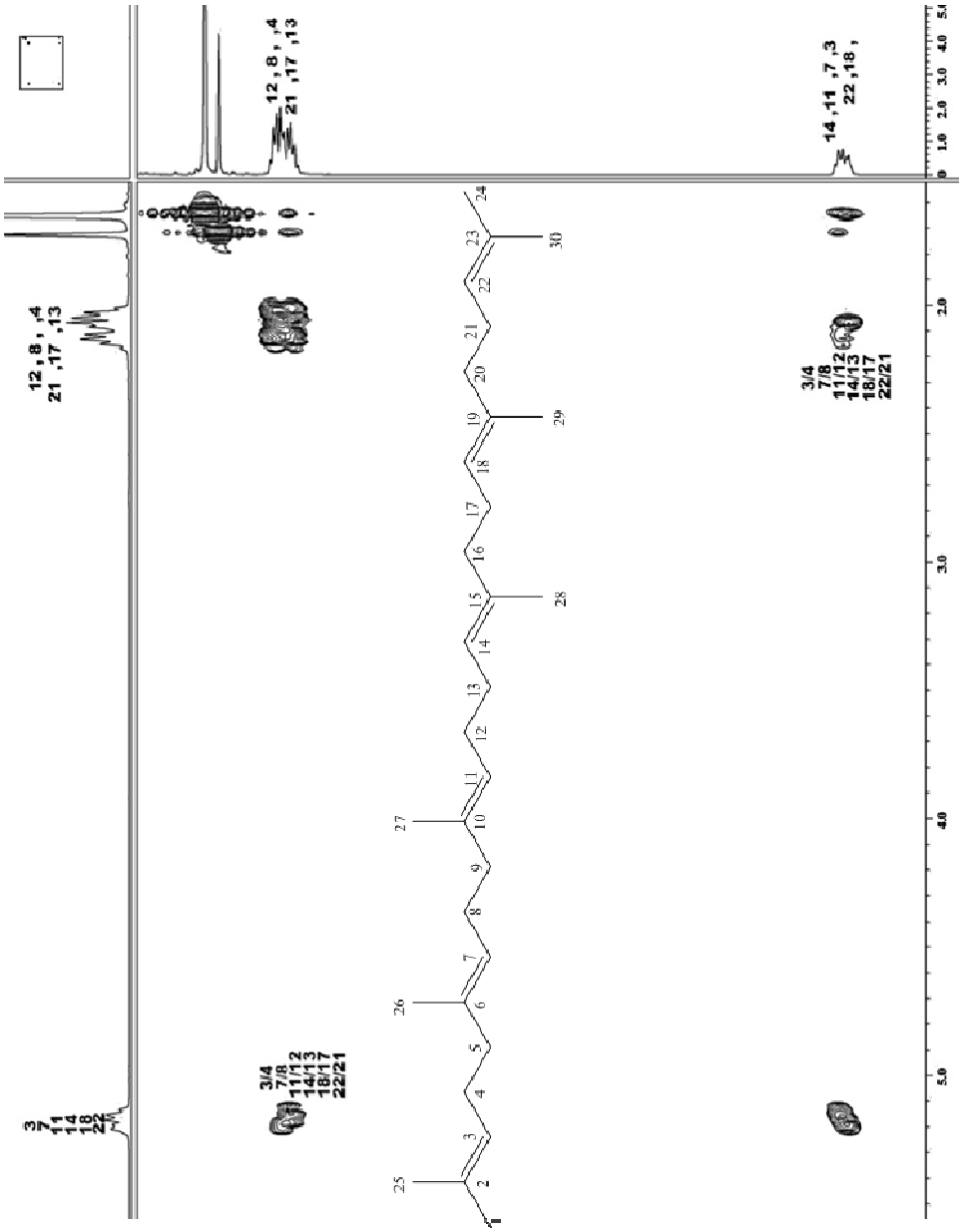

Figure 3.124 : ^{1}H-^{1}H -COSY spectrum of squalene **DM2**

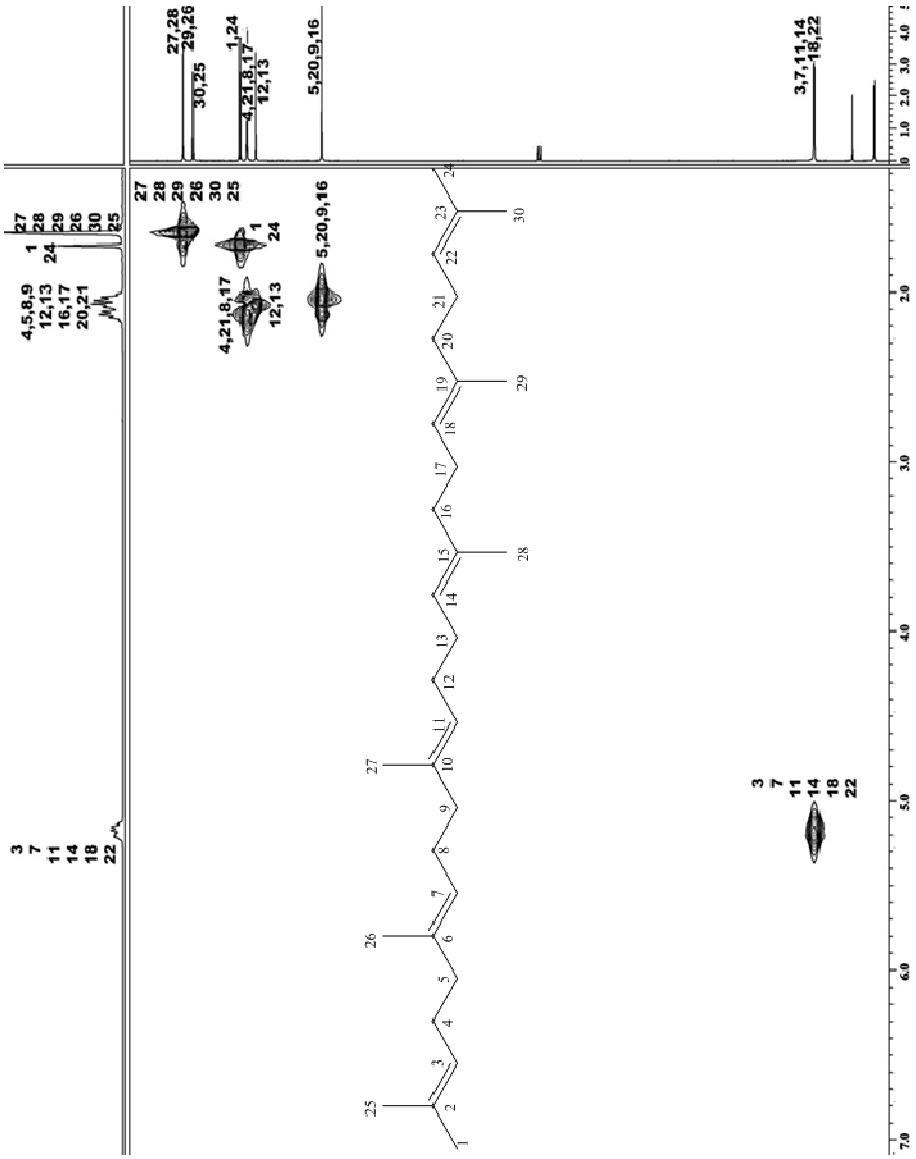

Figure 3.125 : HMQC spectrum of squalene **DM2**

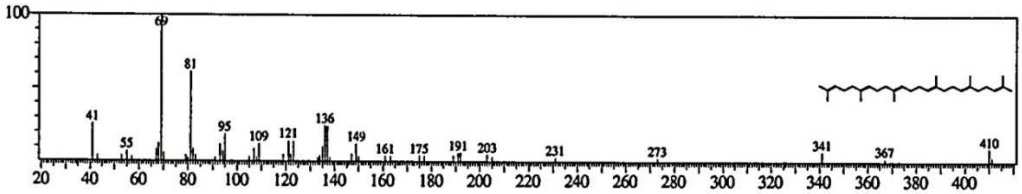

Figure 3.126 : GCMS of squalene **DM2**

3.3.3 Stigmasterol CT3 and *β*-Sitosterol CT4

Two compounds were isolated in the bark of *Dysoxylum macrocarpum*, the physical properties, MS, UV, IR, NMR data show that the two compounds are similar to those in stigmasterol **CT3** and *β*-sitosterol **CT4,** for their data see table 3.12.

CHAPTER FOUR

BIOACTIVITY

4.0 Introduction

Cancer is an ancient illness, in recent years; it has been increased, this topic forms a part of our objectives. Due to this reason, the author screened some isolated compounds against various types of cancer cell lines. Five limonoids, chisomicine A **CC1**, chisomicine B **CC2**, chisomicine C **CC3**, 14-deoxyxyloccensin K **CC6**, and proceranolide **CC7** have been selected for biological activity on their nitric oxide NO inhibitory properties in view of their traditional use for various medicinal purposes in Meliaceae family. Meanwhile, three of the above limonoids **CC1**, **CC2,** and **CC6** as well as 7-hydroxy-*β*- sitosterol **CT1,** along with one portion of hydroxy acid derivatives of ferulate **CT5A-P,** and ferulaldehyde **CT7** were tested for *in-vitro* cytotoxicity activities.

4.1 Materials

Human cancer cell lines were obtained from American Type Culture Collection (ATCC) (Manassas, VA, USA). Roswell Park Memorial Institute (RPMI), Dulbecco's modified Eagle's medium (DMEM), 100 mM non-essential amino acids, phosphate buffer solution (pH 7.2), 50 µg/ml gentamycin and 2.5 µg/ml amphotericin B were purchased from Invitrogen Corporation (Carlsbad, CA, USA). 200 mM L-glutamine, foetal bovine serum, 0.25% trypsin-EDTA, dimethyl sulphoxide (DMSO), 1X PBS (MediaTech, USA), cisplatin and vinblastine sulphate were purchased from Sigma–Aldrich (St. Louis, MO, USA). MTS assay kit [3-(4,5-dimethylthiazol-2-yl)-5-(3-carboxymethoxyphenyl)-2-(4-sulphophenyl)-2*H*-tetrazolium, inner salt] was supplied by Promega (Madison, WI, USA). MTT reagent, Griess reagent (1% sulfanilamide, 0.1% N- lnaphthylethylenediamine dihydrochloride in 2.5% H_3PO4 was added), LPS (5

µg/mL), Annexin V-FITC. Apoptosis Detection Kit (Calbiochem, USA), PI (30.0 µg/ml) (Calbiochem, USA), 1X ice cold binding buffer (Calbiochem, USA), cisplastin, vinblastine and tamoxifan (Merck, USA).

4.2 Methods

4.2.1 Cell lines culture

Nine types of cancer cell lines; mouse macrophage (J774.1), lung (A549), prostate (DU-145), skin (SK-MEL-5), pancreatic (BxPC-3), liver (Hep G2), colon (HT-29), breast (MCF-7) and (MDA-MB-231) and one normal human mammary epithelia cell (HMEC) were cultured either in RPMI or DMEM media supplemented with 2 mM L-glutamine, 10% foetal bovine serum, 50 µg/ml gentamycin and 2.5 µg/ml amphotericin B, maintained in a 37 ºC humidified atmosphere of 5% CO_2 cell incubator. The cultures were sub-cultured every 2 or 3 days and routinely checked under an Eclipe TS-100 fluorescence microscope (Nikon, Japan) for any contamination. Cells were split when 80-90% confluency was attained on the culture flask surface. Spent media was aspirated using a vacuum pump connected to a Pasteur pipette and discarded. Cells were washed with 1X PBS (MediaTech, USA) to remove any residual serum that could inactive trypsin activity. The PBS was removed and 1.0 ml of 0.25% (v/v) Trypsin (SAFC Biosciences, USA)–EDTA (Gibco, USA) solution was added. Cells were then incubated at 37°C for 10 minute to completely detach cells from the T-25cm^2 flask (Nunc, Denmark) surface, 4X volumes of media containing 10.0% (v/v) FBS (JRScientific, USA) was added to inactive trypsin activity, and pipette into a 15.0 ml falcon tube. Neutralized cells were then centrifuge at 1,500 rpm for 10 minute, and the supernatant was discarded. The cell pellet was re-suspended in fresh media containing 10.0% (v/v) FBS (JRScientific, USA), 100.0 U/ml penicillin (Lonza, USA) and 100.0 µg/ml streptomycin (Lonza, USA) and split into two or three flask for further usage.

4.2.2 NO Production assay

J774.1 cells were cultured in the medium containing LPS (5 μg/mL) with or without the test sample at different concentrations for 24 h. NO production was then determined by the Griess assay. 100 μL of the supernatant of the cultured medium was transferred to a 96-well microtiter plate, and then 100 μL of Griess reagent (1% sulfanilamide, 0.1% N- lnaphthylethylenediamine dihydrochloride in 2.5% H_3PO_4 was added). After incubation at room temperature for 15 min, the absorbance at 540 nm and 620 nm was measured with a microplate reader.

4.2.3 MTS/MTT Cytotoxicity assay

Cytotoxicity of the compounds chisomicine A **CC1**, chisomicine B **CC2,** 14-deoxyxyloccensin K **CC6** 7-hydroxy-*β*- sitosterol **CT1,** one portion of hydroxy acid derivatives of ferulate **CT5A-P**, and ferulaldehyde **CT7** were evaluated against 8 types of cancer cell lines; lung (A549), prostate (DU-145), skin (SK-MEL-5), pancreatic (BxPC-3), liver (Hep G2), colon (HT-29), breast (MCF-7) and (MDA-MB-231). Samples and drug standards (cisplatin, vinblastine sulphate and tamoxifan) were dissolved in DMSO and further diluted with DMEM or RPMI media to yield a final DMSO concentration of less than 0.5% v/v. Cells were plated into 96-well microplates at 5,000-10,000 cells per well and maintained in the cell incubator for 24 hour. Then, samples were introduced in triplicates to a final concentration of 0- 100 μM. Drug standards were also introduced to a final concentration of 0-2000 μM (cisplatin), 0-100 μM (vinblastine sulphate) and 0-100 μM (tamoxifan). Cells were further incubated for 48hrs and at the end of the period, cell viability was determined. After incubation, 20 μL per well of MTS or MTT reagent was added into each well and mixed by gently tapping the plate. Microplates were returned to the incubator for 1-2 hours until a purple formazon precipitate was clearly visible. The media was then aspirated, and 200.0 μl of

DMSO (Merck, Germany) was then added to all wells to dissolve the purple formazon precipitate. The plate was left to stand for one hour on shaker in the dark to allow complete color stabilization of the formazon compound. Absorbance of the formazan product was read on a microplate reader at 490 nm with 690 nm as the background wavelength (Infinite 200, Tecan, Männedorf, Swizerland). IC_{50} of samples and drug standards were determined using dose-response curves in Prism 5.02 software (Graph Pad Software Inc., La Jolla, CA, USA) and excel graph.

4.2.4 Apoptosis assay

Detection and differentiation of various apoptosis stages were conducted using the Annexin V-FITC. Apoptosis Detection Kit (Calbiochem, USA). Tumour cells were treated with **CT1** for 24 and 48 hrs at IC_{50} values before harvesting. After treatment, spent media containing detached cells were collected in 15.0 ml tubes. The remaining adherent cells were trypsinized, neutralized by media containing 10.0% (v/v) FBS (JRScientific, USA) and centrifuged at 3,300 rpm for 5 min. The supernantants were discarded and the cell pellets were rinse with 1 ml 1X ice-cold PBS (MediaTech, USA) and centrifuged at 3,300 rpm for 5 min. All cells were re-suspended and diluted in 6.0 ml of media to a final concentration of 1.0×10^5 cell/ml. Aliquots containing 500.0 µl of media (5.0×10^5 cells/ml) were transferred into microcentrifuge tubes, and 10.0 µl of media binding reagent (Calbiochem, USA) was added. Exposure of externalized PS was detected by adding 1.25 µl of FITC-conjugated Annexin-V anticongulant (200.0 µg/ml) (Calbiochem, USA) into each tube, and incubating at 15 minute at room temperature in the dark. All tubes were then centrifuged at 1,000 rpm for 5 minute, and the supernantant was discarded. The pellet was then re-suspended in 500.0 µl of 1X ice cold binding buffer (Calbiochem,USA), followed by the addition of 10.0 µl of PI (30.0 µg/ml) (Calbiochem, USA). All tubes were kept on ice in the dark until analyzed via

flow cytometry. All assays were carried out using the BD FACSCanto 11^{TM} flow cytometer (Becton Dickenson, USA). [159-164].

4.3 Result and Discussion

4.3.1 NO Production assay

Chisomicine A **CC1** showed NO production inhibitory activity in J774.1 cell culture line and dose-dependently stimulated by LPS but showed little effect on cell viability (Figure 4.1). However, chisomicine B **CC2** and C **CC3** as well as 14-deoxyxyloccensin K **CC6** and proceranolide **CC7** did not show NO production inhibitory activity. The activity of Chisomicine A **CC1** maybe related to its structure A2, B-seco rings in comparison with the structures of other limonoids. These findings are the first report of the NO production inhibitory activity in J774.1 cell culture line of these natural chemicals.

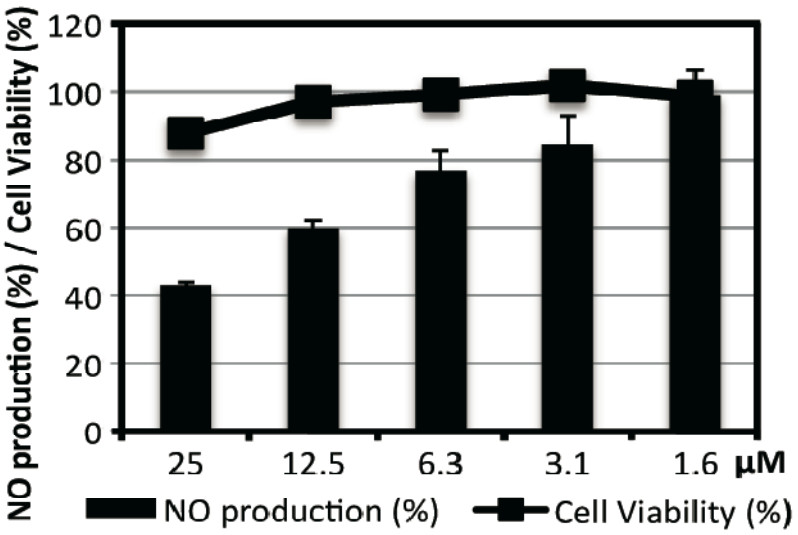

Figure 4.1 : Effect of chisomicine A **CC1** on NO production inhibitory activity in J774.1 cell line culture stimulated by LPS (assay was performed n=3).

4.3.2 MTS/MTT Cytotoxicity Assay

Chisomicine A **CC1**, Chisomicine B **CC2,** and 14-deoxyxyloccensin K **CC6** were evaluated for its cytotoxic effects against 8 types of cancer cell lines; lung (A549), prostate (DU-145), skin (SK-MEL-5), pancreatic (BxPC-3), liver (Hep G2), colon (HT-

29), breast (MCF-7) and (MDA-MB-231) using MTS assay.

Within the eight cancer cell lines used in this experiment, Chisomicine A **CC1** showed an IC_{50} of 87.69 ± 5.04 μM for colon (HT-29) cells (Table 4.1 a), in contrast to both chisomicine B **CC2** and 14-deoxyxyloccensin K **CC6**, no anti-proliferative effect observed in all cancer cells. No IC_{50} were recorded. However an IC_{50} of 87.69 ± 5.04 μM for colon (HT-29) cells treated with Chisomicine A **CC1** showed too low cytotoxic effect compared to the US NCI plant screening program that stated a pure compound is generally considered to have in vitro toxicity activity if the concentration that causes a 50% cell death is less than 4 μM/ml [163-164].

Cisplastin and vinblastine, a standard therapeutic drug used as a positive control in this experiment showed a great toxicity towards all the cancer cell lines used. Both drugs have been studied intensely particularly on the cancer cells and it is approved by FDA for the treatment of cancer. As we can see from the graph in Table 4.1 b, cisplastin show very low IC_{50} values with 12.07 ± 0.64 μM towards HepG2 cells and vinblastine with 0.16 ± 0.05 μM also towards HepG2 cells. Figure 4.2 (a and b).

Table 4.1 : **(a)** IC_{50} of samples tested on 8 different cell lines at 48 hours treatment periods

Cell lines culture	Samples (compounds)		
	Chisomicine A CC1	**Chisomicine B CC2**	**14-deoxyxyloccensin K CC6**
	(Mean ± SD, n=3)	**(Mean ± SD, n=3)**	**(Mean ± SD, n=3)**
Lung (A549)	>150 µM	>150 µM	>150 µM
Prostate (DU-145)	>150 µM	>150 µM	>150 µM
Skin (SK-MEL-5)	>150 µM	>150 µM	>150 µM
Pancreatic (BxPC-3)	>150 µM	>150 µM	>150 µM
Liver (Hep G2)	>150 µM	>150 µM	>150 µM
Colon (HT-29)	87.69 ± 5.04 µM	>150 µM	>150 µM
Breast (MCF-7)	>150 µM	>150 µM	>150 µM
Breast (MDA-MB-231)	>150 µM	>150 µM	>150 µM

Table 4.1 : **(b)** IC_{50} of drugs tested. Each value is the mean ± SD of three determinations.

Cell lines culture	Standard drugs	
	Cisplatin	**Vinblastine**
	(Mean ± SD, n=3)	**(Mean ± SD, n=3)**
Lung (A549)	37.37 ± 3.00 µM	2.36 ± 1.06 µM
Prostate (DU-145)	15.18 ± 0.49 µM	4.25 ± 1.68 µM
Skin (SK-MEL-5)	31.82 ± 0.23 µM	1.74 ± 0.67 µM
Pancreatic (BxPC-3)	20.10 ± 1.21 µM	1.13 ± 0.88 µM
Liver (Hep G2)	12.07 ± 0.64 µM	0.16 ± 0.05 µM
Colon (HT-29)	77.24 ± 3.23 µM	11.18 ± 1.88 nM
Breast (MCF-7)	91.49 ± 6.54 µM	24.08 ± 2.41 µM
Breast (MDA-MB-231)	276.53 ± 1.29 µM	31.52 ± 2.38 µM

(a)

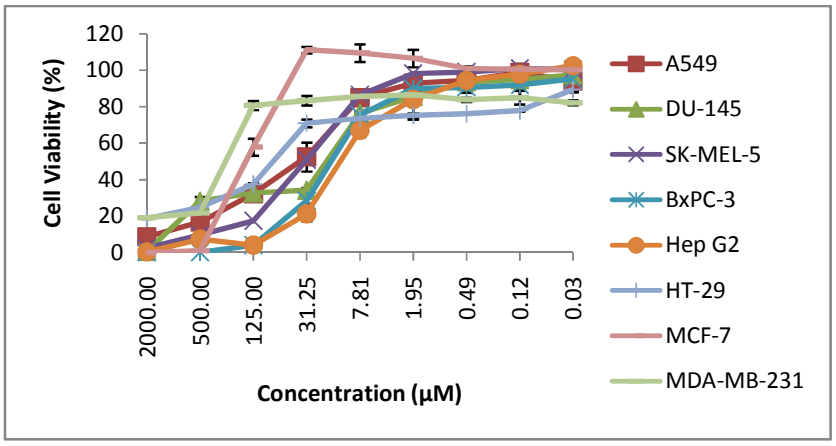

(b)

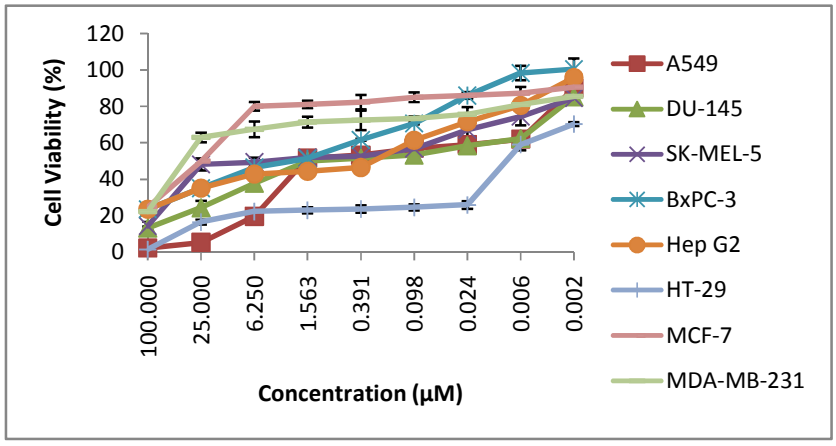

Figure 4.2 : The cytotoxic effects of (a) cisplastin and (b) vinblastine on various cancer lines at 48 hours treatment periods. Each value is the mean ± SD of three determinations.

On other hand, isolated compounds from *Chisocheton tomentosus*, 7-hydroxy-*β*-sitosterol **CT1,** hydroxy acid derivatives of ferulate **CT5A-P** and ferulaldehyde **CT7** were tested for *in-vitro* cytotoxicity activity against MCF7 cells using MTT assay. The results showed one compound exhibited cytotoxicity activity. Among the compounds, 7-hydroxy-*β*- sitosterol **CT1** had the most potent cytotoxicity effect, with the IC_{50} value of 9.0 µM (Figure 4.3) close together as that reported for a well known anti-cancer drug, tamoxifen (IC_{50}, 6.0 µM). The other compounds showed no cytotoxicity effect against MCF7 cells (Table 4.2)

7*α*-Hydroxy-*β*-sitosterol **CT1** was further study for its cytotoxicity activity against normal cell; human mammary epithelia cell (HMEC). 7-hydroxy-*β*- sitosterol

CT1 treatment exhibited cytoselectivity towards normal mammary epithelia cell (HMEC), which gave no IC_{50} value. The cytoselectivity effect was different to the treatment with Tamoxifen. However, Tamoxifen is more cytotoxic towards normal mammary epithelia cells, which inhibit 50% cells viability at 40 ± 0.31μM. As compared to Tamoxifen, 7*α*-Hydroxy-*β*-sitosterol **CT1** was 3 times less toxic against normal human mammary epithelia cells.

Table 4.2 : Summary of compound IC_{50} values as obtained from MTT cytotoxicity assay in human breast adenocarcinoma cell at 24 hours treatment periods.

Cell line	Compound	Exposure (hour)	IC_{50}(μM)	% Cell * viability
MCF7(Human Breast Adenocarcinoma)	**CT1**	24	9.0	30.1
	CT5A-P	24	n/a	95.0
	CT7	24	n/a	97.0
	Tamoxifen	24	6.0	10.3
HMEC (Human Mammary Epithelia Cell)	**CT1**	24	80.0	80.5
	Tamoxifen	24	80.0	40.0

*Percentage of cell viability after 24 hrs incubation upon maximum treatment with 100.0 μM of each compound

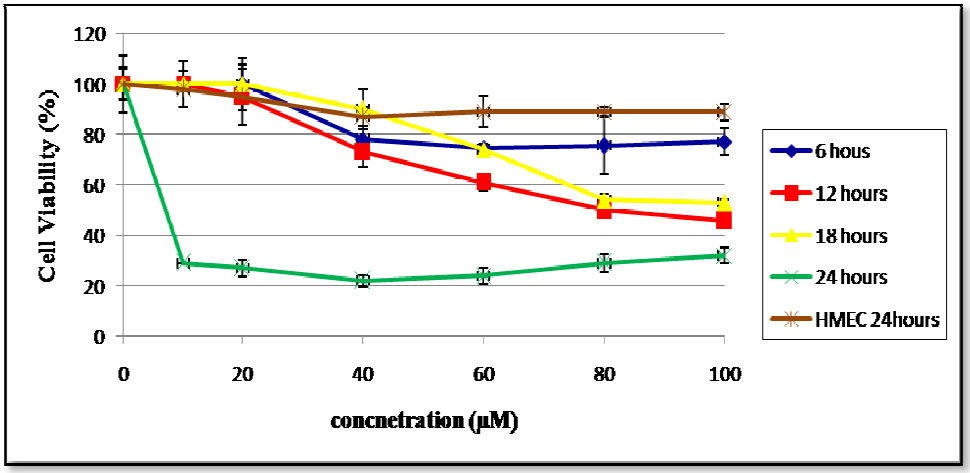

Figure 4.3 : The cytotoxic effects of 7-hydroxy-*β*- sitosterol **CT1** on MCF7 and HMEC (Brown Line) cells were assessed using MTT cell viability assay. Comparison of total relative cell viability (%) between various incubation hours after treatment with 7-hydroxy-*β*- sitosterol **CT1** at different concentrations (0 to 100µM). Results were expressed as total percentage of viable cells. Each value is the mean ± SD of three determinations.

4.3.3 Apoptosis assay

The cytotoxicity mechanism by most anticancer agents is by which apoptosis to further examined the mode of cell death in MCF7 in respond to 7-hydroxy-*β*- sitosterol **CT1**. Both control and 7-hydroxy-*β*- sitosterol **CT1** treat cells were stained with Annexin V-FITC and analyzed by flow cytometry.

Results showed that 7-hydroxy-*β*- sitosterol **CT1** induce mode of death via apoptosis (Table 4.3). Using same IC_{50} value and different incubation hours (24 and 48), induction of apoptosis was achieved at high rate at 48 hours treatment period. Most of the cells for both treatment duration 24 and 48 hours were 32.6% and 78.3% percentage death respectively (Figure 4.4). This result significantly showed that in treated MCF7 cells, cells undergoing an apoptosis process and just appeared as a normal process in every cell lives.

Table 4.3 : Summary of percentage values for each stage obtained from Annexin V assay in human breast adenocarcinoma cell, MCF7 at 24 and 48 hours treatment periods with **CT1**

Incubation (hours)	**% of viable cell**	**% of early apoptosis**	**% of late apoptosis**	**% of necrosis**
0	92.2	2.9	4.4	0.5
24	67.4	5.1	23.4	4.2
48	21.7	2.8	66.2	9.2

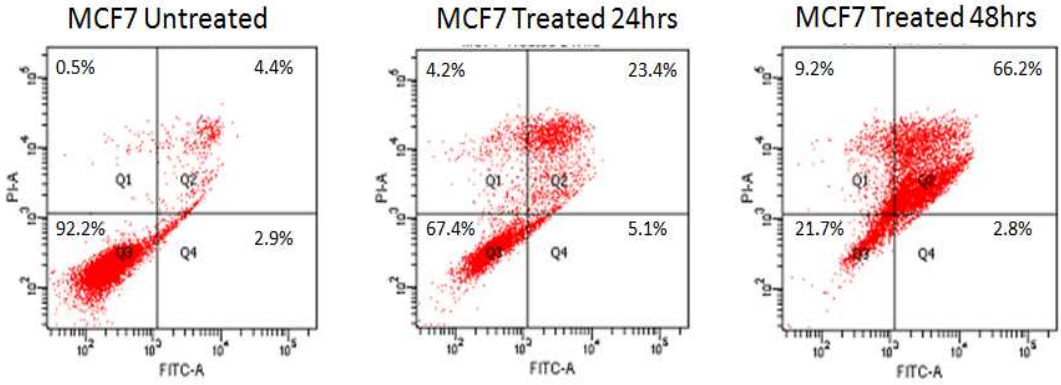

Figure 4.4 : Detection of apoptosis using annexin V-FITC and PI dual staining on MCF7 .Untreated cells (left panel) before and treated cells (right panel) after **CT1** treatment for 24 and 48 hours. Quadrants were designed as follows – Q3: non-stained cells indicating live cells; Q4: annexin V stained cells indicating early apoptosis; Q2: annexin V and PI stained cells indicating late apoptosis; and Q1: PI stained cells indicating necrosis.All dot plots are a representation of an equal cell population (n=10,000).

CHAPTER FIVE

CONCLUSION

Three species from Meliaceae family have been studied for their chemical constituents. They are *Chisocheton ceramicus* (KL-4973), *Chisocheton tomentosus* KL 4251, and *Dysoxylum macrocarpum* KL 4302, as shown in Table 5.1. Phytochemical studies of these three species from Meliaceae family led to the isolation of different types of compounds; limonoids, steroids, triterpenoids, phenolic, and coumaric compounds.

Structural elucidation was established through several spectroscopic methods, notably UV, IR**,** MS (HRMS, GCMS, and LCMS), and 1D, 2D-NMR (^{1}H-NMR, ^{13}C NMR, COSY, DEPT, HMQC, HMBC, NOESY, and single crystal X-ray diffraction analysis.

Studies on the bark of *Chisochetn ceramicus* yielded seven limonoids, among them five were new, they were chisomicine A **CC1,** chisomicine B **CC2,** chisomicine C **CC3,** chisomicine D **CC4,** and chisomicine E **CC5,** while the sixth one, 14-deoxyxyloccensin K **CC6,** was new in its occurrence as natural product and as crystal but it has been synthesized from xyloccensin K, and the last one was known compound; proceranolide **CC7**.

Isolation, identification and characterization of *Chisocheton tomentosus* afforded thirty eight compounds among them fifteen were new and one new as crystal, they were four steroids; 7α-Hydroxy-β-sitosterol **CT1** (new as crystal), stigmasta-4,6-diene-3-one **CT2**, stigmasterol **CT3** and sitosterol **CT4**, and thirty two phenolic compounds; hydroxy acid derivatives of ferulate **CT5A-P** among them **CT5A, CT5C, CT5D, CT5K, CT5L, CT5M, CT5N, CT5O, CT5P** were new, *E*-alkyl-*p*-coumarate **CT6A-O** among them **CT6B**, **CT6C, CT6L**, **CT6M**, **CT6N**, **CT6O** were new, ferulaldehyde **CT7**, and vanillin **CT8** and the last one was styryl lactone (goniothalamin) **CT9**.

While the bark and leaves of the last plant species *Dysoxylum macrocarpum* yielded four compounds among them two compounds from the leaves of *Dysoxylum macrocarpum,* which are 5-Hydroxy-7-methoxy-2-methyl-4*H*-chromen-4-one (Eugenin) **DM1,** it was new as crystal and squalene **DM2**, while two more compounds were found from the leaves of *Dysoxylum macrocarpum*; they were stigmasterol **CT3** and sitosterol **CT4**.

From the bibliographic reviews it was found that these last two species; *Chisocheton tomentosus* and *Dysoxylum macrocarpum* have not been studied before.

Five limonoids were tested for inhibitory activity against NO production. The results showed that chisomicine A **CC1** inhibited NO production in J774.1 dose-dependently stimulated by LPS and also showed little effect on cell viability. However, chisomicine B **CC2** and C **CC3** as well as 14-deoxyxyloccensin K **CC6** and proceranolide **CC7** did not show NO production inhibitory activity. Three of above limonoids chisomicine A **CC1,** chisomicine B **CC2,** 14-deoxyxyloccensin K **CC6** have been selected for further eight cancer cell lines. Only chisomicine A **CC1** showed an IC_{50} of 87.69 ± 5.04 μM for colon (HT-29) cells, in contrast to both chisomicine B **CC2** and 14-deoxyxyloccensin K **CC6**, no anti-proliferative effect observed in all cancer cells.

Some isolated compounds from *Chisocheton tomentosus* 7-hydroxy-*β*- sitosterol **CT1,** hydroxy acid derivatives of ferulate **CT5A-P,** and ferulaldehyde **CT7** were tested for *in-vitro* cytotoxicity activity against MCF7 cells. The results showed one compound showed cytotoxicity activity. Among the compounds, 7-hydroxy-*β*- -sitosterol **CT1** had the most potent cytotoxicity effect, with the IC_{50} value of 9.0 μM the same as that reported for a well known anti-cancer drug, tamoxifan (IC_{50}, 6.0 μM). The other compounds showed very weak or no cytotoxicity effect against MCF7 cells.

CHAPTER SIX

EXPERIMENTAL

6.1 Solvents

The industrial grade solvents (hexane, dichloromethane, and methanol) were used for bulk extractions, these solvents were distilled twice before use. The HPLC and analytical grade solvents were used for chromatographic separation of compounds,

6.2 Instrumentation

- NMR spectra were obtained using JEOL LA 400 FT NMR and JEOL ECA400 FT NMR Spectrometer System using deuterated chloroform as solvent. Chemical shifts were reported in ppm and coupling constants were given in Hertz (Hz).
- Mass spectra were carried out on Agilent Technologies 6530 Accurate-Mass Q-TOF LC/MS, with ZORBAX Eclipse XDB-C18 Rapid Resolution HT 4.6 mm i.d. x 50 mm x 1.8 μm column, the EI MS spectra were obtained on Shimadzu GC-MS QP2000A spectrometer 70 eV , the high-resolution ESI MS were measured on a LTQ Orbitrap XL (Thermo Scientific).
- UV spectra were recorded on a Shimadzu UV-Visible Recording Spectrophotometer using HPLC grade ethanol as solvent with mirror UV cell.
- The infrared (IR) spectra were obtained through Perkin Elmer FT-IR Spectrometer Spectrum RX1 using chloroform as solvent.
- Melting points were taken on hot stage Gallen Kamp melting point apparatus and were uncorrected.
- Optical rotations were determined on JASCO (Japan) P1000 automatic digital polarimeter.

6.3 Chromatography

6.3.1 Thin Layer Chromatography (TLC)

Aluminium supported silica gel 60 F_{254} plates was used to see the spots of the isolated compound. UV Light Model UVGL-58 Mineralight Lamp 230V, 50/60 Hz was used to examine spots or bands on the TLC after spraying with the required reagents.

6.3.2 Column Chromatography (CC)

All solvents used in this experiment are distilled industrial grade. Silica gel 60, 230-400 mesh ASTM (Merck 9385) was used for column chromatography. A slurry of silica gel 60 (approximately 30:1 silica gel to sample ratio) in hexane solvent system was poured into a glass column of appropriate size with gentle tapping to remove trapped air bubbles. The crude extract was initially dissolved in minimum amount of solvent and loaded on top the packed column. The extract was eluted with an appropriate solvent system at a certain flow rate. Fractions were collected in conical flasks and evaporated for the next step. Fractions with similar spots were then combined by TLC monitoring.

6.3.3 Preparative Thin Layer Chromatography (PTLC)

PTLC silica gel 60 F_{254} glass plates of size 20 cm x 20 cm (Merck 1.05715.0001) were used for the separation of compounds. UV Light Model UVGL-58 Mineralight Lamp 230V-50/60 Hz was used to examine bands on the PTLC.

6.3.4 High Performance Liquid Chromatography (HPLC)

Waters HPLC System was used for HPLC separation, equipped with Binary Gradient Module, System Fluidics Organizer and UV detector set at the range from 200-400 nm. Chromatographic analysis and separations were performed on ZORBAX

Eclipse Plus C18 (9.6 mm i.d. x 250 mm x 3.5 μm) HPLC columns. HPLC grade methanol, HPLC grade acetonitrile and deionized water were used as mobile phase solvents with HPLC grade formic acid as buffer. All solvents and samples were filtered with 0.45 μm nylon membrane filter (Waters) prior to HPLC analysis. The data were collected and analysed by using MassLynx software.

6.4 Detector Reagent — Vanillin-Sulphuric Acid Vapour

1.0 g vanillin in 10 mL of concentrated H_2SO_4 was added upon cooling to 90 mL of ethanol before spraying onto the TLC plate. The TLC plate was then heated at 50 °C until full development of colours had been observed. The occurrence of blue, purple, dark green, grey or brown indicated the presence of terpenes, steroids and limonoids.

6.5 Plant Materials

The plant materials were collected and identified by phytochemical team, Chemistry Department, Faculty of Science, University of Malaya. The specimens were deposited at the Chemistry Herbarium, Faculty of Science, University of Malaya, the locality and the times of collection are shown in the Table 6.1.

Table 6.1 : Plant species and locality

Species	Herbarium Specimen No.	Locality and time of collection
Chischeton ceramicus	KL 4973	Hutan Simpan Bukit Enggang in 2000
Chisocheton tomentosus	KL4251	Mersing, Johor in 1993
Dysoxylum macrococarpum	KL4302	Jeli – Dabong, Kelantan in 1993

6.6 Extraction and Isolation

6.6.1 Extraction and Isolation of *Chisocheton ceramicus*

The dried and powdered bark of *Chisocheton ceramicus* (900g) was extracted successively with methanol and the methanol extract (200g) was partitioned with 10% MeOH/H_2O and EtOAc. EtOAc soluble materials (10g) were subjected to a silica gel column (hexane/ EtOAc, 1:0→0:1), in which a fraction eluted by hexane/EtOAc (3:7) was further purified on a silica gel column with CH_2Cl_2/hexane/EtOAc (5:3:2) to afford chisomicine A **CC1** (250 mg; 2.5% yield). The second fraction eluted by hexane/EtOAc (1:4) was further purified on a silica gel column with EtOAc/acetone/hexane (65:10:25). The first sub-fraction has been subjected to an ODS HPLC (80% MeOH aqueous with 0.1% formic acid, 3.0 ml/min, 254 nm) to give pure proceranolide **CC7** (15mg, 0.15%) along with a mixture of chisomicine D **CC4** and chisomicine E **CC5,** then the mixture was subjected to an ODS HPLC using chiral column (77:23 water:acetonotrile 2.4ml/min, 210) to get pure chisomicine D **CC4** and chisomicine E **CC5** , the second subfraction has been subjected to an ODS HPLC (75% MeOH aqueous with 0.1% formic acid, 2.5 mL/min, 254 nm) to give chisomicine B **CC2** (25 mg, 0.25%) and 14-deoxyxyloccensin K **CC6** (19 mg, 0.19%). The third sub-fraction was subjected to the preparative TLC with EtOAc/acetone/hexane (65:10:25) to give chisomicine C **CC3**, (16 mg, 0.16%).scheme 6.1 showed the isolation and fractionation of compounds **CC1-CC7**.

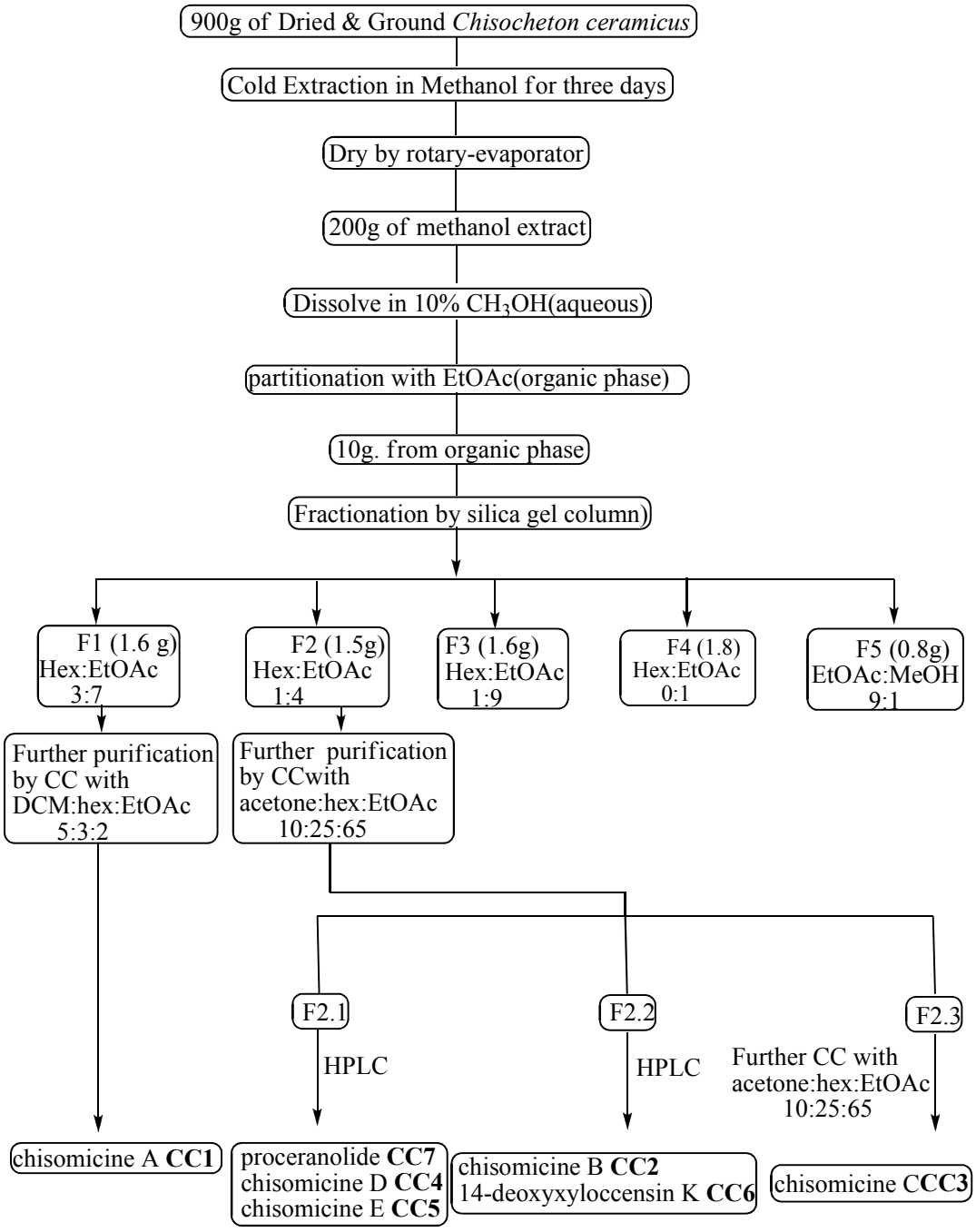

Scheme 6.1 : Extraction and purification of limonoids from *Chisocheton ceramicus*

6.6.2 Extraction and Isolation of *Chisocheton tomentosus* and *Dysoxylum Macrocarpum*

The dried samples of *Chisocheton tomentosus and Dysoxylum macrocarpum* were ground and the extraction was carried out by cold percolation method using *n*-hexane, dichloromethane (CH_2Cl_2) and methanol (MeOH) (scheme 6.2). Initially, the dried samples were extracted by using *n*-hexane for 3 to 5 days. The *n*-hexane eluent was dried using the rotary-evaporator. The *n*-hexane solvent was replaced by CH_2Cl_2 and MeOH for another 3-5 days respectively by applying the same methods as above. Then, the CH_2Cl_2 and MeOH extracts were undergone the fractionation using silica gel column chromatography. The fractions from the column were subjected to analytical Thin Layer Chromatography (TLC). The fractions were purified by using preparative TLC, micro-column. The structures of pure compounds were determined by spectroscopic methods such as UV, Infra Red, 1D and 2D Nuclear Magnetic Resonance, Mass Spectroscopy as well as X-Ray reflectometer. The crude extracts, various fractions and pure compounds were submitted to biological testing (anticancer). The extraction of each plant is shown in schemes 6.2, 6.3, 6.4, 6.5, 6.6.

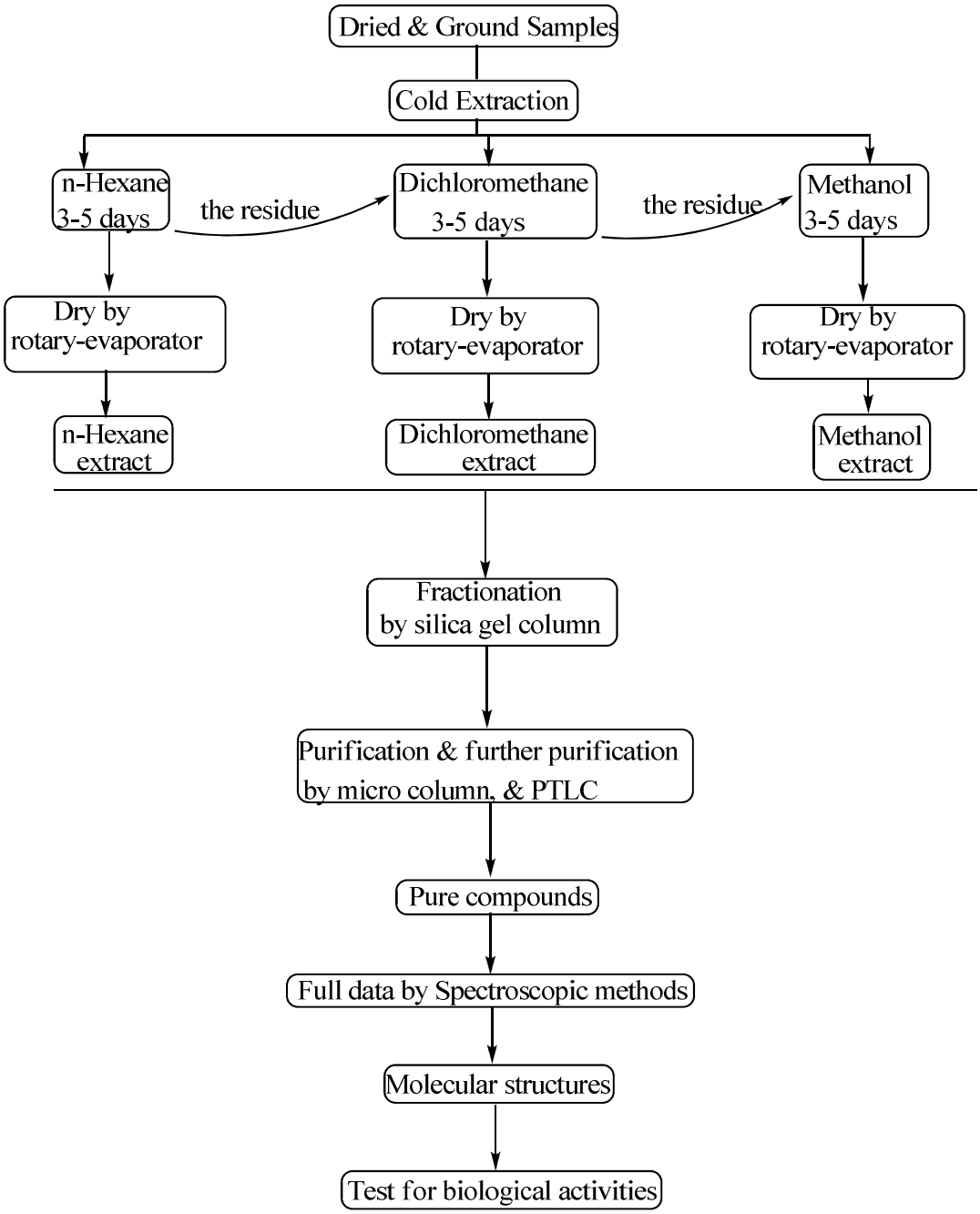

Scheme 6.2 : Extraction and isolation of chemical constituents from *Chisocheton tomentosus* and *Dysoxylum macrocarpum*

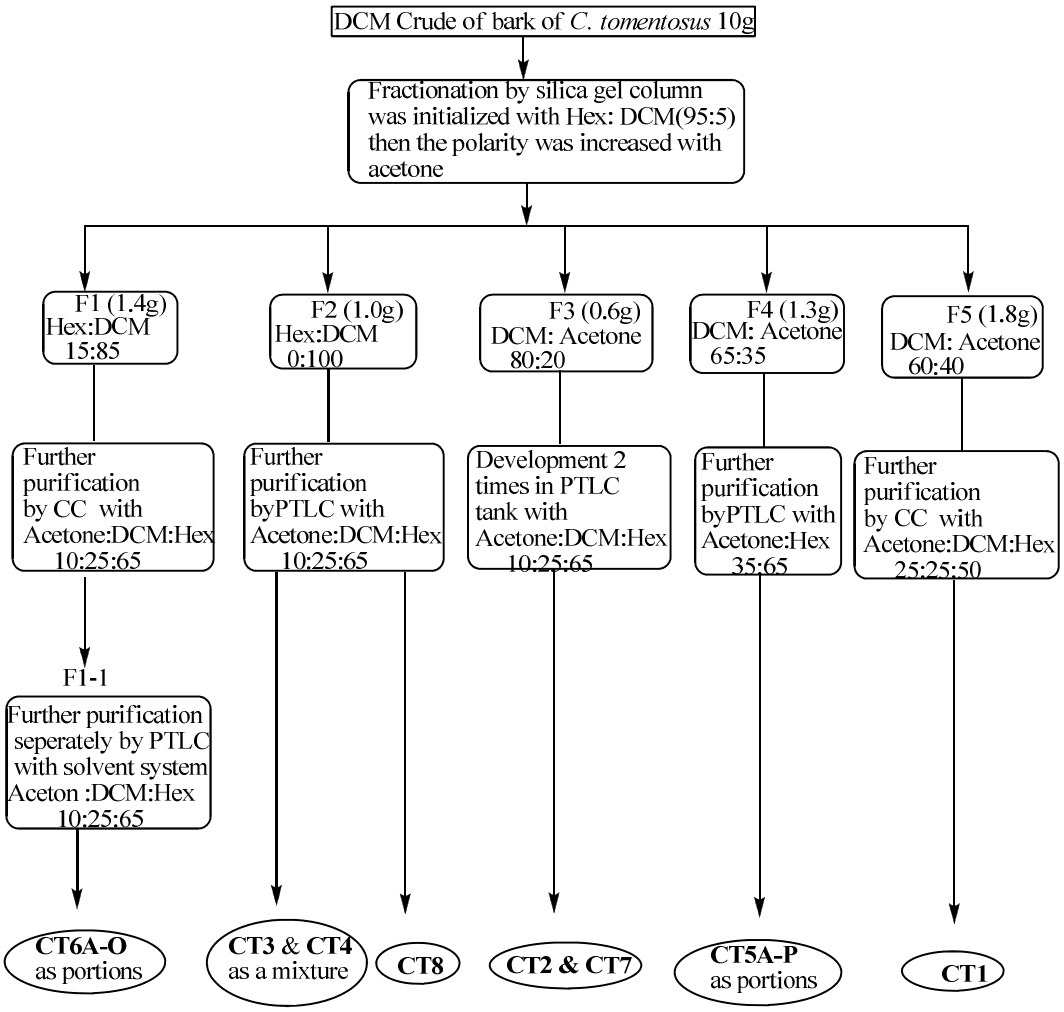

Scheme 6.3 : Isolation and Purification of chemical constituents from *Chisocheton tomentosus*

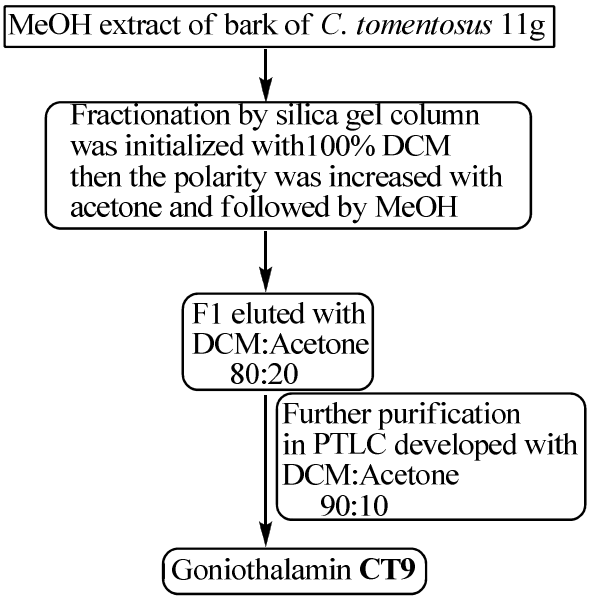

Scheme 6.4 : Isolation and purification of goniothalamin from *Chisocheton tomentosus*

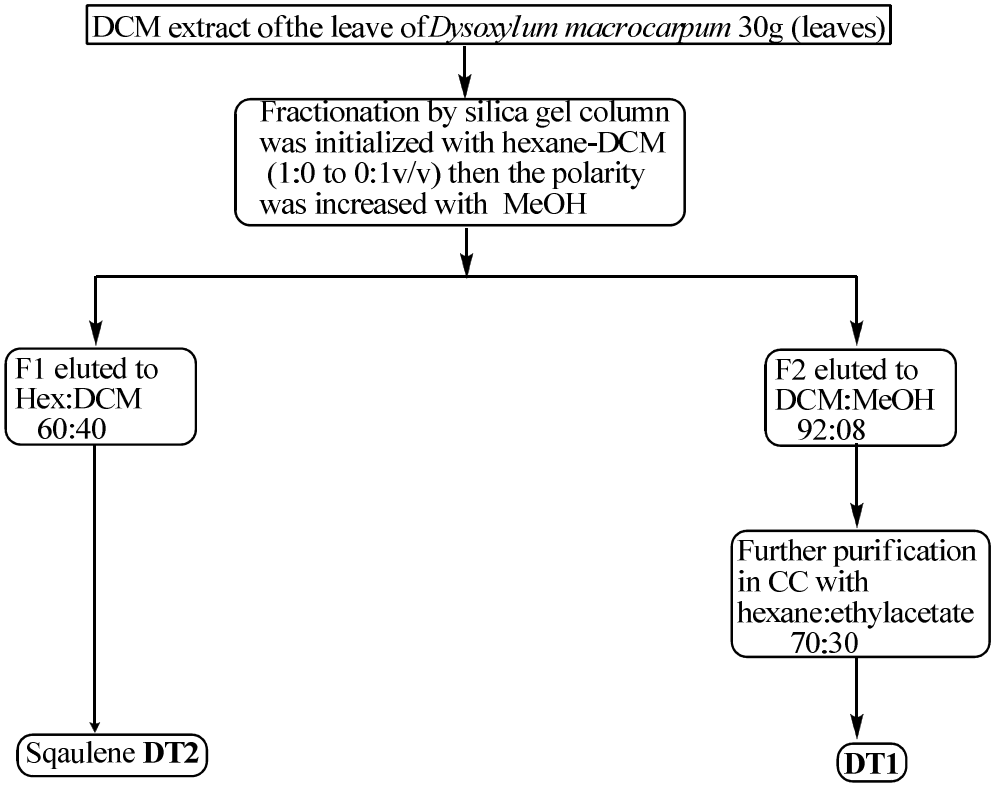

Scheme 6.5 : Isolation and purification of chemical constituents from *Dysoxylum macrocarpum*

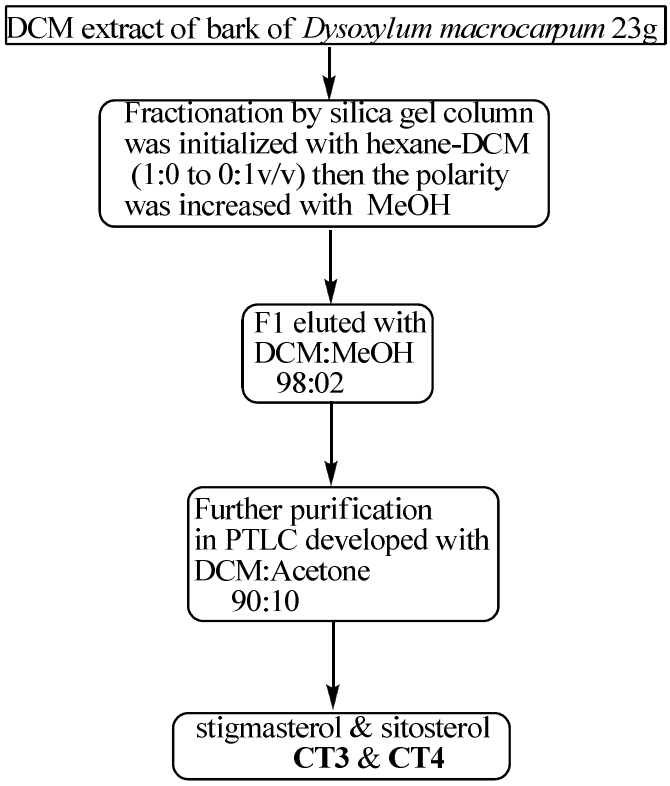

Scheme 6.6 : Isolation and purification of stigmasterol and sitosterol from *Dysoxylum macrocarpum*

6.7 Physical and Spectral Data of Isolated Compounds

6.7.1 *Chisocheton ceramicus*

6.7.1.1 Chisomicine A CC1 : **($C_{32}H_{38}O_8$)**

State	:	White amorphous solid
CD (MeOH) λ_{max} nm ($\Delta\varepsilon$)	:	201 (- 36.2), 213 (0), 227 (7.73), 290 (1.24)
$[\alpha]_D^{25}$	:	-125 (c 0.7, MeOH)
UV λ_{max} nm (log ε)	:	202(4.15), 214(4.02)
IR (KBr) ν_{max} cm^{-1}	:	2938, 1734, 1266
Mass spectrum $[M+Na]^+$	:	573.2464 (573.629 calculated)
^1H NMR ($CDCl_3$) ppm	:	Refer Table 3.2
^{13}C NMR ($CDCl_3$) ppm	:	Refer Table 3.2

6.7.1.2 Chisomicine B CC2 : **$C_{32}H_{40}O_9$**

State	:	colourless needle crystal($CHCl_3$+ MeOH)
Melting Point	:	176-178 ^oC
CD (MeOH) λ_{max} nm ($\Delta\varepsilon$)	:	209 (0.71), 213 (0), 223 (-3.42), 236 (0), 245 (0.92)
$[\alpha]_D^{27}$	:	-66 (*c* 1.0, MeOH)
UV λ_{max} nm (log ε)	:	216 (3.92)
IR (KBr) ν_{max} cm^{-1}	:	3391, 2972, 1735, 1703, 1268
Mass spectrum $[M+H]^+$	:	569.2706 (569.663 calculated)
^1H NMR ($CDCl_3$) ppm	:	Refer Table 3.3
^{13}C NMR ($CDCl_3$) ppm	:	Refer Table 3.3

6.7.1.3 Chisomicine C CC3 : **$C_{32}H_{40}O_{10}$**

State	:	White amorphous solid
CD (MeOH) λ_{max} nm ($\Delta\varepsilon$)	:	201 (-4.86), 208 (0), 211 (0.44), 217 (0),

		221(-0.3), 227(0), 235(0.48), 263(0.93)
$[\alpha]_D^{27}$	:	-86 (*c* 1.0, MeOH)
UV λ_{max} nm (log ε)	:	206 (4.16)
IR (KBr) ν_{max} cm^{-1}	:	3441, 2980, 1732, 1718, 1706, 1269
Mass spectrum $[M+Na]^+$	:	607.2519 (607.644 calculated)
^1H NMR ($CDCl_3$) ppm	:	Refer Table 3.4
^{13}C NMR ($CDCl_3$) ppm	:	Refer Table 3.4

6.7.1.4 Chisomicine D CC4 : **$C_{31}H_{40}O_9$**

State	:	white amorphous solid
$[\alpha]_D^{20}$	:	23 (*c* 1.0, $CDCl_3$)
UV λ_{max} nm (log ε)	:	202 (3.28)
IR (KBr) ν_{max} cm^{-1}	:	3391, 1735
Mass spectrum $[M+H]^+$	:	557.2693 (557.659 calculated)
^1H-NMR ($CDCl_3$) ppm	:	Refer Table 3.5
^{13}C-NMR ($CDCl_3$) ppm	:	Refer Table 3.5

6.7.1.5 Chisomicine E CC5 : **$C_{31}H_{38}O_9$**

State	:	White amorphous solid
$[\alpha]_D^{20}$	:	-23 (*c* 1.0, $CDCl_3$)
UV λ_{max} nm (log ε)	:	202 (3.24)
IR (KBr) ν_{max} cm^{-1}	:	3390, 1733
Mass spectrum $[M+H]^+$	:	555.2551 (555.636 calculated)
^1H-NMR ($CDCl_3$) ppm	:	Refer Table 3.5
^{13}C-NMR ($CDCl_3$) ppm	:	Refer Table 3.5

6.7.1.6 14-deoxyxyloccensin K CC6: **$C_{27}H_{34}O_7$**

State	:	colourless needle crystal in ($CHCl_3$+ MeOH)
Melting Point	:	207-208 °C
$[\alpha]_D^{20}$	:	+98.7 (*c* 0.12, $CHCl_3$)
UV λ_{max} nm (log ε)	:	200, 283, 291
IR (KBr) ν_{max} cm^{-1}	:	2971, 2879, 1733, 1459, 1263
Mass spectrum $[M+H]^+$	:	471.1822
^1H NMR ($CDCl_3$) ppm	:	Refer Table 3.7
^{13}C NMR ($CDCl_3$) ppm	:	Refer Table 3.7

6.7.1.7 Proceranolide CC7 : **$C_{27}H_{34}O_7$**

State	:	yellow pale oil
UV λ_{max} nm	:	200, 281
IR (KBr) ν_{max} cm^{-1}	:	3435, 2971, 2877, 1732, 1460, 1256
Mass spectrum $[M+H]^+$	:	471.1822
^1H NMR ($CDCl_3$) ppm	:	Refer Table 3.8
^{13}C NMR ($CDCl_3$) ppm	:	Refer Table 3.8

6.7.2 *Chisocheton tomentosus*

6.7.2.1 7*α*-Hydroxy-*β*-sitosterol CT1 : **$C_{29}H_{50}O_2$**

State	:	colourless needle crystal in ($CHCl_3$)
Melting point	:	138-140 °C
UV λ_{max} nm	:	302, 254
IR (KBr) ν_{max} cm^{-1}	:	3430, 2936, 2868, 1661, 1464
Mass spectrum $[M]^+$	:	430

^{1}H NMR ($CDCl_3$) ppm	:	Refer Table 3.10
^{13}C NMR ($CDCl_3$) ppm	:	Refer Table 3.10

6.7.2.2 4,6-stigmastadiene-3-one CT2: **$C_{29}H_{46}O$**

State	:	white amorphous
UV λ_{max} nm	:	284
IR (KBr) ν_{max} cm^{-1}	:	3040, 1670, 1620, 1588, 870
Mass spectrum $[M]^+$	:	410
^{1}H NMR ($CDCl_3$) ppm	:	Refer Table 3.11
^{13}C NMR ($CDCl_3$) ppm	:	Refer Table 3.11

6.7.2.3 Mixture of stigmasterol CT3 and sitosterol CT4: $C_{29}H_{48}O$ and $C_{29}H_{50}O$

State	:	white crystal
UV λ_{max} nm	:	302, 254
IR (KBr) ν_{max} cm^{-1}	:	3430, 1598
Mass spectrum $[M+H]^+$	:	413 and 415 respectively
^{1}H NMR ($CDCl_3$) ppm	:	Refer Table 3.12
^{13}C NMR ($CDCl_3$) ppm	:	Refer Table 3.12

6.7.2.4 Mixture of hydroxy acid derivatives of ferulate CT5A-P: $C_{11}H_{10}O_6(CH_2)n$, n=14-16, 18-19, 21-23, 25, 27, 31, 33, 34, 36, 37, 39

State	:	white amorphous
UV λ_{max} nm	:	324, 236
IR (KBr) ν_{max} cm^{-1}	:	3583-3592, 3200-2800, 2926- 2917, 1736-1709, 1678-1673, 1515-1513, 1465
Mass spectrum $[M+Na]^+$	:	457, 471, 485, 513, 527, 555, 569, 583, 611, 637, 693, 723, 737, 765, 779, 807, 194, 144.

^{1}H NMR ($CDCl_3$) ppm : Refer Table 3.13

^{13}C NMR ($CDCl_3$) ppm : Refer Table 3.13

6.7.2.5 Mixture of alkyl coumarate CT6A-O: $C_{10}H_{10}O_3$ $(CH_2)n$, n=11, 12, 14, 16, 19, 20, 21, 24, 25, 29, 31, 34, 37, 39, 40

State : white amorphous

UV λ_{max} nm : 214, 230, 310, 360

IR (KBr) ν_{max} cm^{-1} : 3375, 2912, 2849, 1718, 1607, 1516, 1462, 1172 and 835.

Mass spectrum $[M-H]^+$: 331, 345, 373, 401, 443, 457, 471, 513, 527, 583, 611, 653, 695, 723, 737

^{1}H NMR ($CDCl_3$) ppm : Refer Table 3.14

^{13}C NMR ($CDCl_3$) ppm : Refer Table 3.14

6.7.2.6 Ferulaldehyde CT7 : **$C_{10}H_{10}O_3$**

State : brown oil

UV λ_{max} nm : 314

IR (KBr) ν_{max} cm^{-1} : 3366, 2880, 1660

Mass spectrum $[M]^+$: 178.1

^{1}H NMR ($CDCl_3$) ppm : Refer Table 3.15

^{13}C NMR ($CDCl_3$) ppm : Refer Table 3.15

6.7.2.7 Vanillin CT8 : **$C_8H_8O_3$**

State : light yellow needle crystal

UV λ_{max} nm : 308, 278

IR (KBr) ν_{max} cm^{-1} : 3600-2730, 2680

Mass spectrum $[M+H]^+$: 153.05

^{1}H NMR ($CDCl_3$) ppm : Refer Table 3.16

^{13}C NMR ($CDCl_3$) ppm	:	Refer Table 3.16

6.7.2.8 Goniothalamin CT9 : **$C_{13}H_{12}O_2$**

State	:	brown amorphous crystal
Melting bpoint	:	85-87°C
UV λ_{max} nm	:	210, 258, 300, 310
IR (KBr) ν_{max} cm^{-1}	:	1718, 1244 , 750
Mass spectrum$[M]^+$	:	200
^{1}H NMR ($CDCl_3$) ppm	:	Refer Table 3.17
^{13}C NMR ($CDCl_3$) ppm	:	Refer Table 3.17

6.7.2.9 Eugenin DM1 : **$C_{11}H_{10}O_4$**

State	:	white crystal
Melting point	:	118-119°C
UV λ_{max} nm	:	207, 232, 250, 256, 290, 316
IR (KBr) ν_{max} cm^{-1}	:	3434, 2957, 2842, 1636, 1495
Mass spectrum$[M+H]^+$	:	207
^{1}H NMR ($CDCl_3$) ppm	:	Refer Table 3.19
^{13}C NMR ($CDCl_3$) ppm	:	Refer Table 3.19

6.7.2.10 Squalene DM2 : **$C_{30}H_{50}$**

State	:	yellow colored oil
Boiling point	:	285°C
UV λ_{max} nm	:	344
IR (KBr) ν_{max} cm^{-1}	:	2914, 2728, 1668, 1446, 1382, 1330, 1224, 1151, 1188, 964, 835
Mass spectrum $[M]^+$	:	410
^{1}H NMR ($CDCl_3$) ppm	:	Refer Table 3.20
^{13}C NMR ($CDCl_3$) ppm	:	Refer Table 3.20